MALAYSIAN JOURNAL OF SCIENCE

MJS

ISSN 1394-3065

Malaysian Journal of Science

Vol 44 | No 2 | June 2025

MJS in indexed in Scopus, Google Scholar, Chemical Abstracts Service Database, ASEAN Citation Index (ACI), & MyCite.

MALAYSIAN JOURNAL OF SCIENCE
MJS
ISSN 1394-3065

Regular Issue

Malaysian Journal of Science 44 (2): 1-7 (June 2025) https://mjs.um.edu.my

Purification and Characterization of Bromelain from Pineapple Variety Josapine

Muhammad Yazid Abd Halim[1a], Siti Aimi Sarah Zainal Abidin[2ab] and Siti Roha Ab Mutalib[3ab]*

Abstract: Pineapple (*Ananas comosus (L) Merr*) is a plant that contains the bromelain enzyme which can be found in the crown, flesh, stem, and leaves of the pineapple plant. The bromelain enzyme has the ability to break down the structure of protein into amino acids. Pineapple peels waste from processing are usually discarded and not utilized properly. This study aimed to purify and characterize the bromelain enzyme from pineapple variety Josapine's peels. The production of bromelain powder in this study was done in four steps, the extraction of crude bromelain from pineapple peel extracts, the purification of bromelain using ammonium sulphate precipitation, desalting using the diafiltration process and, finally, freeze drying using a freeze dryer. The protease activity was determined using casein digestion unit (CDU), meanwhile the protein content was determined using Lowry's Method. Results showed that the highest bromelain activity was observed in maturity index 5 in powder form with 2132.78±18.01 CDU/ml, the highest protein content was observed in maturity index 5 in crude extract form with 4.19±0.17 mg/ml and the highest specific enzyme activity was observed in maturity index 5 in powder form with 15234.14 CDU/mg protein. The agroindustry waste product, Josapine pineapple peel, has potential as a future alternative bromelain source.

Keywords: *Purification, bromelain activity, protein content.*

1. Introduction

The pineapple is believed to originate from Brazil. Once discovered, the pineapple was imported to Europe. Christopher Columbus and his men are thought to have tasted the pineapple initially. The word pineapple started to be used in English in 1938 which refers to the organs of conifer trees (Jungle Dragon, 2024). The European pioneers named the fruit as a 'pineapple' according to what is known as a pinecone. The term pinecone was first recorded in 1694, that is to supplant the importance of the pineapple (Hoque *et al*., 2019). According to Sun, (2015), the pineapple or *Ananas comosus L. Merr*. is widely accepted to have come from South America, Argentina, and Paraguay. The pineapple is known by the people of South America just before Christopher Columbus arrived in 1493. The European pilgrims use the word pineapple to present the natural product as to have come from pinecones. Meanwhile, the word Ananas is the initial name of the natural product that comes from the word for pine 'nanas' and 'comosus' referring to the tuft of the stem of the natural product (Jungle Dragon, 2024).

Pineapple is a significant nourishment crop which is planted widely in the tropical and sub-tropical regions of the world. It is a significantly produced natural product for business in Malaysia and is, for the most part, utilized as organic ingredients for pastry or to produce canned pineapple as cuts or rings, squeezes, and sticks. There are five assortments of pineapples in Malaysia; these include the Morris, Sarawak, Gandol, Josapine and N36 (Lasekan & Hussein, 2018). Pineapple processing such as canning and juice produces wastes including pineapple peels. Discharge of pineapple peels during this process will produce waste and lead to serious environmental pollution. In artificial practices, pineapple waste is either used as animal feed or disposed to the soil as waste. Natural enzyme contained in pineapple is called bromelain. Bromelain is an enzyme which is believed to have numerous benefits and is veritably promising to the development of food and medicinal diligence. Bromelain can be found in several parts of the pineapple. The specific part from which it is extracted lends its name to the enzyme; thus, we have fruit bromelain and stem bromelain (Bala *et al*., 2012). Bromelain activity has been reported to be within a pH range of 3 to 8 and a temperature range of 30–70 ºC (Kumar *et al*., 2011;Liang *et al*., 2012;Ramli *et al*., 2018). The natural bromelain enzyme has been used as a meat tenderizer, anti-browning agent and in the processing of formulas for babies (Tochi et al., 2008). As a protease, it hydrolyses proteins in these formulas, therefore making amino acids more readily available to babies. Bromelain is utilized in some applications including cosmetic and pharmaceutical and in textile industry as reported by (Aehle, 2007;B.K. Bhattacharrya, 2008;Ataide *et al*., 2018;Sancesario *et al*., 2018).

Some successful methods have been used for bromelain extraction and purification. Purification of enzymes is important to determine the three-dimensional structure of an enzyme and its impact on the functionality of the enzyme (A. Illanes, 2008). The successful methods in bromelain purification include aqueous two phase systems (Ketnawa *et al*., 2010;Ferreira *et al*., 2011), ammonium sulphate precipitation (G & Viswanathan,

Authors information:
[a]School of Industrial Technology, Faculty of Applied Sciences, Universiti Teknologi MARA, 40450 Shah Alam, Selangor, MALAYSIA. E-mail: muhdyazidhalim@gmail.com[1]; sitiaimi@uitm.edu.my[2]
[b]Malaysian Institute of Transport, Universiti Teknologi MARA, 40450 Shah Alam, Selangor, MALAYSIA. E-mail: sitiroha7796@uitm.edu.my[3]
*Corresponding Author: sitiroha7796@uitm.edu.my

Received: June 8, 2023
Accepted: June 20, 2024
Published: June 30, 2025

DOI:https//doi.org/10.22452/mjs.vol44no2.1
Malaysian Journal of Science 44(2): 1-7 (June 2025)

2013;Gautam *et al*., 2010), ethanol precipitation (Martins *et al*., 2014), ion exchange chromatography (G & Viswanathan, 2013;Gautam *et al*., 2010; Bresolin *et al*., 2013), membrane separation (Seguí & Fito Maupoey, 2018) and adsorption using functionalized Santa Barbara Acid-15 (Arumugam & Ponnusami, 2013).

The pineapple variety Josapine was chosen because it is abundantly planted in Malaysia which covers about 41.5% or 6725 hectares. This shows that the waste produced by the pineapple industry is large at about 150 000 kg. Other than that, the pineapple variety Josapine was easily obtained aIB, 2022). The main reason to select the maturity index 5 and 7 is to determine whether there is a significant difference of bromelain activity among them. As a justification, the maturity index 3 and 4 is not chosen because their difference is too narrow while maturity index 5 is in the middle and maturity index 7 is overripe. Maturity index 1 is too young while maturity index 2 is usually selected for harvesting. Thus, the aim of this study was to determine the bromelain activity, protein content and specific enzyme activity of bromelain extracted from pineapple variety Josapine peel with maturity indices 2, 5 and 7.

2. Materials and Methods

Preparation of Samples

Pineapple of the Josapine variety with different maturity indices of 2, 5 and 7 used in this study were purchased from a local market in Seksyen 6, Shah Alam, Selangor, Malaysia. Table 1 shows the seven-maturity index of pineapple according to the standard specification by Federal Agriculture Marketing Authority (FAMA) (FAMA, 2020). The pineapple peel with maturity index 2, 5 and 7 were cut into small pieces and crushed in a food processor (Model PB-3203L, Brand Pensonic, Country Malaysia) with the addition of water at a ratio of 1:1 to produce pineapple peel extract. Extraction was done in a chilled temperature (4^{o}C). Next, the extract was filtered through a muslin cloth to remove the solid parts. The filtrate was collected and kept in a freezer (-20^{o}C) to be used in further experiments (Gautam *et al*., 2010).

Table 1. Maturity Indices of Pineapple

Index	Characteristics
1	Young or immature. The entire surface of the skin or the eye is slightly oval-shaped upward, dark green with reddish bractea. Flesh is very solid, firm, and sour. Not yet ready for harvest.
2	Early maturity stage. All eyes are quite rounder with glossy dark green and traces of yellow between eyes at the base. The bractea is whitish in colour and dry. Flesh is solid, firm, and sourish. Inedible flesh. Suitable to be harvested for export.
3	Mature fruit. All eyes are green with 1-2 eyes yellowish green at the base. Flesh is solid, crunchy, and sourish. Edible flesh but not palatable. Suitable to be harvested for export.
4	Underripe. An average of 25% of the eyes from the base of the fruit turns into yellowish-orange. Flesh is solid, firm, crunchy and sweet sour. Edible flesh. Suitable to be harvested for domestic market
5	Early ripe. Almost 50% of the eyes are yellowish-orange from the base of the fruit. Flesh is less spongy, yet juicy, sweet, and fragrant. The best level to be eaten fresh.
6	Ripe. Over 75% of their eyes are yellowish-orange. Flesh is a little flaccid, yet spongy, very juicy, sweet, and fragrant. Less suitable to be harvested for export but more suitable for domestic market.
7	Overripe. The whole eyes are yellowish-orange. Flesh is flaccid, soft, very juicy, and sweet sour. Still edible flesh. Not suitable for any domestic market or export.

Production of Bromelain Powder

Purification of Bromelain Extract

Firstly, the purification of the crude bromelain extract was carried out using the ammonium sulphate precipitation method. About 10 mL of crude bromelain extract was transferred into a centrifuge tube and placed in an ice bath. Then, about 6 g of ammonium sulphate was added pinch by pinch. Then, the sample was left for incubation for 1 hour until the appearance of precipitation is observed. Then, the cold incubated sample was centrifuged (Model 5420, Brand Kubota, Country Japan) at 3500 rpm for 30 mins. Then, the pellet was collected by dissolving in 10 mL Tris buffer, while the supernatant was removed. The purified bromelain was stored in a chiller for further analysis (Devakate *et al*., 2009).

Desalting

The dialysis process was performed using a diafiltrator machine. Firstly, about 1 L of deionised water was allowed to run into the diafiltrator machine for washing. Then, before running the sample, the initial salinity of purified extract was checked using a salinity meter (Model RSA0100, Brand Trans Instruments, Country Singapore). Then, the purified extract sample was allowed to run into the diafiltrator machine, until the salinity percentage reached 0%. The purified extract sample was dialysed using the deionised water. After the salinity reached 0%, the dialysed sample was stored in a freezer for further analysis (Devakate *et al*., 2009).

Drying of Desalted Bromelain

Desalted bromelain was dried using a vacuum freeze dryer (Model Alpha 1-4 LD Plus, Brand Christ, Country Germany) which took 4 days for complete drying at -60^{o}C. The desalted bromelain was frozen at -20^{o}C before undergoing the freeze-drying process to provide a necessary condition for low temperature drying (Devakate *et al*., 2009).

DOI:https//doi.org/10.22452/mjs.vol44no2.1
Malaysian Journal of Science 44(2): 1-7 (June 2025)

Protein Content

Preparation of Reagents

Firstly, two solutions were prepared namely solution A and solution B. For solution A, 50 ml of 2% (w/v) of sodium carbonate (Na_2CO_3) solution was mixed with 50 ml of 0.1 N sodium hydroxide (NaOH) solution. For solution B, 10 ml of 1.56% (w/v) of copper sulphate ($CuSO_4.5H_2O$) solution was mixed with 10 ml of 2.37% (w/v) of sodium potassium tartarate ($C_4H_4O_6KNa.4H_2O$) solution. Then, 100 ml of solution A and 2 ml of solution B were mixed to prepare Lowry's solution. To prepare the Folin-Ciocalteau reagent, about 2 ml of Folin-Ciocalteau was mixed with 2 ml of distilled water.

Protein Assay (Lowry's Method)

Firstly, about 1 ml of the sample was transferred into a test tube. Then, about 5 ml of Lowry solution was added into the test tube. The test tube was vortexed and incubated at room temperature for 10 minutes. Then, about 0.5 mL of Folin was added into the test tube. Then, the test tube was incubated in the dark for 30 minutes at room temperature. Next, the sample was transferred into a beaker. Afterwards, the absorbance of sample was measured at 595 nm using a UV-Visible spectrophotometer (Model Lamda 35, Brand Perkin Elmer, Country USA). The amount of protein content was determined using the BSA standard calibration curve (Ketnawa *et al.*, 2012).

Bromelain Activity

Bromelain activity in the sample was determined using the casein digestion unit (CDU) method (Enzyme Development Corporation, 2015). Firstly, approximately 5 ml of the casein substrate was transferred into a test tube. The test tube was then immersed in a water bath at 37°C for 10 minutes. Next, about 5 mL of trichloroacetic acid (TCA) stopping reagent and 1 mL of the enzyme solution were added to the blank test tube, while only about 1 mL of the enzyme solution was added to the sample test tube. The test tubes were vortexed and placed back into the water bath at 37°C for 10 minutes. Subsequently, about 5 mL of the TCA stopping reagent was added to both the blank test tube and sample test tube, and they were vortexed again before being placed back into the water bath at 37°C for 30 minutes. Afterwards, the blank test tube and sample test tube were removed from the water bath and left to cool to room temperature. The blank test tube and sample test tube were then filtered using filter paper, and the filtrate was collected in a beaker. The absorbance was measured at 280 nm using a UV-Visible spectrophotometer (Soares *et al*., 2012). The bromelain activity was calculated using the formula.

$$CDU/mg = [(Et - Eb)/Es] \times 50 \times (11/10) \times DF$$

Where;
DF: Dilution Factor
Et = Absorbance of enzyme sample tube
Eb = Absorbance of blank sample tube
Es = Absorbance of standard Tyrosine

Standard Tyrosine

A standard solution containing exactly 50µg/ ml of L-Tyrosine was prepared in 0.1N HCl. The absorbance of the standard was measured and recorded at 275 nm using distilled water for the blank test tube (Enzyme Development Corporation, 2015).

Specific Enzyme Activity

The specific enzyme activity in pineapple peels will be calculated using the following formula.

$$\text{Specific enzyme activity} = \frac{\textit{Bromelain Activity}}{\textit{Protein Content}}$$

Data Analysis

All experiments were performed in triplicate. The data obtained were analyzed using the software, Statistical Package for the Social Sciences (SPSS). The analysis of variance (ANOVA) tests was performed.

DOI:https//doi.org/10.22452/mjs.vol44no2.1
Malaysian Journal of Science 44(2): 1-7 (June 2025)

Table 2. Activity of pineapple Josapine

Sample	Bromelain activity (CDU/ml)	Protein content (mg/ml)	Specific bromelain enzyme activity (CDU/mg protein)	Purification level
Index 2				
Pineapple peel extract	659.16±10.14^{d}	3.72±0.11^{a}	177.19^{d}	1.00^{d}
Purified bromelain	791.66±33.18^{c}	0.80±0.05^{b}	989.57^{c}	5.58^{c}
Desalted bromelain	1004.95±5.02^{b}	0.21±0.01^{c}	4785.47^{b}	27.00^{b}
Bromelain powder	1440.63±63.87^{a}	0.14±0.00^{d}	10290.21^{a}	58.07^{a}
Index 5				
Pineapple peel extract	877.89±35.71^{d}	4.19±0.17^{a}	209.52^{d}	1.00^{d}
Purified bromelain	1574.43±24.64^{c}	0.74±0.05^{b}	2127.60^{c}	10.15^{c}
Desalted bromelain	1728.31±63.49^{b}	0.19±0.01^{c}	9096.36^{b}	43.41^{b}
Bromelain powder	2132.78±18.01^{a}	0.14±0.01^{d}	15234.14^{a}	72.70^{a}
Index 7				
Pineapple peel extract	505.96±14.49^{d}	3.84±0.14^{a}	131.76^{d}	1.00^{d}
Purified bromelain	1012.36±9.64^{c}	1.15±0.06^{b}	880.31^{c}	6.68^{c}
Desalted bromelain	1281.75±16.32^{b}	0.22±0.01^{c}	5826.13^{b}	44.21^{b}
Bromelain powder	1611.83±8.57^{a}	0.13±0.01^{d}	12398.69^{a}	94.10^{a}

Means within each column with different superscript are significantly different at $p < 0.05$

DOI:https//doi.org/10.22452/mjs.vol44no2.1
Malaysian Journal of Science 44(2): 1-20 (June 2025)

3. Results and Discussion

In this study, bromelain powder was produced in four steps. The production steps included the extraction of crude bromelain from pineapple peel extract, followed by bromelain purification using ammonium sulphate precipitation. Then, a desalting process was performed using a diafiltration machine, and, finally, freeze drying was done using a freeze dryer. Subsequently, the samples obtained from each processing step were analysed for bromelain activity, protein content, and specific bromelain enzyme activity.

The bromelain activity measures the quantity of active enzymes present in the sample, while the protein content measures the total level of protein in a solution. The specific bromelain enzyme activity measures the enzyme purity in a mixture. The purification level, on the other hand, shows whether the sample became purer following the purification technique.

The bromelain activity, protein content, and specific bromelain enzyme activity were tested for pineapple peel extract, purified bromelain, desalted bromelain, and bromelain powder at maturity indices 2, 5, and 7. Table 2 shows the bromelain activity, protein content, and specific enzyme activity for each sample.

For maturity index 2, the bromelain activity, protein content, and specific enzyme activity of pineapple peel extract were 659.16 CDU/ml, 3.72 mg/ml, and 177.19 CDU/mg of protein, respectively. This step was to isolate most of the protein present in the pineapple peel extract since it could affect the bromelain activity as well as protein content in the following steps. The value of bromelain activity, protein content and specific bromelain enzyme activity in the purified bromelain were 791.66 CDU/ml, 0.80 mg/ml, and 989.57 CDU/mg of protein, respectively. For the desalted bromelain, its value of bromelain activity, protein content and specific bromelain enzyme activity were 1004.95 CDU/ml, 0.21 mg/ml, and 4785.47 CDU/mg of protein, respectively. While the value of bromelain activity, protein content and specific bromelain enzyme activity in the bromelain powder were 1440.63 CDU/ml, 0.14 mg/ml, and 10290.21 CDU/mg of protein, respectively.

Similarly, for maturity index 5, the bromelain activity, protein content, and specific enzyme activity of pineapple peel extract were 877.89 CDU/ml, 4.19 mg/ml, and 209.52 CDU/mg of protein, respectively. The value of bromelain activity, protein content and specific bromelain enzyme activity in the purified bromelain were 1574.43 CDU/ml, 0.74 mg/ml, and 2127.60 CDU/mg of protein, respectively. For the desalted bromelain, its value of bromelain activity, protein content and specific bromelain enzyme activity were 1728.31 CDU/ml, 0.19 mg/ml, and 9096.36 CDU/mg of protein, respectively. While the value of bromelain activity, protein content and specific bromelain enzyme activity in the bromelain powder were 2132.78 CDU/ml, 0.14 mg/ml, and 15234.14 CDU/mg of protein, respectively.

Lastly, for maturity index 7, the corresponding values of bromelain activity, protein content, and specific enzyme activity of pineapple peel extract were 505.96 CDU/ml, 3.84 mg/ml, and 131.76 CDU/mg of protein, respectively. The value of bromelain activity, protein content and specific bromelain enzyme activity in the purified bromelain were 1012.36 CDU/ml, 1.15 mg/ml, and 880.31 CDU/mg of protein, respectively. For the desalted bromelain, its value of bromelain activity, protein content and specific bromelain enzyme activity were 1281.75 CDU/ml, 0.22 mg/ml, and 5826.13 CDU/mg of protein, respectively. While the value of bromelain activity, protein content and specific bromelain enzyme activity in the bromelain powder were 1611.83 CDU/ml, 0.13 mg/ml, and 12398.69 CDU/mg of protein, respectively.

The determination of bromelain activity, protein content and specific enzyme activity were important to know the trend loss of bromelain enzyme during the purification processing studied. Every step of the process gives different results for bromelain activity, protein content and specific enzyme activity. The purification level was estimated by dividing the specific enzyme activity at each purification step with that of crude pineapple peel extract.

Table 2 shows that the bromelain activity was significantly higher in the bromelain powder at the 5% level followed by those in the purified bromelain, desalted bromelain, and pineapple peel extract of those maturity indices. Bromelain activity increased after the purification process. This is because only bromelain was purified from the pineapple peel extract. A previous study done by Nadzirah *et al*., (2012) on the extraction of bromelain form pineapple crown variety N36 by using distilled water as the extraction medium found that the bromelain activity was significantly higher in bromelain powder (529.77 CDU/ml), followed by purified (501.08 CDU/ml), desalted (485.78 CDU/ml), and pineapple extract (426.49 CDU/ml). Furthermore, Misran *et al*., (2019) conducted a study on pineapple variety Morris and found that the highest bromelain activity was observed in the peel (229.64 CDU/ml). Another study by Nor *et al*., (2015) found that the bromelain activity for pineapple peel variety Smooth Cayenne is 429.70 CDU/ml. In this study, the values of bromelain activity ranges between 505.96 to 2132.78 CDU/ml which was higher than the findings by Nadzirah *et al*. (2012) and Nor *et al*. (2015) which ranged between 229.64 to 529.77 CDU/ml. The different results obtained from this study compared to the previous findings may have been due to the difference in species of pineapple used. Different varieties of pineapples will influence the quality of bromelain extracted. Environmental factors such as climatic growth conditions, growth, ripening stage, temperature, duration of storage and thermal treatment may have influenced the bromelain activity (Ramli & Munir, 2022). Therefore, pineapple peel variety Josapine can provide a better source of bromelain enzyme compared to N36 and Smooth Cayenne variety.

In this study, the protein content was significantly higher in the pineapple peel extract while specific enzyme activity was significantly higher in the powdered bromelain. A previous study done by Gul et al., (2021) found that protein content in pineapple variety Phu Lae (0.215 mg/ml) and Nang Lae (0.337 mg/ml). Another study by Misran et al., (2019) found that the protein content for pineapple peel variety Morris was 83.33 mg/ml.

Furthermore, Nor et al., (2015) found that the protein content of pineapple peel variety Smooth Cayenne was 1.37 mg/ml. To compare, the protein content obtained in this research study was lower than the above previous studies. The range of protein content obtained in this study was between 0.13 to 4.19 mg/ml meanwhile the protein content for the above previous studies was between 0.2 to 83.33 mg/ml. According to Ramli & Munir, (2022) the difference in the protein content is influenced by the variety of pineapple, climate during culture, the stage of ripeness, the timing of harvest, and the extraction technique.

Lastly, regarding specific enzyme activity, (Gul *et al*., 2021) studied the specific enzyme activity of pineapple variety Phu Lae extract purified with 60% ammonium sulphate. The highest specific enzyme activity was observed in the core (105.17 CDU/mg), followed by the crown (64.20 CDU/mg) and peel (54.69 CDU/mg). Additionally, Umesh Hebbar *et al*., (2008) examined the specific enzyme activity of pineapple variety Kew, and the results showed that the highest specific enzyme activity was observed in the crown (49.41 CDU/mg), followed by the core (40.32 CDU/mg), stem (14.72 CDU/mg), and peel (10.22 CDU/mg). For comparison, the specific bromelain enzyme activity obtained from this research study was higher than reported in the previous studies. The range for specific bromelain enzyme activity for this research was between 131.76 to 15234.14 CDU/mg protein meanwhile for the reported above previous studies was between 10.22 to 105.17 CDU/mg protein. According to Susanti *et al*., (2022) the differences in specific bromelain enzyme activity may due to the number of impurities decreasing after the purification steps. This shows that the level of purity value of bromelain enzyme is higher when the value of specific bromelain enzyme activity is higher.

For pineapple peel extract, it has lower bromelain activity, specific bromelain enzyme activity and purification level compared to bromelain powder, but it has the highest protein content. High protein content indicates the presence of other proteins in the sample while low protein content indicates the presence of target bromelain in sample (Nadzirah *et al*., 2012) From the data in Table 2, the purification of enzyme through the drying process (powdered bromelain) yielded the highest purification level at 58.07, 72.70 and 94.10 for maturity index 2, 5 and 7 respectively. The increasing trend in purification level showed that the samples are successfully purified at each stage.

4. Conclusion

The extraction process to produce bromelain was carried out consecutively. Therefore, one step might affect the following steps. Bromelain activity and purification level in powdered bromelain was significantly higher compared to those from pineapple peel extract, purified bromelain, and desalted bromelain.

5. Acknowledgement

Special thanks to Ministry of Higher Education, Malaysia for funding this project under Fundamental Research Grant Scheme [600-IRMI/FRGS-RACER 5/3 (097/2019].

5. References

A. Illanes. (2008). Enzyme Biocatalysis. In *Springer eBooks.*

Aehle, W. (2007). Enzymes in Industry: Production and Applications, 3rd edition. In Wiley.com.

Arumugam, A., & Ponnusami, V. (2013). Pineapple fruit bromelain recovery using recyclable functionalized ordered mesoporous silica synthesized from sugarcane leaf ash. *Brazilian Journal of Chemical Engineering*, *30*(3), 477–486.

Ataide, J. A., Gérios, E. F., Mazzola, P. G., & Souto, E. B. (2018). Bromelain-loaded nanoparticles: A comprehensive review of the state of the art. *Advances in Colloid and Interface Science*, *254*, 48–55.

Bala, M., Azira Ismail, N., Mel, M., Saedi Jami, M., Mohd Salleh, H., Amid, A., Saedi JAMI, M., & Azira ISMAIL, N. (2012). Bromelain Production: Current Trends and Perspective. *Archives Des Sciences*, *65*(11), 370.

B.K. Bhattacharrya. (2008). Bromelain: Overview. *Natural Product Radiance*. *7*(4), 359–363.

Bresolin, I. R. A. P., Bresolin, I. T. L., Silveira, E., Tambourgi, E. B., & Mazzola, P. G. (2013). Isolation and purification of bromelain from waste peel of pineapple for therapeutic application. *Brazilian Archives of Biology and Technology*, *56*(6), 971–979.

Devakate, R. V., Patil, V. V., Waje, S. S., & Thorat, B. N. (2009). Purification and drying of bromelain. *Separation and Purification Technology*, *64*(3), 259–264.

Enzyme Development Corporation. (2015). Casein Digestion Unit Analytical Method (CDU). *Enzyme Development Corporation*.

FAMA. (2020). Menuju ke arah kualiti Malaysia's BEST. *Federal Agricultural Marketing Authority (FAMA)*.

Ferreira, J. F., Bresolin, L. R. P., Silveira, E., & Tambourgi, E. B. (2011). Purification of bromelain from ananas comosus by PEG/phosphate ATPS. *Chemical Engineering Transactions*, *24*, 931–936.

G, S., & Viswanathan, G. (2013). Isolation and Characterization of Bromelain (BML) Proteases from Ananas cosmosus an asset to Cancer Chemotherapy. *International Journal of Pharmacology and Toxicology*, *1*(2).

Gautam, S. S., Mishra, S. K., Dash, V., Goyal, A. K., & Rath, G. (2010). Comparative study of extraction, purification and estimation of bromelain from stem and fruit of pineapple plant. *Thai Journal of Pharmaceutical Sciences*, *34*(2), 67–76.

Gul, A., Siddiqui, M., Arain, H., Khan, S., Khan, H., & Ishrat, U. (2021). Extraction, partial purification and characterization of bromelain from pineapple (Ananas Comosus) crown, core and peel waste. *Brazilian Archives of Biology and Technology*, *64*(e21200639), 1–10.

Hoque, S. S., Rashid, M. H.-A., & Sharmin, S. (2019). Comparative profitability of sole pineapple, pineapple-papaya and pineapple-banana-arum cultivation in Tangail District of Bangladesh. *Journal of the Bangladesh Agricultural University*, *17*(2), 236–243.

Jungle Dragon. (2024). Pineapple (Ananas comosus). *JungleDragon*.

Ketnawa, S., Chaiwut, P., & Rawdkuen, S. (2012). Pineapple wastes: A potential source for bromelain extraction. *Food and Bioproducts Processing*, *90*(3), 385–391.

Ketnawa, S., Rawdkuen, S., & Chaiwut, P. (2010). Two phase partitioning and collagen hydrolysis of bromelain from pineapple peel Nang Lae cultivar. *Biochemical Engineering Journal*, *52*(2–3), 205–211.

Kumar, S., Hemavathi, A. B., & Hebbar, H. U. (2011). Affinity based reverse micellar extraction and purification of bromelain from pineapple (Ananas comosus L. Merryl) waste. *Process Biochemistry*, *46*(5), 1216–1220.

Lasekan, O., & Hussein, F. K. (2018). Classification of different pineapple varieties grown in Malaysia based on volatile fingerprinting and sensory analysis. *Chemistry Central Journal*, *12*(1), 1–12.

Liang, H., Li, M., Shi, M., Liao, A., & Wu, R. (2012). Study on the Stability of Fruit Bromelain. *Advanced Materials Research*, *421*, 19–22.

Martins, B. C., Rescolino, R., Coelho, D. F., Zanchetta, B., Tambourgi, E. B., & Silveira, E. (2014). Characterization of bromelain from ananas comosus agroindustrial residues purified by ethanol factional precipitation. *Chemical Engineering Transactions*, *37*, 781–786.

Misran, E., Idris, A., Mat Sarip, S. H., & Ya'akob, H. (2019). Properties of bromelain extract from different parts of the pineapple variety Morris. *Biocatalysis and Agricultural Biotechnology*, *18*(101095), 1–4.

MPIB. (2022). Malaysian Pineapple Industry Board, Report of pineapple production statistics according to variety 2019. *MPIB*.

Nadzirah, K. Z., Zainal, S., Normah, A., & Roha, S. (2012). Physicochemical properties of pineapple crown extract variety N36 and bromelain activity in different forms. *APCBEE Procedia*, *4*, 130–134.

Nor, M. Z. M., Ramchandran, L., Duke, & M., & Vasiljevic, T. (2015). Characteristic properties of crude pineapple waste extract for bromelain purification by membrane processing. *Journal Food Science Technology*, *52*(11), 7103–7112.

Ramli, A. N. M., Manas, N. H. A., Hamid, A. A. A., Hamid, H. A., & Illias, R. M. (2018). Comparative structural analysis of fruit and stem bromelain from Ananas comosus. *Food Chemistry*, *266*, 183–191.

Ramli, A. N. M., & Munir, N. (2022). Enzymatic Analysis and Characterization of Bromelain from Two Varieties of Pineapple (Ananas comosus) Fruit and Stem Extracts. *Current Science and Technology*, *2*(2), 13–19.

Sancesario, G. M., Nuccetelli, M., Cerri, A., Zegeer, J., Severini, C., Ciotti, M. T., Pieri, M., Martorana, A., Caltagirone, C., Nistico, R., & Bernardini, S. (2018). Bromelain Degrades Aβ1-42 Monomers and Soluble Aggregates: An In Vitro Study in Cerebrospinal Fluid of Alzheimer's Disease Patients. *Current Alzheimer Research*, *15*(7), 628–636.

Seguí, L., & Fito Maupoey, P. (2018). An integrated approach for pineapple waste valorisation. Bioethanol production and bromelain extraction from pineapple residues. *Journal of Cleaner Production*, *172*, 1224–1231.

Soares, P. A. G., Vaz, A. F. M., Correia, M. T. S., Pessoa, A., & Carneiro-Da-Cunha, M. G. (2012). Purification of bromelain from pineapple wastes by ethanol precipitation. *Separation and Purification Technology*, *98*, 389–395.

Sun. (2015). Nutritional Composition of Pineapple (Ananas comosus (L.) Merr.). In *Nutritional Composition of Fruit Cultivars* (pp. 609–637). Elsevier Inc.

Susanti, S., Rizqiati, H., Pratama, Y., Arifan, F., & Reza, S. P. (2022). Characteristics of Bromelain enzyme from Queen variety pineapple crown at different drying temperatures. *IOP Conference Series: Earth and Environmental Science*, *977*(012029), 1–7.

Tochi, B. N., Wang, Z., Xu, S. Y., & Zhang, W. (2008). Therapeutic application of pineapple protease (Bromelain): A review. *Pakistan Journal of Nutrition*, *7*(4), 513–520.

Umesh Hebbar, H., Sumana, B., & Raghavarao, K. S. M. S. (2008). Use of reverse micellar systems for the extraction and purification of bromelain from pineapple wastes. *Bioresource Technology*, *99*(11), 4896–4902.

MALAYSIAN JOURNAL OF SCIENCE
MJS
ISSN 1394-3065

Regular Issue

Malaysian Journal of Science 44 (2): 8-17 (June 2025) https://mjs.um.edu.my

Reproductive Biology of Pokea Clams (*Batissa violacea var. celebensis*, von Martens 1897) at Langkumbe River, Southeast Sulawesi, Indonesia

Bahtiar[1a]*, Muhammad Nur Findra[2b], Yustika Intan Permatahati[3a] and Ma'ruf Kasim[4a]

Abstract: Pokea clams (*Batissa violacea*) are bivalves that possess different reproductive patterns depending on the location. However, their reproductive pattern in Langkumbe River (Southeast Sulawesi, Indonesia) is unknown. This study aims to determine the sex ratio, gonad maturity level (GML), gonadosomatic index (GSI), fecundity and size of the first gonad maturity of the clams. The samples were collected randomly using iron baskets in all parts of the river and were combined together. The sex ratio, GML, GSI and size at first maturity were calculated using a standard formula, each of which was analyzed using the Chi-Square test, quantitative descriptive analysis as well as simple and non-linear regression. The results showed that the clams were gonochoric with more males than females. Male clams were relatively smaller and ranged from 3.28-3.75 cm in size. Furthermore, gonadal early and late development occurred in February through March and final gonad maturation occurred in April. Gonadal maturation and spawning occurred over a long period from March to October with a pattern of 1 peak spawning marked by an increase in the GSI value in the particular month. The GSI values in males and females were relatively the same, i.e., 36.47±16.79 and 34.80±17.71 as well as 18.37±9.46 and 18.57±8.86, respectively. Male pokea clams matured earlier than female with sizes of 1.4 cm or 0.23% and 2 cm or 0.50%, respectively. The reproductive potential of pokea clams in the Langkumbe River is high.

Keywords: *Batissa violacea, Langkumbe River, reproduction, Southeast Sulawesi.*

1. Introduction

Batissa violacea var. *celebensis* von Martens 1897 (Kusnoto, 1953) is a species of bivalves that has important economic potential and can be found distributed in several large rivers in Southeast Sulawesi among them: Pohara River (Bahtiar et al., 2015), Lasolo River (Bahtiar et al., 2016), Langkumbe River (Alkadri et al., 2018) and Laeya River (Bahtiar et al., 2022a; Bahtiar et al., 2023a). The local community people named this species pokea or keha (Bahtiar et al., 2021). Clams of the same genus (*Batissa*) are widely distributed and found in the western (Sumatera) to the eastern part of Indonesia (Papua), the Philippine and the southern Pacific (Fiji Islands) (Kusnoto, 1953; Layugan et al., 2013; Mayor et al., 2016).

Ecologically, these clams live immersed in a substrate that can be found from the texture of the substrate of mud, clay, sand and gravel. These clams are relatively distributed in groups and are only found in the estuary area, namely in the tidal area farthest upstream until the meeting of fresh water and seawater towards the sea (Bahtiar et al., 2012b). Similar to other clams, this species plays an important role in the ecosystems of rivers. These clams are able to reduce the turbidity of waters through their filter feeder mechanism. This shellfish is an environmental architect capable of producing and stabilizing the bottom substrate of the water so that it can be useful for the life of other organisms at the bottom of the water (Vaughn et al., 2008). They are also economically viable, providing the community with resources to establish food businesses (Bahtiar et al., 2014a, 2012a, 2023b; Layugan et al., 2013; Mayor & Ancog, 2016) due to their highly nutritious and efficacious nature in healing several types of diseases (Bahtiar et al., 2014b; Yeni, 2012). Pokea clams also provide a source of living for many and are frequently being sold in local markets in Kendari City.

Batissa clams are overexploited in several locations including the Pohara River (Bahtiar et al., 2012b) as well as Lasolo River (Bahtiar, 2017), Laeya River, Langkumbe River (Bahtiar et al., 2022a); and have become an endangered species in the Philippines' Cagayan River (Layugan et al., 2013; Mayor et al., 2016). The catch/production of pokea shellfish by fishermen can reach 155 tons in the Pohara River (Bahtiar, 2012), 1500-1750 tons in the Lasolo River (Bahtiar et al., 2016) and 3.40-24.77 kg/trip/boat in Cagayan River, Northern Philippines (Mayor & Ancog, 2016). Overexploitation potentially leads to a decline in the quality (low condition index and b value) and quantity (the number and size of clams are getting smaller) of pokea clams (Bahtiar, 2012; Bahtiar et al., 2015, 2016, 2022a) as well as severely disturbs their reproduction pattern or cycle in nature. Clams in areas with high ecological stress adopt reproductive strategies to maintain their existence in nature (Bone & Marshall, 1982) such as prompting early gonad maturity. However, depending on their specific habitats, pokea clams can have different environments that shape food consumption and

Authors information:
[a]Department of Aquatic Resources Management, Faculty of Fisheries and Marine Science, Halu Oleo University, Kendari, INDONESIA. E-mail: bahtiarfpikuho@gmail.com[1]; intanintanaa@gmail.com[3]; marufkasim@uho.ac.id[4]
[b]Department of Aquatic Resources Management, Faculty of Fisheries and Marine Science, Khairun University, Ternate, INDONESIA. E-mail: muhammad.findra@gmail.com[2]
*Corresponding Author: bahtiarfpikuho@gmail.com

Received: June, 2023
Accepted: June, 2024
Published: June, 2025

DOI:https//doi.org/10.22452/mjs.vol44no2.2
Malaysian Journal of Science 44(2): 8-17 (June 2025)

regulate their activities (Bahtiar et al., 2021)

Existing studies on reproduction cycles and activity related to pokea were limited and often restricted to areas within Indonesia. Previous studies have been conducted in various locations such as the Pohara River (Bahtiar et al., 2021), Batang Anai River, Padang West Sumatra (Puteri, 2005) and Lasolo River (Bahtiar, 2017). Still, sufficient report on reproduction of the clams in Langkumbe River is yet to be identified and established. This information is crucial to guide in managing clam resources in the future (Bahtiar et al., 2022b; Camilo et al., 2017). Consequently, investigations on the reproduction biology of pokea clams in the river are needed. This study aims to determine several parameters reproduction biology of pokea clams in Langkumbe River, Southeast Sulawesi, specifically on the analysis of sex ratio, Gonad Maturity Level (GML), Gonadosomatic Index (GSI) and size at first gonadal maturity.

2. Materials and Methods

This study was carried out in Langkumbe River, Southeast Sulawesi, Indonesia, for one year from February 2017 to January 2018 at the location of 04°21'58.1" S and 122°29'54.0" W to 04°22'24.6" S and 122°29'54.9" W (Figure 1). Pokea clam samples were collected randomly and periodically every month in all parts of the river waters using iron baskets. A total of 10 batches were later brought to the laboratory and separated by sex, identified by the color of the gonads. Male gonads are milky white, while female is brown. Furthermore, the reproductive parameters of pokea clams observed include sex ratio, GML, GSI, fecundity and size at first gonad maturity. The number of samples observed to determine sex ratio was all the clams caught at all observation points. In contrast, GML, GSI, fecundity and size at first maturity of gonads were observed from 120 individuals from each sex.

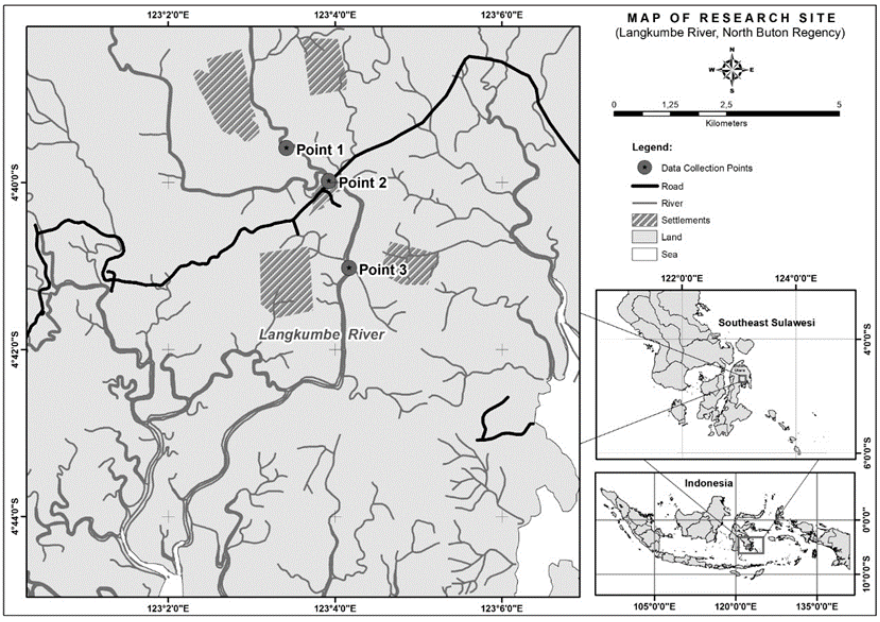

Figure 1. Map of study sites on Langkumbe River, Southeast Sulawesi.

The sex ratio was determined by calculating the ratio of the number of males and females in each month. Gonad development was observed using a microscope with a magnification of 40x10. The clams were subsequently categorized into 5 (five) different levels based on their stage of development: inactive, preparatory/early, late, mature and spawning/post-spawning. Each sample was grouped into the respective category based on the gonad morphology as observed using a microscope with histology preparation (Bahtiar et al., 2021). Furthermore, GSI observation was carried out by weighing the body and gonad weight (Bahtiar, 2017), while size at first gonad maturity was assessed by measuring the widths of all clams with mature gonads (Bahtiar et al., 2023c). Water samples were analyzed for their quality at the Laboratory of the Faculty of Fisheries and Marine Science, Halu Oleo University. The samples were taken at the same time as the pokea clams, while the quality aspects observed were the total organic and sediment organic matter and chlorophyll-a content.

The sex ratio of male to female pokea was determined by Chi-square test (χ^2) (Mzighani, 2005).

The GSI value (gonadosomatic index) was calculated using the formula described by (Bahtiar, 2017; Bahtiar et al., 2024):

$$GSI = \frac{Wg}{Wb} \times 100\ \% \qquad (1)$$

Descriptions:

GSI = gonadosomatic Index
Wg = weight of gonad (g)
Wt = weight of body including Gonad (g)

DOI:https//doi.org/10.22452/mjs.vol44no2.2
Malaysian Journal of Science 44(2): 8-17 (June 2025)

The 50% probability of gonad maturity was determined with the non-linear regression analysis on the logistic curve (Bahtiar et al., 2023c; Mzighani, 2005) using the Sigma plot 6.0 software as shown in the following equation:

$$Y = \frac{a}{1 + e^{\frac{-x + xo}{b}}} \quad (2)$$

Descriptions:
Y = probability of pokea with mature gonad (%)
e = exponential constant
a = intercept
b = slope
x, xo = i-th width (cm)

3. Results and Discussion

Sex Ratio

Pokea shells were observed to be dominatingly gonochorism with both male and female sexes found in each month. A relatively greater trend of gonochorism was found in February and later decreased up until January. Females were smaller in proportion in February and increased onwards until October. In general, males had the larger ratios to females ranging from 34.51-71.16% and 19.04-45.98%, respectively. The χ^2 test obtained a P-value of 0.23 (p >0.05) indicating that the male to female ratio was close to 1:1, or relatively the same. Gonochorism was found in the smallest clams with a size range of 3.28-3.75 cm. Moreover, males were dominant up to the size range of 3.28-3.75 cm, above which females became generally more numerous (Figure 2). The male and female reproductive organs of pokea clams were found to be separated (dioecious) (Bahtiar, 2012; Bahtiar et al., 2021) and there was no indication of micro or true hermaphroditic nature compared to several other freshwater clams including Corbicula fluminea (Sousa et al., 2008). Pokea clams were primarily gonochoritic at a size below 1.4 cm and progressively smaller as the shells increased. Gonochorism is common in several types of shellfish including Potomida littoralis (Şereflişan et al., 2013), Chambardia rubens (Morad et al., 2018) and Atrina maura (Gongora-Gomez et al., 2016). Based on the results, it was dominant in February and was still detected every month. This condition is indicative of successful spawning and recruitment into the population implied by the dominance of young clams present at the river beds. In some species of shellfish, an equal sex ratio of 1:1 is common but this might vary depending on the conditions. This deviation was showcased in different sex ratios found in various clam colonies or population and aquatic condition. The numbers of male and female pokea found in Langkumbe River were not significantly different although males were generally larger in number. This is not the case in several rivers in Southeast Sulawesi with high fishing pressure where immoderate or significant disproportionality was found between males and females, with the former dominating the latter as in Lasolo (Bahtiar, 2017) and Pohara (Bahtiar et al., 2021). Equal sex ratio of male and female clams was shown in studies by Mayor et al. (2016) and Layugan et al. (2013), Mya arenaria (Cross et al., 2012), Cerastoderma glaucum (Tarnowska et al., 2012), Potomida littoralis (Şereflişan et al., 2013), Choromytilus chorus (Ruiz-Velásquez et al., 2017), Megapitaria squalida (Álvarez-Dagnino et al., 2017), Mytella guyanensis (Camilo et al., 2017) and Donax trunculus (Hamdani et al., 2020).

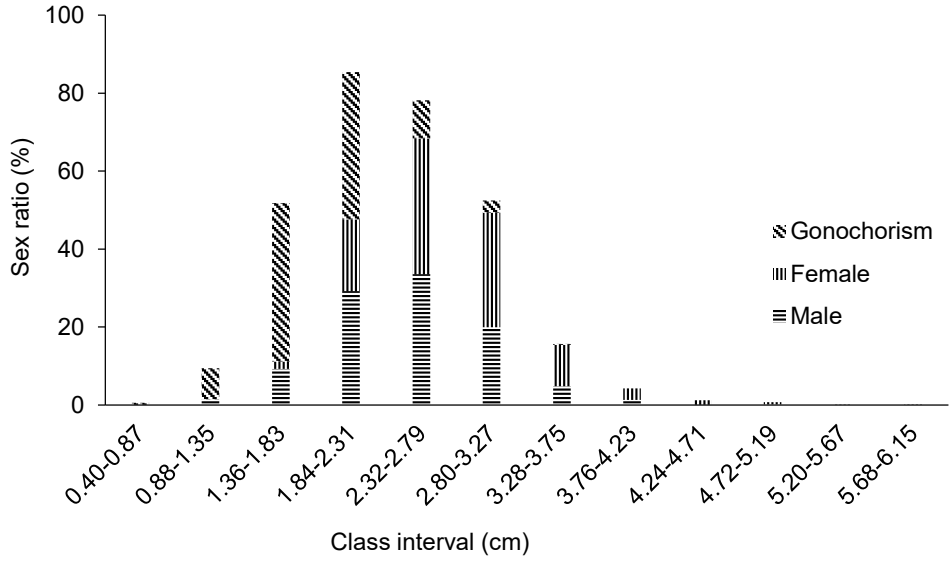

Figure 2. Sex ratio of pokea clams in Langkumbe River.

Gonad Maturity Level (GML) and Gonadosomatic Index (GSI)

The inactive phase of male and female clams occurred in February, followed by the early gonad development in March and continued to advance into the late phase in April. Furthermore, the gonad maturation and spawning took place over a long time, peaking in September and later in October. Lastly, the pokea shells experienced an inactive phase from November to January, although some were found to spawn continuously (Figure 3). The

DOI:https//doi.org/10.22452/mjs.vol44no2.2
Malaysian Journal of Science 44(2): 8-17 (June 2025)

GSI of male and female pokea found during this study were relatively similar with values ranging from 36.47±16.79 and 34.80±17.71 to 18.37±9.46 and 18.57±86, respectively. Changes in the GSI values of both sexes were simultaneous during the peak in August and declined sharply in October (Figure 4). The water quality at the sampling sites varied temporally in the course of this study. The TOM (total organic matter) measured was within the range of 0.67-9.62 mgL^{-1} which was higher at the beginning of this study and decreased from May to the end. Sediment organic matter (SOM) observed in the water samples ranged from 0.42-4.51%. Similar to TOM, SOM was higher at the beginning, but decreased from June to September. Chlorophyll-a was measured at 0.42 to 2.93, which was relatively low in the middle of this study (August) and high at the beginning and end (Figure 5). The results showed that male and female pokea clams underwent a relatively synchronous process of gonadal maturation each month. The reproductive cycle was consistent with gonad development activity/process occurring in early February, peak reproduction in September, and long spawning in October-January. Moreover, local spawning was also found monthly in small proportions. The continuous reproductive cycle over a long period implies that pokea clams in the river observed had relatively high productivity. This was indicated by: 1) the large range in the GSI value observed suggesting that spawning occurred every month and its increase at certain times indicates a peak of maturity, while a drastic decline implies spawning (Şereflişan et al., 2013), 2) recruitment of the gonochorism phase found almost in the observation period suggests an early phase of the clam life cycle. The reproductive pattern of pokea clams in Langkumbe River was relatively the same as those found in Pohara (Bahtiar et al., 2021) and Lasolo (Bahtiar, 2017). The clams experience gonadal development in February, peak maturity and spawning in July-October, while partial spawning every month was only found in one other place namely Pohara River. It is hypothesized that the differences in reproductive patterns among these rivers were due to the conditions of sufficient food supply in Langkumbe and Pohara Rivers, which allowed the clams to reproduce in the year (Bahtiar, 2012). The gonad maturation in these rivers was relatively the same as several other shellfish in the tropical region with a long spawning period, specifically in the year, including Iphigenia brasiliana (Silva et al., 2013), Tagelus plebeuis (Ceuta & Boehs, 2012), Mytella guyanensis (Camilo et al., 2017) and Geloina expansa (Bahtiar et al., 2023c). The spawning pattern observed in this study is commonly found in the tropics when the availability of food is sufficient, thereby providing prime environmental conditions for reproduction in the year (Bahtiar et al., 2023c; Boukadida et al., 2019). Furthermore, water quality and food availability play an important role in the early development of gonadal maturity as well as during peak spawning until the shellfish larvae are released (Álvarez-Dagnino et al., 2017; Boukadida et al., 2019). Improvements in water quality aspects such as the value of total organic matter and chlorophyll-a content were followed by gonad maturation and prominent release of larvae, specifically in February. Additionally, pokea clams had sufficient nutritional intake that increased energy reserves for the reproductive process. This condition was also observed in Pohara River which was adequately supplied with nutrients as marked by an increase in the amount of food due to the high value of sedimentary organic matter originating from the Aopa Swamp that entered during the rainy season, thereby promoting peak development and maturity (Bahtiar et al., 2021). It can be inferred that gonadal maturation and early spawning were triggered by an increase in the amount of organic matter as the food source of pokea clams. Food availability accompanied by gonadal development was also found in Gari elongate with gonad maturity taking place during the rainy season (Nabuab & Norte-Campos, 2006). Similarly, food availability influences larvae spawning of Megapitaria squalida (Álvarez-Dagnino et al., 2017). Other environmental factors such as temperature and salinity also play major roles in gonad maturation and spawning (Hafsaoui et al., 2016; Hashizume et al., 2012; Khalil, 2013; Razek et al., 2014). Differences in the development of early gonadal maturity and the end of spawning period, including the release of glochidia larvae in Pseudanodonta complanata were found to be affected by changes in temperature (Ram et al., 2012; Yanovych, 2015). This was similarly reported in Paphia malabarica with changes in salinity (Thomas, 2013).

DOI:https//doi.org/10.22452/mjs.vol44no2.2
Malaysian Journal of Science 44(2): 8-17 (June 2025)

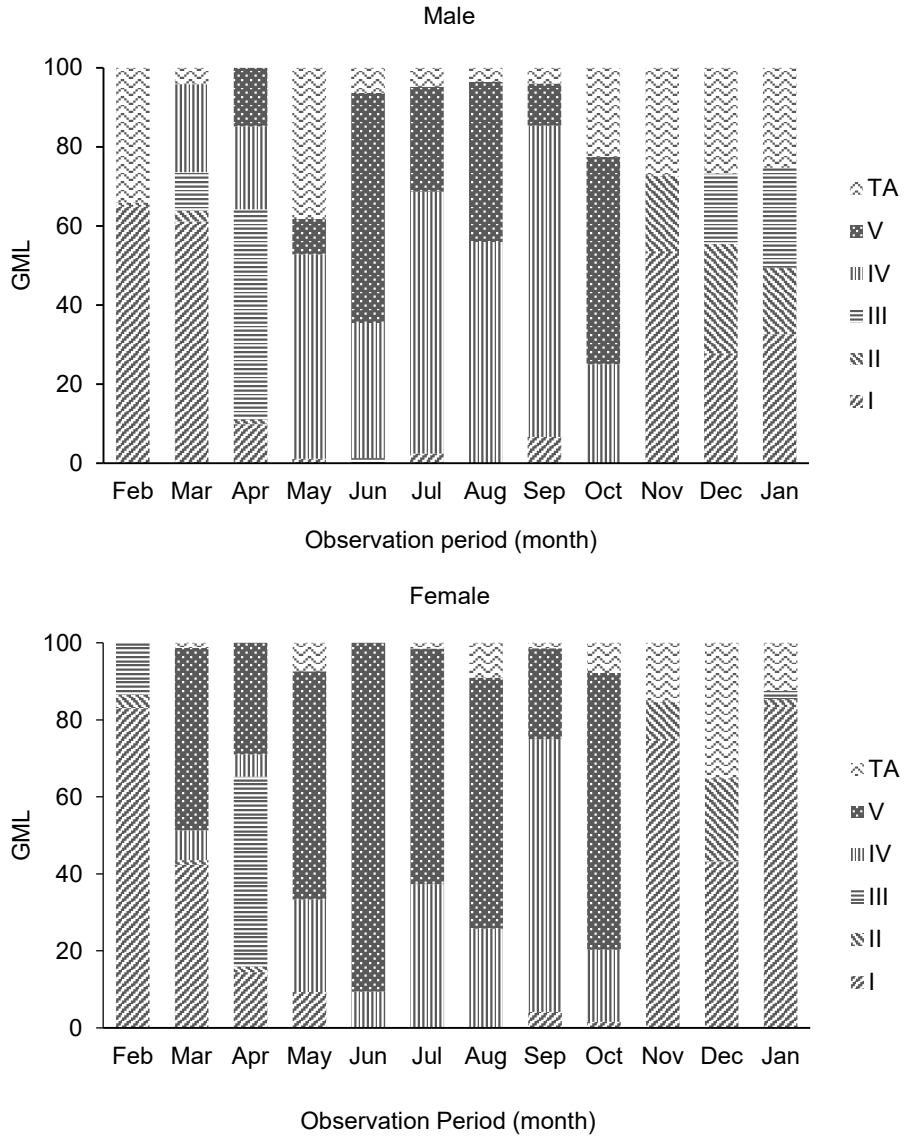

Figure 3. Gonadal maturity level of pokea clams in Langkumbe River. Description: TA = Inactive Phase.

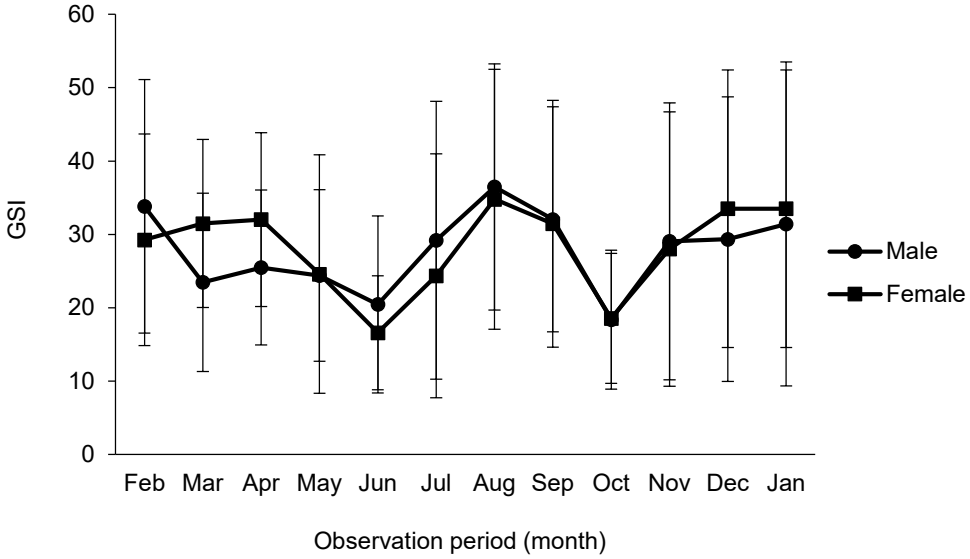

Figure 4. Average GSI values of male and female pokea during this study.

DOI:https//doi.org/10.22452/mjs.vol44no2.2
Malaysian Journal of Science 44(2): 8-17 (June 2025)

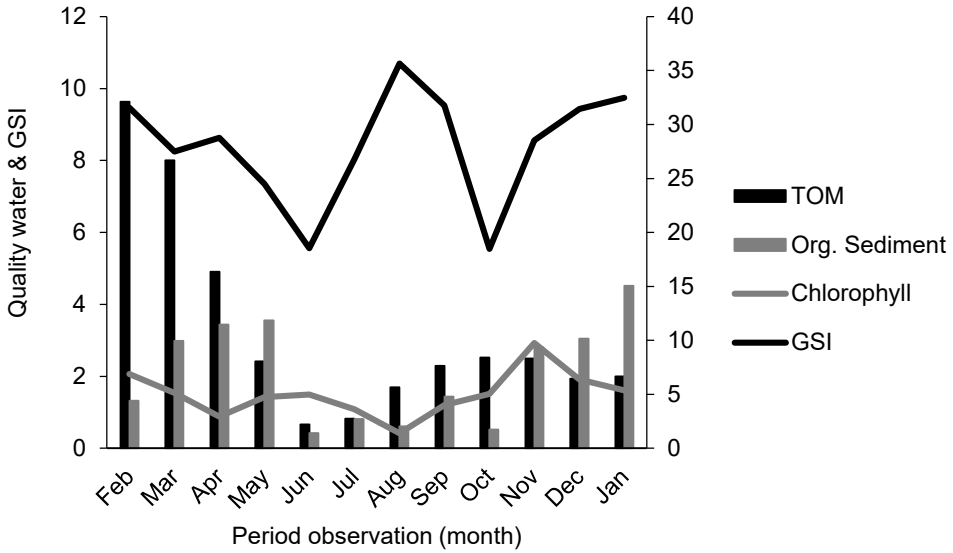

Figure 5. Langkumbe River water quality over the study period. Descriptions: TOM = total organic matter, SOM = sedimentary organic matter.

Temporarily, the reproduction pattern of pokea clams observed was not significantly different from other shellfish. Maturity in both males and females in several shellfish developed almost proportionally with the tendency to experience multiple spawning or group synchronous spawner (Sousa et al., 2008). Gonadal maturity was observed in Mya arenaria before spawning occurred in March-October (Cross et al., 2012). Potomida littoralis initiates gonad maturity in January, with a peak in May and spawning occurring in June (Şereflişan et al., 2013). The development of Paphia malabarica entails gonad maturity in March, peak maturity in September-October, and partial spawning until February (Thomas, 2013). Anodontidae bivalves of the species Pseudanodonta complanata spawns in June-August (Yanovych, 2015) which is very different from Anodontites trapezoidal cultivated in ponds and produce eggs in the season (Silva-Souza & Guardia-Felipi, 2014). Different cycles were demonstrated in freshwater clams such as Geloina erosa (Sarong et al., 2015) which showed non-concurrent spawning patterns at a specific time (asynchronous spawner).

Size at First Gonad Maturity

The non-linear regression analysis on the sigmoid pattern obtained P = 0.0001, which is α = 0.05, and a coefficient of determination (R^2) in males and females ranging from 99.88-99.96%. This means that the model established between gonad maturity and width of the pokea clams showed an appropriate relationship. The width of males with matured gonads was smaller than females at 1.4 cm and 2 cm, with a chance of gonad maturity amounting to 0.23% and 0.50%, respectively (Figure 6). Pokea clams experienced early gonadal maturation at a small size of 1.4-2 cm namely ±1/4 of the maximum length, with a quicker rate in males than females. Early gonad maturity was also found in Pohara (Bahtiar et al., 2021) and Lasolo (Bahtiar, 2017) rivers with values of 2.1-2.5 cm and 1.75-2.15 cm, respectively, all occurring at a small size. Other clams also exhibit early spawning at a small size including Paphia malabarica (1.5-2 cm) in Kerala and the West Coast of India (Thomas, 2013), and Cerastoderma glaucum (12-14 mm) on the coast of Tunisia (Derbali et al., 2009). In contrast, some species initiate gonad maturity at a size significantly larger than pokea clams such as Gari elongate and Geloina expansa with early maturation of male and female gonads at widths of 45.4 and 44.8 mm (Nabuab & Norte-Campos, 2006) and 30-52 mm (Bahtiar et al., 2023c), respectively, as well as Anadara antiquata (Mzighani, 2005). Variations in the size of clams with mature gonads can occur within the same and different species (Darrigran et al., 1999). Additionally, those in the tropical region tend to have earlier gonad maturity than others in the subtropics with sizes reaching 60% (Sato, 1994) of their asymptotic length compared to the 30-35% of the clams in the tropics. Optimum temperature and availability of food in the year trigger clams to reach gonad maturity earlier (Galimany et al., 2015). Alternatively, rapid maturity can also be caused by high environmental stress due to fishing activities. This condition is a manifestation of the strategy developed by living things to maintain the sustainability of their populations in nature. Pokea clams in Langkumbe as well as other rivers (Lasolo and Pohara) in Southeast Sulawesi, where overexploitation along with low water quality and high TSS are present, also have the proclivity to adopt such strategy when the two conditions occur. A reproductive strategy namely r-type selection pattern can be developed by initiating gonad maturity at a smaller size with multiple reproduction over a year as prompted by the less stable and unfavorable water conditions to maintain population sustainability (Bone & Marshall, 1982). This study is limited because the main cause of early initiation of gonadal maturity is not known. The following factors assumed to cause this includes: 1) adequate food availability, 2) fishing pressure or a combination of both, or 3) genetic tendency of pokea clams to have a small size when gonads mature. However, there are no previous studies that confirm these assumptions.

DOI:https//doi.org/10.22452/mjs.vol44no2.2
Malaysian Journal of Science 44(2): 8-17 (June 2025)

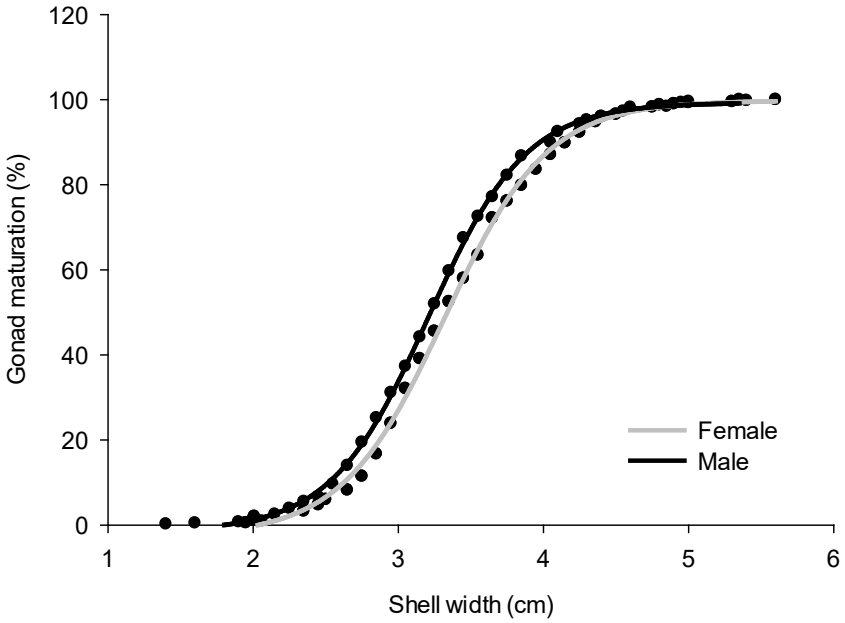

Figure 6. Size at first gonad maturity of male and female pokea.

4. Conclusion

Pokea clams in the Langkumbe river have high reproductive potential, namely: a balanced sex ratio. Although there is a tendency for certain sizes to be dominated by certain sexes, long spawning followed by partial spawning that occurs every time, small size at early gonad maturity, and water quality and food availability are sufficient to support reproduction in nature so that they can balance the fishing pressure that occurred.

5. Acknowledgement

The authors are grateful to all students who have helped in conducting this study and to all motorboat crews who have helped in the field.

6. References

Alkadri, Muh. A., Bahtiar, Yasidi, F. (2018). Preferensi habitat kerang pokea (Batissa violacea var. celebensis von Martens, 1897) di Sungai Langkumbe Kecamatan Kulisusu Barat Kabupaten Buton Utara. Jurnal Manajemen Sumber Daya Perairan, 3(2), 105–115.

Álvarez-Dagnino, E., Santamaría-Miranda, A., García-Ulloa, M., Góngora-Gómez, A. M. (2017). Reproduction of Megapitaria squalida (Bivalvia: Veneridae) in the Southeast Gulf of California, Mexico. Revista de Biología Tropical, 65(3), 881. https://doi.org/10.15517/rbt.v65i3.26371

Bahtiar. (2012). Studi Bioekologi dan Dinamika Populasi Pokea (Batissa violacea var. celebensis von Martens, 1897) yang Tereksploitasi Sebagai Dasar Pengelolaan di Sungai Pohara Sulawesi Tenggara [Disertasi]. Institut Pertanian Bogor.

Bahtiar. (2017). Biologi reproduksi kerang pokea Batissa violacea var. celebensis, von Martens 1897 di Muara Lasolo, Sulawesi Tenggara. Jurnal Ilmu Dan Teknologi Kelautan Tropis, 9(1), 9–18.

Bahtiar, Anadi, L., Nurgayah, W., Emiyarti, Hari, H. (2016). Pertumbuhan, kematian dan tingkat eksploitasi kerang pokea (Batissa violacea var. celebensis, von Martens 1897) pada segmen muara Sungai Lasolo Sulawesi Tenggara. Marine Fisheries : Journal of Marine Fisheries Technology and Management, 7(2), 137–147. https://doi.org/10.29244/jmf.7.2.137-147

Bahtiar, Anadi, L., Nurgayah, W., Hamzah, M., Hernawan, U. E. (2021). Reproductive biology of the freshwater clam pokea (Batissa violacea var. celebensis, von Marten 1897) (Bivalvia: Corbiculidae) in the Pohara River, Southeast Sulawesi, Indonesia. Biotropia, 28(1), 1–10.

Bahtiar, B., Findra, M. N., Ishak, E. (2023a). Length-weight relationships and condition index of Pokea clams (Batissa violacea var. celebensis, von Martens 1897) in the Laeya River, Southeast Sulawesi, Indonesia. Aceh Journal of Animal Science, 8(2), 45–52. https://doi.org/https://doi.org/10.13170/ajas.8.2.30994

Bahtiar, Emiyarti, Nurgayah, W. (2014a). Model Pengelolaan Spatial dan Temporal Sumberdaya Kerang Pokea Yang Tereksploitasi (Batissa volacea var. celebensis, von Martens

DOI:https//doi.org/10.22452/mjs.vol44no2.2
Malaysian Journal of Science 44(2): 8-17 (June 2025)

1897) Berbasis Ekobiologi dan Dinamika Populasi dalam Penguatan Pangan Lokal di Sulawesi Tenggara.

Bahtiar, B., Jiwani, Y. E., Findra, M. N., Ishak, E. (2024). Temporal variation of peanut worm (Siphonosoma australe-australe) reproduction in Toronipa Beach of Southeast Sulawesi, Indonesia. Biodiversitas Journal of Biological Diversity, 25(8), 2533–2540. https://doi.org/10.13057/biodiv/d250825

Bahtiar, Hamzah, M., Hari, H. (2015). Studi struktur dan pertumbuhan populasi kerang pokea (Batissa violacea var. celebensis, von Martens 1897) di Sungai Pohara Sulawesi Tenggara. Jurnal Biologi Tropis, 15(2), 112–124. https://doi.org/10.29303/jbt.v15i2.200

Bahtiar, Nurgayah, W., Irawati, N. (2014b). Studi kebiasaan makanan kerang pokea (Batissa violacea var celebensis, von Martens 1897) saat penambangan pasir di Sungai Pohara Sulawesi Tenggara. Jurnal Biologi Tropis, 14(2), 75–82. https://doi.org/10.29303/jbt.v14i2.135

Bahtiar, Permatahati, Y. I., Findra, M. N., & Fekri, L. (2023b). Production, biomass, and turnover of exploited mangrove clams (Geloina expansa, Mousson 1849) in Kendari Bay mangrove forest, Southeast Sulawesi Indonesia. BIO Web of Conferences, 74, 03009. https://doi.org/10.1051/bioconf/20237403009

Bahtiar, Purnama, M. F., Kasim, M., Ishak, E. (2023c). Reproductive biology of mangrove clams Geloina expansa (Mousson, 1849) from mangrove at Kendari Bay, Southeast Sulawesi, Indonesia. Marine Biology Research, 1–11. https://doi.org/10.1080/17451000.2023.2185639

Bahtiar, Purnama, M. F., Muis, Ishak, E., Kasim, M. (2022). The size structure, growth, mortality, and exploitation rate of freshwater clam (Batissa violacea var. celebensis) from Southeast Sulawesi, Indonesia. Journal of Shellfish Research, 41(1), 145–152. https://doi.org/10.2983/035.041.0112

Bahtiar, Purnama, M. F., Rahmadhani, & Findra, M. N. (2022b). Reproduksi kerang tahu (Meretrix meretrix) di muara Sungai Kambu, Sulawesi Tenggara. Journal of Tropical Fisheries Management, 6(1), 54–60. https://doi.org/10.29244/jppt.v6i1.44443

Bahtiar, Riani, E., Setyobudiandi, I., Muchsin, I. (2012a). Kepadatan dan distribusi pokea (Batissa violacea var. celebensis, von Martens 1897) pada substrat berbeda di Sungai Pohara Kendari Sulawesi Tenggara. Aqua Hayati, 8(2), 115–123.

Bahtiar, Riani, E., Setyobudiandi, I., Muchsin, I. (2012b). Pengaruh aktivitas penambangan pasir terhadap kepadatan dan distribusi pokea (Batissa violacea var. celebensis, von Martens 1897) di Sungai Pohara Kendari Sulawesi Tenggara. Agriplus, 22(1), 58–64.

Bone, Q., Marshall, N. B. (1982). Biology of Fishes (First). Blackkie and Sons Limited.

Boukadida, K., Cachot, J., Morin, B., Clerandeau, C., Banni, M. (2019). Moderate temperature elevation increase susceptibility of early-life stage of the Mediterranean mussel, Mytilus galloprovincialis to metal-induced genotoxicity. Science of The Total Environment, 663, 351–360. https://doi.org/10.1016/j.scitotenv.2019.01.215

Camilo, V. M. A., Souza, J. da C., Conceição, E. de J., Luz, J. R., Boehs, G., Campiolo, S. (2017). Reproductive cycle of Mytella guyanensis (Lamarck, 1819) in a Marine Reserve (RESEX Bay of Iguape), Bahia, Brazil. Brazilian Journal of Biology, 78(2), 255–264. https://doi.org/10.1590/1519-6984.05716

Ceuta, L. O., Boehs, G. (2012). Reproductive cycle of Tagelus plebeius (Mollusca: Bivalvia) in the estuary of the Cachoeira River, Ilhéus, Bahia, Brazil. Brazilian Journal of Biology, 72(3), 569–576.

Cross, M. E., Lynch, S., Whitaker, A., O'Riordan, R. M., Culloty, S. C. (2012). The reproductive biology of the softshell clam, Mya arenaria, in Ireland, and the possible impacts of climate variability. Journal of Marine Biology, 2012, 1–9. https://doi.org/10.1155/2012/908163

Darrigran, G. A., Penchaszadeh, P. E., Damborenea, M. C. (1999). The reproductive cycle of Limnoperna fortunei (Dunker, 1857) (Mytilidae) from a neotropical temperate locality. Journal of Shellfish Research, 18, 361–365.

Derbali, A., Jarboui, O., Ghorbel, M. (2009). Reproductive biology of cockle Cerastoderma glaucum (Mollusca : Bivalvia) from the North Coast of Sfax (Gulf of Gabes, Tunisia). Ciencias Marinas, 35(2), 141–152.

Galimany, E., Baeta, M., Durfort, M., Lleonart, J., Ramón, M. (2015). Reproduction and size at first maturity in a Mediterranean exploited Callista chione bivalve bed. Scientia Marina, 79(2), 233–242. https://doi.org/10.3989/scimar.04155.13A

Gongora-Gomez, A., Garcia-Ulloa, M., Arellano-Martínez, M., Abad, S., Dominguez, A., Ponce-Palafox, J. (2016). Annual reproductive cycle and growth of the pen shell Atrina maura (Pterioidea: Pinnidae) on sand-bottom culture in the Ensenada Pabellones lagoon system, Gulf of California,

DOI:https//doi.org/10.22452/mjs.vol44no2.2
Malaysian Journal of Science 44(2): 8-17 (June 2025)

Mexico. Invertebrate Reproduction & Development, 60(1), 28–38. https://doi.org/10.1080/07924259.2015.1126535

Hafsaoui, I., Bouaziz, R., Draredja, B., Beldi, H. (2016). Reproduction cycle of Donax trunculus (Mollusca. Bivalvia) in the Gulf of Annaba (Northeast Algeria). Adv Environ Biol., 10(5), 82–95.

Hamdani, A., Soltani, N., Zaidi, N. (2020). Growth and reproduction of Donax trunculus from the Gulf of Annaba (Northeast Algeria) in relation to environmental conditions. Environmental Science and Pollution Research, 27(33), 41656–41667. https://doi.org/10.1007/s11356-020-10103-9

Hashizume, K., Tatarazako, N., Kohata, K., Nakamura, Y., Morita, M. (2012). Life history characteristics of the surf clam Mactra veneriformis (Bivalvia: Veneroida: Mactridae) on a sandy tidal flat in Tokyo Bay, Japan. Pacific Science, 66(3), 335–346. https://doi.org/10.2984/66.3.7

Khalil, M. (2013). The effect of environmental condition on the spawning period of blood cockle Anadara granosa (Bivalvia: Arcidae) In Lhokseumawe, The Northern Straits of Malacca. Jurnal Agrium, 10(2), 69. https://doi.org/10.29103/agrium.v10i2.499

Kusnoto. (1953). Kebun Raya Indonesia (Botanic Gardens of Indonesia). Treubia A Journal of Zoology, Hydrobiology and Oceanography of the Indo-Australian Archipelago, 22, 53–57.

Layugan, E. A., Segawa, S., Laureta, L. V, Ronquillo, J. D. (2013). Gametogenesis and spawning induction in Batissa violacea Lamarck, (1806) at Cagayan River, Philippines. IAMURE International Journal of Ecology and Conservation, 5(1), 1–23. https://doi.org/10.7718/ijec.v5i1.504

Mayor, A. D., Ancog, R. (2016). Fishery status of freshwater clam (Batissa violacea, Corbiculidae) (Bivalvia) (Lamarck, 1818) in Cagayan River, Northern Philippines. International Journal of Fisheries and Aquatic Studies, 4(3), 500–506.

Mayor, A. D., Ancog, R. C., Guerrero, R. D., Camacho, M. V. C. (2016). Environmental factors influencing population density of freshwater clam Batissa violacea (Bivalvia) (Lamarck, 1818) in Cagayan River, Northern Philippines. International Journal of Aquatic Science, 7(2), 69–72.

Morad, M., Fol, M., Gamil, I., Mansour, R. (2018). Gonad variation and development of freshwater mussel Chambardia rubens Lamarck, 1819 (Bivalvia: Mutelidae) from the River Nile in Egypt. Journal of Bioscience and Applied Research, 4(4), 495–506. https://doi.org/10.21608/jbaar.2018.154710

Mzighani, S. (2005). Fecundity and population structure of cockles Anadara antiquata L. 1758 (Bivalvia: Arcidae) from a sandy/muddy beach near Dar es Salaam, Tanzania. Western Indian Ocean Journal of Marine Science, 4(1). https://doi.org/10.4314/wiojms.v4i1.28475

Nabuab, F., Norte-Campos, A. D. (2006). Some aspects of the reproduction in the elongate sunset clam, Gari elongate (Lamarck, 1818) from Banate Bay Area, West Central Philippines. J. Science Diliman, 18(2), 34–46.

Puteri, R. E. (2005). Analisis Populasi dan Habitat : Sebaran Ukuran dan Kematangan Gonad Kerang Lokan Batissa violacea Lamarck (1818) di Muara Sungai Batang Anai Padang Sumatera Barat [Tesis]. Institut Pertanian Bogor.

Ram, J. L., Karim, A. S., Acharya, P., Jagtap, P., Purohit, S., Kashian, D. R. (2012). Reproduction and genetic detection of veligers in changing Dreissena populations in the Great Lakes. Ecosphere, 2(1), 1–13.

Razek, F. A. A., Abdel-Gaid, S. E., Abu-Zaid, M. M., & Aziz, T. A. (2014). Aspects on the reproduction of eared horse mussel, Modiolus auriculatus (Krauss, 1848) in Red Sea, Egypt. The Egyptian Journal of Aquatic Research, 40(2), 191–198. https://doi.org/10.1016/j.ejar.2014.04.003

Ruiz-Velásquez, M., Zapata, M., Gonzalez, M. T., Ordenes, D., Escalona, M. (2017). Sexual differentiation and size at first maturity of the mussel Choromytilus chorus (Molina, 1782) (Mollusca, Bivalvia) in Northern Chile. American Malacological Bulletin, 35(1), 31–41. https://doi.org/10.4003/006.035.0104

Sarong, M. A., Asiah, M., Daud, W., Wardiah, I., Dewiyanti, Z. A., Muchlisin. (2015). Gonadal histological characteristics of mud clam (Geloina erosa) in the estuary of Reuleung River, Aceh Besar District, Indonesia. AACL Bioflux, 8(5), 708–713.

Sato, S. (1994). Analysis of the relationship between growth and sexual maturation in Phacosoma japonicum (Bivalvia: Veneridae). Marine Biology, 118(4), 663–672. https://doi.org/10.1007/BF00347514

Şereflişan, H., Çek, Ş., Şereflişan, M. (2013). The reproductive cycle of Potomida littoralis (Cuvier, 1798) (Bivalvia : Unionidae) in Lake Golbasi, Turkey. Pakistan J. Zool, 45(5), 1311–1319.

Silva, P. P., Peso-Aguiar, M. C., Ribeiro, G. (2013). Ciclo gametogênico e comportamento reprodutivo de Iphigenia brasiliana (Mollusca, Bivalvia, Donacidae) no estuário do rio Subaé, Baía de Todos os Santos, Bahia, Brasil. Iheringia. Série Zoologia, 102(4), 359–369. https://doi.org/10.1590/S0073-47212012005000011

DOI:https//doi.org/10.22452/mjs.vol44no2.2
Malaysian Journal of Science 44(2): 8-17 (June 2025)

Silva-Souza, A. T., Guardia-Felipi, P. (2014). Incubation cycle of eggs and larvae of Anodontites trapesialis (Lamarck, 1819) (Bivalvia, Mycetopodidae) in fish farming. Pan-American Journal of Aquatic Science, 9(4), 312–319.

Sousa, R., Antunes, C., Guilhermino, L. (2008). Ecology of the invasive Asian clam Corbicula fluminea (Müller, 1774) in aquatic ecosystems: an overview. Annales de Limnologie - International Journal of Limnology, 44(2), 85–94. https://doi.org/10.1051/limn:2008017

Tarnowska, K., Verney, A., Wolowicz, M., Féral, J.-P., Chenuil, A. (2012). Survival of male and female Cerastoderma glaucum (Bivalvia) during aerial exposure. Vie et Milieu - Life and Environment, 62(1), 23–28.

Thomas, S. (2013). Reproductive studies on the short neck clam Paphia malabarica (Chemnitz) from Dharmadom Estuary, Kerala, India. Indian J. Fish, 60(4), 47–50.

Vaughn, C. C., Nichols, S. J., Spooner, D. E. (2008). Community and foodweb ecology of freshwater mussels. Journal of the North American Benthological Society, 27(2), 409–423.

Yanovych, L. M. (2015). Reproductive features of indigenous and the invasive Chinese freshwater mussels (Mollusca, Bivalvia, Anodontinae) in Ukraine. Vestnik Zoologii, 49(5), 433–438. https://doi.org/10.1515/vzoo-2015-0050

Yeni. (2012). Aktivitas Antioksidan dan Pengaruh Pengolahan Terhadap Kandungan Gizi Kerang Pokea (Batissa violacea celebensis, Martens 1897) di Sungai Pohara Sulawesi Tenggara. Institut Pertanian Bogor.

DOI:https//doi.org/10.22452/mjs.vol44no2.2
Malaysian Journal of Science 44(2): 8-17 (June 2025)

MALAYSIAN JOURNAL OF SCIENCE
MJS
ISSN 1394-3065

Regular Issue

Malaysian Journal of Science 44 (2): 18-41 (June 2025) https://mjs.um.edu.my

Assessing Bacterial Communities in Bulk Soil and Rhizosphere Associated with NPK Fertilizer in Oil Palm Seedlings via Amplicon Sequencing

Mohd Khairil Radzali[1a], Amalia Mohd Hashim[2ab], Ho Li Sim[3c], Joyce Ding Yoon Mei[4c], Julia Ibrahim[5c], Miratul Hada Mohd Ali[6a], Mohd Termizi Yusof[7a], Noor Azizah Musa[8c], Nuha Hassim[9c] and Wan Zuhainis Saad[10a]*

Abstract: Malaysia's palm oil industry relies heavily on chemical fertilizers, leading to significant environmental concerns such as nutrient loss and declining biodiversity. This study aims to evaluate the impact of post-fertilizer application on bacterial communities in soil, particularly focusing on bulk soil and rhizosphere. Through amplicon sequencing, we investigated the response of bacterial diversity to unfertilized and NPK-fertilized soil treatments. Fertilizer application increased soil phosphorus, potassium, and magnesium levels, enhancing seedlings' growth but reducing bacterial diversity, particularly sensitive groups such as Acidobacteria and Verrucomicrobia. *Candidatus Solibacter* and *Acidothermus* were consistent biomarkers for unfertilized soil, while *Mizugakiibacter* and *Castellaniella* were for fertilized treatment. For the inferred bacterial community functions, the unfertilized bulk soil demonstrated enhanced function related to carbohydrate metabolism, and the unfertilized rhizosphere exhibited functions related to energy metabolism, stress tolerance, bioremediation, and plant defense. During fertilized treatment, functions related to secondary metabolites were enriched in the bulk soil, and bacterial colonization functions were enriched in both compartments. For network analysis, the fertilizer application reduced bacterial network interactions and complexity. Environmental drivers, namely, pH and soil total phosphorus (TP), influenced the bacterial biomarkers' abundance in the bulk soil and rhizosphere. These findings demonstrate the need to optimize chemical fertilizer applications and identify beneficial bacterial taxa to foster sustainable agricultural practices in the palm oil industry.

Keywords: *Palm oil, fertilizer, bacterial communities, amplicon sequencing, oil palm seedlings.*

1. Introduction

Oil palm (*Elaeis guineensis*) is Malaysia's most cultivated agricultural crop and has been among the country's top economic contributors. This crop is cultivated on 5.73 million hectares as of 2021, with Sarawak having the second-largest area (1.61 million hectares) and Peninsular Malaysia having the biggest oil palm plantations (2.61 million hectares) (MPOB, 2022a). The Malaysian palm oil industry generated an average of RM 108.52 billion in export earnings in 2021, making it Malaysia's most profitable agricultural crop (MPOB, 2022b). The demand for palm oil is projected to increase as the world's population grows, and it is estimated that between 93 and 156 million tonnes of palm oil might be needed by 2050 (Pirker et al., 2016; Murphy et al., 2021). Previous studies have shown that the use of NPK (nitrogen, phosphorus, potassium) chemical fertilizer increased nutrient availability in both soil and leaves which subsequently improved the production of commercialized crops (Kavvadias et al., 2023; Wang et al., 2023). Thus, optimized fertilizer usage and strategic production techniques can accomplish a higher yield.

Bulk soil is termed an area not penetrated by plant roots. In contrast, the rhizosphere is a zone of soil immediately surrounding the root of plants since plants may secrete root exudates to encourage the growth of microbes that can improve plant nutrient uptake (Vives-Peris et al., 2020; Jamil et al., 2022). The response of the bacterial community in soil-and-plant root systems, including bulk soil and rhizosphere, can vary depending on the amount of fertilizer applied, soil type, and plant species. Proteobacteria became increasingly dominant in both bulk soil and rhizosphere of *Larix* seed orchard over time after initial fertilization (Wang et al., 2024). After phosphorus-potassium (PK) fertilization, Actinobacteria demonstrated increased relative abundance in the bulk soil of buckwheat fields compared to post-fertilization (Morigasaki et al., 2024). While short-term effects may vary, the development of plants, the makeup of the

Authors information:
[a]Department of Microbiology, Faculty of Biotechnology and Biomolecular Sciences, Universiti Putra Malaysia, 43400, Serdang, Selangor, MALAYSIA. Email: gs50774@student.upm.edu.my[1]; amalia@upm.edu.my[2]; miratulali@gmail.com[6]; mohdtermizi@upm.edu.my[7]; zuhainis@upm.edu.my[10]
[b]Halal Produt Research Institute, Universiti Putra Malaysia, 43400, Serdang, Selangor, MALAYSIA. E-mail: amalia@upm.edu.my[2]
[c]SD Guthrie Technology Centre Sdn. Bhd., UPM-MTDC Technology Centre III Malaysia, Lebuh Silikon, Putra Square, 43400 Serdang, Selangor, MALAYSIA. Email: ho.li.sim@simedarbyplantation.com[3]; joyce.ding.yoonmei@simedarbyplantation.com[4]; julia.ibrahim@simedarbyplantation.com[5]; noor.azizah.musa@simedarbyplantation.com[8]; nuha.hassim@simedarbyplantation.com[9]
*Corresponding Author: zuhainis@upm.edu.my

Received: June 8, 2023
Accepted: June 20, 2024
Published: June 30, 2025

DOI:https//doi.org/10.22452/mjs.vol44no2.3
Malaysian Journal of Science 44(2): 18-41 (June 2025)

microbiome, and the agricultural management practices can be intertwined and have long-term detrimental effects on the ecosystem. Prior studies via the amplicon approach have demonstrated that the chemical fertilizer application decreased bacterial diversity in the roots of wheat and rice, suggesting rational rate fertilizer application for environmental and sustainable development (Liu et al., 2020a; Sinong et al., 2021). NPK fertilization was also found to reduce microbial connections based on network analysis (Ji et al., 2023; Yang et al., 2023).

NPK fertilization led to the enrichment of genera such as *Dyella*, *Thermomonas*, *Massilia*, and *Devosia*, known for promoting plant growth (Zhao et al., 2013; Zheng et al., 2017; O'Brien et al., 2018). This contradicts Sinong et al. (2021), who found that low nutrient input is preferable for optimizing beneficial bacterial population structure and promoting plant health and growth. The application of chemical fertilizer also enhanced the specialized functions of soil and root-associated bacterial communities, potentially impacting plant growth and health (Caradonia et al., 2019). Tang et al. (2023) demonstrated that soil physicochemical parameters drove the microbial community succession in response to the NPK fertilizer. However, there remains a lack of studies concentrated on how chemical fertilizer application influences the bacterial changes in the compartments of oil palm seedlings.

Therefore, we hypothesize that: (i) post-NPK fertilizer application will potentially lead to increased availability of soil nutrients, resulting in enhanced foliar nutrient content of oil palm seedlings and a shift towards enrichment of bacterial populations and functions associated with plant growth promotion within soil-plant compartments; (ii) the fertilizer application will induce a reduction in bacterial diversity in both bulk soil and rhizosphere, possibly due to altered nutrient availability and shifts in microbial interactions within soil-plant compartments. The primary objectives of this study were: (i) to analyze the effects of post-NPK fertilizer application on soil and foliar nutrient availability, bulk soil and rhizosphere bacterial diversity and co-occurrence network, and microbial functions associated with plant growth promotion; and (ii) to understand the role of environmental drivers, such as soil physicochemical properties and foliar nutrient contents, in shaping the abundance and composition of bacterial populations within soil-plant compartments.

2. Materials and Methods

Experimental Design and Sample Collection

The experimental design and sample collection were conducted by Sime Darby Plantation Technology Centre (SDPTC) Sdn. Bhd. The crossing type of oil palm germinated seeds (*Dura* x *Pisifera*, Calix 600) were sown in polybags (10 × 12 inches) and grew in a controlled nursery environment. The polybag contained inland soil, which was perceived to be less fertile than coastal soil, but the encroachment of oil palm cultivation land has been extended to inland soil (Tarmizi & Tayeb, 2006; Arifin et al., 2022). The study was conducted in a randomized block pattern, and the germinated seedlings were subjected to unfertilized soil (control) and a fertilized treatment using commercial NPK chemical fertilizer (CCM25, N:P:K: Mg-14:13:9:2.5). Each type of soil had five replicates. According to standard agronomic practice, the chemical fertilizer was applied once every two weeks until the 30th week (approximately seven months). The seedlings were watered daily. Destructive sampling was carried out following the completion of NPK fertilization at the oil palm seedlings' ideal development stage of the eighth month. The seedling phenotypes, including height and biomass, were recorded during sampling. All the soil samples were flash-frozen in liquid nitrogen and stored at -80°C before DNA extraction. The soil and plant samples were homogenized and sent to an accredited MS ISO/IEC 17025 certified laboratory (Estate Research and Advisory Services RISDA Estates, ERAS Lab) for further analysis, as described below.

Soil Physicochemical Properties

For soil physicochemical analysis, soil samples underwent air drying until constant readings were achieved. About 150 g of soil was used for the analysis. pH, electrical conductivity (EC), total carbon (TC), organic carbon (OC), total nitrogen (TN), carbon-to-nitrogen (C/N) ratio, total phosphorus (TP), available phosphorus (AP), potassium (K), calcium (Ca), magnesium (Mg), sodium (Na), cation exchange capacity (CEC), base saturation (BS), and mechanical analysis (clay, silt, coarse, fine sand) were evaluated for the soil samples.

The soil was suspended in distilled water (1:2.5 WV^{-1}) to determine soil pH using a pH meter. By using the same ratio of 1:2.5 WV^{-1}, the soil-water suspension was mixed and allowed to stand for 30 minutes before measuring the EC using an EC meter. Approximately 100 grams of soil samples were subjected to combustion, converting them into gases, before being analyzed for carbon (C), nitrogen (N), and the C/N ratio using the dry combustion method (Matejovic, 1993) with an Elemental Analyzer (EA, Thermo Fisher). Total phosphorus (TP) and available phosphorus (AP) concentrations were analyzed using the vanadate-molybdate method, as described by Tandon et al. in 1968. Soil samples, weighing approximately 10 g, underwent treatment with specific extractant solutions to dissolve the phosphorus compounds. Subsequently, the TP and AP levels were quantified by measuring the absorbance of colored complexes formed during the chemical reactions, utilizing an Ultraviolet-Visible Spectrometer (UV-Vis, Thermo Fisher). CEC and exchangeable cations (Ca, Mg, K, Na) were then determined using ammonium acetate solution (David, 1960). Approximately 10 g of soil was treated with ammonium acetate solution to release the cations, which were then quantitatively measured using Inductively Coupled Plasma Optical Emission Spectrometry (ICP-EOS, Thermo Fisher). The soil texture, including clay, silt, coarse, and fine sand, was estimated using a soil hydrometer. A minimum of 100 g of soil was used to observe the settling rate over time in water before comparing it to standard classifications. All the parameters were evaluated using three biological replicates. The analyses were performed by ERAS Laboratory, adhering to the M.S 678 (soil) method outlined by the Standard and Industrial Research Institute of Malaysia (Malaysian Standard [MS], 1980).

Foliar Nutrient Content Analysis

DOI:https//doi.org/10.22452/mjs.vol44no2.3
Malaysian Journal of Science 44(2): 18-41 (June 2025)

The leaf samples also underwent air drying until constant readings were achieved, and an approximation of 5 g of dried leaves was used for the analysis. The samples were subjected to the same method mentioned in the soil physicochemical analysis for TN, TC, C/N, P, K, Mg, and Ca. Moreover, trace elements such as boron (B), copper (Cu), manganese (Mn), iron (Fe), and zinc (Zn) were quantified. Plant tissue samples underwent preparation via dry ashing, following the method outlined by Heanes in 1981, utilizing a muffle furnace, and were determined using Inductively Coupled Plasma-Optical Emission Spectrometry (ICP-EOS, Thermo Fisher). All the above parameters were tested with three biological replicates.

Soil-Root Fraction and DNA Extraction

Bacterial DNA for the bulk soil and rhizosphere was extracted as described (Wieland et al., 2001). For the bulk soil fraction, 100 g of non-adhering soil was collected after the seedling was removed from the polybag. For the rhizosphere fraction, 50 g of the primary roots with loosely attached soil were cut into smaller pieces (1-2 cm length) to increase surface area and enhance DNA extraction efficiency, followed by mixing in 500 ml of 0.85% NaCl in a shaker incubator (15 mins, 150 rpm). The washing solutions were centrifuged (10 mins, 10,000 rpm, 4°C) to obtain rhizosphere pellets. All processed samples were kept at -20°C before DNA extraction. According to the manufacturer's protocols, two hundred fifty milligrams of soil-processed samples were utilized to extract the genomic DNA using the FastDNA SPIN Kit for Soil (MP Bio, USA). The quality of DNA was determined by 1% agarose gel electrophoresis and a Nanodrop 1000 spectrophotometer according to the manufacturer's protocols (Thermo Scientific, USA).

Amplicon Sequencing and Amplicon Data Pre-Processing

A final concentration of 1 ng/µl was used for subsequent analysis. The amplification of the V3–V4 region of the 16S rRNA gene employed forward primer 341 F (5'-CCTACGGGNGGCWGCAG-3') and reverse primer 805R (5'-GACTACHVGGGTATCTAATCC-3'), both barcoded. PCR reactions utilized Phusion® High-Fidelity PCR Master Mix (New England Biolabs) with a composition of Phusion Master Mix (1X), primers (0.5 µM), genomic DNA (250 ng), and dd H2O to reach a final volume of 25 µl. The PCR program involved an initial denaturation at 98°C for 1 min, followed by 30 cycles at 98°C for 10 s, 50°C for 30 s, and 72°C for 30 s, with a final extension at 72°C for 5 min. Sequencing libraries were prepared with TruSeq® DNA PCR-Free Sample Preparation Kit (Illumina, USA) and assessed for quality using Qubit@ 2.0 Fluorometer (Thermo Scientific) and Agilent Bioanalyzer 2100 system. Sequencing was performed on a Novaseq PE250 platform, generating 250 bp paired-end reads.

Paired-end reads were assigned to samples based on unique barcodes. The barcode and primer sequences were removed. Paired reads were then merged using FLASH (V 1.2.7) (Magoč & Salzberg, 2011). Quality filtering followed specific filtering conditions in QIIME (V1.7.0) (Bolyen et al., 2019) to achieve high-quality clean tags. Chimeric sequences were removed using the UCHIME algorithm (Quast et al., 2013). Clean amplicon data were then clustered into operational taxonomic units (OTUs) with Uparse (V 7.0.1001) (Edgar, 2013) at a similarity threshold of ≥97%. A representative sequence was selected for each OTU, and taxonomic affiliations were determined by aligning them against the Greengenes database (V.05/2013) for 16S rRNA sequences (DeSantis et al., 2006; McDonald et al., 2012).

Statistical and Bioinformatic Analysis

Operational taxonomic units (OTUs) assigned to the chloroplasts and mitochondria were removed. Bacterial relative abundance (>2%), and alpha and beta diversities were performed using the phyloseq R package V 1.4.1106 (McMurdie & Holmes, 2013). The significant difference of taxa was analyzed with Statistical Analysis of Metagenomic Profile (STAMP) V2.1.3 using a two-sided Welch's t-test (Parks et al., 2014). The alpha diversity of the microbiome was evaluated using richness (Chao1) and diversity (Shannon and Simpson) indices. The Wilcoxon rank sum test was employed to perform statistical comparisons between the treatments. Beta diversity was visualized using Principal Coordinate Analysis (PCoA) based on Bray-Curtis dissimilarity. Analysis of Similarities (ANOSIM) was used to determine the significant differences between the groups (Legendre & Gallagher, 2001).

The Kruskal-Wallis sum rank test and linear discriminant analysis size effect (LEfSe) were used to identify discriminatory taxa and functions in the soil-plant compartments. The LEfSe analysis was used with default parameters (LDA>2, $p < 0.05$) in the Galaxy server (V. 1.0) (Goecks et al., 2010; Segata et al., 2011). The predictive functional analysis based on an operational taxonomic unit (OTU) was performed using Tax4Fun as described (Chong et al., 2020). For network analysis, correlations between bacterial genera (LDA>2) were calculated based on Spearman rank coefficient ($r > \pm 0.7$, $p < 0.01$) using the iGraph R package (Csardi & Nepusz, 2006). The network was then visualized in Cytoscape V 3.8.3 (Shannon et al., 2003). The network analysis identified the bacterial keystone within the community based on high mean degree, high closeness centrality, and low betweenness centrality (Banerjee et al., 2018). Canonical correspondence analysis (CCA) was used to investigate the relationship between significant physicochemical parameters and biomarker taxa using the vegan R package (V 2.6-2). A variance inflation factor (VIF) of less than 10 was set to avoid multicollinearity between variables (Oksanen, 2015).

3. Results and Discussion

The Chemical Fertilizer Application Increased Soil Nutrient Availability Yet Not Directly Proportionate to Foliar Nutrient Contents

Tables 1 and 2 show the impact of fertilizer application on soil physicochemical properties and foliar nutrient content. The fertilized soil showed higher levels of TP, K, and Mg, indicating increased nutrient availability (Table 1). Prior work also

DOI:https//doi.org/10.22452/mjs.vol44no2.3
Malaysian Journal of Science 44(2): 18-41 (June 2025)

demonstrates the positive impact of fertilizer application on soil nutrients, such as TP level (Mao et al., 2015; Ahmed et al., 2019). The fertilized soil also showed higher levels of acidity, EC, and BS (Table 1). The release of hydrogen ions (H+) during fertilizer reactions and the use of ammonium-based fertilizers, which may cause soil acidification (Gu et al., 2017; Tkaczyk et al., 2020), are responsible for the increase in EC (Aizat et al., 2014). Consequently, the fertilized soil had a lower soil pH than the unfertilized soil. The higher base cations (K+, Mg2+) and base saturation in the fertilized soil are likely a response to mitigate soil acidification caused by the fertilizer application (Havlin, 2005; Goulding, 2016). These buffering effects aid to maintain soil fertility and nutrient availability for plant uptake (Ng et al., 2022).

Table 1. Soil physicochemical properties

Parameter	Unit	Unfertilized		Fertilized	
		Mean	S.D.	Mean	S.D.
pH*	%	4.66	0.18	4.13	0.21
EC*		49.67	1.53	217.67	39.40
TC		0.59	0.03	0.58	0.05
TOC		0.45	0.02	0.45	0.04
TN		0.22	0.03	0.24	0.02
C/N		2.67	0.58	2.33	0.58
BS*		2.50	0.01	3.39	0.22
Clay		65.33	7.57	62.67	1.15
Slit		13.67	2.08	13.67	1.15
Coarse Sand		13.00	1.73	14.67	0.58
Fine Sand		8.00	5.29	9.00	1.00
TP*	ppm	318.33	45.06	1029.00	377.13
AP		3.00	0.00	120.33	80.09
K*	meq/ 100g	0.08	0.02	0.25	0.05
Ca		0.80	0.10	0.79	0.04
Mg*		0.14	0.02	0.40	0.05
Na		0.06	0.01	0.01	0.03
CEC		41.06	4.29	42.62	1.71

Data are presented as mean and standard deviation (n = 3). An asterisk within the parameter column indicates a significant difference ($p < 0.05$) between treatments for two independent means. EC – electrical conductivity; TC – total carbon; TOC – total organic carbon; TN – total nitrogen; C/N – carbon to nitrogen ratio; BS – base saturation; TP – total phosphorus (P); AP – available P; K – potassium; Ca – calcium; Mg – magnesium; Na – Sodium; CEC – cation exchange capacity.

Despite increased soil nutrient availability, the foliar nutrient analysis (Table 2) revealed that the fertilized soil did not significantly ($p < 0.05$) reflect higher foliar nutrient concentrations of P, K, Ca, Mn, Fe, and Zn. These findings suggest that the increased soil nutrient content did not translate into proportional increases in foliar nutrient concentrations. This discrepancy is likely due to the complex nutrient uptake, translocation, and utilization processes within plants. The absorption and distribution of nutrients in plant tissues are regulated based on the demands of the plants (Han et al., 2016). Nutrients in leaves are mobile and can be rapidly transferred from leaves to other plant parts, such as the stems and roots, to promote the development of new tissues (Kim et al., 2018). Despite the increased availability of soil nutrients due to fertilizer application, there was minimal effect on the leaf nutrient concentrations.

Table 2. Foliar nutrient contents

Parameter	Unit	Unfertilized		Fertilized	
		Mean	S.D.	Mean	S.D.
TN	%	3.06	0.14	2.98	0.35
TC*		43.86	0.20	45.65	1.39
C/N		14.33	0.58	15.46	1.49
P*		0.20	0.01	0.11	0.01
K*		3.01	0.13	2.06	0.21
Mg		0.26	0.02	0.28	0.04
Ca*		1.02	0.10	0.31	0.05
B	ppm	21.33	4.16	13.33	6.51
Cu		9.79	1.50	9.54	1.80
Mn*		173.00	11.53	73.67	8.39
Fe*		371.19	50.47	198.41	46.13
Zn*		35.89	6.04	24.87	0.21
Plant dry weight (DW)*	g	442.32	77.62	576.16	74.92
Plant height*	cm	50.67	3.06	70.33	6.81

Data are presented as mean and standard deviation (n = 3). An asterisk within the parameter column indicates a significant difference ($p < 0.05$) between treatments for two independent means. TN – total nitrogen; TC – total carbon; C/N – carbon to nitrogen ratio; P – phosphorus; K – exchangeable potassium (K+); Mg – exchangeable magnesium (Mg2+); Ca – exchangeable calcium (Ca2+); B – boron; Cu – copper; Mn – manganese; Fe – Iron; Zn – Zinc.

Beneficial Phyla for Plant Growth in Response to Soil Nutrient Availability

Proteobacteria constituted the top predominant taxon up to 43.15% of the total bacterial community, followed by Acidobacteria (18.79%), Chloroflexi (12.51%), Actinobacteria (9.34%), and Firmicutes (4.20%) (Figure 1A). The fertilizer application significantly increased the abundance of Proteobacteria in the bulk soil (Figure 1A, S1A), consistent with prior studies (Xu et al., 2022; Bai et al., 2022). Proteobacteria, particularly copiotrophic members like Pseudomonas and Bacillus, thrive in nutrient-rich environments such as agricultural soils and around plant roots (Wei et al., 2018; Angelina et al., 2020). The flourishing of these bacteria in the fertilized soil is likely attributed to the nitrogen-containing fertilizers used, as genes associated with nitrogen metabolism were linked to the Proteobacteria phylum (Ren et al., 2018). This proposes that the current use of chemical fertilizers that contain nitrogen stimulates Proteobacteria to thrive in the soil. The significant increase in

DOI:https//doi.org/10.22452/mjs.vol44no2.3
Malaysian Journal of Science 44(2): 18-41 (June 2025)

Proteobacteria abundance (Figure 1A, S1A) in response to substantially higher K (Table 1) in the fertilizer bulk soil may promote the growth of the seedlings. Proteobacteria aid crop growth by producing organic acids, siderophores, biofilms, and plant growth hormones, enhancing yield and quality through improved nutrient availability and stress resistance (Bright et al., 2022). Conversely, the chemical fertilizer substantially reduced the abundance of Acidobacteria in the bulk soil (Figure 1A, S1A), in line with other studies (Dai et al., 2018; Shi et al., 2020). This could be because Acidobacteria genera such as Terriglobus and Granulicella are oligotrophs that enable them to flourish in low-nutrient soil (Tebo et al., 2015; Dedysh & Damsté, 2018; Noble et al., 2020). Given that Acidobacteria prefer oligotrophic environments, this suggests that fertilizing soil might harm their abundance.

Whereas for the rhizosphere, the average abundance of phyla Proteobacteria constituted the top predominant taxon by 54% of the total bacterial community, followed by Actinobacteria (10.73%), Acidobacteria (10.39%), Chloroflexi (6.28%), and Bacteroidetes (5.33%) (Figure 1B). Moreover, the fertilizer application caused a noticeably greater abundance of Saccharibacteria and Actinobacteria (Figure 1B, S1B) and aligns with earlier research (Shen et al., 2018; Liu et al., 2020b). These phyla likely grew and proliferated because of the increasing availability of nutrients, particularly nitrogen and phosphorus (Figueroa-Gonzalez et al., 2020; Boubekri et al., 2021). As a source of carbon and energy for these bacteria in the rhizosphere, N-containing fertilizer can also encourage plant root development, resulting in larger production of root exudates (Zhu et al., 2016). Therefore, this implies that the fertilizer application increases the abundance of Saccharibacteria and Actinobacteria in the rhizosphere because of improved nutrient availability and root exudation. In contrast, the abundance of Verrucomicrobia and Acidobacteria were significantly reduced in the fertilized soil (Figure 1B, S1B) and the pattern was similarly found in several other crops including wheat, corn, soybeans, and rice (Wang et al., 2015; Singh et al., 2018; Kandel et al., 2019). These phyla thrive in low-nutrient environments, playing crucial roles in nutrient cycling, plant development, and health (Feng et al., 2019; Kalam et al., 2020; Bünger et al., 2020). Their ability to efficiently use limited nutrients suggests they are oligotrophs, potentially enhancing plant growth in nutrient-poor soil, as seen in their prevalent abundance in the unfertilized treatment (Figure 1B, S1B).

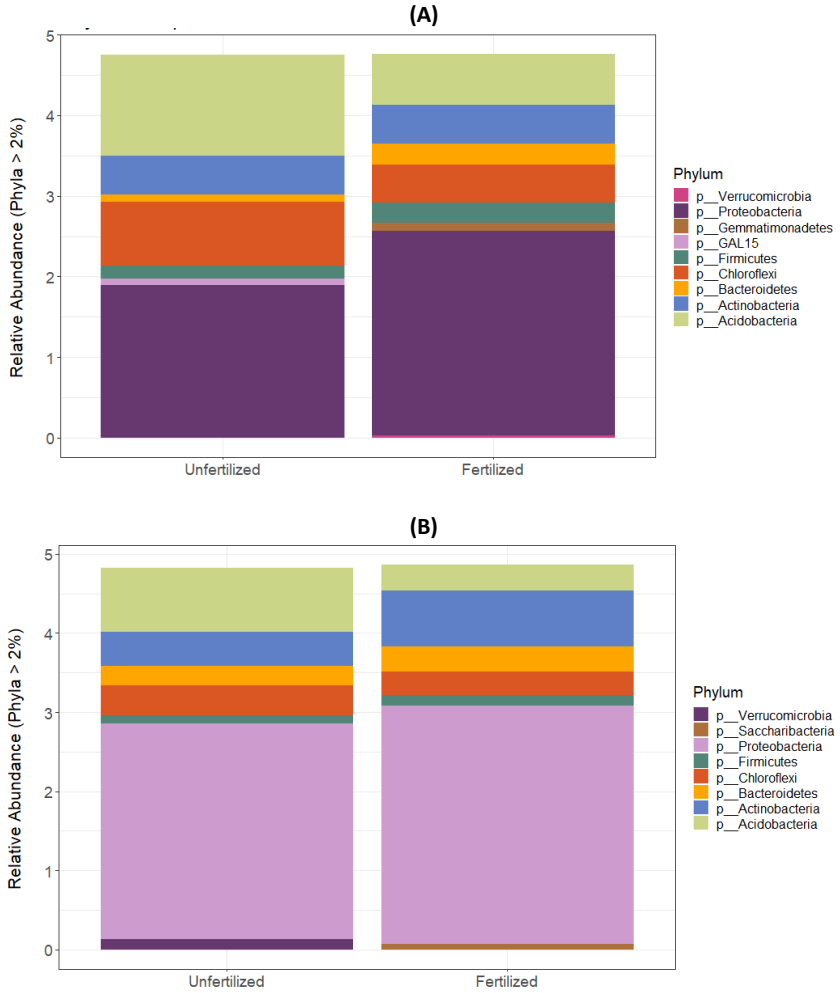

Figure 1. Relative abundance of bacterial phyla (> 2%) between unfertilized and fertilized soil in the (A) bulk soil and (B) rhizosphere

DOI:https//doi.org/10.22452/mjs.vol44no2.3
Malaysian Journal of Science 44(2): 18-41 (June 2025)

Reduced Bacterial Diversity Following the Chemical Fertilizer Application

The chemical fertilizer application significantly reduced the bacterial richness and diversity in the bulk soil and rhizosphere (Figure 2A, B) aligning with previous studies (Wang et al., 2018; Liu et al., 2020a; Chen et al., 2020; Semenov et al., 2020; Xu et al., 2020). This adverse impact, particularly on sensitive oligotrophs like Acidobacteria, suggests a potential early indicator of declining soil fertility due to agricultural activities (Feng et al., 2022). The fertilizer application also reduces soil organic matter, hindering bacterial growth while favoring antibiotic-producing bacteria and compromising community diversity and richness (Lin et al., 2019). Additionally, root exudates such as phenols and flavonoids also contribute to the rhizosphere's declining bacterial richness and diversity, as they contain allelopathic properties, releasing antibacterial chemicals that reduce microbial diversity (Wen et al., 2022; Kakar et al., 2023). Therefore, applying fertilizer can decrease bacterial richness and diversity in both bulk soil and the rhizosphere, signaling potential early signs of declining soil fertility. Root exudates, with allelopathic compounds, may contribute to reducing microbial diversity in this context.

Diversity loss due to nitrogen addition could also be due to the Resource Competition theory (Eliot, 2011). The existing evidence suggests that, similar to its impact on plant communities, the enhancement of dominant microbial species, possibly due to nitrogen additions, may contribute to diversity losses of subservient species through competitive exclusion for the resource (Wu et al., 2022). While the theory has been extensively investigated with plant diversity (Farrer et al., 2016; Wu et al., 2022), its application to microbial diversity requires further exploration to alleviate the species loss caused by nutrient enrichment and maintain the diversity of ecosystems.

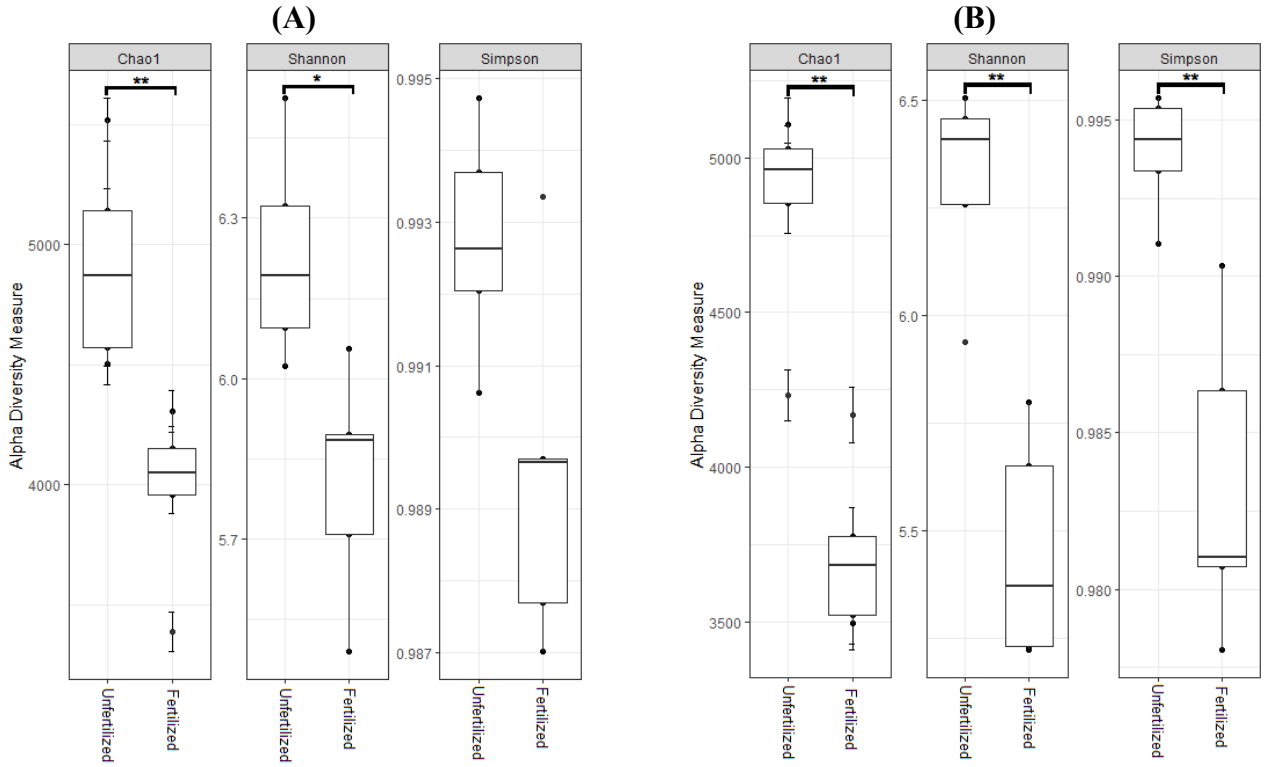

Figure 2. Box-whisker plots depicting bacterial richness (Chao1) and alpha diversity (Shannon and Simpson) between unfertilized and fertilized soil in the (A) bulk soil and (B) rhizosphere at the feature level. Statistical significance *p*-values were assessed by the Wilcoxon rank sum test. *$p < 0.05$, **$p < 0.01$, ***$p < 0.001$

The PCoA analysis revealed no clear grouping between the soil types in the bulk soil, indicating that the treatment likely did not affect the bacterial composition (Figure 3A). Previous research has suggested that soil bacteria can be resilient to disturbances caused by chemical fertilizers (Čuhel et al., 2019). In contrast, a distinct, clear separation between the soil types was found in the rhizosphere, suggesting that the fertilizer application may have significantly impacted the bacterial community (Figure 3B). Exposure to nitrogen fertilizer has been observed to stimulate the growth of microbial genera possessing identifiable pathogenic characteristics (Zhou et al., 2016). Consequently, plant roots may actively choose certain microorganisms to inhabit the rhizosphere (Berendsen et al., 2012). This selective process ultimately attracts and supports beneficial microorganisms, enhancing nutrient absorption and counteracting potentially harmful taxa (Dennis et al., 2010). These findings support previous research indicating that chemical fertilizer can selectively affect bacterial populations in the rhizosphere (Zhao et al., 2022).

DOI:https//doi.org/10.22452/mjs.vol44no2.3
Malaysian Journal of Science 44(2): 18-41 (June 2025)

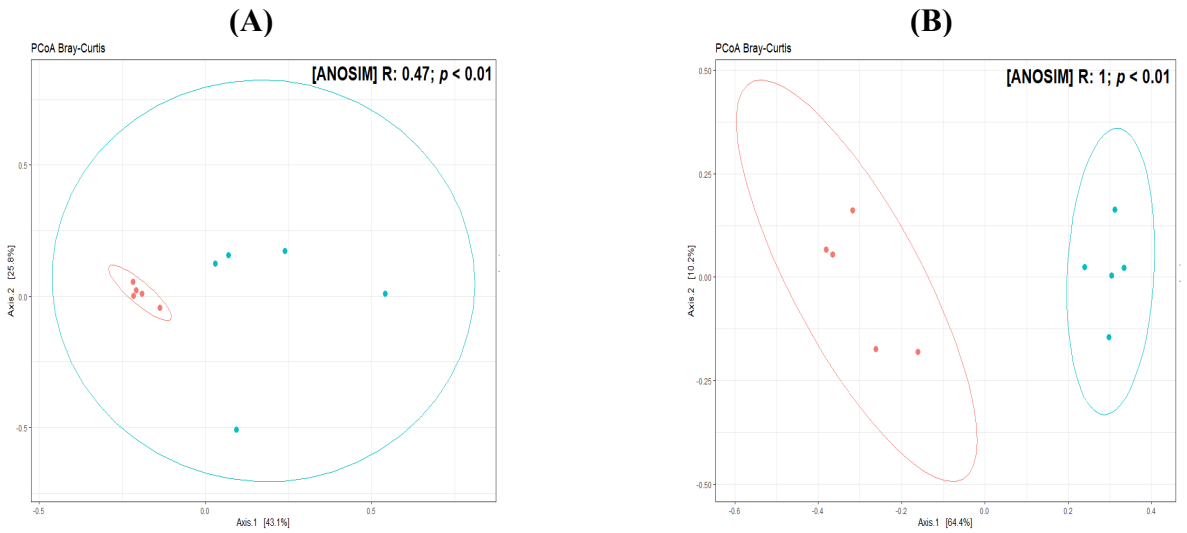

Figure 3. Principal Coordinate Analysis (PCoA) ordination based on the Bray-Curtis dissimilarity matrix of taxonomic bacterial community between the unfertilized and fertilized soil in the (A) bulk soil and (B) rhizosphere. Red indicates unfertilized soil whereas blue indicates NPK-treated soil

Potential Bacterial Biomarkers and Their Role in Soil Fertility and Plant Growth

The research findings suggest that Bryobacter, Candidatus Solibacter, and Acidothermus were more abundant in the unfertilized bulk soil (Figure 4A). Bryobacter and Candidatus Solibacter are known to play a role in mobilizing phosphate and reducing nitrite and nitrate, respectively, which are essential for plant development in nutrient-poor soil (Ward et al., 2009; Zhao et al., 2019; Zhang et al., 2019a). The prevalence of Acidothermus may indicate its potential role in combating pathogens, as suggested by research in tobacco and oil palm crops with limited nutrients (Barabote et al., 2009; Svenningsen et al., 2018; Gao et al., 2019; Goh et al., 2020). These findings could justify the prevalence of these bacteria in unfertilized soil, indicating their potential beneficial roles in promoting nutrient cycling and plant defense under nutrient limitations. In contrast, Mizugakiibacter and Castellaniella were found to be more abundant in the fertilized bulk soil (Figure 4A). These bacteria are involved in nitrogen cycling and can act as biocontrol agents by competing with harmful pathogens for nutrients (Kojima et al., 2014; Lin et al., 2018; Yin et al., 2022). Additionally, a previous study has shown that Castellaniella has the potential to degrade harmful pollutants like polychlorinated biphenyls (PCBs) (Su et al., 2019), suggesting they could be useful for bioremediation. These findings suggest that Mizugakiibacter and Castellaniella may be important in promoting plant growth, defending against pathogens, and maintaining a healthy soil ecosystem.

Meanwhile, in the rhizosphere, Rhizomicrobium, Acidibacter, Bradyrhizobium, Candidatus Solibacter, and Acidothermus were more abundant in the unfertilized soil (Figure 4B). These genera have been reported to symbiotically interact and promote plant growth by fixing nitrogen, producing plant hormones, and converting ammonium to nitrate (Antoun et al., 1998; Bárta et al., 2017; Arocha-Garza et al., 2017; Bei et al., 2018; Halifu et al., 2019; Liu et al., 2019). Thus, these beneficial bacteria could suggest a mutually beneficial relationship with the plant roots to support plant survival in a nutrient-limited environment. Applying chemical fertilizer in the rhizosphere enriched Proteobacteria members, including Mizugakiibacter, unidentified Xanthomonadaceae, and Castellaniella (Figure 4B). Previous studies have linked Mizugakiibacter and Castellaniella with nitrification and denitrification (Lin et al., 2018), while Xanthomonadaceae is recognized for its significant contribution to nitrogen, phosphorus, and carbon transformation in the soil (Li et al., 2017). Granulicella was also enriched by the fertilizer application (Figure 4B). Granulicella boosts plant growth by producing indole-3-acetic acid and siderophores (Kalam et al., 2020). Additionally, it carries genes involved in exopolysaccharide synthesis, enhancing soil structure and water retention (Rawat et al., 2012; Kalam et al., 2020; Morcillo & Manzanera, 2021). These findings demonstrate that the enriched genera may play important roles in maintaining soil fertility, nutrient cycling, and promoting plant development.

DOI:https//doi.org/10.22452/mjs.vol44no2.3
Malaysian Journal of Science 44(2): 18-41 (June 2025)

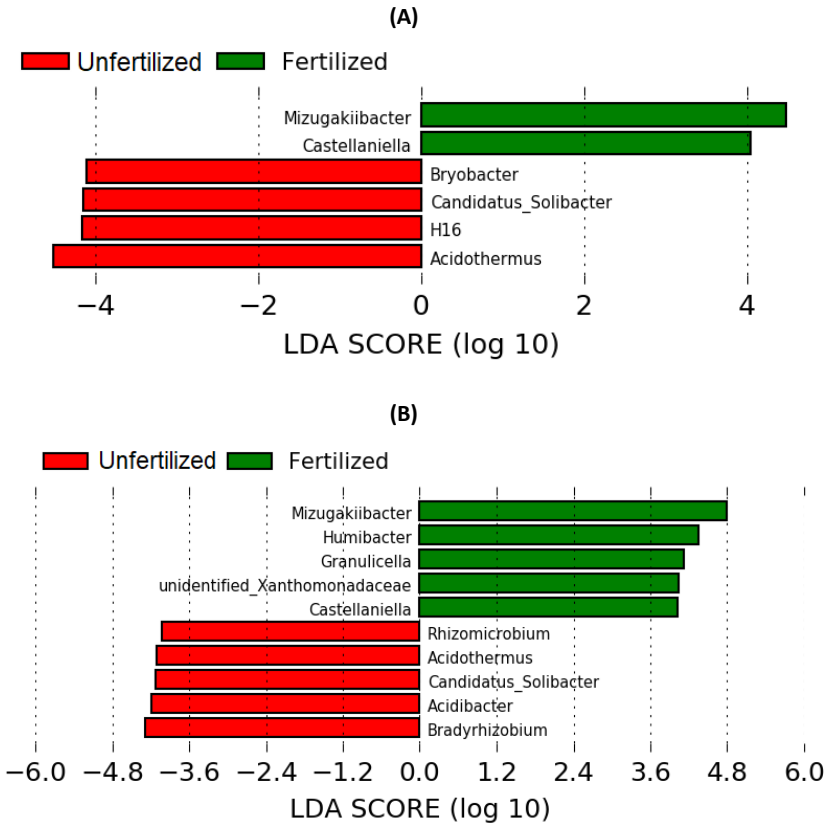

Figure 4. Linear discriminant analysis effect size (LEfSe) (LDA > 4) in the (A) bulk soil and (B) rhizosphere. Red indicates unfertilized soil-enriched taxa while green indicates fertilized soil-enriched taxa

Inferred Functional Responses of Bacterial Community Associated with Soil Fertility and Plant Growth

The fertilizer application enriched glycan biosynthesis and metabolism in the bulk soil and rhizosphere (Figure 5), which may suggest beneficial plant-microbe interactions. Rhizobacteria produce lipochitooligosaccharides, a glycan group, to distinguish between harmful pathogens and beneficial microorganisms in the plant-microbe relationship (Wanke et al., 2021). The enrichment of other secondary metabolites in the fertilized bulk soil and rhizosphere (Figure 5) may be linked to the increased abundance of Proteobacteria and Actinobacteria (Figure S1A) as these phyla produce various secondary metabolites such as siderophores, which help plants acquire iron, and indole acetic acid (IAA), a hormone that promotes root growth and enhances plant tolerance to stress (Duncan et al., 2021; Chhetri et al., 2021; Selim et al., 2021). These enhanced functions in response to the fertilizer application may improve the growth of oil palm seedlings, as evidenced by higher dry weight and height measurements (Table 2). Moreover, the constant enrichment of these functions in the bulk soil and rhizosphere may suggest a successful association between plants and beneficial microbes in the fertilized soil.

Carbohydrate metabolism was enriched in the unfertilized bulk soil (Figure 5A). Bacteria produce extracellular enzymes such as phosphatase and nitrate reductase to promote plant growth as part of carbohydrate metabolism (Ndabankulu et al., 2022). However, carbohydrate metabolism enrichment was shifted from the unfertilized bulk soil to the fertilized rhizosphere (Figure 5). It may be attributed to fertilization's increased availability of nutrients and root exudates in the rhizosphere. Chemical fertilizers enhance soil microbial carbon utilization, producing carbohydrates, carboxylic acids, and amino acids (Haiming et al., 2020). These products benefit plant growth, as carbohydrates provide structural support, carboxylic acids aid in photosynthesis, and amino acids serve as building blocks for plant tissue (Mallhi et al., 2019; Guo et al., 2021). Furthermore, the enrichment of carbohydrate metabolism by plant growth-promoting bacteria has increased plant biomass and nutrient uptake (Dhawi et al., 2017), which could explain the higher total carbon content and better seedling traits (Table 2) observed in this study.

For the unfertilized soil in the rhizosphere, amino acid metabolism, xenobiotics biodegradation and metabolism, metabolism of cofactors and vitamins, and metabolism of terpenoids and polyketides were enriched (Figure 5B). These metabolisms may be important for basic cellular functioning, defense mechanisms, nutrient cycling, and plant stress tolerance (Lewis et al., 2018). Rhizospheric bacteria enhance amino acid metabolism by extracting amino groups and converting them into ammonia, providing nitrogen for plant energy and growth. The xenobiotic degradation was enriched in the unfertilized soil (Figure 5B) as a fitness response to environmental stress. Xenobiotics are toxic substances, including heavy metals, insecticides, herbicides, and naturally occurring substances such as lignin and cellulose (Arora, 2020; Kathiravan & Gnanadoss,

DOI:https//doi.org/10.22452/mjs.vol44no2.3
Malaysian Journal of Science 44(2): 18-41 (June 2025)

2021). The bacteria can degrade them through enzymatic conversion into less toxic compounds or by storing them in their cells to prevent environmental harm (Kathiravan & Gnanadoss, 2021; Verma & Rawat, 2021).

Enriching cofactors and vitamins in the unfertilized rhizosphere (Figure 5B) may mitigate adverse effects in stressful environments (Lu et al., 2020; Loutet et al., 2021; Amjad et al., 2021). Based on the foliar physicochemical result (Table 2), significantly higher Fe and Zn as cofactors and vitamins in the unfertilized soil could potentially be utilized by the bacterial community via root exudation for cellular strategies (Merchant & Helmann, 2012). Lastly, the metabolism of terpenoids and polyketides was enriched in the unfertilized rhizosphere (Figure 5B), indicating that the bacterial community may serve in antimicrobial activities, plant growth promotion, yield increase, and stress alleviation (Piccoli & Bottini, 2013). These findings highlight the functional roles of bacteria in the rhizosphere in the absence of NPK fertilizer, particularly in nutrient cycling, plant stress response, and the reduction of environmental contaminants. However, these inferred observations are speculative because of database coverage restrictions and potential variations in microbial functions across various phases of plant growth (Aßhauer et al., 2015; Breitkreuz et al., 2021). When evaluating Tax4Fun results, care should be practiced, and experimental validation is advised for more accurate functional evaluations.

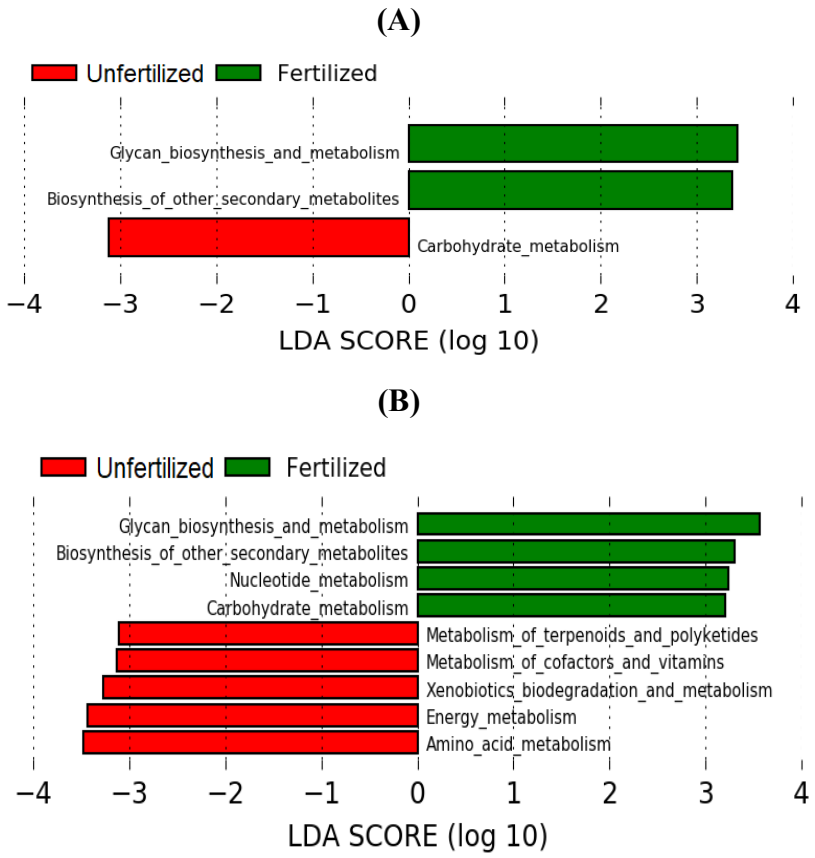

Figure 5. Linear discriminant analysis effect size (LEfSe) of inferred bacterial functions (LDA > 2) using Tax4Fun in the (A) bulk soil and (B) rhizosphere. Red indicates unfertilized soil-enriched function while green indicates the fertilized soil-enriched function

The Chemical Fertilizer Application Reduced Bacterial Network Complexity

The complexity of the bacterial networks was analyzed using topological data (Qiu et al., 2021; Price et al., 2021; Yang et al., 2021). The fertilizer application reduced the bacterial network complexity in the bulk soil and rhizosphere compared to the unfertilized soil (Table 3). Chemical fertilizer addition decreased bacterial diversity (Figure 2A), which could further simplify the complexity of species co-occurrence and redundancy of bacterial interaction (Yu et al., 2019). Bacteria may compete for available resources from fertilizer and root exudates, which causes some bacteria to thrive better than others (McNear, 2013). In contrast, the unfertilized soil encompassed more intricate bacterial networks in the bulk soil and rhizosphere (Table 3). This complexity may be linked to higher diversity (Figure 2) in nutrient-limited ecosystems through feedback processes related to nutrient recycling (Aerts & Chapin, 1999). The trend of network complexity can be supported by the Stress Gradient hypothesis, where microbial interactions become increasingly important in response to low nutrient availability and extreme environmental conditions (Bertness & Callaway, 1994; Mandakovic et al., 2023).

DOI:https//doi.org/10.22452/mjs.vol44no2.3
Malaysian Journal of Science 44(2): 18-41 (June 2025)

Table 3. The topological properties of bacterial in the bulk soil and rhizosphere

Summary Statistic	Bulk Soil		Rhizosphere	
	C	F	C	F
Number of nodes	69	23	112	47
Number of edges	68	36	267	42
Positive correlation (%)	52.94	100	73.78	52.38
Negative correlation (%)	47.06	0	26.22	47.62
Avg. number of neighbours	1.971	3.13	4.768	1.787
Network diameter	3	1	2	2
Network radius	1	1	1	1
Characteristic path length	1.284	1	1.187	1.256
Clustering coefficient	0.199	0.37	0.445	0.185
Network density	0.014	0.071	0.021	0.019
Connected components	21	7	18	16

C – Unfertilized, F – Fertilized

The potential association between the bacterial keystones and the network members is further determined in the context of plant growth-promotion. An Acidobacteria member, 11-24 was the keystone taxa in unfertilized bulk soil and formed positive correlations with Proteobacteria members (Figure 6A), yet literature on this genus (11-24) is limited. At the phylum level, Acidobacteria breaks down various complex compounds like carbohydrates, amino acids, and alcohols which are subsequently used by Proteobacteria, aiding in the cycling of nitrogen, phosphorus, and sulfur in ecosystems. (Ward et al., 2009; Belova et al., 2018; Zhou et al., 2020; Song et al., 2021; Berza et al., 2022). In the unfertilized rhizosphere, a Planctomycetes member (Gemmata) was a key player and formed positive correlations with the genera belonging to the Actinobacteria, Bacteroidetes, Proteobacteria, and Verrucomicrobia (Figure 7). These bacterial phyla thrive in chitin-rich environments, which can be found in fungal cell walls (Zegeye et al., 2019). They play a crucial role in the plant's defense system by breaking down the chitin-based cell walls of pathogenic fungi (Esperschütz et al., 2011; Ren et al., 2015; Kramer et al., 2016), thereby cooperating within the network to protect the seedlings in nutrient-poor soil.

In the fertilized bulk soil, Paenibacillus and Nitrospira formed a positive correlation (Figure 6B). Paenibacillus could convert nitrogen into ammonia, which is further converted into nitrate by Nitrospira for plant utilization (Liu et al., 2019; Sakoula et al., 2021). Nitrospira and Sporosarcina exhibited a positive correlation, suggesting a potential cooperative relationship within the nitrogen cycle. Nitrospira is involved in nitrification, whereas Sporosarcina plays a crucial role by producing urease, an enzyme essential for nitrogen cycling (Zhang et al., 2019b; Ma et al., 2020). These findings suggest that chemical fertilizers could positively impact these two genera, promoting soil health and optimizing nutrient cycling. Gordonia, a genus belonging to Actinobacteria, was found as a network keystone in the rhizosphere of fertilized treatment and formed a positive association with Lysinibacillus (Figure 8). Gordonia is involved in nitrogen fixation, converting atmospheric nitrogen into ammonia, whereas Lysinibacillus has genes related to ammonia conversion, specifically ammonia monooxygenase and ammonium transporter, suggesting its involvement in nitrification. This may imply that both bacteria likely cooperate in the nitrogen cycle, with Gordonia fixing nitrogen and Lysinibacillus converting ammonia into nitrite and nitrate for the plants' benefit (Gomez-Garzon et al., 2017).

DOI:https//doi.org/10.22452/mjs.vol44no2.3
Malaysian Journal of Science 44(2): 18-41 (June 2025)

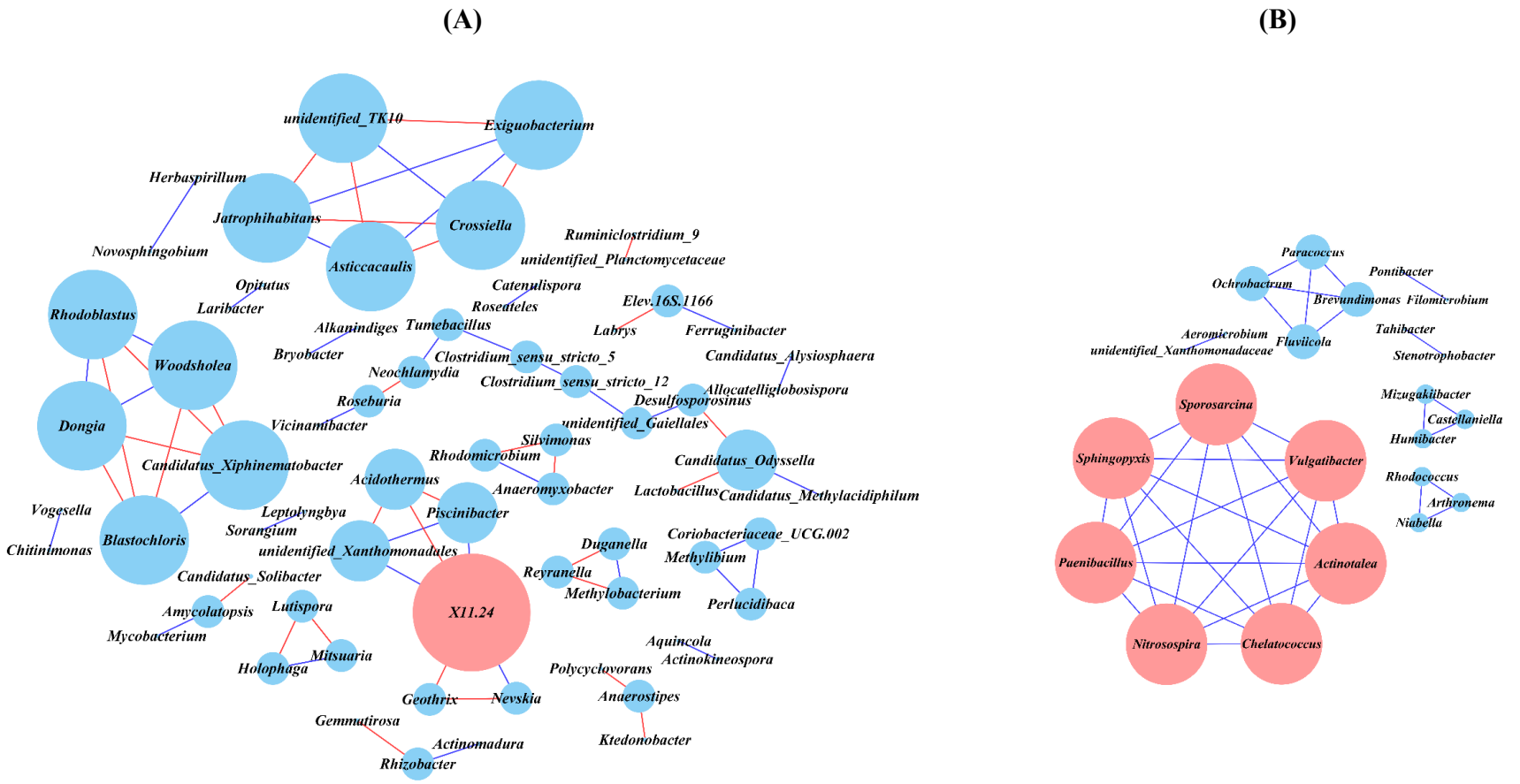

Figure 6. Bacterial co-occurrence network of (A) unfertilized and (B) fertilized soil in the bulk soil. The connection between genera (LDA > 2) is visualized based on the Spearman coefficient (r > ±0.7) and significant ($p < 0.01$) correlation. The node size is proportioned to the number of connections (degree) and the edge width (weight) is proportioned to the r-value. The edge is colored blue and red for positive and negative correlation, respectively

DOI:https//doi.org/10.22452/mjs.vol44no2.3
Malaysian Journal of Science 44(2): 18-41 (June 2025)

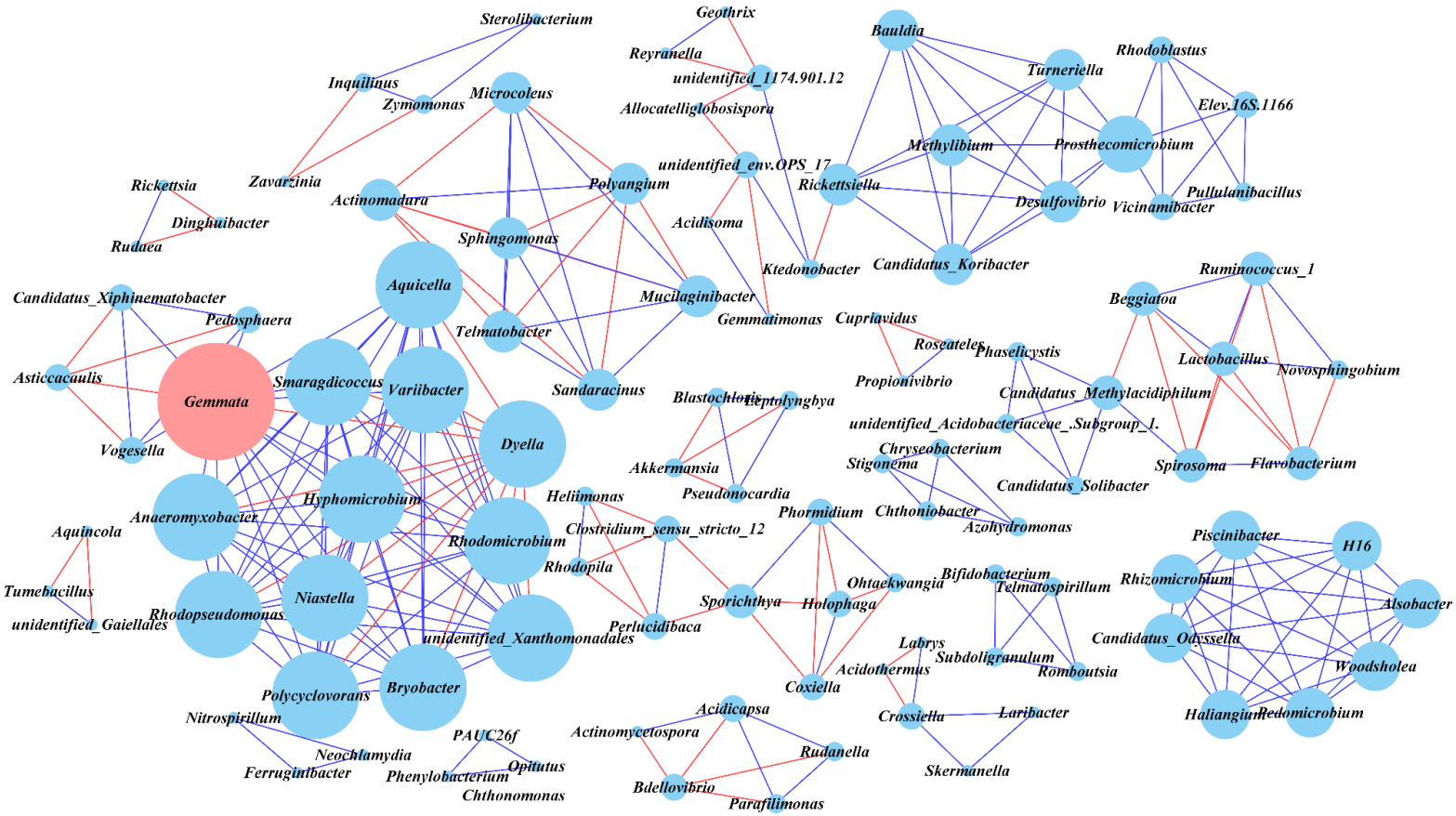

Figure 7. Bacterial co-occurrence network of the unfertilized soil in the rhizosphere. The connection between genera (LDA > 2) is visualized based on the Spearman coefficient ($r > \pm 0.7$) and significant ($p < 0.01$) correlation. The node size is proportioned to the number of connections (degree) and the edge width (weight) is proportioned to the r-value. The edge is colored blue and red for positive and negative correlation, respectively

DOI:https//doi.org/10.22452/mjs.vol44no2.3
Malaysian Journal of Science 44(2): 18-41 (June 2025)

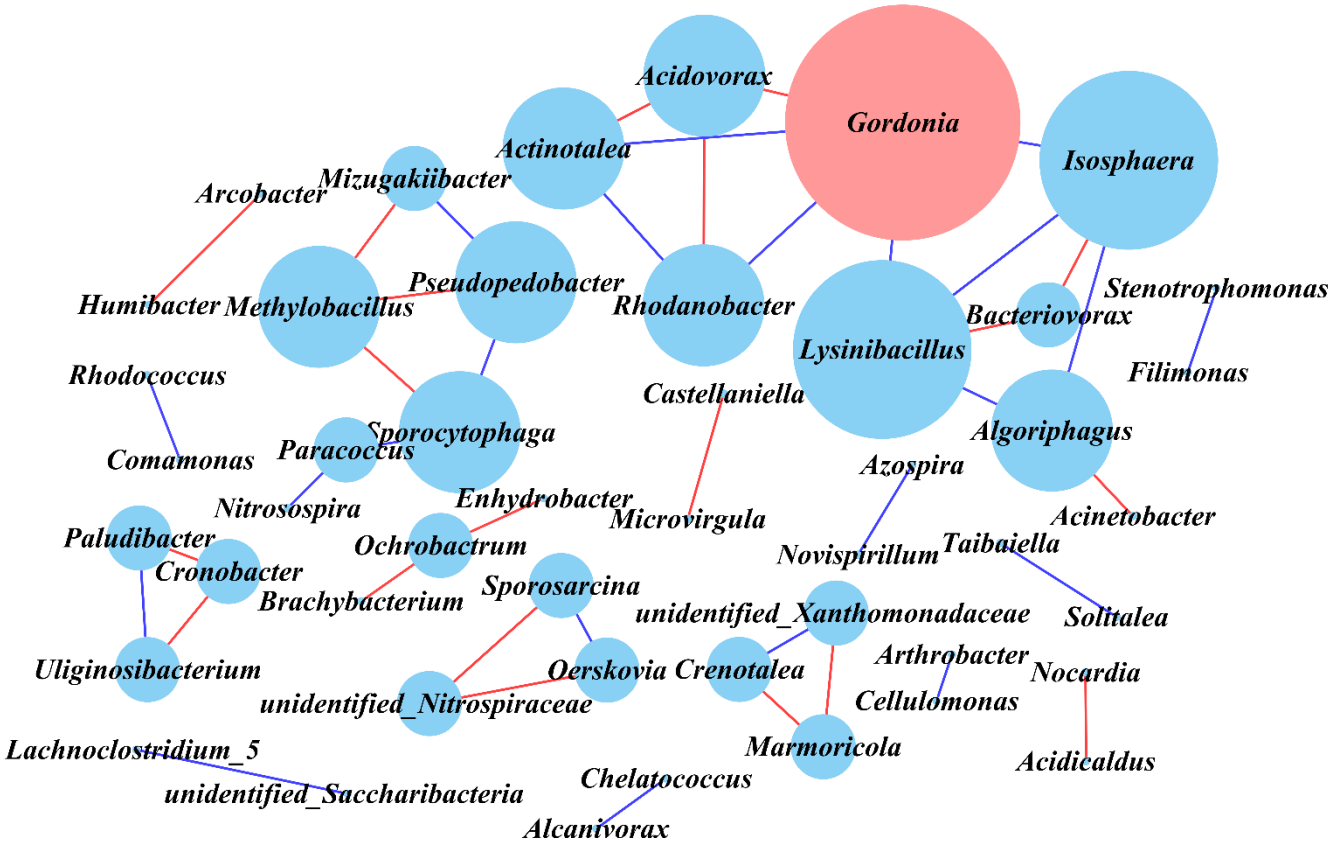

Figure 8. Bacterial co-occurrence network of the fertilized soil in the rhizosphere. The connection between genera (LDA > 2) is visualized based on the Spearman coefficient (r > ±0.7) and significant (p < 0.01) correlation. The node size is proportioned to the number of connections (degree) and the edge width (weight) is proportioned to the r-value. The edge is colored blue and red for positive and negative correlation, respectively

0

DOI:https//doi.org/10.22452/mjs.vol44no2.3
Malaysian Journal of Science 44(2): 18-41 (June 2025)

Significant Environmental Factors Drove the Abundance of Potentially Beneficial Biomarkers

The relationship between the potential biomarkers (LDA > 4) with significant soil physicochemical parameters and foliar nutrient contents was further investigated (Figure 9). In the unfertilized bulk soil, Acidothermus (OTU14) was positively correlated with pH (Figure 9A), suggesting that lower soil pH (Table 1) may drive the genus' abundance as proposed (Kim et al., 2016; Ogola et al., 2021; Ren et al., 2021). The decreased soil pH causes Mg to be more soluble, yet appears to diverge from the anticipated outcome with significantly lower Mg in the unfertilized soil (Table 1). As proposed in Liebig's Law of the Minimum, the plant's growth will be limited by the scarcest nutrient (van der Ploeg et al., 1999), hence suggesting that Mg may be further utilized by the seedlings rather than stored in the soil. Additionally, Castellaniella (OTU10) in the fertilized bulk soil was positively correlated with soil TP (Figure 9A), suggesting that soil phosphorus may influence the genus's abundance. Phosphate helps Castellaniella (OTU10), a denitrifying bacterium, by stabilizing pH, boosting their activity, causing zinc phosphate to form, and lessening the impact of ZnO nanoparticles on interactions with extracellular polymeric substances. This positively affects the abundance and activity of denitrifying bacteria (Cheng et al., 2019). This may explain its dependence on soil TP.

In terms of the rhizosphere, Acidothermus (OTU12) and Bradyrhizobium (OTU13) were strongly associated with pH in the unfertilized soil (Figure 9B). Acidothermus (OTU12) may be driven by an acidic environment and is known to break down plant tissues, leading to increased organic matter and nutrients available to plants (Ren et al., 2021; Ogola et al., 2021). Bradyrhizobium (OTU13) can adapt to acidic soil, despite generally not thriving in low pH environments (Jaiswal & Dakora, 2019), and effectively fix nitrogen (Holland et al., 2023). It also produces a siderophore that improves iron availability for plants and inhibits pathogens (Kumawat et al., 2019; Seraj et al., 2020). This may explain the higher foliar Fe content (Table 2), promoting plant growth and defense in nutrient-deficient conditions. In addition, Mizugakiibacter (OTU16) in the rhizosphere was positively correlated with fertilized soil TP (Figure 9B), and this pattern was consistent with a prior study (Li et al., 2021). During the hydrolysis of P-containing substrates, Mizugakiibacter (OTU16) produces phosphatase to release orthophosphates for utilization by soil biota and plants. (Kojima et al. 2014; Dotaniya et al. 2019). This implies that their abundance was influenced by the availability of phosphate and may aid to solubilize phosphate for plant development.

(A)

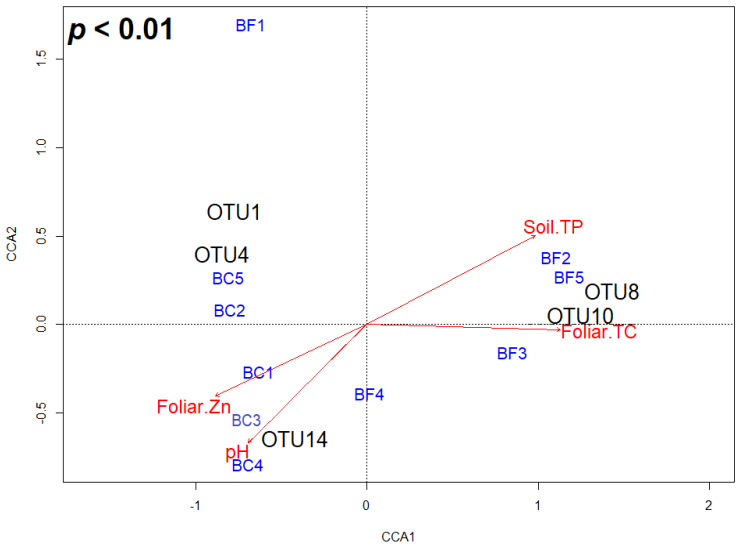

(B)

DOI:https//doi.org/10.22452/mjs.vol44no2.3
Malaysian Journal of Science 44(2): 18-41 (June 2025)

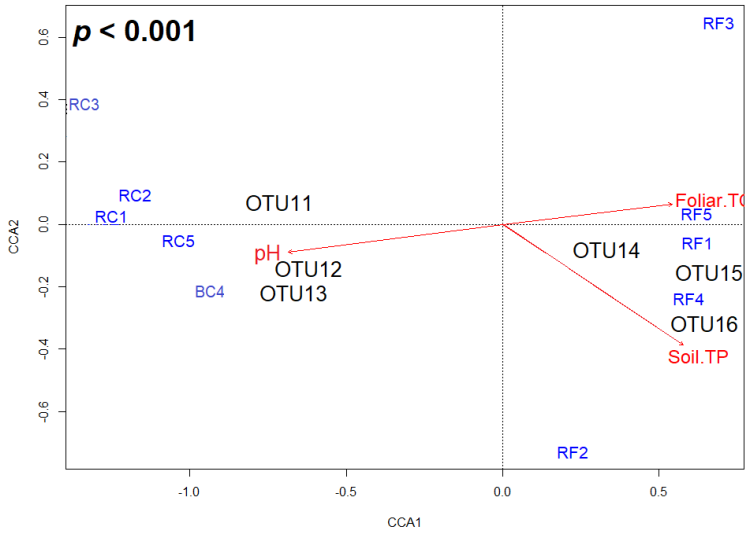

Figure 9. Canonical correspondence analysis (CCA) shows a correlation between significant physicochemical parameters and bacterial biomarkers (LDA > 4) for (A) bulk soil and (B) rhizosphere. The closeness of the points indicates the similarity of the samples, the arrowhead of variables shows a degree of association, and the length represents strength that explains the biomarker dispersion observed. B – Bulk soil, R – Rhizosphere, C – Unfertilized, F – Fertilized

4. Conclusion

While fertilizer application increased soil nutrient availability, it did not necessarily produce proportional increases in foliar nutrient concentrations. The abundance of Proteobacteria, Saccharibacteria, and Actinobacteria significantly increased in response to the fertilizer application, suggesting their succession as dominant phyla due to the nutrient-rich conditions. However, the fertilizer application also reduced bacterial diversity in the soil and root systems, especially in sensitive bacterial groups like Acidobacteria, indicating potential early indicators of declining soil fertility due to agricultural activities. The consistent enrichment of *Mizugakiibacter* and *Castellaniella* in the fertilized bulk soil and rhizosphere may suggest potential capabilities to utilize the nutrients present in the fertilizer. Current findings also revealed a higher number of genera belonging to Proteobacteria (*Rhizomicrobium*, *Bradyrhizobium*), Actinobacteria (*Acidothermus*), and Acidobacteria (*Candidatus Solibacter*, *Bryobacter*) compared to the fertilized soil, suggesting that the unfertilized soil may represent an early successional stage in bacterial community development in the absence of fertilizer application. Moreover, the fertilizer application enhanced the enrichment of specific metabolic processes in bacteria, such as glycan biosynthesis, nucleotide metabolism, and carbohydrate metabolism, which likely contribute to improved plant-microbe interactions and plant growth in the fertilized treatment. Alternatively, the enriched bacterial functions in the unfertilized soil may suggest cellular functioning strategies.

Regarding network analysis, the fertilizer application resulted in a simpler bacterial network. However, it can also promote positive interactions and contribute to nutrient cycling. In contrast, the unfertilized soil exhibits more complex networks, potentially associated with nutrient limitation and the recruitment of beneficial bacteria for growth support. The CCA demonstrated that the presence of *Acidothermus* and *Castellaniella* was positively associated with specific nutrient levels in the unfertilized soil, suggesting their potential role in nutrient cycling and plant health. Acidothermus, Bradyrhizobium, and Mizugakiibacter also showed associations with different nutrient conditions in the fertilized treatment, indicating their potential contributions to nutrient availability and plant growth. Understanding the impact of fertilizer application on the bacterial community composition, diversity, functionality, and networks will aid in promoting the seedlings' growth. Future studies should focus on optimizing chemical fertilizer applications to address the presence of pathogens and highlight the enrichment of beneficial taxa for sustainable agriculture practices.

5. Acknowledgements

We express our heartfelt appreciation to Sime Darby Plantation Technology Centre Sdn. Bhd. for their pivotal role in our research conducted at the Department of Microbiology, Faculty of Biotechnology and Biomolecular Sciences, Universiti Putra Malaysia. Their provision of cutting-edge facilities, valuable samples, and expert guidance significantly enhanced the quality and scope of our study. We are truly grateful for their unwavering support, which has been instrumental in the success of our research endeavors.

6. References

Abhauer, K. P., Wemheuer, B., Daniel, R., & Meinicke, P. (2015). Tax4Fun: predicting functional profiles from metagenomic 16S rRNA data. *Bioinformatics, 31*(17), 2882-2884. https://doi.org/10.1093/bioinformatics/btv287

Aerts, R., & Chapin III, F. S. (1999). The mineral nutrition of wild plants revisited: a re-evaluation of processes and patterns.

DOI:https//doi.org/10.22452/mjs.vol44no2.3
Malaysian Journal of Science 44(2): 18-41 (June 2025)

Advances in Ecological Research, 30, 1-67. https://doi.org/10.1016/S0065-2504(08)60016-1

Ahmed, W., Jing, H., Kaillou, L., Qaswar, M., Khan, M. N., Jin, C., Geng, S., Qinghai, H., Yiren, L., Guangrong, L., Mei, S., Chao, L., Dongchu, L., Ali, S., Normatov, Y., Mehmood, S., & Zhang, H. (2019). Changes in phosphorus fractions associated with soil chemical properties under long-term organic and inorganic fertilization in paddy soils of southern China. *PloS One, 14*(5), 1-17. https://doi.org/10.1371/journal.pone.0216881

Aizat, A. M., Roslan, M. K., Sulaiman, W. N. A., & Karam, D. S. (2014). The relationship between soil pH and selected soil properties in 48 years logged-over forest. *International Journal of Environmental Sciences, 4*(6), 1129-1140. https://doi.org/10.6088/ijes.2014040600004

Amjad, S. F., Mansoora, N., Yaseen, S., Kamal, A., Butt, B., Matloob, H., Alamri, S. A. M., Alrumman, S. A., Eid, E. M., & Shahbaz, M. (2021). Combined use of endophytic bacteria and pre-sowing treatment of thiamine mitigates the adverse effects of drought stress in wheat (*Triticum aestivum* L.) cultivars. *Sustainability*, *13*(12), 6582. https://doi.org/10.3390/su13126582

Angelina, E., Papatheodorou, E. M., Demirtzoglou, T., & Monokrousos, N. (2020). Effects of *Bacillus subtilis* and *Pseudomonas fluorescens* inoculation on attributes of the lettuce (*Lactuca sativa* L.) soil rhizosphere microbial community: The role of the management system. *Agronomy*, *10*(9), 1428. https://doi.org/10.3390/agronomy10091428

Antoun, H., Beauchamp, C. J., Goussard, N., Chabot, R., & Lalande, R. (1998). Potential of *Rhizobium* and *Bradyrhizobium* species as plant growth promoting rhizobacteria on non-legumes: effect on radishes (*Raphanus sativus* L.). In *Molecular Microbial Ecology of The Soil* (pp. 57-67). Springer, Dordrecht. https://doi.org/10.1007/978-94-017-2321-3_5

Arifin, I., Hanafi, M. M., Roslan, I., Ubaydah, M. U., Abd Karim, Y., Tui, L. C., & Hamzah, S. (2022). Responses of irrigated oil palm to nitrogen, phosphorus and potassium fertilizers on clayey soil. *Agricultural Water Management, 274*, 107922. https://doi.org/10.1016/j.agwat.2022.107922

Arocha-Garza, H. F., Canales-Del Castillo, R., Eguiarte, L. E., Souza, V., & De la Torre-Zavala, S. (2017). High diversity and suggested endemicity of culturable Actinobacteria in an extremely oligotrophic desert oasis. *PeerJ, 5*, 1-21. https://doi.org/10.7717/peerj.3247

Arora, P. K. (2020). Bacilli-mediated degradation of xenobiotic compounds and heavy metals. *Frontiers in Bioengineering and Biotechnology*, *8*, 570307. https://doi.org/10.3389/fbioe.2020.570307

Bai, L., Wang, Y., Li, Y., Zhang, X., Lu, Z., Zhang, D., Sun, F., & Zhao, X. (2022). Changes in the Microbial Community in Maize (*Zea mays* L.) Root Spatial Structure Following Short-Term Nitrogen Application. *ACS Omega*, *8*(1), 208–218. https://doi.org/10.1021/acsomega.2c01711

Banerjee, S., Schlaeppi, K., & van der Heijden, M. G. (2018). Keystone taxa as drivers of microbiome structure and functioning. *Nature Reviews Microbiology, 16*(9), 567-576. https://doi.org/10.1038/s41579-018-0024-1

Barabote, R. D., Xie, G., Leu, D. H., Normand, P., Necsulea, A., Daubin, V., Médigue, C., Adney, W. S., Xu, X. C., Lapidus, A., Parales, R. E., Detter, C., Pujic, P., Bruce, D., Lavire, C., Challacombe, J. F., Brettin, T. S., & Berry, A. M. (2009). Complete genome of the cellulolytic thermophile *Acidothermus cellulolyticus* 11B provides insights into its ecophysiological and evolutionary adaptations. *Genome Research, 19*(6), 1033-1043. http://www.genome.org/cgi/doi/10.1101/gr.084848.108

Barta, J., Tahovská, K., Šantrůčková, H., & Oulehle, F. (2017). Microbial communities with distinct denitrification potential in spruce and beech soils differing in nitrate leaching. *Scientific Reports, 7*(1), 1-15. https://doi.org/10.1038/s41598-017-08554-1

Bei, S., Zhang, Y., Li, T., Christie, P., Li, X., & Zhang, J. (2018). Response of the soil microbial community to different fertilizer inputs in a wheat-maize rotation on a calcareous soil. *Agriculture, Ecosystems & Environment, 260*, 58-69. https://doi.org/10.1016/j.agee.2018.03.014

Belova, S. E., Ravin, N. V., Pankratov, T. A., Rakitin, A. L., Ivanova, A. A., Beletsky, A. V., Damste, J. S. S., & Dedysh, S. N. (2018). Hydrolytic capabilities as a key to environmental success: chitinolytic and cellulolytic Acidobacteria from acidic sub-arctic soils and boreal peatlands. *Frontiers in Microbiology*, *9*, 2775. https://doi.org/10.3389/fmicb.2018.02775

Berendsen, R. L., Pieterse, C. M., & Bakker, P. A. (2012). The rhizosphere microbiome and plant health. *Trends in plant science, 17*(8), 478-486. https://doi.org/10.1016/j.tplants.2012.04.001

Bertness, M. D., & Callaway, R. (1994). Positive interactions in communities. *Trends in Ecology & Evolution, 9*(5), 191-193.

Berza, B., Sekar, J., Vaiyapuri, P., Pagano, M. C., & Assefa, F. (2022). Evaluation of inorganic phosphate solubilizing efficiency and multiple plant growth promoting properties of endophytic bacteria isolated from root nodules *Erythrina brucei. BMC Microbiology*, *22*(1), 276. https://doi.org/10.1186/s12866-022-02688-7

DOI:https//doi.org/10.22452/mjs.vol44no2.3
Malaysian Journal of Science 44(2): 18-41 (June 2025)

Bolyen, E., Rideout, J. R., Dillon, M. R., Bokulich, N. A., Abnet, C. C., Al-Ghalith, G. A., Alexander, H., Alm, E. J., Arumugam, M., Asnicar, F., Bai, Y., Bisanz, J. E., Bittinger, K., Brejnrod, A., Brislawn, C. J., Brown, C. T., Callahan, B. J., Caraballo-Rodríguez, A. M., Chase, J., Cope, E. K., Da Silva, R., Diener, C., Dorrestein, P. C., Douglas, G. M., Durall, D. M., Duvallet, C., Edwardson, C. F., Ernst, M., Estaki, M., Fouquier, J., Gauglitz, J. M., Gibbon, S. M., Gibson, D. L., Gonzalez, A., Gorlick, K., Guo, J., Hillman, B., Holmes, S., Holste, H., Huttenhower, C., Huttley, G. A., Janssen, S., Jarmusch, A. K., Jiang, L., Kaehler, B. D., Kang, K. B., Keefe, C. R., Keim, P., Kelley, S. T., Knights, D., Koester, I., Kosciolek, T., Kreps, J., Langille, M. G. I., Lee, J., Ley, R., Liu, Y. X., Loftfield, E., Lazupone, C., Maher, M., Marotz, C., Martin, B. D., McDonald, D., Mclver, L. J., Melnik, A. V., Metcalf, J. L., Morgan, S. C., Morton, J. T., Naimey, A. T., Navas-Molina, J. A., Nothias, L. F., Orchanian, S. B., Pearson, T., Peoples, S. L., Petras, D., Preuss, M. L., Pruesse, E., Rasmussen, L. B., Rivers, A., Robeson II, M. S., Rosenthal, P., Segata, N., Shaffer, M., Shiffer, A., Sinha, R., Song, S. J., Spear, J. R., Swafford, A. D., Thompson, L. R., Torres, P. J., Trinh, P., Tripathi, A., Turnbaugh, P., J., Ul-Hasan, S., van der Hooft, J. J. J., Vargas, F., Vázquez-Baeza, Y., Vogtmann, E., von Hippel, M., Walters, W., Wan, Y., Wang, M., Warren, J., Weber, K. C., Williamson, C. H. D., Willis, A. D., Xu, Z., Z., Zaneveld, J. R., Zhang, Y., Zhu, Q., Knight, R., & Caporaso, J. G. (2019). Reproducible, interactive, scalable and extensible microbiome data science using QIIME 2. *Nature Biotechnology, 37*(8), 852-857. https://doi.org/10.1038/s41587-019-0252-6

Boubekri, K., Soumare, A., Mardad, I., Lyamlouli, K., Hafidi, M., Ouhdouch, Y., & Kouisni, L. (2021). The screening of potassium- and phosphate-solubilizing actinobacteria and the assessment of their ability to promote wheat growth parameters. *Microorganisms, 9*(3), 470. https://doi.org/10.3390/microorganisms9030470

Breitkreuz, C., Heintz-Buschart, A., Buscot, F., Wahdan, S. F. M., Tarkka, M., & Reitz, T. (2021). Can we estimate functionality of soil microbial communities from structure-derived predictions? A reality test in agricultural soils. *Microbiology Spectrum, 9*(1), 10-1128. https://doi.org/10.1128/Spectrum.00278-21

Bright, J. P., Baby, A. S., Thankappan, S., George, A. S., Maheshwari, H. S., Nataraj, R., Judson, S., & Binodh, A. K. (2022). Potassium releasing bacteria for unlocking soil potassium-a way forward for judicious use of chemical fertilizers. *International Journal of Plant & Soil Science, 34*, 49-61. https://doi.org/10.9734/IJPSS/2022/v34i1931088

Bunger, W., Jiang, X., Müller, J., Hurek, T., & Reinhold-Hurek, B. (2020). Novel cultivated endophytic Verrucomicrobia reveal deep-rooting traits of bacteria to associate with plants. *Scientific Reports, 10*(1), 8692. https://doi.org/10.1038/s41598-020-65277-6

Caradonia, F., Ronga, D., Catellani, M., Giaretta Azevedo, C. V., Terrazas, R. A., Robertson-Albertyn, S., Francia, E., & Bulgarelli, D. (2019). Nitrogen fertilizers shape the composition and predicted functions of the microbiota of field-grown tomato plants. *Phytobiomes Journal, 3*(4), 315-325. https://doi.org/10.1094/PBIOMES-06-19-0028-R

Chen, L., Li, F., Li, W., Ning, Q., Li, J., Zhang, J., Ma, D., & Zhang, C. (2020). Organic amendment mitigates the negative impacts of mineral fertilization on bacterial communities in Shajiang black soil. *Applied Soil Ecology*, *150*, 103457. https://doi.org/10.1016/j.apsoil.2019.103457

Cheng, Y. F., Zhang, Z. Z., Li, G. F., Zhu, B. Q., Zhang, Q., Liu, Y. Y., Zhu, W. Q., Fan, N. S., & Jin, R. C. (2019). Effects of ZnO nanoparticles on high-rate denitrifying granular sludge and the role of phosphate in toxicity attenuation. *Environmental Pollution*, *251*, 166-174. https://doi.org/10.1016/j.envpol.2019.04.138

Chhetri, G., Kang, M., Kim, J., Kim, I., So, Y., & Seo, T. (2021). *Sphingosinicella flava* sp. nov., indole acetic acid producing bacteria isolated from maize field soil. *International Journal of Systematic and Evolutionary Microbiology, 71*(10), 005038. https://doi.org/10.1099/ijsem.0.005038

Chong, J., Liu, P., Zhou, G., & Xia, J. (2020). Using MicrobiomeAnalyst for comprehensive statistical, functional, and meta-analysis of microbiome data. *Nature Protocols, 15*(3), 799-821. https://doi.org/10.1038/s41596-019-0264-1

Csardi, G., & Nepusz, T. (2006). The igraph software package for complex network research. *InterJournal Complex Systems*, *1695*(5), 1–9. http://igraph.sf.net

Cuhel, J., Malý, S., & Královec, J. (2019). Shifts and recovery of soil microbial communities in a 40-year field trial under mineral fertilization. Pedobiologia, 77, 150575. https://doi.org/10.1016/j.pedobi.2019.150575

Dai, Z., Su, W., Chen, H., Barberán, A., Zhao, H., Yu, M., Yu, L., Brookes, P. C., Schadt, C. W., Chang, S. X., & Xu, J. (2018). Long-term nitrogen fertilization decreases bacterial diversity and favors the growth of Actinobacteria and Proteobacteria in agro-ecosystems across the globe. *Global Change Biology*, *24*(8), 3452-3461. https://doi.org/10.1111/gcb.14163

David, D. J. (1960). The determination of exchangeable sodium, potassium, calcium and magnesium in soils by atomic-absorption spectrophotometry. *Analyst, 85*(1012), 495-503.

Dedysh, S. N., & Damsté, J. S. S. (2018). Acidobacteria. *eLS*, 1-10. https://doi.org/10.1002/9780470015902.a0027685

Dennis, P. G., Miller, A. J., & Hirsch, P. R. (2010). Are root exudates more important than other sources of rhizodeposits in

DOI:https//doi.org/10.22452/mjs.vol44no2.3
Malaysian Journal of Science 44(2): 18-41 (June 2025)

structuring rhizosphere bacterial communities?. *FEMS Microbiology Ecology, 72*(3), 313-327. https://doi.org/10.1111/j.1574-6941.2010.00860.x

DeSantis, T. Z., Hugenholtz, P., Larsen, N., Rojas, M., Brodie, E. L., Keller, K., Huber, T., Dalevi, D., Hu, P., & Andersen, G. L. (2006). Greengenes, a chimera-checked 16S rRNA gene database and workbench compatible with ARB. *Applied and Environmental Microbiology, 72*(7), 5069-5072. https://doi.org/10.1128/AEM.03006-05

Dhawi, F., Datta, R., & Ramakrishna, W. (2017). Proteomics provides insights into biological pathways altered by plant growth promoting bacteria and arbuscular mycorrhiza in sorghum grown in marginal soil. *Biochimica et Biophysica Acta (BBA)-Proteins and Proteomics, 1865*(2), 243-251. https://doi.org/10.1016/j.bbapap.2016.11.015

Dotaniya, M. L., Aparna, K., Dotaniya, C. K., Singh, M., & Regar, K. L. (2019). Role of soil enzymes in sustainable crop production. In *Enzymes in Food Biotechnology* (pp. 569-589). Academic Press. https://doi.org/10.1016/B978-0-12-813280-7.00033-5

Duncan, T. R., Werner-Washburne, M., & Northup, D. E. (2021). Diversity of Siderophore-Producing Bacterial Cultures From Carlsbad Caverns National Park (Ccnp) Caves, Carlsbad, New Mexico. *Journal of Cave and Karst Studies: the National Speleological Society bulletin*, *83*(1), 29-43. https://doi.org/10.4311%2F2019es0118

Edgar, R. C. (2013). UPARSE: highly accurate OTU sequences from microbial amplicon reads. *Nature Methods, 10*(10), 996-998. https://doi.org/10.1038/nmeth.2604

Eliot, C. H. (2011). Competition theory and channeling explanation. *Philosophy, Theory, and Practice in Biology, 3* (20130604), 1-16. https://doi.org/10.3998/ptb.6959004.0003.001

Esperschütz, J., Pérez-de-Mora, A., Schreiner, K., Welzl, G., Buegger, F., Zeyer, J., Hagedorn, F., Munch, J. C., & Schloter, M. (2011). Microbial food web dynamics along a soil chronosequence of a glacier forefield. *Biogeosciences, 8*(11), 3283-3294. https://doi.org/10.5194/bg-8-3283-2011

Farrer, E. C., & Suding, K. N. (2016). Teasing apart plant community responses to N enrichment: the roles of resource limitation, competition and soil microbes. Ecology letters, 19(10), 1287-1296. https://doi.org/10.1111/ele.12665

Feng, C., Jia, J., Wang, C., Han, M., Dong, C., Huo, B., Li, D., & Liu, X. (2019). Phytoplankton and bacterial community structure in two chinese lakes of different trophic status. *Microorganisms, 7*(12), 621. https://doi.org/10.3390/microorganisms7120621

Feng, Y., Delgado-Baquerizo, M., Zhu, Y., Han, X., Han, X., Xin, X., Li, W., Guo, Z., Dang, T., Li, C., Zhu, B., Cai, Z., Li, D., & Zhang, J. (2022). Responses of soil bacterial diversity to fertilization are driven by local environmental context across China. *Engineering*, *12*, 164-170. https://doi.org/10.1016/j.eng.2021.09.012

Figueroa-Gonzalez, P. A., Bornemann, T. L., Adam, P. S., Plewka, J., Révész, F., Von Hagen, C. A., Táncsics, A., & Probst, A. J. (2020). Saccharibacteria as organic carbon sinks in hydrocarbon-fueled communities. *Frontiers in Microbiology, 11*, 587782. https://doi.org/10.3389/fmicb.2020.587782

Gao, L., Wang, R., Gao, J., Li, F., Huang, G., Huo, G., Liu, Z., Tang, W., & Shen, G. (2019). Analysis of the structure of bacterial and fungal communities in disease suppressive and disease conducive tobacco-planting soils in China. *Soil Research, 58*(1), 35-40. https://doi.org/10.1071/SR19204

Goecks, J., Nekrutenko, A., Taylor, J., Afgan, E., Ananda, G., Baker, D., Blankenberg, D., Chakrabarty, R., Coraor, N., Goecks, J., Von Kuster, G., Lazarus, R., Li, K., Taylor, J., & Vincent, K. (2010). Galaxy: a comprehensive approach for supporting accessible, reproducible, and transparent computational research in the life sciences. *Genome Biology*, *11*(8), 1–13. https://doi.org/10.1186/gb-2010-11-8-r86

Goh, Y. K., Zoqratt, M. Z. H. M., Goh, Y. K., Ayub, Q., & Ting, A. S. Y. (2020). Determining soil microbial communities and their influence on *Ganoderma* disease incidences in oil palm (*Elaeis guineensis*) via high-throughput sequencing. *Biology, 9*(12), 1-21. https://doi.org/10.3390/biology9120424

Gomez-Garzon, C., Hernández-Santana, A., & Dussan, J. (2017). A genome-scale metabolic reconstruction of *Lysinibacillus sphaericus* unveils unexploited biotechnological potentials. *PLoS One, 12*(6), 1-21. https://doi.org/10.1371%2Fjournal.pone.0179666

Goulding, K. W. T. (2016). Soil acidification and the importance of liming agricultural soils with particular reference to the United Kingdom. *Soil Use and Management, 32*(3), 390-399. https://doi.org/10.1111/sum.12270

Gu, Y., Wang, Y., Lu, S. E., Xiang, Q., Yu, X., Zhao, K., Zou, L., Chen, Q., Tu, S., & Zhang, X. (2017). Long-term fertilization structures bacterial and archaeal communities along soil depth gradient in a paddy soil. *Frontiers in Microbiology, 8*, 1-15. https://doi.org/10.3389/fmicb.2017.01516

Guo, N., Zhang, S., Gu, M., & Xu, G. (2021). Function, transport, and regulation of amino acids: What is missing in rice?. *The Crop Journal*, *9*(3), 530-542. https://doi.org/10.1016/j.cj.2021.04.002

Haiming, T., Xiaoping, X., Chao, L., Xiaochen, P., Kaikai, C., Weiyan,

DOI:https//doi.org/10.22452/mjs.vol44no2.3
Malaysian Journal of Science 44(2): 18-41 (June 2025)

L., & Ke, W. (2020). Microbial carbon source utilization in rice rhizosphere and nonrhizosphere soils with short-term manure N input rate in paddy field. *Scientific Reports*, *10*(1), 6487. https://doi.org/10.1038/s41598-020-63639-8

Halifu, S., Deng, X., Song, X., An, Y., & Song, R. (2019). Effects of Sphaeropsis Blight on Rhizosphere Soil Bacterial Community Structure and Soil Physicochemical Properties of *Pinus sylvestris* var. *mongolica* in Zhanggutai, China. *Forests, 10*(11), 1-18. https://doi.org/10.3390/f10110954

Han, S. H., An, J. Y., Hwang, J., Kim, S. B., & Park, B. B. (2016). The effects of organic manure and chemical fertilizer on the growth and nutrient concentrations of yellow poplar (*Liriodendron tulipifera* Lin.) in a nursery system. *Forest Science and Technology, 12*(3), 137-143. https://doi.org/10.1080/21580103.2015.1135827

Havlin, J. L. (2005). Fertility. In *Encyclopedia of Soils in the Environme*nt (pp. 10-19). Elsevier.

Heanes, D. L. (1981). Determination of trace elements in plant materials by a dry-ashing procedure. Part II. Copper, manganese and zinc. *Analyst, 106*(1259), 182-187. https://doi.org/10.1039/AN9810600172

Hernandez, D., Cardell, E., & Zarate, V. (2005). Antimicrobial activity of lactic acid bacteria isolated from Tenerife cheese: initial characterization of plantaricin TF711, a bacteriocin-like substance produced by *Lactobacillus plantarum* TF711. *Journal of Applied Microbiology*, *99*(1), 77-84. https://doi.org/10.1111/j.1365-2672.2005.02576.x

Holland, B. L., Matthews, M. L., Bota, P., Sweetlove, L. J., Long, S. P., & diCenzo, G. C. (2023). A genome-scale metabolic reconstruction of soybean and Bradyrhizobium diazoefficiens reveals the cost–benefit of nitrogen fixation. *New Phytologist.* https://doi.org/10.1111/nph.19203

Jaiswal, S. K., & Dakora, F. D. (2019). Widespread distribution of highly adapted Bradyrhizobium species nodulating diverse legumes in Africa. *Frontiers in microbiology*, *10*, 310. https://doi.org/10.3389/fmicb.2019.00310

Jamil, F., Mukhtar, H., Fouillaud, M., & Dufossé, L. (2022). Rhizosphere signaling: Insights into plant–rhizomicrobiome interactions for sustainable agronomy. *Microorganisms*, *10*(5), 899. https://doi.org/10.3390/microorganisms10050899

Ji, L., Xu, X., Zhang, F., Si, H., Li, L., & Mao, G. (2023). The Preliminary Research on Shifts in Maize Rhizosphere Soil Microbial Communities and Symbiotic Networks under Different Fertilizer Sources. *Agronomy*, *13*(8), 2111. https://doi.org/10.3390/agronomy13082111

Kakar, K., Xuan, T. D., & Khanh, T. D. (2023). Allelopathic Potential of Sweet Sorghum Root Exudates and Identification of the Relevant Allelochemicals. *Agrochemicals*, *2*(1), 96-105. https://doi.org/10.3390/agrochemicals2010007

Kalam, S., Basu, A., Ahmad, I., Sayyed, R. Z., El Enshasy, H. A., Dailin, D. J., & Suriani, N. (2020). Recent understanding of soil Acidobacteria and their ecological significance: A critical review. *Frontiers in Microbiology, 11*, 1-15. https://doi.org/10.3389/fmicb.2020.580024

Kandel, S., Kim, Y., Park, J., & Lee, J. (2019). Nitrogen and phosphorus fertilization effects on bacterial community structure and functional gene diversity of the rice rhizosphere. Frontiers in Microbiology, 10, 1498.

Kathiravan, A., & Gnanadoss, J. J. (2021). White-rot fungi-mediated bioremediation as a sustainable method for xenobiotic degradation. *Environmental and Experimental Biology, 19*(3), 103-119. https://doi.org/10.22364/eeb.19.11

Kavvadias, V., Ioannou, Z., Vavoulidou, E., & Paschalidis, C. (2023). Short Term Effects of Chemical Fertilizer, Compost and Zeolite on Yield of Lettuce, Nutrient Composition and Soil Properties. *Agriculture, 13(5), 1022.* https://doi.org/10.3390/agriculture13051022

Kim, C., Baek, G., Yoo, B. O., Jung, S. Y., & Lee, K. S. (2018). Regular fertilization effects on the nutrient distribution of bamboo components in a moso bamboo (*Phyllostachys pubescens* (Mazel) Ohwi) stand in South Korea. *Forests, 9*(11), 1-12. https://doi.org/10.3390/f9110671

Kim, S. K., Chung, D., Himmel, M. E., Bomble, Y. J., & Westpheling, J. (2016). Heterologous expression of family 10 xylanases from *Acidothermus cellulolyticus* enhances the exoproteome of *Caldicellulosiruptor bescii* and growth on xylan substrates. *Biotechnology for Biofuels*, *9*, 1-10. https://doi.org/10.1186/s13068-016-0588-9

Kojima, H., Tokizawa, R., & Fukui, M. (2014). *Mizugakiibacter sediminis* gen. nov., sp. nov., isolated from a freshwater lake. *International Journal of Systematic and Evolutionary Microbiology*, *64*(Pt_12), 3983-3987. https://doi.org/10.1099/ijs.0.064659-0

Kramer, S., Dibbern, D., Moll, J., Huenninghaus, M., Koller, R., Krueger, D., Marhan, S., Urich, T., Wubet, T., Bonkowski, M., Buscot, F., Leuders, T., & Kandeler, E. (2016). Resource partitioning between bacteria, fungi, and protists in the detritusphere of an agricultural soil. *Frontiers in Microbiology, 7*, 1-12. https://doi.org/10.3389/fmicb.2016.01524

Kumawat, K. C., Sharma, P., Sirari, A., Singh, I., Gill, B. S., Singh, U., & Saharan, K. (2019). Synergism of *Pseudomonas aeruginosa*

DOI:https//doi.org/10.22452/mjs.vol44no2.3
Malaysian Journal of Science 44(2): 18-41 (June 2025)

(LSE-2) nodule endophyte with *Bradyrhizobium* sp. (LSBR-3) for improving plant growth, nutrient acquisition and soil health in soybean. *World Journal of Microbiology and Biotechnology, 35*(3), 1-17. https://doi.org/10.1007/s11274-019-2622-0

Legendre, P., & Gallagher, E. D. (2001). Ecologically meaningful transformations for ordination of species data. *Oecologia*, *129*, 271-280. https://doi.org/10.1007/s004420100716

Lewis, R. W., Barth, V. P., Coffey, T., McFarland, C., Huggins, D. R., & Sullivan, T. S. (2018). Altered bacterial communities in long-term no-till soils associated with stratification of soluble aluminum and soil pH. *Soil Systems, 2*(1), 1-13. https://doi.org/10.3390/soils2010007

Li, F., Chen, L., Zhang, J., Yin, J., & Huang, S. (2017). Bacterial community structure after long-term organic and inorganic fertilization reveals important associations between soil nutrients and specific taxa involved in nutrient transformations. *Frontiers in Microbiology, 8*, 1-12. https://doi.org/10.3389/fmicb.2017.00187

Li, K., Han, X., Ni, R., Shi, G., De-Miguel, S., Li, C., Shen, W., Zhang, Y., & Zhang, X. (2021). Impact of *Robinia pseudoacacia* stand conversion on soil properties and bacterial community composition in Mount Tai, China. *Forest Ecosystems, 8*(1), 1-12. https://doi.org/10.1186/s40663-021-00296-x

Lin, S. Y., Hameed, A., Hsieh, Y. T., Hsu, Y. H., Lai, W. A., & Young, C. C. (2018). *Castellaniella fermenti* sp. nov., isolated from a fermented meal. *International Journal of Systematic and Evolutionary Microbiology, 68*(1), 52-57. https://doi.org/10.1099/ijsem.0.002436

Lin, W., Lin, M., Zhou, H., Wu, H., Li, Z., & Lin, W. (2019). The effects of chemical and organic fertilizer usage on rhizosphere soil in tea orchards. *PloS One, 14*(5), e0217018. https://doi.org/10.1371/journal.pone.0217018

Liu, C., Gong, X., Dang, K., Li, J., Yang, P., Gao, X., Deng, X., & Feng, B. (2020b). Linkages between nutrient ratio and the microbial community in rhizosphere soil following fertilizer management. *Environmental Research, 184*, 109261. https://doi.org/10.1016/j.envres.2020.109261

Liu, J., Ma, Q., Hui, X., Ran, J., Ma, Q., Wang, X., & Wang, Z. (2020a). Long-term high-P fertilizer input decreased the total bacterial diversity but not phoD-harboring bacteria in wheat rhizosphere soil with available-P deficiency. *Soil Biology and Biochemistry*, *149*, 107918. https://doi.org/10.1016/j.soilbio.2020.107918

Liu, K., Cai, M., Hu, C., Sun, X., Cheng, Q., Jia, W., Yang, T., Nie, M., & Zhao, X. (2019). Selenium (Se) reduces *Sclerotinia* stem rot disease incidence of oilseed rape by increasing plant Se concentration and shifting soil microbial community and functional profiles. *Environmental Pollution, 254*, 1-10. https://doi.org/10.1016/j.envpol.2019.113051

Loutet, S. A., Chan, A. C., Kobylarz, M. J., Verstraete, M. M., Pfaffen, S., Ye, B., Arrieta, A. L., & Murphy, M. E. (2021). The fate of intracellular metal ions in microbes.

Lu, X., Heal, K. R., Ingalls, A. E., Doxey, A. C., & Neufeld, J. D. (2020). Metagenomic and chemical characterization of soil cobalamin production. *The ISME Journal*, *14*(1), 53-66. https://doi.org/10.1038/s41396-019-0502-0

Ma, L., Pang, A. P., Luo, Y., Lu, X., & Lin, F. (2020). Beneficial factors for biomineralization by ureolytic bacterium *Sporosarcina pasteurii*. *Microbial Cell Factories*, *19*(1), 1-12. https://doi.org/10.1186/s12934-020-1281-z

Magoč, T., & Salzberg, S. L. (2011). FLASH: fast length adjustment of short reads to improve genome assemblies. *Bioinformatics, 27*(21), 2957-2963. https://doi.org/10.1093/bioinformatics/btr507

Malaysian Standard [MS] (1980). *MS 678–Recommended methods for soil chemical analysis: Part I–V*. Shah Alam: Standards and Industrial Research Institute of Malaysia.

Mallhi, Z. I., Rizwan, M., Mansha, A., Ali, Q., Asim, S., Ali, S., Hussain, A., Alrokayan, S. H., Khan, H. A., Alam, P., & Ahmad, P. (2019). Citric acid enhances plant growth, photosynthesis, and phytoextraction of lead by alleviating the oxidative stress in castor beans. *Plants, 8*(11), 525. https://doi.org/10.3390/plants8110525

Mandakovic, D., Aguado-Norese, C., García-Jiménez, B., Hodar, C., Maldonado, J. E., Gaete, A., Latorre, M., Wilkinson, M. D., Gutiérrez, R. A., Cavierres, L. A., Medina, J., Cambiazo, V., & Gonzalez, M. (2023). Testing the stress gradient hypothesis in soil bacterial communities associated with vegetation belts in the Andean Atacama Desert. *Environmental Microbiome, 18*(1), 1-17. https://doi.org/10.1186/s40793-023-00486-w

Mao, X., Xu, X., Lu, K., Gielen, G., Luo, J., He, L., Donnison, A., Xu, Z., Xu, J., Yang, W., Song, Z., & Wang, H. (2015). Effect of 17 years of organic and inorganic fertilizer applications on soil phosphorus dynamics in a rice–wheat rotation cropping system in eastern China. *Journal of Soils and Sediments, 15*(9), 1889-1899. https://doi.org/10.1007/s11368-015-1137-z

Matejovic, I. (1993). Determination of carbon, hydrogen, and nitrogen in soils by automated elemental analysis (dry combustion method). *Communications in Soil Science and Plant Analysis, 24*(17-18), 2213-2222. https://doi.org/10.1080/00103629309368950

DOI:https//doi.org/10.22452/mjs.vol44no2.3
Malaysian Journal of Science 44(2): 18-41 (June 2025)

McDonald, D., Price, M. N., Goodrich, J., Nawrocki, E. P., DeSantis, T. Z., Probst, A., Andersen, G. L., Knight, R., & Hugenholtz, P. (2012). An improved Greengenes taxonomy with explicit ranks for ecological and evolutionary analyses of bacteria and archaea. *The ISME Journal, 6*(3), 610-618. https://doi.org/10.1038/ismej.2011.139

McMurdie, P. J., & Holmes, S. (2013). Phyloseq: An R Package for Reproducible Interactive Analysis and Graphics of Microbiome Census Data. *PLoS One*, *8*(4), 1–11. https://doi.org/10.1371/journal.pone.0061217

McNear Jr., D. H. (2013) The Rhizosphere - Roots, Soil and Everything In Between. Nature Education Knowledge 4(3), 1. https://www.nature.com/scitable/knowledge/library/the-rhizosphere-roots-soil-and-67500617/ (accessed 22 February 2023)

Merchant, S. S., & Helmann, J. D. (2012). Elemental economy: microbial strategies for optimizing growth in the face of nutrient limitation. *Advances in Microbial Physiology, 60*, 91-210. https://doi.org/10.1016/B978-0-12-398264-3.00002-4

Morcillo, R. J., & Manzanera, M. (2021). The effects of plant-associated bacterial exopolysaccharides on plant abiotic stress tolerance. *Metabolites*, *11*(6), 337. https://doi.org/10.3390/metabo11060337

Morigasaki, S., Matsui, M., Ohtsu, I., Doi, Y., Kawano, Y., Nakai, R., Iwasaki, W., Hayashi, H., & Takaya, N. (2024). Temporal and fertilizer-dependent dynamics of soil bacterial communities in buckwheat fields under long-term management. *Scientific Reports, 14*(1), 9896. https://doi.org/10.1038/s41598-024-60655-w

MPOB (2022a). Malaysian Oil Palm Statistics 2021. 41st edition. MPOB, Bangi

MPOB (2022b). Review of the Malaysian Oil Palm Industry 2021. MPOB, Bangi.

Murphy, D. J., Goggin, K., & Paterson, R. R. M. (2021). Oil palm in the 2020s and beyond: challenges and solutions. *CABI Agriculture and Bioscience*, *2*(1), 1–22. https://doi.org/10.1186/s43170-021-00058-3

Ndabankulu, K., Egbewale, S. O., Tsvuura, Z., & Magadlela, A. (2022). Soil microbes and associated extracellular enzymes largely impact nutrient bioavailability in acidic and nutrient poor grassland ecosystem soils. *Scientific Reports, 12(1), 12601.* https://doi.org/10.1038/s41598-022-16949-y

Ng, J. F., Ahmed, O. H., Jalloh, M. B., Omar, L., Kwan, Y. M., Musah, A. A., & Poong, K. H. (2022). Soil nutrient retention and pH buffering capacity are enhanced by calciprill and sodium silicate. *Agronomy, 12*(1), 219. https://doi.org/10.3390/agronomy12010219

Noble, A. S., Noe, S., Clearwater, M. J., & Lee, C. K. (2020). A core phyllosphere microbiome exists across distant populations of a tree species indigenous to New Zealand. *PLoS One*, *15*(8), e0237079. https://doi.org/10.1371/journal.pone.0237079

O'Brien, F. J., Dumont, M. G., Webb, J. S., & Poppy, G. M. (2018). Rhizosphere bacterial communities differ according to fertilizer regimes and cabbage (*Brassica oleracea* var. capitata L.) harvest time, but not aphid herbivory. *Frontiers in Microbiology, 9*, 1620. https://doi.org/10.3389/fmicb.2018.01620

Ogola, H. J. O., Selvarajan, R., & Tekere, M. (2021). Local geomorphological gradients and land use patterns play key role on the soil bacterial community diversity and dynamics in the highly endemic indigenous afrotemperate coastal scarp forest biome. *Frontiers in Microbiology*, *12*, 592725. https://doi.org/10.3389/fmicb.2021.592725

Oksanen, J. (2015). Vegan: an introduction to ordination. URL http://cran. r-project. org/web/packages/vegan/vignettes/introvegan. pdf, 8, 1-19.

Parks, D. H., Tyson, G. W., Hugenholtz, P., & Beiko, R. G. (2014). STAMP: Statistical analysis of taxonomic and functional profiles. *Bioinformatics*, *30*(21), 3123–3124. https://doi.org/10.1093/bioinformatics/btu494

Piccoli, P., & Bottini, R. (2013). Terpene production by bacteria and its involvement in plant growth promotion, stress alleviation, and yield increase. *Molecular Microbial Ecology of the Rhizosphere, 1,* 335-343. https://doi.org/10.1002/9781118297674.ch31

Pirker, J., Mosnier, A., Kraxner, F., Havlík, P., & Obersteiner, M. (2016). What are the limits to oil palm expansion? *Global Environmental Change*, *40*, 73–81. https://doi.org/10.1016/j.gloenvcha.2016.06.007

Price, G. W., Langille, M. G., & Yurgel, S. N. (2021). Microbial co-occurrence network analysis of soils receiving short-and long-term applications of alkaline treated biosolids. *Science of The Total Environment, 751*, 1-11. https://doi.org/10.1016/j.scitotenv.2020.141687

Qiu, L., Zhang, Q., Zhu, H., Reich, P. B., Banerjee, S., van der Heijden, M. G. A., Sadowsky, M. J., Ishii, S., Jia, X., Shao, M., Liu, B., Jiao, H., Li, H., & Wei, X. (2021). Erosion reduces soil microbial diversity, network complexity and multifunctionality. *The ISME Journal*, *15*(8), 2474-2489. https://doi.org/10.1038/s41396-021-00913-1

Quast, C., Pruesse, E., Yilmaz, P., Gerken, J., Schweer, T., Yarza, P., Peplies, J., & Glöckner, F. O. (2012). The SILVA ribosomal RNA

DOI:https//doi.org/10.22452/mjs.vol44no2.3
Malaysian Journal of Science 44(2): 18-41 (June 2025)

gene database project: improved data processing and web-based tools. *Nucleic Acids Research, 41*(D1), D590-D596. https://doi.org/10.1093/nar/gks1219

Rawat, S. R., Männistö, M. K., Bromberg, Y., & Häggblom, M. M. (2012). Comparative genomic and physiological analysis provides insights into the role of Acidobacteria in organic carbon utilization in Arctic tundra soils. *FEMS Microbiology Ecology, 82*(2), 341-355. https://doi.org/10.1111/j.1574-6941.2012.01381.x

Ren, D., Madsen, J. S., Sørensen, S. J., & Burmølle, M. (2015). High prevalence of biofilm synergy among bacterial soil isolates in cocultures indicates bacterial interspecific cooperation. *The ISME Journal, 9*(1), 81-89. https://doi.org/10.1038/ismej.2014.96

Ren, H., Wang, H., Qi, X., Yu, Z., Zheng, X., Zhang, S., Wang, Z., Zhang, M., Ahmed, T., & Li, B. (2021). The damage caused by decline disease in bayberry plants through changes in soil properties, rhizosphere microbial community structure and metabolites. *Plants*, *10*(10), 2083. https://doi.org/10.3390/plants10102083

Ren, M., Zhang, Z., Wang, X., Zhou, Z., Chen, D., Zeng, H., Zhao, S., Chen, L., Hu, Y., Zhang, C., Liang, Y., She, Q., Zhang, Y., & Peng, N. (2018). Diversity and contributions to nitrogen cycling and carbon fixation of soil salinity shaped microbial communities in Tarim Basin. *Frontiers in Microbiology, 9*, 1-14. https://doi.org/10.3389/fmicb.2018.00431

Sakoula, D., Koch, H., Frank, J., Jetten, M. S., van Kessel, M. A., & Lücker, S. (2021). Enrichment and physiological characterization of a novel comammox *Nitrospira* indicates ammonium inhibition of complete nitrification. *The ISME Journal, 15*(4), 1010-1024. https://doi.org/10.1038/s41396-020-00827-4

Segata, N., Izard, J., Waldron, L., Gevers, D., Miropolsky, L., Garrett, W. S., & Huttenhower, C. (2011). Metagenomic biomarker discovery and explanation. *Genome Biology*, *12*(6), 1–18. https://doi.org/doi.org/10.1186/gb-2011-12-6-r60

Selim, M. S. M., Abdelhamid, S. A., & Mohamed, S. S. (2021). Secondary metabolites and biodiversity of actinomycetes. *Journal of Genetic Engineering and Biotechnology*, *19*(1), 72. https://doi.org/10.1186/s43141-021-00156-9

Semenov, M. V., Krasnov, G. S., Semenov, V. M., & van Bruggen, A. H. (2020). Long-term fertilization rather than plant species shapes rhizosphere and bulk soil prokaryotic communities in agroecosystems. *Applied Soil Ecology*, *154*, 103641. https://doi.org/10.1016/j.apsoil.2020.103641

Seraj, M. F., Rahman, T., Lawrie, A. C., & Reichman, S. M. (2020). Assessing the plant growth promoting and arsenic tolerance potential of *Bradyrhizobium japonicum* CB1809. *Environmental Management, 66*(5), 930-939. https://doi.org/10.1007/s00267-020-01351-z

Shannon, P., Markiel, A., Ozier, O., Baliga, N. S., Wang, J. T., Ramage, D., Amin, N., Schwikowski, B., & Ideker, T. (2003). Cytoscape: A Software Environment for Integrated Models. *Genome Research*, *13*(11), 24980–2504. https://doi.org/10.1101/gr.1239303.metabolite

Shen, G., Zhang, S., Liu, X., Jiang, Q., & Ding, W. (2018). Soil acidification amendments change the rhizosphere bacterial community of tobacco in a bacterial wilt affected field. *Applied Microbiology and Biotechnology, 102*, 9781-9791. https://doi.org/10.1007/s00253-018-9347-0

Shi, Y., Qiu, L., Guo, L., Man, J., Shang, B., Pu, R., Ou, X., Dai, C., Liu, P., Yang, Y., & Cui, X. (2020). K fertilizers reduce the accumulation of Cd in *Panax notoginseng* (Burk.) FH by improving the quality of the microbial community. *Frontiers in Plant Science*, *11*, 888. https://doi.org/10.3389/fpls.2020.00888

Singh, B. K., Jha, B., Tripathi, S., Singh, D. K., & Trivedi, P. (2018). Impact of long-term fertilizer application on rhizosphere bacterial community structure of wheat and barley. MicrobiologyOpen, 7(5), e00637.

Sinong, G. F., Yasuda, M., Nara, Y., Lee, C. G., Dastogeer, K. M. G., Tabuchi, H., Nakai, H., Djedidi, S., & Okazaki, S. (2021). Distinct root microbial communities in nature farming rice harbor bacterial strains with plant growth-promoting traits. *Frontiers in Sustainable Food Systems*, *4*, 629942. https://doi.org/10.3389/fsufs.2020.629942

Song, J., Min, L., Wu, J., He, Q., Chen, F., & Wang, Y. (2021). Response of the microbial community to phosphate-solubilizing bacterial inoculants on *Ulmus chenmoui* Cheng in Eastern China. *Plos One, 16*(2), e0247309. https://doi.org/10.1371/journal.pone.0247309

Su, X., Li, S., Cai, J., Xiao, Y., Tao, L., Hashmi, M. Z., Lin, H., Chen, J., Mei, R., & Sun, F. (2019). Aerobic degradation of 3, 3', 4, 4'-tetrachlorobiphenyl by a resuscitated strain *Castellaniella* sp. SPC4: kinetics model and pathway for biodegradation. *Science of the Total Environment*, *688*, 917-925. https://doi.org/10.1016/j.scitotenv.2019.06.364

Svenningsen, N. B., Watts-Williams, S. J., Joner, E. J., Battini, F., Efthymiou, A., Cruz-Paredes, C., Nybroe, O., & Jakobsen, I. (2018). Suppression of the activity of arbuscular mycorrhizal fungi by the soil microbiota. *The ISME Journal, 12*(5), 1296-1307. https://doi.org/10.1038/s41396-018-0059-3

DOI:https//doi.org/10.22452/mjs.vol44no2.3
Malaysian Journal of Science 44(2): 18-41 (June 2025)

Tandon, H. L. S., Cescas, M. P., & Tyner, E. H. (1968). An acid-free vanadate-molybdate reagent for the determination of total phosphorus in soils. *Soil Science Society of America Journal, 32*(1), 48-51. https://doi.org/10.2136/sssaj1968.03615995003200010012x

Tang, S., Zhou, J., Pan, W., Sun, T., Liu, M., Tang, R., Li, Z., Ma, Q., & Wu, L. (2023). Effects of combined application of nitrogen, phosphorus, and potassium fertilizers on tea (*Camellia sinensis*) growth and fungal community. *Applied Soil Ecology, 181*, 104661. https://doi.org/10.1016/j.apsoil.2022.104661

Tarmizi, A. M., & Mohd Tayeb, D. (2006). Nutrient demands of *tenera* oil palm planted on inland soil of Malaysia. *Journal of Oil Palm Research, 18*, 204.

Tebo, B. M., Davis, R. E., Anitori, R. P., Connell, L. B., Schiffman, P., & Staudigel, H. (2015). Microbial communities in dark oligotrophic volcanic ice cave ecosystems of Mt. Erebus, Antarctica. *Frontiers In Microbiology*, *6*, 179. https://doi.org/10.3389/fmicb.2015.00179

Tkaczyk, P., Mocek-Płóciniak, A., Skowrońska, M., Bednarek, W., Kuśmierz, S., & Zawierucha, E. (2020). The mineral fertilizer-dependent chemical parameters of soil acidification under field conditions. *Sustainability, 12*(17), 1-11. https://doi.org/10.3390/su12177165

van der Ploeg, R. R., Böhm, W., & Kirkham, M. B. (1999). On the origin of the theory of mineral nutrition of plants and the law of the minimum. *Soil Science Society of America Journal*, *63*(5), 1055-1062. https://doi.org/10.2136/sssaj1999.6351055x

Verma, P., & Rawat, S. (2021). Rhizoremediation of heavy metal- and xenobiotic-contaminated soil: an eco-friendly approach. *Removal of Emerging Contaminants Through Microbial Processes*, 95-113. https://doi.org/10.1007/978-981-15-5901-3_5

Vives-Peris, V., De Ollas, C., Gómez-Cadenas, A., & Pérez-Clemente, R. M. (2020). Root exudates: from plant to rhizosphere and beyond. *Plant Cell Reports, 39*, 3-17. https://doi.org/10.1007/s00299-019-02447-5

Wang, M., Xu, Y., Ni, H., Ren, S., Li, N., Wu, Y., Yang, Y., Liu, Y., Liu, Z., Liu, Y., Shi, J., Zhang, Y., Jiang, L., & Tu, Q. (2023). Effect of fertilization combination on cucumber quality and soil microbial community. *Frontiers in Microbiology*, *14*, 1122278. https://doi.org/10.3389/fmicb.2023.1122278

Wang, Q., Jiang, X., Guan, D., Wei, D., Zhao, B., Ma, M., Chen, S., Li, L., Cao, F., & Li, J. (2018). Long-term fertilization changes bacterial diversity and bacterial communities in the maize rhizosphere of Chinese Mollisols. *Applied Soil Ecology, 125*, 88-96. https://doi.org/10.1016/j.apsoil.2017.12.007

Wang, W., Yang, Y., Li, J., Bu, P., Lu, A., Wang, H., He, W., Bermudez, R. S., & Feng, J. (2024). Consecutive Fertilization-Promoted Soil Nutrient Availability and Altered Rhizosphere Bacterial and Bulk Fungal Community Composition. *Forests, 15*(3), 514. https://doi.org/10.3390/f15030514

Wang, Y., Zhang, L., Zhang, X., Wang, S., & Zhou, J. (2015). Nitrogen fertilization alters bacterial community structure and diversity in the soybean rhizosphere. *Applied and Environmental Microbiology, 81*(20), 7113-7121.

Wanke, A., Malisic, M., Wawra, S., & Zuccaro, A. (2021). Unraveling the sugar code: the role of microbial extracellular glycans in plant–microbe interactions. *Journal of Experimental Botany, 72*(1), 15-35. https://doi.org/10.1093/jxb/eraa414

Ward, N. L., Challacombe, J. F., Janssen, P. H., Henrissat, B., Coutinho, P. M., Wu, M., Xie, G., Haft, D. H., Sait, M., Badger, J., Barabote, R. D., Bradley, B., Brettin, T. S., Brinkac, L. M., Bruce, D., Creasy, T., Daugherty, S. C., Davidsen, T. M., DeBoy, R. T., Detter, J. C., Dodson, R. J., Durkin, A. S., Ganapathy, A., Gwinn-Giglio, M., Han, C. S., Khouri, H., Kiss, H., Kothari, S. P., Madupu, R., Nelson, K. E., Nelson, W. C., Paulsen, I., Penn, K., Ren, Q., Rosovitz, M. J., Selengut, J. D., Shrivastava, S., Sullivan, S. A., Tapia, R., Thompson, L. S., Watkins, K. L., Yang, Q., Yu, C., Zafar, N., Zhou, L., & Kuske, C. R. (2009). Three genomes from the phylum Acidobacteria provide insight into the lifestyles of these microorganisms in soils. *Applied and Environmental Microbiology*, *75*(7), 2046-2056. https://doi.org/10.1128/AEM.02294-08

Wei, W., Yang, M., Liu, Y., Huang, H., Ye, C., Zheng, J., Guo, C., Hao, M., He, X., & Zhu, S. (2018). Fertilizer N application rate impacts plant-soil feedback in a sanqi production system. *Science of the Total Environment*, *633*, 796-807. https://doi.org/10.1016/j.scitotenv.2018.03.219

Wen, T., Yu, G. H., Hong, W. D., Yuan, J., Niu, G. Q., Xie, P. H., Sun, F. S., Guo, L. D., Kuzyakov, Y., & Shen, Q. R. (2022). Root exudate chemistry affects soil carbon mobilization via microbial community reassembly. *Fundamental Research, 2*(5), 697-707. https://doi.org/10.1016/j.fmre.2021.12.016

Wieland, G., Neumann, R., & Backhaus, H. (2001). Variation of Microbial Communities in Soil, Rhizosphere, and Rhizoplane in Response to Crop Species, Soil Type, and Crop Development. *Applied and Environmental Microbiology*, *67*(12), 5849–5854. https://doi.org/10.1128/AEM.67.12.5849-5854.2001

Wu, W., Wang, X., Ren, Z., Zhou, X., & Du, G. (2022). N-Induced Species Loss Dampened by Clipping Mainly Through Suppressing Dominant Species in an Alpine Meadow. *Frontiers in Plant Science, 13*, 815011. https://doi.org/10.3389%2Ffpls.2022.815011

DOI:https//doi.org/10.22452/mjs.vol44no2.3
Malaysian Journal of Science 44(2): 18-41 (June 2025)

Xu, A., Li, L., Xie, J., Zhang, R., Luo, Z., Cai, L., Liu, C., Wang, L., Anwar, S., & Jiang, Y. (2022). Bacterial Diversity and Potential Functions in Response to Long-Term Nitrogen Fertilizer on the Semiarid Loess Plateau. *Microorganisms*, *10*(8), 1579. https://doi.org/10.3390/microorganisms10081579

Xu, Q., Ling, N., Chen, H., Duan, Y., Wang, S., Shen, Q., & Vandenkoornhuyse, P. (2020). Long-term chemical-only fertilization induces a diversity decline and deep selection on the soil bacteria. *Msystems*, *5*(4), e00337-20. https://doi.org/10.1128/mSystems.00337-20

Yang, L., Sun, R., Li, J., Zhai, L., Cui, H., Fan, B., Wang, H., & Liu, H. (2023). Combined organic-inorganic fertilization builds higher stability of soil and root microbial networks than exclusive mineral or organic fertilization. *Soil Ecology Letters, 5(2), 220142.* https://doi.org/10.1007/s42832-022-0142-6

Yang, L., Sun, R., Li, J., Zhai, L., Cui, H., Fan, B., Wang, H., & Liu, H. (2021). Organic-inorganic fertilization built higher stability of soil and root microbial networks than exclusive mineral or organic fertilization. *ResearchSquare*, 1-26. https://doi.org/10.21203/rs.3.rs-652488/v1

Yin, X., Li, T., Jiang, X., Tang, X., Zhang, J., Yuan, L., & Wei, Y. (2022). Suppression of grape white rot caused by *Coniella vitis* using the potential biocontrol agent *Bacillus Velezensis* GSBZ09. *Pathogens*, *11*(2), 248. https://doi.org/10.3390/pathogens11020248

Yu, Z., Hu, X., Wei, D., Liu, J., Zhou, B., Jin, J., Liu, X., & Wang, G. (2019). Long-term inorganic fertilizer use influences bacterial communities in Mollisols of Northeast China based on high-throughput sequencing and network analyses. *Archives of Agronomy and Soil Science*. 1-13. https://doi.org/10.1080/03650340.2018.1563685

Zegeye, E. K., Brislawn, C. J., Farris, Y., Fansler, S. J., Hofmockel, K. S., Jansson, J. K., Wright, A. T., Graham, E. B., Naylor, D., McClure, R. S., & Bernstein, H. C. (2019). Selection, succession, and stabilization of soil microbial consortia. *Msystems, 4*(4), 1-13. https://doi.org/10.1128/mSystems.00055-19

Zhang, C., Song, Z., Zhuang, D., Wang, J., Xie, S., & Liu, G. (2019a). Urea fertilization decreases soil bacterial diversity, but improves microbial biomass, respiration, and N-cycling potential in a semiarid grassland. *Biology and Fertility of Soils*, *55*(3), 229-242. https://doi.org/10.1007/s00374-019-01344-z

Zhang, Q., Li, Y., He, Y., Liu, H., Dumont, M. G., Brookes, P. C., & Xu, J. (2019b). *Nitrosospira* cluster 3-like bacterial ammonia oxidizers and *Nitrospira*-like nitrite oxidizers dominate nitrification activity in acidic terrace paddy soils. *Soil Biology and Biochemistry*, *131*, 229-237. https://doi.org/10.1016/j.soilbio.2019.01.006

Zhao, F., Guo, X. Q., Wang, P., He, L. Y., Huang, Z., & Sheng, X. F. (2013). *Dyella jiangningensis* sp. nov., a γ-proteobacterium isolated from the surface of potassium-bearing rock. *International Journal of Systematic and Evolutionary Microbiology, 63(Pt_9),* 3154-3157. https://doi.org/10.1099/ijs.0.048470-0

Zhao, Z., Zhao, R., Qiu, X., Wan, Y., & Lee, L. (2022). Structural Diversity of Bacterial Communities and Its Relation to Environmental Factors in the Surface Sediments from Main Stream of Qingshui River. *Water, 14*(21), 3356. https://doi.org/10.3390/w14213356

Zheng, B. X., Bi, Q. F., Hao, X. L., Zhou, G. W., & Yang, X. R. (2017). *Massilia phosphatilytica* sp. nov., a phosphate solubilizing bacteria isolated from a long-term fertilized soil. *International Journal of Systematic and Evolutionary Microbiology, 67*(8), 2514-2519. https://doi.org/10.1099/ijsem.0.001916

Zhou, J., Jiang, X., Zhou, B., Zhao, B., Ma, M., Guan, D., Li, J., Chen, S., Cao, F., Shen, D., & Qin, J. (2016). Thirty four years of nitrogen fertilization decreases fungal diversity and alters fungal community composition in black soil in northeast China. *Soil Biology and Biochemistry, 95*, 135-143. https://doi.org/10.1016/j.soilbio.2015.12.012

Zhou, Z., Tran, P. Q., Kieft, K., & Anantharaman, K. (2020). Genome diversification in globally distributed novel marine Proteobacteria is linked to environmental adaptation. *The ISME Journal, 14*(8), 2060-2077. https://doi.org/10.1038/s41396-020-0669-4

Zhou, Z., Yan, T., Zhu, Q., Bu, X., Chen, B., Xue, J., & Wu, Y. (2019). Bacterial community structure shifts induced by biochar amendment to karst calcareous soil in southwestern areas of China. *Journal of Soils and Sediments*, *19*, 356-365. https://doi.org/10.1007/s11368-018-2035-y

Zhu, S., Vivanco, J. M., & Manter, D. K. (2016). Nitrogen fertilizer rate affects root exudation, the rhizosphere microbiome and nitrogen-use-efficiency of maize. *Applied Soil Ecology, 107*, 324-333. https://doi.org/10.1016/j.apsoil.2016.07.009

DOI:https//doi.org/10.22452/mjs.vol44no2.3
Malaysian Journal of Science 44(2): 18-41 (June 2025)

MALAYSIAN JOURNAL OF SCIENCE
MJS
ISSN 1394-3065

Regular Issue

Malaysian Journal of Science 44 (2): 42-51 (June 2025) https://mjs.um.edu.my

The Potential of the *Spatholobus littoralis* Hassk Plant as an Antioxidant and Prediction of the Mechanism of Activity Against ROS1 Kinase Receptor in Silico

Sri Atun[1a*], Nurfina Aznam[2a], Rasningtyaswati[3a], Putri Verdiana Dwi Cahyani[4a], Lusiana Qotimatul Izah[5a], Wiwid Deswantari Danarjati[6a] and Adity Sangal[7b]

Abstract: Various phenolic compounds that exhibit antioxidant, anticancer, and anti-inflammatory activities are found in *Spatholobus.* Therefore, this study aimed to determine the antioxidant potential of *Spatholobus littoralis* wood in vitro and predict the mechanism of its activity against the ROS1 kinase receptor in silico. The ground-dried wood of *S. littoralis* was extracted with ethanol via maceration. The analysis of the total phenolic content (TPC) of extracts and fractions obtained from *S. littoralis* wood was determined by the Folin-Ciocalteu reagent. Similarly, the antioxidant activity was determined by the DPPH (2,2-diphenyl-1-picrylhydrazyl) and FRAP (The ferric reducing antioxidant power) method. The human ROS1 kinase enzyme (4UXL and 3ZBF) was used to determine the molecular mechanism of the interaction from the genus *Spatholobus* in silico. The total ethanol extract, chloroform, and ethyl acetate fraction of *S. littoralis* showed a high content of phenolic compounds and antioxidant activity. Phenolic compounds in plants of the genus *Spatholubus* also showed good activity against ROS1 kinase receptors (3ZBF and 4UXL). In conclusion, the *S. littoralis* plant has the potential to be developed for the discovery of new drugs.

Keywords: *Spatholobus littoralis Hassk, antioxidant, ROS1 kinase receptors, In silico.*

1. Introduction

Spatholobus littoralis Hassk, known locally as Bajakah Tempala, is a plant that climbs on wood trees from the Phaseoleae tribe. This genus was discovered in 1842 by a German botanist and had 28 species that grow in the tropical forests of Indonesia (Ridder-Numan & Wiriadinata, 1985). Ethnopharmacologically, bajakah wood is used in traditional medicine in Kalimantan (Istiqomah & Safitri, 2021). Several studies have shown the pharmacological activities, such as anticancer (Aliviyanti et al., 2021), anti-inflammatory (Nastiti & Nugraha, 2022), antidiabetic (Arysanti et al., 2022) antioxidant (Fitriani et al., 2020; Iskandar et al., 2022), and antihepatotoxic (Adhityasmara & Ramonah, 2022). Furthermore, the chemical content of this genus *Spatholobus* generally contains flavonoids and tannins (Fitriani et al., 2020), phenolics (Iskandar et al., 2022), and steroids (Astuti et al., 2014). A previous study reported that the flavonoid compounds contained in *Spatholobus suberectus* included flavones, flavanones, chalcones, isoflavanes, and isoflavones (Liu et al., 2018; Peng et al., 2019). Some of these flavonoid compounds contain anti-inflammatory and inhibitory tyrosinase activity (Liu et al., 2018) and are cytotoxic against breast cancer cell lines (Peng et al., 2019), antioxidant and anticancer (Li et al., 2015). In silico studies on several compounds from the *Spatholobus* also showed anticancer (Tejasari et al., 2022) and anti-psoriasis (Prasetyorini et al., 2022) activity.

The search for new drugs from natural ingredients is not only based on empirical data but also computational methods to predict the pharmacokinetic and toxicological properties through an in silico study. This method is also beneficial to understanding the interaction between compounds and molecular targets and facilitates the testing of all interactions experimentally (Fang et al., 2018). The strength of the binding affinity can be determined by the Gibbs free energy value (ΔG kcal/mol) (Bajorath, 2015). Gibbs free energy minimizes the thermodynamic potential when a system reaches equilibrium at constant pressure and temperature. Furthermore, Gibbs energy value shows the spontaneity of a molecule or compound to bind to a receptor or target protein. A value of less than zero (0) shows that the bond between the compound and the target protein occurs spontaneously (Hill & Reilly, 2008).

Many studies are currently using ROS1 kinase as a target for new drug discovery. ROS1 kinase plays an essential role in several cellular processes, such as apoptosis, survival, cell migration, and transformation in various malignancies, including colorectal cancer, inflammatory myofibroblast tumors, ovarian cancer, and lung cancer cells (Vanajothi et al., 2022). The human ROS1 kinase receptors used were PDB 4UXL and 3ZBF. This study was conducted to determine the total phenolic content of extracts and wood fractions of *S. littoralis* plant stems and test the activity as antioxidants using the DPPH (1,1-diphenyl-2-picrylhydrazine) and the FRAP (The ferric reducing antioxidant power) methods. The mechanism activity against ROS1 receptor kinase in silico was also predicted.

Authors information:
[a]Department Chemistry Education, Faculty of Mathematics and Natural Science, Universitas Negeri Yogyakarta, Jl. Colombo No.1 Depok, Sleman, Yogyakarta, 55281, INDONESIA. E-mail: sriatun@uny.ac.id[1]; nurfina_aznam@uny.ac.id[2]; rasningtyaswati.2019@student.uny.ac.id[3]; putriverdiana.2020@student.uny.ac.id[4]; lusiana0540fmipa.2020@student.uny.ac.id[5]; wiwiddeswantari.2020@student.uny.ac.id
[b]Department of Chemistry, Amity Institute of Applied Sciences, Amity University, Noida (U.P.) INDIA. E-mail: asangal@amity.edu[7]
*Corresponding Author: sriatun@uny.ac.id

Received: November, 2023
Accepted: May, 2024
Published: June 30, 2025

DOI:https//doi.org/10.22452/mjs.vol44no2.4
Malaysian Journal of Science 44(2): 42-51 (June 2025)

2. Method

Apparatus and Reagent

Glassware, analytical balance, evaporator Buchi Rotavapor R-114, and UV-Vis spectrophotometer were commonly used in this work. Powder and dryed of *S. littoralis*, ethanol, ascorbic acid, chloroform, *n*-hexan, ethyl acetic, aquadest, 1,1-diphenyl-2-picrylhydrazyl (DPPH, Aldrich), and gallic acid, were purchased and used without further purification. A hardware computer with Intel Xeon CPU specifications, 32 Gb RAM, 10 cores, and 500 Gb SSD was used. The software used AutoDock Tools 1.5.7, Pymol, Avogadro 2.0, LigPlot+2.2.8, and GIMP 2.0.

Preparation Extract and Fraction of *S. littoralis*

The wood of *S. littoralis* was obtained from the Pontianak, Indonesia market. The Faculty of Biology of Gadjah Mada University, Indonesia staff identified the plant, which confirmed that it is *Spatholobus littoralis* Hassk. The milled dried steam of *S. littoralis* (3 kg) was extracted exhaustively with ethanol by maceration for 24 hours. The extract was fractionated using solvents with increasing polarity, starting from *n*-hexane, chloroform, and ethyl acetate (Abubakar & Haque, 2020).

Phytochemical Screening

Phytochemical qualitative analysis of extracts and fractions obtained from the wood of the *S. littoralis* plant was carried out using reagents for the terpenoid, alkaloid, phenolic, and saponin tests. Terpenoid and steroid tests were carried out with the Salkowski reagent. Meanwhile, alkaloid, phenolic, and foam tests were carried out with Wagner reagent, iron (III) chloride, and saponins, respectively (Harborne, 1998).

Analysis of Total Phenolic Content (TPC)

Analysis of the TPC of extracts and fractions from *S. littoralis* wood was determined using the Folin-Ciocalteu procedure (Hagerman et al., 2000). The sample was reacted with Folin-Ciocalteu reagent and sodium carbonate solution. The tube was vortexed and heated at 50°C for 10 minutes, and the absorbance of the resulting blue mixture was recorded at 725 nm against a blank containing only solvent. Each sample and blank were replicated three times (n=3). Gallic acid was dissolved in ethanol at various concentrations, and absorbance was measured at the same wavelength. TPC was calculated as gallic acid equivalent (GAE) from a calibration curve of the relationship between absorbance and concentration.

Determination of Antioxidant Activity Using the DPPH Method

The antioxidant activity of each extract and wood fraction of *S. littoralis* was determined using the DPPH (2,2-diphenyl-1-picrylhydrazyl) method (Atun et al., 2018). In this method, DPPH is the source of free radicals and each sample was dissolved in ethanol at various concentrations. Each solution was then added with DPPH reagent and stored in a dark place at room temperature for 30 minutes. Three replications (n=3) of the data were collected for the absorbance which was measured at a wavelength of 516 nm using a spectrophotometer. Antioxidant activity was calculated as the percentage of DPPH that decreased compared to the control. In this study, antioxidant activity was expressed as IC_{50}.

Determination of Antioxidant Activity using FRAP (The Ferric Reducing Antioxidant Power)

The FRAP test was based on the ability to reduce yellow iron (containing Fe^{3+}) to blue iron complexes (containing Fe^{2+}) due to its reaction with electron-donating antioxidants in an acidic medium. The antioxidant test method with FRAP free radicals used is a modification of the procedure reported by Kumar (2012). The sample was dissolved in ethanol at a certain concentration, then 1 mL was taken, 1 mL of 0.2 M phosphate buffer (pH 6.6), and 1 mL of 1% $K_3Fe(CN)_6$ were added, then incubated for 20 minutes at 50° C. Furthermore, 1 mL of TCA was added after incubation and centrifuged at 3000 rpm for 10 minutes. After centrifugation, pipette 1 mL of the top layer into a test tube, and add 1 mL of distilled water and 0.5 mL of 0.1% $FeCl_3$. The solution was left for 10 minutes and the absorbance was measured at 720 nm. A mixture of solutions without samples was used as a blank. Calibration curves were prepared using ascorbic acid solutions with various concentrations. FRAP values were expressed in mg ascorbic acid equivalent/g sample.

Prediction of the Mechanism of Activity Against ROS1 Kinase Receptors in Silico

Phenolic compounds from plants of the genus *Spathollobus* were obtained from data on the KNApSAcK website (http://www.knapsackfamily.com/knapsack_core/top.php) and information on the composition of flavonoid compounds from the *S. littoralis* plant (Sianipar et al., 2023). However, only 14 phenolic compounds most commonly found in the *Spathollobus* were selected, namely dihydroquercetin, butin, (-)-epicatechin, eriodictyol, liquiritigenin, prunasin, afromosin, cajanin, formononetin, 3',4',7-trihydroxyflavone, licochalcone A, (+)-dihydrokaempferol, plathymenin, and 6-methoxyeriodictyol. The 3D structure was obtained from PubChem (https://pubchem.ncbi.nlm.nih.gov/) and stabilized using Avogadro 2.0. Subsequently, the 3D structure of each compound was created in a pdb file using the Pymol software and converted into a pdbqt file using AutodockTools1.5.7 software.

The human ROS1 kinase enzyme protein structures (PDB IDs: 4UXL and 3ZBF) were retrieved from the Protein Data Bank (www.pdb.org) to predict the molecular interaction mechanisms between phenolic compounds from the genus *Spatholobus* in silico. Proteins were separated from solvents and ligands or residues using Pymol software and saved in the pdb extension. The docking process was carried out using AutoDockTools-1.5.7 software. Re-docking between receptors and natural ligands was carried out on a grid box, which can produce an RMSD (Root Mean Square Deviation) value < 2 Å, suggesting that the method used is valid (Balgaria et al, 2016). The binding energy was determined by the Gibbs free energy value (ΔG kcal/mol) (Bajorath, 2015). A Gibbs free energy value of less than zero (0) shows that the bond between the ligand and the target protein occurs spontaneously

DOI:https//doi.org/10.22452/mjs.vol44no2.4
Malaysian Journal of Science 44(2): 42-51 (June 2025)

and is stable (Hill & Reilly, 2008). Furthermore, the binding energy (ΔG kcal/mol) of each ligand is compared with the native ligand and positive control (ascorbic acid). LigPlot+ 2.2.8 software was used to determine the interaction between the ligand and receptor. The result was visualized using the GIMP 2.0 software and saved in jpg format (Forli et al, 2016).

3. Results and Discussion

Several studies reported that the wood or roots of plants from species of the genus *Spathollobus* contain high levels of phenolic compounds and antioxidant activity (Fitriani et al., 2020; Iskandar et al., 2022). This study used samples of *S. littoralis* wood obtained from traditional markets in Pontianak, Kalimantan, Indonesia. A total of 3 kg of *S. littoralis* plant wood was dried and ground. Dry wood powder was extracted by maceration using technical ethanol (95%). The extract was concentrated (around 420 g) and fractionated using successive solvents *n*-hexane, chloroform, and ethyl acetate. After being concentrated, the results of extraction and fractionation resulted in the *n*-hexane fraction (13.63 g), chloroform (104.26 g), ethyl acetate (153.57 g), and 65 g of ethanol extract residue. Each extract and fraction were subjected to phytochemical tests, phenolic content analysis, and antioxidant activity using the DPPH and FRAP methods. Phytochemical test data shows that each *S. littoralis* wood extract and fraction contains phenolic compounds, flavonoids, and triterpenoids, except for the *n*-hexane fraction, which shows negative results for phenolic compounds and flavonoids.

Quantitative analysis of TPC using a spectrophotometer followed the Folin-Ciocalteu method (Hagerman et al., 2000). The sample was reacted with Folin-Ciocalteau reagent, and sodium carbonate was heated at 50°C for 10 minutes. The absorbance of each sample was measured using a spectrophotometer at a wavelength of 760 nm. Gallic acid was used as a standard for phenolic compounds. The calibration curve results obtained have a linear regression equation $y = 0.0043x + 0.0339$, with an R^2 value of 0.993. The TPC of each sample was expressed in mg Gallic Acid Equivalents (GAE) per gram sample.

Inhibitory activity (%I) was calculated as the percentage decrease in absorbance of the sample solution compared to the DPPH solution without a sample. The inhibitory activity obtained from each sample concentration was represented in a graph, and the regression equation was used to calculate the antioxidant activity, expressed as IC_{50} (inhibitory activity at a concentration of 50%). Antioxidant activity was measured using the FRAP method with ascorbic acid solution as a standard. The purpose of adding TCA is for the potassium ferrocyanide complex to precipitate. The addition of $FeCl_3$ also aimed to form a green to blue complex (Berlin blue). Antioxidant ability was measured by the ability of a sample to convert Fe^{3+} to Fe^{2+}. The FRAP value was expressed in mg ascorbic acid equivalent/g extract (Kumar, 2012). Table 1 shows the analysis results of each extract's TPC and antioxidant activity of *S. littoralis*.

The results of the analysis of TPC expressed as Gallic Acid Equivalent (mg/g sample GAE) showed that the ethyl acetate fraction had the highest content. The ethanol extract also showed a high content of phenolic compounds. Due to the mixture of ethanol extract with non-phenolic compounds, the TPC was lower than ethyl acetate. Phenolic compounds generally dissolve in relatively polar and semi-polar solvents. The high content of phenolic compounds is closely related to antioxidant activity. Antioxidant potential is usually associated with the molecular structure of phenolic compounds due to the presence of a conjugated π electron system that facilitates the donation of electrons from the hydroxyl group to radical oxidation.

Table 1. Total phenolic content (TPC) and antioxidant activity of each extract and fraction of *S. littoralis*

No	Sample extract and fraction wood of *S. littoralis*	TPC (mg/g sample GAE)	Antioxidant activity test against DPPH (IC_{50} (µg/mL)	Antioxidant activity using FRAP (mg Ascorbic Acid Equivalent/g sample)
1	Total ethanol extract	545.10 ± 9.81	2.12 ± 0.51	313.25 ± 8.83
2	*n*-Hexane fraction	78.88 ± 1.31	173.47 ± 14.06	6.54 ± 1.80
3	Chloroform fraction	308.67 ± 2.52	1.46 ± 0.98	126.53 ± 19.16
4	Ethyl acetate fraction	909.91 ± 1.00	2.61 ± 0.31	740.24 ± 13.24
5	Ascorbic acid (Positive control)		1.45 ± 0.02	-

The antioxidant activity test using the DPPH method was based on the radical capture reaction formed by releasing hydrogen radicals from phenolic compounds, which will produce DPPH-H molecules in non-radical form (Molyneux, 2003). Total ethanol extract, chloroform fraction, and ethyl acetate fraction from *S. littoralis* wood showed IC_{50} values below 10 µg/mL, suggesting a very high activity. Ascorbic acid, a widely utilized natural antioxidant in various food, pharmaceutical, and cosmetic products, was employed as a positive control. The results of the analysis are consistent with the report of previous studies that plants from the genus *Spatholobus* are rich in phenolic compounds, such as isoflavones, flavanones, flavans, isoflavanols, chalcones, lignans, and others (Huang et al., 2023; Nguyen-Ngoc et al., 2022). The occurrence of cell damage in organisms due to free radicals requires chemical compounds that function as antioxidants in the body. Phenolic compounds from plants generally have strong antioxidant properties and a natural effect in preventing various diseases related to oxidative stress, such as cancer (Dai & Mumper, 2010). Furthermore, the antioxidant activity capacity using the FRAP method was based on the ability of the compounds to reduce Fe^{3+} ions to Fe^{2+}. The antioxidant capacity was calculated from a linear calibration curve and expressed as ascorbic acid equivalent per gram of sample. A weakness of the FRAP method is that not all Fe^{3+} reductants are antioxidants, and some are not able to reduce Fe^{3+} (Hidalgo, 2017). However, the results of this study showed that the data are

DOI:https//doi.org/10.22452/mjs.vol44no2.4
Malaysian Journal of Science 44(2): 42-51 (June 2025)

similar. The total ethanol extract, chloroform fraction, and ethyl acetate fraction of *S. littoralis* showed excellent antioxidant activity, while the *n*-hexane fraction was weak. This is related to the phenolic compound content of each fraction.

Molecular mechanism of interaction from the genus *Spatholobus* on the ROS1 kinase receptor in silico using PDB code proteins include 3ZBF and 4UXL, downloaded from Protein Data Bank (www.pdb.org). Validation of the redocking method for the 3ZBF receptor produced a grid box with center x: 42.521; y: 19.649; z: 3.987, with box size x=y =z =30 Å, with an RMSD (root-mean-square deviation) value of 0.687 Å. The 4UXL receptor produced a grid box with center x: 42.587; y: -19.777; z: -5.719, with box size x=y =z =30 Å, and an RMSD value of 0.143 Å. This value meets the valid criteria for a docking method because the RMSD is <2 Å. Table 2 shows the results of the docking analysis of 14 phenols, redocking of native ligand, and positive control (ascorbic acid) against the 3ZBF receptor, while the 4UXL receptor is in Table 3. The data include binding energy (ΔG kcal/mol), hydrogen bonds, and hydrophobic interactions.

Information obtained from molecular docking includes binding energy and interaction of the ligand with amino acid residues of the receptor (Du, X, 2016). The binding energy between the ligand and receptor was expressed in Gibbs free energy (ΔG kcal/mol). The result of redocking between the 3ZBF receptor and the native ligand VGH {(3-[(1R)-1-(2,6-dichloro-3-fluorophenyl)ethoxy]-5-(1-piperidin-4-yl-1H-pyrazol-4- yl) pyridine-2-amine)} shows the minor binding energy (-10,590 kcal/mol), which is the most stable. Among the 14 phenolic compounds that showed the highest activity, licochalcone-A had the most binding energy of -8.823 kcal/mol. This compound also showed a higher binding energy than ascorbic acid which had a binding energy of -5.028 kcal/mol.

Results from redocking of 4UXL receptor and native ligand 5P8 {(10R)-7-amino-12-fluoro-2,10,16-trimethyl-15-oxo-10,15,16,17-tetrahydro-2H-8,4-(methanol)-pyra-zolo[4,3-h]-[2,5,11] benzoxadiazacyclotetradecine-3-carbonitrile)} shows an energy affinity of -11,400 kcal/mol. This implies that the native binding of the ligand to the 4UXL receptor is relatively stable. The most stable energy affinity of the 14 phenolic compounds tested was licochalcone-A at -9,384 kcal/mol. The antioxidant activity test with the DPPH ascorbic acid reagent had the highest antioxidant activity. However, analysis using the docking method with 3ZBF and 4UXL receptors showed a lower binding energy compared to the phenolic compounds tested from *Spatholobus*. This result shows that the bond between ascorbic acid and the 3ZBF and 4UXL receptors is due to the relatively small size compared to other phenolic compounds. Licochalcone A, is a phenolic compound that has activity as an antibacterial (Tsukiyama et al, 2022), antioxidant, and anti-aging (Ara et al, 2023). The compound also showed anti-inflammatory activity through inhibition of COX-2 synthesis (Cui et al, 2007).

Various factors influence the binding energy between the ligand and the receptor, including electrostatic interactions, Van der Walls forces, hydrophobic bond interactions, hydrogen bonds, and flexibility of the receptor structure. However, the data obtained showed that the greater the number of hydrogen bonds and hydrophobic interactions formed between the ligand and receptor, the stronger the bond (Du et al., 2016). Observation of hydrophobic interaction data between the ligand and the 3ZBF and 4UXL receptors (Tables 2 and 3) showed that the amino acid residue often present in the interaction was Leu 2026, Leu 2028, and Leu 2086.

DOI:https//doi.org/10.22452/mjs.vol44no2.4
Malaysian Journal of Science 44(2): 42-51 (June 2025)

Table 2. The Binding Energy of the Ligands, as Well as Their Interaction with the Amino Acid Residues of the Human ROS1 Kinase Receptor 3ZBF

No	Ligands/ Compound	Binding Energy (kcal/mol)	Hydrogen bond	Hydrophobic interaction
1	VGH (Native ligand)	-10.590	Glu2027	Leu2026, Val1959, Leu2028, Met2029, Ala1978, Gly2032, Leu1951, Leu2086, Leu2010, Arg2083, Lys1980
2	Ascorbic acid (positive control)	-5.028	Met2029	Leu1951, Leu2028, Leu2086, Leu2026, Ala1978, Val1959
3	Licochalcone-A	-8.823	Glu1961	Leu2026, Leu2086, Leu2010, Ala1978, Met2029, Glu2027, Glu2030, Gly2032, Leu2028, Leu1951, Val1959
4	Cajanin	-8.559	Lys1980; Met2029	Leu2026, Leu2086, Ala1978, Leu2028, Gly2032, Glu2030, Leu1951, Val1959, Gly2101, Asp2102
5	6-Methoxyeriodictyol	-8.244	Met2029; Gly2101	Leu2026, Leu2086, Glu2030, Gly2032, Leu1951, Val1959, Asp2102, Leu2010
6	Eriodictyol	-8.105	Met2029; Lys1980 Asp2102	Leu2086, Leu2028, Gly2032, Leu1951, Val1959
7	Dihydroquercetin	-8.036	Met2029; Asp2033	Leu1951, Gly2032, Val1959, Leu2086, Leu2026, Ala1978
8	Dihydrokaempferol	-8.007	Asp2102; Met2029 Lys1980	Leu2028, Ala1978, Leu1951, Gly2032, Leu2086, Val1959
9	Plathymenin	-7.928	Lys1980; Met2029 Asp2102	Val1959, Leu1951, Gly2032, Ala1978, Leu2028, Leu2086
10	Liquiritigenin	-7.924	Lys1980; Met2029 Asp2102	Leu2086, Leu2028, Ala1978, Leu1951, Gly2032, Val1959
11	Epicatechin	-7.870	Asp2102; Lys1980 Met2029	Val1959, Leu1952, Gly2032, Ala1978, Gly2101, Leu2086
12	3', 4', 7'-trihidroxyflavone	-7.779	Asp2102; Lys1980 Met2029	Leu2086, Ala1978, Gly2032, Leu1951, Leu2028, Leu2026
13	Butin	-7.760	Asp2102; Met2029 Lys1980	Leu2086, Leu2028, Ala1978, Gly2032, Leu1951, Val1959
14	Formononetin	-7.540	-	Gly2101, Leu2026, Leu2086, Ala1978, Met2029, Leu2028, Gly2032, Leu1951, Val1959, Lys1980, Asp2102
15	Prunasin	-7.356	Met2029; Glu2027	Ala1978, Arg2083, Asp2102, Asn2084, Gly2101, Leu2026, Lys1980, Leu2086, Leu2028, Gly2032, Leu1951
16	Afrormosin	-7.171	Lys1980	Leu2010, Gly2101, Leu2086, Asp2033, Gly2032, Leu1951, Met2029, Val1959, Leu2026

DOI:https//doi.org/10.22452/mjs.vol44no2.4
Malaysian Journal of Science 44(2): 42-51 (June 2025)

Table 3. The Binding Energy of the Ligands, as Well as Their Interaction with the Amino Acid Residues of the Human ROS1 Kinase Receptor 4UXL

No	Ligands/ Compound	Binding Energy (kcal/mol)	Hydrogen bond	Hydrophobic interaction
1	5P8 (native ligan)	-11.400	Met2029; Glu2027	Glu2030, Ala1978, Leu2026, Leu2010, Leu2086, Gly2101, Arg2083, Val1959, Gly2032, Leu1951, Leu2028
2	Ascorbic acid (positive control)	-5.244	Leu2028; Lys1976 Ser2088; Glu2030	Glu2027
3	Licochalcone-A	-9.384	Glu1961	Glu2030, Met2029, Leu2028, Ala1978, Glu2027, Leu2086, Leu2010, Leu2026, Val1959, Gly1952, Leu1951, Gly2032
4	Eriodictyol	-9.116	Lys1980; Leu1951 Met2029; Asp2102	Val1959, Gly2101, Leu2028, Leu2086
5	Plathymenin	-9.080	Asp2102; Met2029 Lys1980	Leu2086, Gly2101, Ala1978, Leu2028, Leu1951, Val1959
6	Dihydrokaempferol	-9.060	Lys1980; Met2029	Gly2101, Leu2026, Val1959, Leu1951, Leu2028, Ala1978, Leu2086
7	6-methoxyeriodictyol	-8.996	Gly2101; Leu1951 Met2029	Asp2102, Val1959, Gly2032, Glu2030, Leu2086, Leu2026
8	Liquiritigenin	-8.961	Lys1980; Met2029 Asp2102	Leu1951, Ala1978, Leu2028, Leu2086, Gly2101
9	Dihydroquercetin	-8.912	Gly2101; Met2029 Leu1951	Asp2102, Leu2086, Gly2032, Glu2030, Val1959, Leu2026
10	Butin	-8.908	Lys1980; Met2029 Asp2102	Val1959, Leu1951, Leu2028, Ala1978, Leu2086, Gly2101
11	Cajanin	-8.745	Lys1980; Asp2102	Val1959, Leu1951, Met2029, Leu2086, Gly2101
12	3'-4'-7'-Trihidroxyflavone	-8.608	Met2029; Lys1980	Leu2026, Gly2032, Leu1951, Leu2086, Leu2028, Ala1978
13	Epicatechin	-8.587	Leu1951; Met2029 Lys1980	Gly2101, Asp2102, Val1959, Gly2032, Glu2030, Leu2028, Ala1978, Leu2086
14	Formononetin	-8.250	Lys1980	Asp2102, Leu2026, Gly2101, Leu1951, Leu2028, Gly2032, Glu2030, Met2029, Leu2086, Val1959
15	Afrormosin	-7.962	-	Leu2086, Leu1951, Met2029, Glu2030, Val1959, Gly1954
16	Prunasin	-7.624	Met2029; Glu2027	Arg2083, Lys1980, Leu1951, Gly2032, Leu2028, Leu2086, Ala1978, Val1959, Leu2026

Phenolic compounds in plants of the *Spatholobus* genus generally have phenol groups, which allows for interaction with amino acids through hydrogen bonds and hydrophobic interactions. Figure 1 shows the visualization of the interaction of licochalcon-A against the 3ZBF receptor. Meanwhile, Figure 2 shows the visualization of the interaction of licochalcon-A against receptor 4UXL. Hydrogen bonds are between molecules with a hydrogen atom bonded to an atom with high electronegativity.

The partial positive charge in hydrogen bonds comes from the H atom of the ligand. However, the partial negative charge results from from highly electronegative atoms, such as oxygen, nitrogen, flour, and sulfur in the amino acid residues of the receptor. Hydrophobic interactions occur between non-polar groups and enhance protein stability by increasing the entropy of water molecules.

DOI:https//doi.org/10.22452/mjs.vol44no2.4
Malaysian Journal of Science 44(2): 42-51 (June 2025)

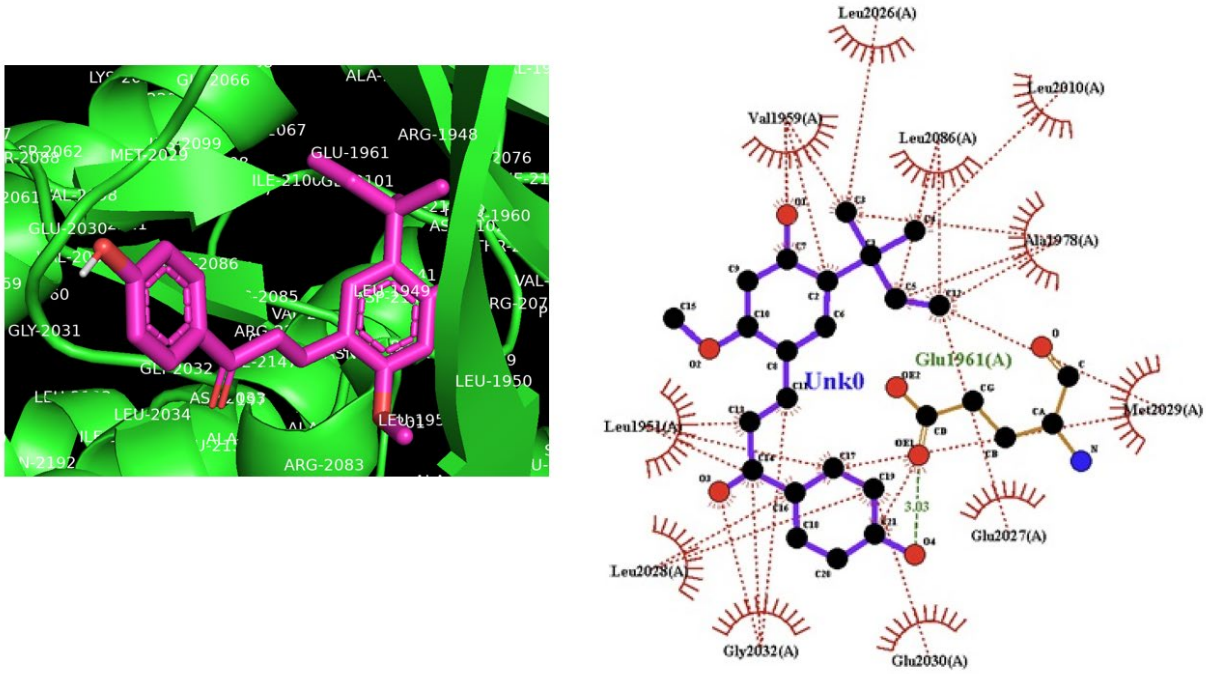

Figure 1. Visualization of interactions between licochalcone-A against receptor 3ZBF (Hydrogen bonds on the green line and hydrophobic interactions on the red line)

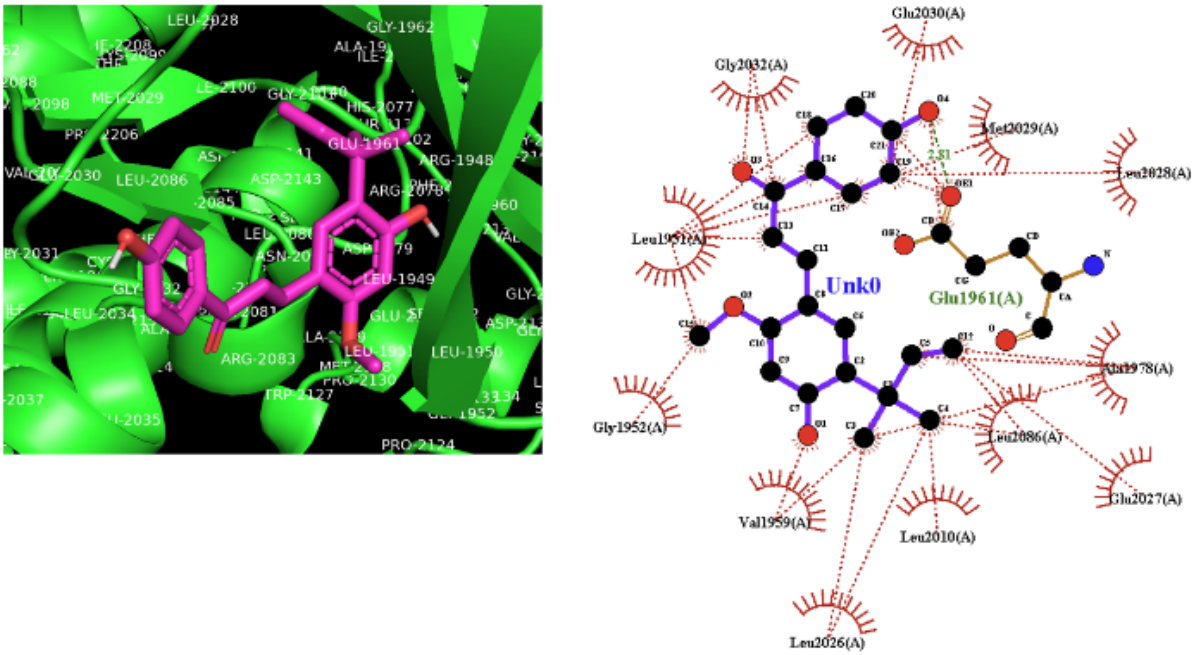

Figure 2. Visualization of interactions between licochalcone-A against receptor 4UXL (Hydrogen bonds on the green line and hydrophobic interactions on the red line)

Several plants of the genus *Spatholobus* have been widely used as part of crucial traditional medicine. For example, *Spatholobus suberectus* grape stems are an essential medicinal ingredient in traditional Chinese, Vietnamese, and Korean medicine (Huang et al., 2023; Nguyen-Ngoc et al., 2022). The plant was used to treat blood disorders, such as anemia, menstrual irregularities, and rheumatic diseases. Similarly, the wood of the *Spatholobus littoralis* plant was widely used in traditional medicine in Kalimantan, Indonesia. The main compounds found in plants of the genus *Spatholobus* are from the phenolic group, especially flavonoids. The results of this study are consistent with previous reports regarding the content of phenolic compounds and

DOI:https//doi.org/10.22452/mjs.vol44no2.4
Malaysian Journal of Science 44(2): 42-51 (June 2025)

antioxidant activity in plants of the genus *Spatholobus*. Proof through molecular docking using ROS1 kinase receptors (3ZBL and 4UXL) showed that there are hydrogen bonds and hydrophobic interactions, and some compounds have relatively small energy affinities, despite being relatively more extensive when compared to the native ligands.

ROS1 is a receptor tyrosine kinase that has been shown to undergo genetic rearrangement in various types of human cancer, including glioblastoma, non-small cell lung cancer (NSCLC), ovarian cancer, and others. This rearrangement can produce fusion proteins, thereby promoting cell proliferation (Davies & Doebele, 2013). Previous studies showed that ROS1 played a significant role in several cellular processes, such as apoptosis, survival, cell migration, and transformation in various malignancies including colorectal, ovarian, and NSCLC, as well as inflammatory myofibroblast tumors. Therefore, ROS1 has become a potential drug target. Several studies showed a relationship between compounds that act as antioxidants and have anticancer activity (Grigalius & Petrikaite, 2017; Milella et al., 2023). Several compounds found in plants of the genus *Spatholobus* show antioxidant and anticancer activity (Huang et al., 2023; Li et al., 2015; Nguyen-Ngoc et al., 2022)

4. Conclusion

In conclusion, *S. littoralis* was a medicinal plant widely used in traditional medicine in Kalimantan, Indonesia, containing phenolic compounds and high levels of antioxidant activity. Phenolic compounds in plants of the genus *Spatholubus* also showed high binding energy to ROS1 kinase receptors (3ZBF and 4UXL). Observation of hydrophobic interaction data between the ligand and the 3ZBF and 4UXL receptors showed that the amino acid residues frequently included in the interaction were Leu2026, Leu2028, and Leu2086.

5. Acknowledgement

The authors are grateful to the DRPM-DIKTI Indonesia for providing financial support in regular fundamental studies with Number: T/13.14 /UN34.9/PT.01.03/2023

6. References

Abubakar, A.R. & Haque, M. (2020). Preparation of Medicinal Plants: Basic Extraction and Fractionation Procedures for Experimental Purposes. *J Pharm Bioallied Sci*. *12*(1):1-10. https://doi.org/ 10.4103/jpbs.JPBS_175_19.

Adhityasmara, D., & Ramonah, D. (2022). Efek hepatoprotektor ekstrak etanol batang bajakah tampala (*Spatholobus littoralis* hassk) pada tikus yang diinduksi isoniazid. *Jurnal Ilmiah Sains*, *22*(1), 40. https://doi.org/10.35799/jis.v22i1.36293

Aliviyanti, R. U. Y., Sudibyo, R. S., & Murwanti, R. (2021). Efek sitotoksik beberapa akar bajakah kalimantan terhadap sel kanker payudara T47D. *Jurnal Penelitian Saintek*, *26*(2). https://doi.org/10.21831/jps.v26i2.41211

Ara, I., Rita Turcio, R., Islam, T., Hossain S., Md., Hasan, K. Md. (2023). Anti-aging related activities and health benefits of Licochalcone A: A review, *Clinical Complementary Medicine and Pharmacology*, 100125:1-32. https://doi.org/10.1016/j.ccmp.2023.100125.

Arysanti, R. D., Wirjatmadi, B., & Winarni, D. (2022). Effect of Bajakah (*Spatholobus littoralis* Hassk.) extracts on malondialdehyde serum of Wistar rats induced by streptozotocin. *Jurnal Kesehatan Prima*, *16*(2), 143. https://doi.org/10.32807/jkp.v16i2.837

Astuti, M. D., Maulana, A., & Kuntowati, E. M. (2014). Isolasi steroid dari fraksi *n*-heksana batang kayu bajakah tempala (*Spatholobus littoralis* Hassk.). *Prosiding Seminar Nasional Kimia, Jurusan Kimia FMIPA Universitas Negeri Surabaya*.

Atun, S., Handayani, S., Rakhmawati, A., Aini Purnamaningsih, N., An Naila, B. I., & Lestari, A. (2018). Study of potential phenolic compounds from stems of *Dendrophthoe falcata* (Loranthaceae) plant as antioxidant and antimicrobial agents. *Oriental Journal of Chemistry*, *34*(5), 2342–2349. https://doi.org/10.13005/ojc/340515

Balgaria, A., Jaravine, V., Huang, Y.J., Montelino, G.T., Güntert, P. (2016). Protein structure validation by generalized linear model root-mean-square deviation prediction. *Protein Science*, *21*(2): 229–238. https://doi.org/10.1002/pro.2007

Bajorath, J. (2015). Computer-aided drug discovery. *F1000Research*, *4*, 630. https://doi.org/10.12688/f1000research.6653.1

Cui, Y., Mingzhang, A. M., Li, W., Hu, J., and Yu L. (2007). Anti-Inflammatory Activity of Licochalcone A Isolated from Glycyrrhiza inflata, *Z. Naturforsch*. *63*(c): 361-365.

Dai, J., & Mumper, R. J. (2010). Plant phenolics: Extraction, analysis and their antioxidant and anticancer properties. *Molecules*, *15*(10), 7313–7352. https://doi.org/10.3390/molecules15107313

Davies, K. D., & Doebele, R. C. (2013). Molecular pathways: ROS1 fusion proteins in cancer. *Clinical Cancer Research*, *19*(15), 4040–4045. https://doi.org/10.1158/1078-0432.CCR-12-2851

Du, X., Li, Y., Xia, Y.L., Ai, S.M., Liang, J., Sang, P., Ji, X.L., & Liu, S.Q. (2016). Insights into protein-ligand interactions: Mechanisms, models, and methods. *International Journal of Molecular Sciences*, *17*(2), 144. https://doi.org/10.3390/ijms17020144

Fang, J., Liu, C., Wang, Q., Lin, P., Cheng, F. (2018) In silico polypharmacology of natural products. *Brief Bioinform*. *19*(6):1153-71. https://doi.org/10.1093/bib/bbx045.

DOI:https//doi.org/10.22452/mjs.vol44no2.4
Malaysian Journal of Science 44(2): 42-51 (June 2025)

Fitriani, F., Sampepana, E., & Saputra, S. H. (2020). Karakterisasi Tumbuhan akar bajakah (*Spatholobus littoralis* Hassk) dari Loa Kulu Kabupaten Kutai Kartanegara. *Jurnal Riset Teknologi Industri*, *14*(2), 365. https://doi.org/10.26578/jrti.v14i2.6590

Forli, S., Huey, R., Pique, M.E., Sanner, M.F., Goodsell, D. S., Olson, A.J. (2016). Computational protein–ligand docking and virtual drug screening with the AutoDock suite. *Nature Protocols 11*(5): 905–919. https://doi.org/10.1038/nprot.2016.051

Grigalius, I., & Petrikaite, V. (2017). Relationship between antioxidant and anticancer activity of Trihydroxyflavones. *Molecules*, *22*(12), 2169. https://doi.org/10.3390/molecules22122169

Hagerman, A., Harvey-Mueller, I., Makkar, A. H., Mueller, I. H., & Makar, H. P. S. (2000). *Quantification of tannins in tree and shrub foliage: A laboratory manual*. FAO/IAEA.

Harborne, A. J. (1998). *Phytochemical methods a guide to modern techniques of plant analysis* (3rd ed.). Springer.

Hidalgo, G.-I., & Almajano, M.P. (2017). Red fruits: extraction of antioxidants, phenolic content, and radical scavenging determination: A Review. *Antioxidants* (Basel). 19, 6(1): 1-27. https://doi.org/10.3390/antiox6010007

Hill, A. D., & Reilly, P. J. (2008). A Gibbs free energy correlation for automated docking of carbohydrates. *Journal of Computational Chemistry*, *29*(7), 1131–1141. https://doi.org/10.1002/jcc.20873

Huang, X., Fei, Q., Yu, S., Liu, S., Zhang, L., Chen, X., Cao, L., Wang, Z., & Shan, M. (2023). A comprehensive review: Botany, phytochemistry, traditional uses, pharmacology, and toxicology of *Spatholobus suberectus* vine stems. *Journal of Ethnopharmacology*, *312*, 116500. https://doi.org/10.1016/j.jep.2023.116500

Iskandar, D., Widodo, N., Warsito, Masruri, Rollando, & Antang, Y. P. P. (2022). Phenolic content, antioxidant, cytotoxic of fractions of *Spatholobus littoralis* Hassk from Kalimantan, Indonesia. *Journal of Hunan University Natural Sciences*, *49*(3), 14–23. https://doi.org/10.55463/issn.1674-2974.49.3.2

Istiqomah, I., & Safitri, D. (2021). Pharmacological activities of *Spatholobus littoralis*. *Infokes: Info Kesehatan*, *11*(2), 463–469.

Kumar, S. (2012). Assay-guided comparison for enzymatic and non-enzymatic antioxidant activities with special reference to medicinal plants. InTech. Egypt. Mansoura University. http:/doi.org/ 10.5772/50782

Li, W., Liu, J., Guan, R., Chen, J., Yang, D., Zhao, Z., & Wang, D. (2015). Chemical characterization of procyanidins from *Spatholobus suberectus* and their antioxidative and anticancer activities. *Journal of Functional Foods*, *12*, 468–477. https://doi.org/10.1016/j.jff.2014.11.009

Liu, R.X., Xu, Y.L., Ma, L.F., Ying, Y.M., & Zhan, Z.J. (2018). A new flavanone from *Spatholobus suberectus* dunn. *Journal of Chemical Research*, *42*(10), 529–530. https://doi.org/10.3184/174751918X15386515371813

Milella, R. A., De Rosso, M., Gasparro, M., Gigante, I., Debiase, G., Forleo, L. R., Marsico, A. D., Perniola, R., Tutino, V., Notarnicola, M., Velasco, R., & Flamini, R. (2023). Correlation between antioxidant and anticancer activity and phenolic profile of new Apulian table grape genotypes (V. Vinifera L.). *Frontiers in Plant Science*, *13*. https://doi.org/10.3389/fpls.2022.1064023

Molyneux, P. (2003). The use of the stable radical Diphenylpicrylhydrazyl (DPPH) for estimating antioxidant activity. *J.Sci. Technol*, *26*(2), 211–219.

Nastiti, K., & Nugraha, D. F. (2022). Aktivitas antiinflamasi ekstrak kayu bajakah (*Spatholobus littoralis* Hask). *Jurnal Surya Medika*, *7*(2), 45–50. https://doi.org/10.33084/jsm.v7i2.3202

Nguyen-Ngoc, H., Vu-Van, T., Pham-Ha-Thanh, T., Le-Dang, Q., & Nguyen-Huu, T. (2022). Ethnopharmacology, phytochemistry, and pharmacological activities of *Spatholobus suberectus* vine stem. *Natural Product Communications*, *17*(12), 1934578X2211427. https://doi.org/10.1177/1934578X221142724

Peng, F., Zhu, H., Meng, C.-W., Ren, Y.-R., Dai, O., & Xiong, L. (2019). New isoflavanes from *Spatholobus suberectus* and their cytotoxicity against human breast cancer cell lines. *Molecules*, *24*(18), 3218. https://doi.org/10.3390/molecules24183218

Prasetyorini, B. E., Kusumawardani, A., Fitriani, F., Rachman, P. O., Amelinda, N., & Ramadhani, A. (2022). Analisis in silico senyawa aktif batang kayu bajakah (*Spatholobus littoralis* hassk) sebagai terapi psoriasis. *Herb-Medicine Journal*, *5*(1), 26. https://doi.org/10.30595/hmj.v5i2.12744

Ridder-Numan, J. W. A., & Wiriadinata, H. (1985). A revision of the genus *Spatholobus* (Leguminosae-Papilionoideae). *Journal on Taxonomic Botany*, *10*(2), 107–270.

Sianipar, R.N.R., Suryanegara, L., Fatriasari, W., Arung, E.T., Kusuma, I.W., Achmadi, S.S., Azelee, N.I.W., Hamid, Z.A.A. (2023). The role of selected flavonoids from bajakah tampala (*Spatholobus littoralis* Hassk.) stem on cosmetic properties: A review, *Saudi Pharmaceutical Journal, 31*(3):382-400. https://doi.org/10.1016/j.jsps.2023.01.006

Tejasari, M., Respati, T., & Yuniarti, L. (2022). Exploring anticancer potential in Bajakah tampala by in silico virtual screening. *KnE Life Sciences*. https://doi.org/10.18502/kls.v7i5.12517

DOI:https//doi.org/10.22452/mjs.vol44no2.4
Malaysian Journal of Science 44(2): 42-51 (June 2025)

Tsukiyama, R., Katsura, H., Tokuriki, N., Kobayashi, M. (2002). Antibacterial activity of licochalcone A against spore-forming bacteria. *Antimicrob Agents Chemother*. *46*(5):1226-30. https://doi.org/ 10.1128/AAC.46.5.1226-1230.2002.

Vanajothi, R., Vedagiri, H., Al-Ansari, M. M., Al-Humaid, L. A., & Kumpati, P. (2022). Pharmacophore-based virtual screening, molecular docking, and molecular dynamic simulation studies for finding ROS1 kinase inhibitors as potential drug molecules. *Journal of Biomolecular Structure and Dynamics*, *40*(8), 3385–3399. https://doi.org/10.1080/07391102.2020.1847195

DOI:https//doi.org/10.22452/mjs.vol44no2.4
Malaysian Journal of Science 44(2): 42-51 (June 2025)

MALAYSIAN JOURNAL OF SCIENCE
MJS
ISSN 1394-3065

Regular Issue

Malaysian Journal of Science 44 (2): 52-62 (June 2025) https://mjs.um.edu.my

Bogdanov-Takens Bifurcation in SIRI Model with Multiple Reinfection of COVID-19

Livia Owen[1]

Abstract: In the presence of cases of COVID-19 reinfection, we propose a SIRI (Susceptible-Infected-Recovery-Infected) spread model of two COVID-19 variants. This model considers the possibility of individuals becoming reinfected with the same or different variants, although the risk of reinfection with the same variant remains lower due to natural immunity from previous infections. Besides analyzing the stability of equilibrium points, we focus on codimension-one bifurcations. Our initial numerical simulations used parameters obtained from real data collected through a British government survey. Our analysis revealed unstable disease-free equilibria and stable endemic equilibria. By varying the Case Fatality Rate parameter, we identified all codimension-one bifurcations. To further investigate the model's dynamics, we introduced a new parameter, the reinfection rate, and utilized AUTO software. Our research led to the discovery of codimension-two bifurcations, specifically the Bogdanov-Takens bifurcation. We identified the parameter domain where a stable limit cycle and homoclinic orbit occur in the presence of the Bogdanov-Takens bifurcation. We also simulated parameter variations that could trigger a pandemic resurgence. This highlights the possibility of emerging variants causing a pandemic return.

Keywords: *SIRI, reinfection, COVID-19, codimension one bifurcation, Bogdanov-Takens bifurcation.*

1. Introduction

Since December 2019, the Coronavirus Disease 2019, commonly known as COVID-19, has been spreading and affecting the world. The origin of COVID-19 is believed to be in a seafood market in Wuhan, China. The World Health Organization (WHO) declared COVID-19 a pandemic on March 11, 2020, and there have been over 770 million reported cases of COVID-19, resulting in over 6.9 million deaths (WHO, 2023). Recently, in August 2023, there were reports of over 1.4 million new COVID-19 cases and 1,800 fatalities. The four major variants of COVID-19 are Alpha, Beta, Delta, and Omicron. Omicron has subvariants such as XBB and Eris, which are still considered "Variants of Interest" because of their high transmission potential. The WHO designates these variants as VOI to monitor their spread. A new highly mutated variant named Pirola has been detected in the UK (Yale, 2023).

During the Omicron wave, there have been instances of reinfection with the same or different variants. Individuals can contract COVID-19 multiple times (Pinto et al., 2021; WHO, 2023). COVID-19 sequences by variant and subvariant of Omicron in each country can be viewed on (Our World in Data, 2023). On average, there are two predominant variants of the epidemic during a given interval, as shown in Figure 1. For example, as of April 12, 2021, the two prevalent varieties were the Alpha and Beta variants. One month later, the two prevalent varieties were the Alpha and Delta variants. On December 20, 2021, the two dominant variants were the Delta and Omicron (BA.1) variants. Currently, two subvariants of Omicron are predominant.

Authors information:
[a]Center for Mathematics and Society, Department of Mathematics, Parahyangan Catholic University, Bandung 40141, INDONESIA. E-mail: livia.owen@unpar.ac.id[1];
*Corresponding Author: livia.owen@unpar.ac.id

Received: June 8, 2023
Accepted: June 20, 2024
Published: June 30, 2025

DOI:https//doi.org/10.22452/mjs.vol44no2.5
Malaysian Journal of Science 44(2): 52-62 (June 2025)

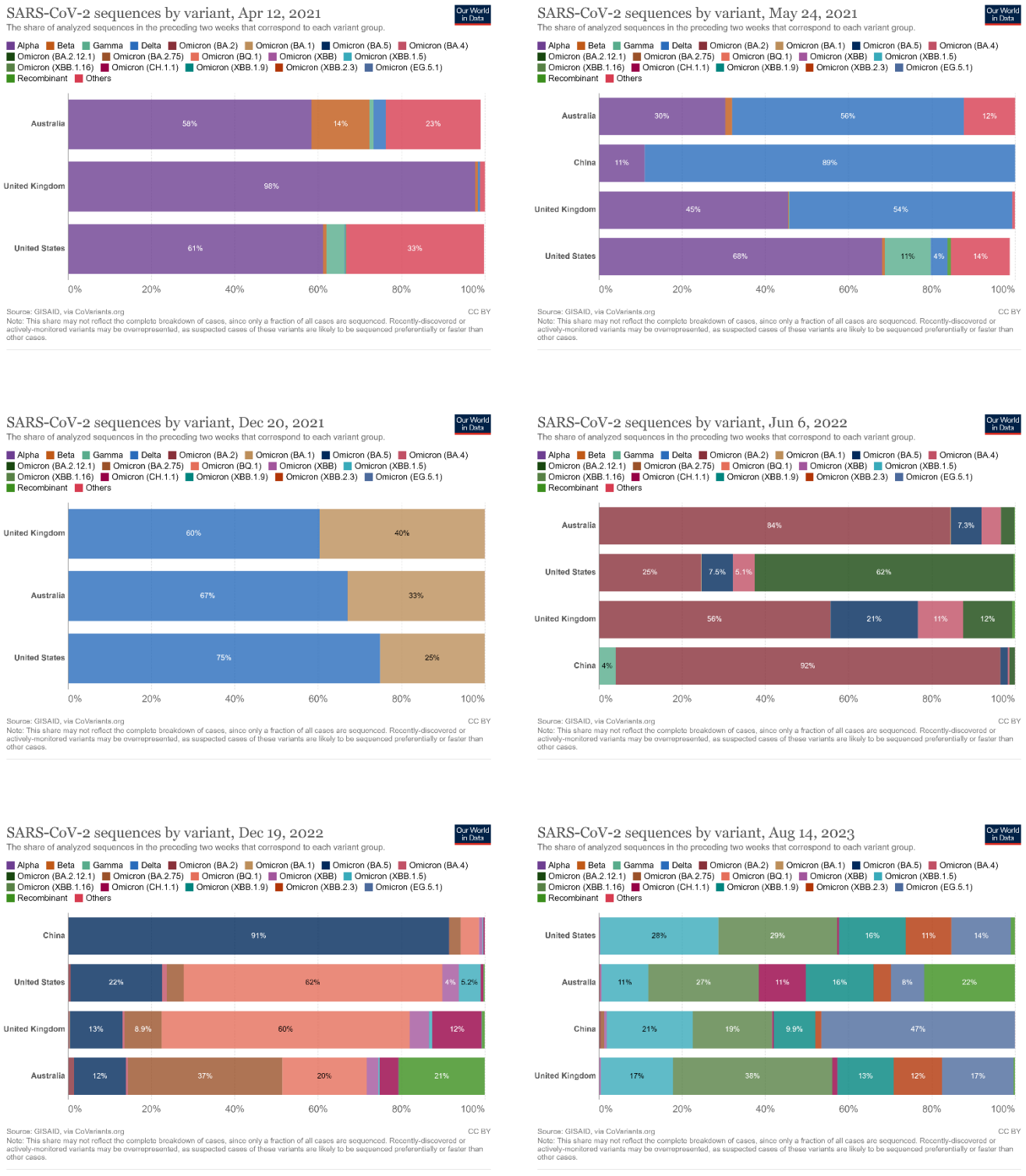

Figure 1. COVID-19 sequences by variant from June 7 in Australia, China, UK, United States, June 7, 2021 until April 26, 2023 (Our World in Data, 2023).

DOI:https//doi.org/10.22452/mjs.vol44no2.5
Malaysian Journal of Science 44(2): 52-62 (June 2025)

The complexity of COVID-19's spread is compounded by the possibility of reinfection with the same or different virus variants. To gain deeper insight into disease spread under these circumstances, we propose a SIRI (Susceptible-Infected-Recovery-Infected) model for two COVID-19 variants. Previous SIRI spread model research appears in studies on TBC and herpes disease spread models (Sharma et al., 2017), SIRI diffusion models (Yang, 2019; Duan, 2021), and vaccination strategies (Martins & Pinto, 2017). Recent SIRI model research on COVID-19 spread is detailed in (Nurjanah, 2022), while the discrete model appears in (McMahon & Robb, 2020). Studies by (Wangari, 2021) and (Salman, 2021) examined COVID-19 reinfection using data from Kenya and Malaysia, respectively. Reinfection in COVID-19 significantly impacts modeling processes. However, these studies considered only one disease variant and have not addressed multi-strain disease spread models. Our paper examines how public awareness affects COVID-19 spread, considering same-strain reinfection possibilities. The study analyzes the virus's multi-strain spread model, helping policymakers and healthcare professionals understand public awareness's role in reducing COVID-19 transmission.

This research develops from studies examining COVID-19 spread models with saturation. A discrete version appears in (Yong et al., 2022a), and proposed government policy design appears in (Yong et al., 2022b). Codimension 1 bifurcation analysis and interpretation appear in (Yong et al., 2022a). The study uses public awareness level as its bifurcation parameter. From basic reproduction numbers, we analyze disease-free equilibria point stability. We derive endemic equilibrium points and analyze their bifurcations. The first numerical simulation uses parameters from British government survey data (ONS, 2023) in Table 1. These data indicate that recovered individuals cannot experience reinfection from previous variants. Consequently, our model assumes reinfection occurs only with the same variant or new variants. Beyond real-data parameters, we simulate parameter variations that could trigger pandemic resurgence, representing potential scenarios if new variants emerge.

Table 1. Percentage of first and second infections by period in which different variants were dominant, UK, 2 July 2020 to 23 November 2022 (ONS, 2023)

First infection variant	Second infection variant	Estimated percentage (%) of total reinfection
Alpha	Alpha	1.1
Alpha	Delta	4.4
Alpha	Omicron BA.1	9.9
Alpha	Omicron BA.2	10.6
Alpha	Omicron BA.4/BA.5	9.5
Delta	Delta	0.6
Delta	Omicron BA.1	8.2
Delta	Omicron BA.2	11.5
Delta	Omicron BA.4/BA.5	12.9
Omicron BA.1	Omicron BA.1	0.3
Omicron BA.1	Omicron BA.2	4.9
Omicron BA.1	Omicron BA.4/BA.5	16.6
Omicron BA.2	Omicron BA.2	0.3
Omicron BA.2	Omicron BA.4/BA.5	8.5
Omicron BA.4/BA.5	Omicron BA.4/BA.5	0.7

2. Model

After the recent case of reinfection, we modified the SIRS model to use the SIRI model due to the multi-strain variant we work with. This model allows individuals with recovery to become infected with the same or a different variant. We constructed our model based on the following assumptions, see Figure 2.

We denoted two main variants of COVID-19, i.e., $i = 1$ for the past variant and $i = 2$ for the new or current variant (including all of the subvariants). Let $S = S(t)$, $I_i = I_i(t)$, and $R_i = R_i(t)$ respectively, the number of susceptible individuals, infected by i-variant individuals, and recovered individuals at time $t \geq 0$.

We excluded the exposed individual because, according to the European Centre for Disease Prevention and Control, the incubation time for the new variant is shorter (3-4 days).

The recruitment of individuals due to births and migrations is constant, Λ and also proportional to the number of recovery individuals: $\lambda(R_1 + R_2)$ for Λ, $\lambda > 0$, and they assumed as susceptible individuals.

The incidence rate is proportional to the possible contacts between susceptible individuals and infected individuals and has a denominator which increases with S. The parameter γ_1 measuring the level of a susceptible's cautiousness. So we have the incidence rate: $\frac{\beta_i S I_i}{1+\gamma_1 S}$ for some $\beta_i > 0$.

Infected individuals I_i become recovered R_i at the rate $\mu_i > 0$.

The proportions of each individual leaving the population as a result of deaths are proportional to the mortality rate $\delta > 0$. Infected individuals die at a greater rate than susceptible and recovered individuals, so we add the Case Fatality Rate (CFR) of each variant, δ_i.

Recovery individuals R_1 can be reinfected with the same variant with rate α_{11} or by new variant with rate α_{12}. Recovery individuals

DOI:https//doi.org/10.22452/mjs.vol44no2.5
Malaysian Journal of Science 44(2): 52-62 (June 2025)

R_2 only reinfected with the same variant with rate α_{22} and cannot be reinfected by the old variant, see Table 1. This incidence rate is proportional to the possible contacts of recovery and infected individuals and also the reinfection rate from i variant to j variant, $i, j = 1, 2$. The level of recovery's cautiousness is assumed to be less than or equal to the level of susceptible's one, $\gamma_2 \leq \gamma_1$, thus we have the incidence rate: $\frac{\alpha_{ij}\beta_i R_i I_j}{1+\gamma_2 R_i}$ for some $i, j = 1,2, i \leq j$.

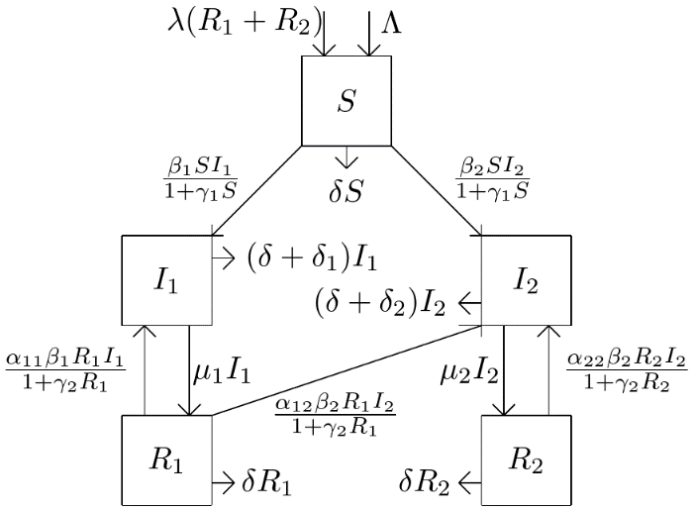

Figure 2. Transmission diagram of COVID-19

Table 2. The model parameters with their biological meanings

Parameters	Biological meanings	Estimated values	Sources
α_{ij}	Reinfection rate from i to j variant, $i \leq j$,	(0.01,0.35)	(ONS, 2023)
β_i	Transmission coefficient from susceptible to infected individuals with i variant.	(0.58,0.95)	(Ndairou et al., 2020)
δ	Mortality rate	0.002	(Ud Din et al., 2020)
δ_i	Case Fatality Rate (CFR) i variant	(0.01,0.05)	(Ndairou et al., 2020)
Λ	Recruitment of susceptible individuals (birth rate, etc.)	$\frac{10000}{59 \times 365}$	(Agusto, 2013)
λ	Birth rate of recovery individual	(0.01, 0.2)	(Ud Din et al., 2020)
μ_i	Recovery rate of i variant	(0.5, 0,8)	(Ndairou et al., 2020)
γ_1	The susceptible individual's cautiousness level	(0.3,0.8)	(Yong et al., 2022b)
γ_2	The recovery individual's cautiousness level, $\gamma_2 < \gamma_1$	(0.3,0.8)	(Yong et al., 2022b)

The above assumptions lead to the following model:

$$\begin{cases} \frac{dS}{dt} &= \Lambda + \lambda(R_1 + R_2) - \delta S - \frac{\beta_1 SI_1}{1+\gamma_1 S} - \frac{\beta_2 SI_2}{1+\gamma_1 S}, \\ \frac{dI_1}{dt} &= \frac{\beta_1 SI_1}{1+\gamma_1 S} - \delta I_1 - \delta_1 I_1 - \mu_1 I_1 + \frac{\alpha_{11}\beta_1 I_1 R_1}{1+\gamma_2 R_1}, \\ \frac{dI_2}{dt} &= \frac{\beta_2 SI_2}{1+\gamma_1 S} - \delta I_2 - \delta_2 I_2 - \mu_2 I_2 + \frac{\alpha_{22}\beta_2 I_2 R_2}{1+\gamma_2 R_2} + \frac{\alpha_{12}\beta_2 I_2 R_1}{1+\gamma_2 R_1}, \\ \frac{dR_1}{dt} &= \mu_1 I_1 - \delta R_1 - \frac{\alpha_{11}\beta_1 I_1 R_1}{1+\gamma_2 R_1} - \frac{\alpha_{12}\beta_2 I_2 R_1}{1+\gamma_2 R_1}, \\ \frac{dR_2}{dt} &= \mu_2 I_2 - \delta R_2 - \frac{\alpha_{22}\beta_2 I_2 R_2}{1+\gamma_2 R_2}, \end{cases} \quad (1)$$

DOI:https//doi.org/10.22452/mjs.vol44no2.5
Malaysian Journal of Science 44(2): 52-62 (June 2025)

3. Results and Discussion

Firstly, we applied the following proposition regarding the System's positiveness solution.

Proposition 1. (The System's positiveness solution.) Let the initial conditions: $S(0), I_i(0), R_i(0) \geq 0, i, j = 1,2$, then the solutions $S(t), I_i(t), R_i(t), i, j = 1,2$ of system (1) are non- negative for $t \geq 0$.

Proof 1. Rewrite the right hand side of $\frac{dI_1}{dt}$ and $\frac{dI_2}{dt}$ on System (1) as

$$\begin{aligned} \frac{dI_1}{dt} &= I_1\left(\frac{\beta_1 S}{1+\gamma_1 S} - \delta - \delta_1 - \mu_1 + \frac{\alpha_{11}\beta_1 R_1}{1+\gamma_2 R_1}\right), \\ \frac{dI_2}{dt} &= I_2\left(\frac{\beta_2 S}{1+\gamma_1 S} - \delta - \delta_2 - \mu_2 + \frac{\alpha_{22}\beta_2 R_2}{1+\gamma_2 R_2} + \frac{\alpha_{12}\beta_2 R_1}{1+\gamma_2 R_1}\right). \end{aligned}$$

Both planes $I_1 = 0$ and $I_2 = 0$ are invariant manifolds since it imply $\frac{dI_1}{dt} = 0$ and $\frac{dI_2}{dt} = 0$.

Since $\frac{dS}{dt}\Big|_{S=0,I_1,I_2,R_1,R_2\geq 0} = \Lambda + \lambda(R_1 + R_2), \frac{dR_1}{dt}\Big|_{R_1=0,S,I_1,I_2,R_2\geq 0} = \mu_1 I_1, \frac{dR_2}{dt}\Big|_{R_2=0,S,I_1,I_2,R_1\geq 0} = \mu_2 I_2$, the rates listed above are all non-negative over their $\mathbb{R}^5_+$ boundary planes. As a result, we have the vector fields intended inward direction from their boundaries. Starting with non-negative initial conditions so that all of the System's solutions (1) remain positive for all $t \geq 0$. ■

The Basic Reproduction Number and The Stability of the Disease-Free Equilibrium

The disease-free equilibrium is $E_0 = \left(\frac{\Lambda}{\delta}, 0,0,0,0\right)$ and the linearized vector field of (1) in the vicinity of E_0 is

$$\begin{pmatrix} -\delta & -\frac{\beta_1\Lambda}{\gamma_1\Lambda+\delta} & -\frac{\beta_2\Lambda}{\gamma_1\Lambda+\delta} & \lambda & \lambda \\ 0 & -\delta-\delta_1-\mu_1+\frac{\beta_1\Lambda}{\gamma_1\Lambda+\delta} & 0 & 0 & 0 \\ 0 & 0 & -\delta-\delta_2-\mu_2+\frac{\beta_2\Lambda}{\gamma_1\Lambda+\delta} & 0 & 0 \\ 0 & \mu_1 & 0 & -\delta & 0 \\ 0 & 0 & \mu_2 & 0 & -\delta \end{pmatrix} \quad (2)$$

The eigenvalues of (2) are

$$-\delta, -\delta, -\delta, \frac{\beta_1\Lambda}{\gamma_1\Lambda+\delta} - (\delta+\delta_1+\mu_1), \frac{\beta_2\Lambda}{\gamma_1\Lambda+\delta} - (\delta+\delta_2+\mu_2) \quad (3)$$

We determine the basic reproduction number, $\mathcal{R}_0$, by using the next generation method (Driessche, 2017), i.e.

$$\mathcal{R}_0 = \max(\mathcal{R}_{01}, \mathcal{R}_{02}) \quad (4)$$

where

$$\mathcal{R}_{01} = \frac{\beta_1\Lambda}{(\gamma_1\Lambda+\delta)(\delta+\delta_1+\mu_1)}, \mathcal{R}_{02} = \frac{\beta_2\Lambda}{(\gamma_1\Lambda+\delta)(\delta+\delta_2+\mu_2)}.$$

Equation (3) is rewritten as

$$-\delta, -\delta, -\delta, \mathcal{R}_{01} - 1, \mathcal{R}_{02} - 1 \quad (5)$$

We conclude the following proposition for the stability of disease-free equilibrium.

Proposition 2. (The stability of disease-free equilibrium.) The disease-free equilibrium is $E_0 = \left(\frac{\Lambda}{\delta}, 0,0,0,0\right)$ is a stable node if $\mathcal{R}_0 < 1$ and it is a saddle point if $\mathcal{R}_0 > 1$.

For condition $\mathcal{R}_0 = 1$ will be discuss in section 3.4.

One Variant Exists

Assume $I_2, R_2 \neq 0$. The condition $I_1 = 0$ implies $R_1 = 0$, the dynamic of the System (1) follows the subsystem

$$\begin{aligned} \frac{dS}{dt} &= \Lambda + \lambda R_2 - S\left(\delta + \frac{\beta_2 I_2}{1+\gamma_1 S}\right), \\ \frac{dI_2}{dt} &= \frac{\beta_2 S}{1+\gamma_1 S} - \delta - \delta_2 - \mu_2 + \frac{\alpha_{22}\beta_2 R_2}{1+\gamma_2 R_2}, \\ \frac{dR_2}{dt} &= \mu_2 I_2 - R_2\left(\delta + \frac{\alpha_{22}\beta_2 I_2}{1+\gamma_2 R_2}\right). \end{aligned} \quad (6)$$

DOI:https//doi.org/10.22452/mjs.vol44no2.5
Malaysian Journal of Science 44(2): 52-62 (June 2025)

We get an equilibrium $E_2 = (S_2, 0, I_{22}, 0, R_{22})$ whose the R_{22}-component satisfies:

$$a_3(R_{22})^3 + a_2(R_{22})^2 + a_1 R_{22} + a_0 = 0 \quad (7)$$

where

$$\begin{aligned} k &= \delta + \delta_2 + \mu_2 \\ a_3 &= (\alpha_{22}\beta_2\gamma_1 - \gamma_1\gamma_2 k + \beta_2\gamma_2)(\alpha_{22}\beta_2(\lambda - \delta) + \delta\gamma_2 k - \gamma_2\lambda\mu 2) \\ a_2 &= (\alpha_{22}\beta_2)^2(\Lambda\gamma_1 + \delta) + (\alpha_{22}\beta_2)((2\delta k - \Lambda(k+\mu_2))\gamma_2 - \lambda(k+\mu_2))\gamma_1 + \\ &\quad (\Lambda\beta_2 - \delta(k+\mu_2))\gamma_2 - \beta_2(\delta - \lambda)) + \gamma_2(((\Lambda\gamma_2 + 2\lambda)\gamma_1 + \delta\gamma_2)k - \beta_2(\Lambda\gamma_2 + 2\lambda))\mu_2 - 2k\delta(\gamma_1 k - \beta_2) \\ a_1 &= -\alpha_{22}\beta_2\left(((k+\mu_2)\gamma_1 - \beta_2)\Lambda + \delta(k+\mu_2)\right) + \left(((2\Lambda\gamma_2 + \lambda)\gamma_1 + 2\delta\gamma_2)k - (2\Lambda\gamma_2 + \lambda)\beta_2\right)\mu_2 - k\delta(\gamma_1 k - \beta_2) \\ a_0 &= \mu_2(\Lambda\gamma_1 k + \delta k - \Lambda\beta_2) \end{aligned}$$

and

$$\begin{aligned} S_2 &= \frac{(\delta + \delta_2 + \mu_2)(\gamma_2 R_{22} + 1) - \alpha_{22}\beta_2 R_{22}}{(\gamma_2 R_{22} + 1)(\beta_2 - \gamma_1(\delta + \delta_2 + \mu_2) + \alpha_{22}\beta_2\gamma_1 R_{22})} \\ I_{22} &= \frac{\delta R_{22}(\gamma_2 R_{22} + 1)}{\mu_2 + \mu_2\gamma_2 R_{22} - \alpha_{22}\beta_2 R_{22}} \end{aligned}$$

With a similar analysis, assume $I_1, R_1 \neq 0$. The condition $I_2 = 0$ implies $R_2 = 0$, we get an equlibrium $E_1 = (S_1, I_{11}, 0, R_{11}, 0)$ and the expression for S_1, I_{11}, R_{11} is similar with S_2, I_{22}, R_{22} by replacing $\alpha_{22}, \beta_2, \delta_2, \mu_2$ with $\alpha_{11}, \beta_1, \delta_1, \mu_1$.

Two Variant Exist

The double endemic equilibrium $\bar{E} = (\bar{S}, \bar{I_1}, \bar{I_2}, \bar{R_1}, \bar{R_2})$ exist if

$$\begin{aligned} \Lambda + \lambda(\bar{R_1} + \bar{R_2}) - \bar{S}\left(\delta + \frac{\beta_1\bar{I_1}}{1+\gamma_1\bar{S}} + \frac{\beta_2\bar{I_2}}{1+\gamma_1\bar{S}}\right) &= 0, \\ \frac{\beta_1\bar{S}}{1+\gamma_1\bar{S}} - \delta - \delta_1 - \mu_1 + \frac{\alpha_{11}\beta_1\bar{R_1}}{1+\gamma_2\bar{R_1}} &= 0, \\ \frac{\beta_2\bar{S}}{1+\gamma_1\bar{S}} - \delta - \delta_2 - \mu_2 + \frac{\alpha_{22}\beta_2\bar{R_2}}{1+\gamma_2\bar{R_2}} + \frac{\alpha_{12}\beta_2\bar{R_1}}{1+\gamma_2\bar{R_1}} &= 0, \\ \mu_1\bar{I_1} - \bar{R_1}\left(\delta + \frac{\alpha_{11}\beta_1\bar{I_1}}{1+\gamma_2\bar{R_1}} + \frac{\alpha_{12}\beta_2\bar{I_2}}{1+\gamma_2\bar{R_1}}\right) &= 0, \\ \mu_2\bar{I_2} - \bar{R_2}\left(\delta + \frac{\alpha_{22}\beta_2\bar{I_2}}{1+\gamma_2\bar{R_2}}\right) &= 0. \end{aligned}$$

has a solution for $\bar{S}, \bar{I_1}, \bar{I_2}, \bar{R_1}, \bar{R_2} > 0$ or equivalently with

$$\delta\gamma_1\bar{S^2} + \left(\delta + \beta_1\bar{I_1} + \beta_2\bar{I_2} - \gamma_1(\Lambda + \lambda\bar{R_1} + \lambda\bar{R_2})\right)\bar{S} - (\Lambda + \lambda\bar{R_1} + \lambda\bar{R_2}) = 0 \quad (8)$$

Since $\Lambda + \lambda\bar{R_1} + \lambda\bar{R_2} > 0$, we conclude that only one positive $\bar{S}$ if discriminant of (8) is positive

$$\begin{aligned} &(\lambda\gamma_1)^2\left(\bar{R_1}^2 + \bar{R_2}^2\right) + 2\lambda\gamma_1(\delta + \gamma_1\lambda\bar{R_2} + \Lambda\gamma_1 - \beta_1\bar{I_1} - \beta_2\bar{I_2})\bar{R_1} + 2\lambda\gamma_1(\delta + \Lambda\gamma_1 - \beta_1\bar{I_1} \\ &-\beta_2\bar{I_2})\bar{R_2} + (\Lambda\gamma_1 + \delta)^2 + (\beta_1\bar{I_1} + \beta_2\bar{I_2})^2 + 2\beta_1\bar{I_1}(\delta - \Lambda\gamma_1) + 2\beta_2\bar{I_2}(\delta - \Lambda\gamma_1) > 0 \end{aligned}$$

Bifurcation Analysis

In the following propositions, we analytically demonstrate the conditions that make transcritical or fold bifurcations occur (see Strogatz (2018) for the bifurcation theory).

Proposition 3. (Transcritical bifurcation) At $\mathcal{R}_{0i} = 1$ or equivalently with $\delta_i = \frac{\Lambda\beta_i}{\Lambda\gamma_1 + \delta} - \delta - \mu_i$, the equilibria E_0 and E_i undergo transcritical bifurcation.

Proof 3. It is simple to get that

i) E_0 and E_1 collide when $\delta_1 = \frac{\Lambda\beta_1}{\Lambda\gamma_1 + \delta} - \delta - \mu_1$ or equivelently with $\mathcal{R}_{01} = 1$, and

ii) E_0 and E_2 collide when $\delta_1 = \frac{\Lambda\beta_1}{\Lambda\gamma_1 + \delta} - \delta - \mu_1$ or equivelently with $\mathcal{R}_{02} = 1$.

At the transcritical point, they become degenerate equilibrium with one zero eigenvalue.

DOI:https//doi.org/10.22452/mjs.vol44no2.5
Malaysian Journal of Science 44(2): 52-62 (June 2025)

Proposition 4. (Fold bifurcation of E_i) Let $D := 18a_3a_2a_1a_0 - 4a_3a_1^3 - 4{a_2}^3a_0 + {a_2}^2{a_1}^2 - 27a_3^2a_0^2 = 0$
where

$k = \delta + \delta_i + \mu_i$

$a_3 = (\alpha_{ii}\beta_i\gamma_1 - \gamma_1\gamma_2 k + \beta_i\gamma_2)(\alpha_{ii}\beta_i(\lambda - \delta) + \delta\gamma_2 k - \gamma_2\lambda\mu_i)$

$a_2 = (\alpha_{ii}\beta_i)^2(\Lambda\gamma_1 + \delta) + (\alpha_{ii}\beta_i)((2\delta k - \Lambda(k + \mu_i)\gamma_2 - \lambda(k + \mu_i))\gamma_1 +$
$(\Lambda\beta_i - \delta(k + \mu_i))\gamma_2 - \beta_i(\delta - \lambda)) + \gamma_2(((\Lambda\gamma_2 + 2\lambda)\gamma_1 + \delta\gamma_2)k - \beta_i(\Lambda\gamma_2 + 2\lambda))\mu_i - 2k\delta(\gamma_1 k - \beta_i)$

$a_1 = -\alpha_{ii}\beta_i\left(((k + \mu_2)\gamma_1 - \beta_i)\Lambda + \delta(k + \mu_i)\right) + + \left(((2\Lambda\gamma_2 + \lambda)\gamma_1 + 2\delta\gamma_2)k - (2\Lambda\gamma_2 + \lambda)\beta_i\right)\mu_i - k\delta(\gamma_1 k - \beta_i)$

$a_0 = \mu_i(\Lambda\gamma_1 k + \delta k - \Lambda\beta_i)$

Fold bifurcation of E_i occurs when $D = 0$.

Proof 4. Without loss of generality, we prove the fold bifurcation of E_2. Since R_i is the root of the cubic equation (7), the discriminant of it (10) can be computed using the Cardano formula (Wituła & Słota, 2010). If $D = 0$, then the cubic equation (7) has multiple roots, and all of its roots are real.

4. Numerical Simulation

This section presents the codimension two bifurcation diagram, from which we can show some interesting phase portraits and time series. The initial parameters are given in Table 3. We vary the parameters α_{22} and δ_2 to analyze how the new variant impacts the pandemic situation.

Table 3. The initial parameter set.

α_{11}	α_{12}	α_{22}	β_1	β_2	δ	δ_1	δ_2	Λ	λ	μ_1	μ_2	γ_1	γ_2
0.01	0.35	0.24	0.08	0.5	0.0065	0.04	0.02	0.02	0.0125	0.8	0.7	0.1	0.05

We have the saddle point $e_0 = (3.076923077, 0, 0, 0, 0)$ and the stable node $e_2 = (0.09463959107, 0, 2.520380824, 0, 7.900874864)$. So one variant exists, for the phase portrait (see Figure 4 (Left)).

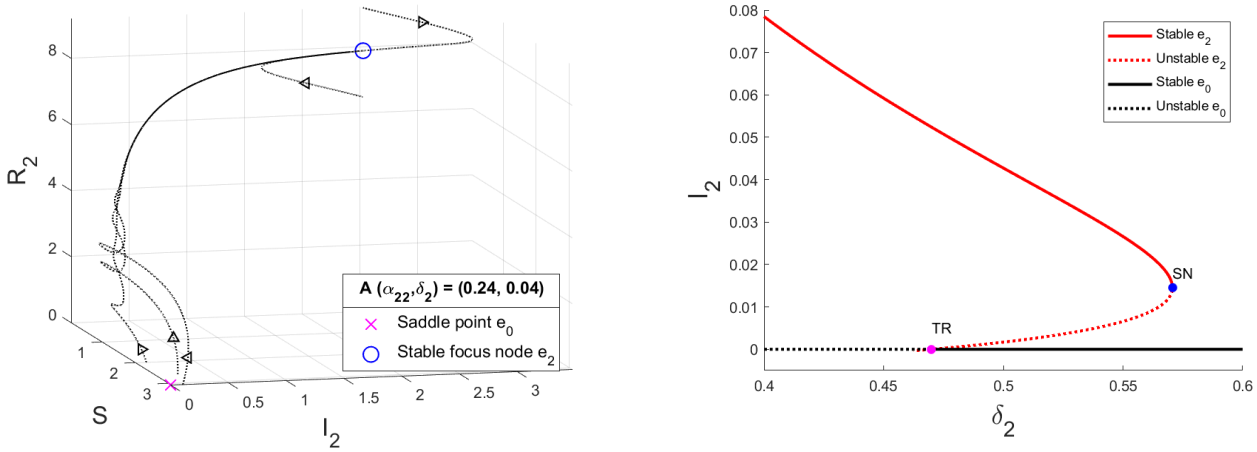

Figure 4. (Left) Some orbits for the initial parameter set in Table 3 or the A parameter set. (Right) The I_2-coordinate of the branch of continuation equilibrium as variation on parameter δ_2.

Codimension One Bifurcation

Using the numerical continuation AUTO, we vary δ_2 and obtain a transcritical bifurcation point (between e_0 and e_2) and a fold (or saddle node) bifurcation point for e_2 (see Table 4). These are the same results with Propositions 3 and 4.

Table 4. Transcritical and fold bifurcations list.

Bifurcation	**Label**	δ_2	S	I_1	I_2	R_1	R_2
Transcritical	TR	0.469970711	3.076923077	0	0	0	0
Fold	SN	0.570633209	2.939313201	0	0.014559724	0	1.251406177

Figure 4 (Right) displays the branch of continuation nontrivial equilibrium (red curve), which undergoes a fold bifurcation and a transcritical bifurcation with disease-free equilibrium (black line) as a variation on parameter δ_2. Their stability alternates from stable (solid style) to unstable (dashed style), and vice versa.

DOI:https//doi.org/10.22452/mjs.vol44no2.5
Malaysian Journal of Science 44(2): 52-62 (June 2025)

Codimension Two Bifurcation

In this section, we add α_{22} (which is the reinfection rate parameter of the new variant) as a new free parameter. We then follow the loci of the fold bifurcation and obtain the fold bifurcation curve. As we increase α_{22}, we find the Bogdanov-Takens bifurcation point

$$BT := (\delta_2, \alpha_{22}) = (0.70518678919, 2.0727176300)$$

which means there is a Hopf bifurcation near that point. After we found one Hopf bifurcation point, we followed its loci and obtained the Hopf bifurcation curve. These results are shown in Figure 5 (Left). We give four examples to illustrate the dynamic for each region in Figures 4 (Left), 5 (Right), and 6.

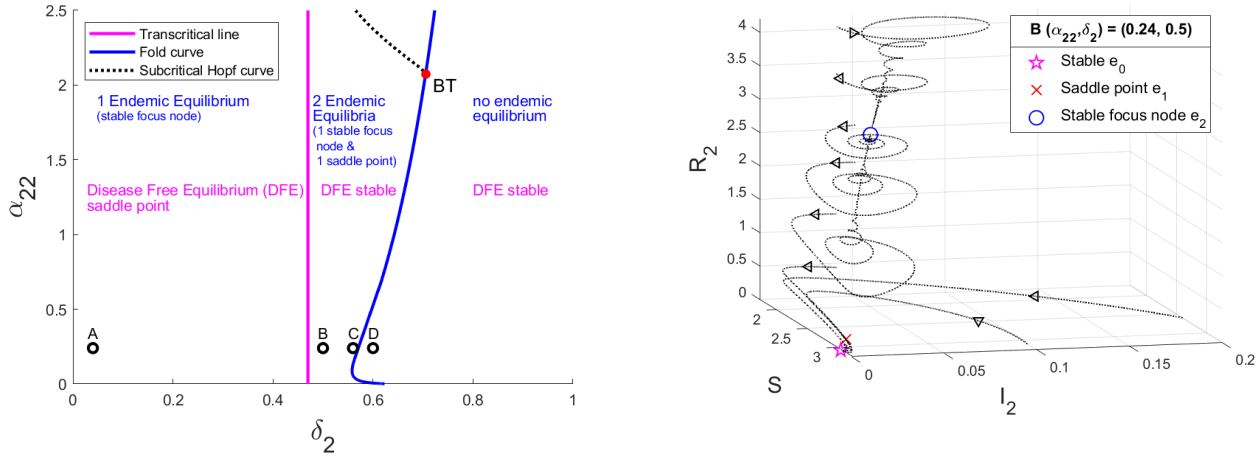

Figure 5. (Left) Two parameter bifurcation diagram of the nontrivial equilibrium of System (1) for $0 \leq \delta_2 \leq 1{,}0 \leq \alpha_{22} \leq 2.5$. (Right) Some orbits for the B parameter set.

The transcritical bifurcation point does not depend on parameter α_{22}, since $\mathcal{R}_0$ does not either, according to formula (4). For $\delta_2 < 0.469970711$, for example, in the A parameter sets in Figure 4 (Left), we have the disease-free equilibria e_0, which is saddle point typed (magenta cross symbol), and the stable focus node e_2 (blue circle symbol). We have two nontrivial equilibriums, e_1 and e_2, but e_1 is negative. By passing through the transcritical line, e_1 becomes positive. Then, e_0 and e_1 switch their stability, so e_0 becomes stable (magenta star symbol), and we obtain the new saddle point e_1 (Figure 5 (Right)). These nontrivials become closer (Figure 6 (Left)), collide and vanish at the fold bifurcation point. As a result, we only have one stable disease-free equilibria e_0, as in Figure 6 (Right).

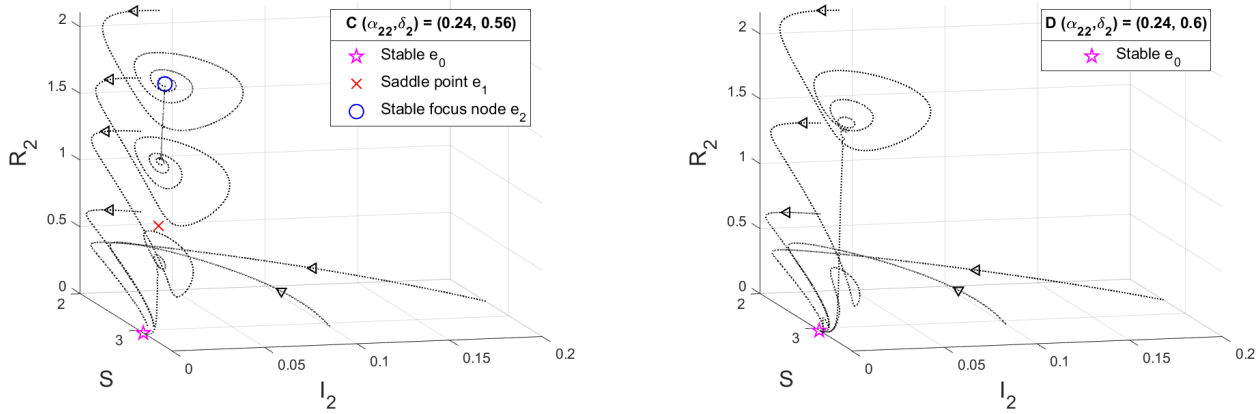

Figure 6. Some orbits for the C and D parameter sets.

We are interested in seeing the dynamics near the Bogdanov-Takens point and focusing on the nontrivial equilibrium e_2. We present four different topological examples to illustrate the dynamics between the C parameter set and the D parameter set (see Figures 8 and 9).

In the previous set of parameters, labeled as the E parameter set and illustrated in Figure 8 (Left), e_2 is a stable focus node (blue circle symbol). However, in the F parameter set, the system undergoes a homoclinic bifurcation. The solution for some initial conditions near the homoclinic orbit (dash-dotted red orbit) will have a very large period (see Figure 8 (Right)).

By increasing δ_2, in the G parameter set, the homoclinic orbit has shrunk and become an unstable limit cycle (dashed blue orbit), as shown in Figure 9 (Left). After passing through the subcritical Hopf curve in the H parameter set, the unstable limit cycle collides with e_2, and e_2 becomes an unstable focus node (blue square symbol), as shown in Figure 9 (Right).

DOI:https//doi.org/10.22452/mjs.vol44no2.5
Malaysian Journal of Science 44(2): 52-62 (June 2025)

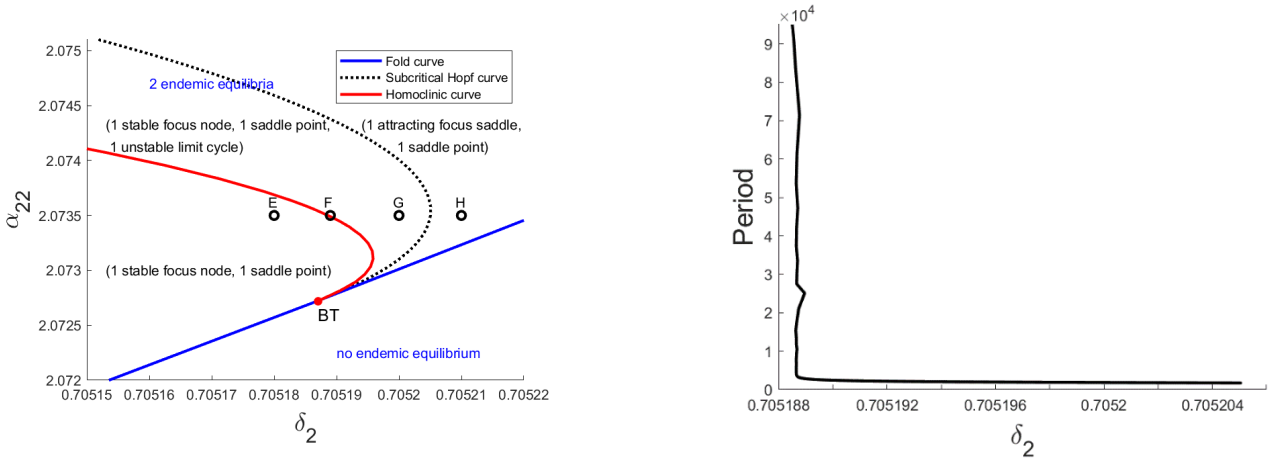

Figure 7. (Left) Two parameter bifurcation diagram of the nontrivial equilibrium of System (1) near the Bogdanov-Takens bifurcation point. (Right) The branch of periodic solution at $\alpha_{22} = 2.0735$ as variation on parameter δ_2. By numerical observation, the homoclinic orbit occurs at $\delta_2 = 0.70518803536$.

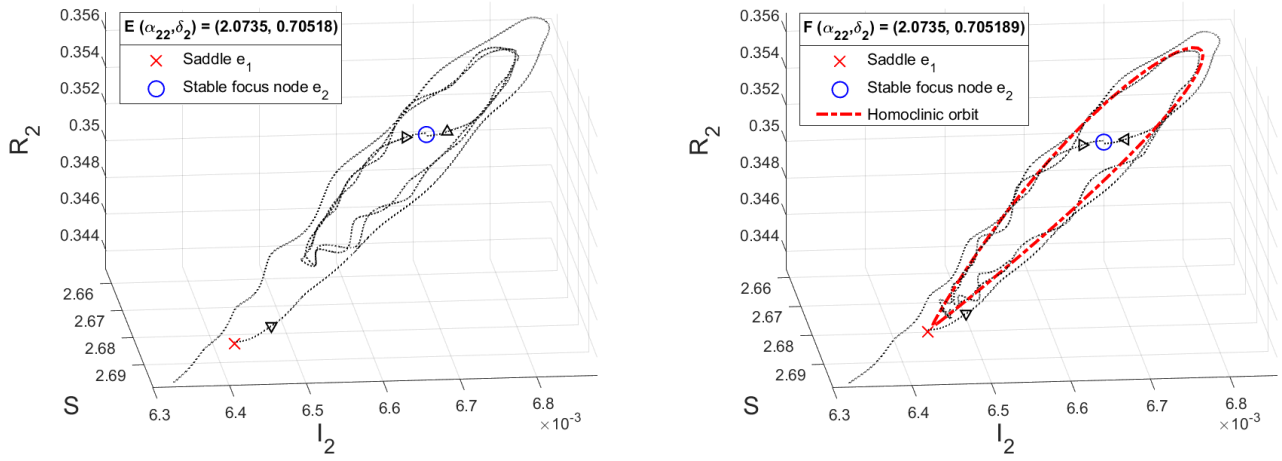

Figure 8. Some orbits for the E dan F parameter set.

5. Conclusion Remarks

We developed a SIRI model to investigate the reinfection rate, α_{22}, and Case Fatality Rate, δ_2, of a new COVID-19 variant in preventing the spread of COVID-19. Our calculations yielded the basic reproduction number $\mathcal{R}_0$, which revealed a stable disease-free equilibrium for all parameter values, provided $\mathcal{R}_0 < 1$. By varying α_{22} and δ_2, we discovered a codimension two bifurcation, known as the Bogdanov-Takens bifurcation. Further numerical analysis allowed us to gain a better understanding of the behavior near this bifurcation point, including the identification of a domain of parameters containing a stable limit cycle and a homoclinic orbit.

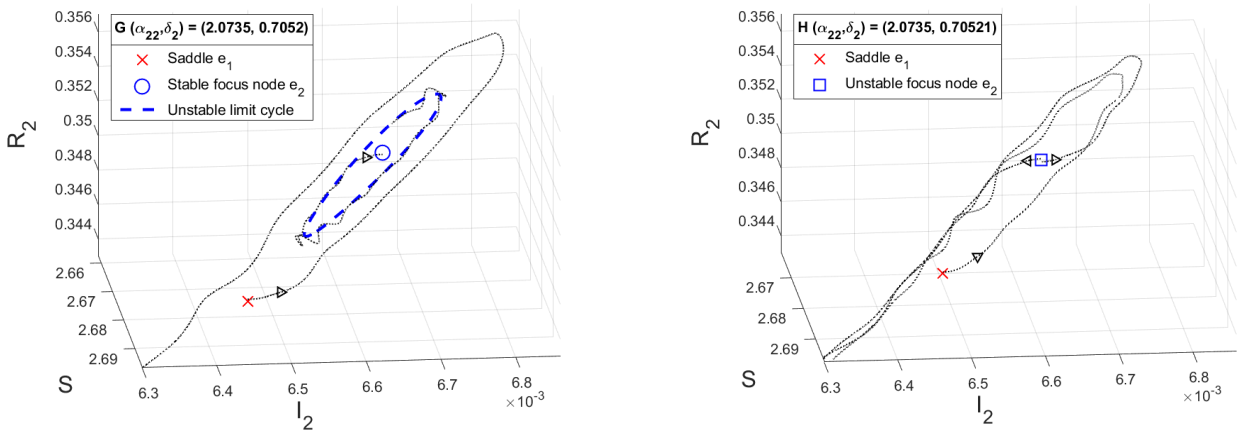

Figure 9. Some orbits for the G and H parameter set.

DOI:https//doi.org/10.22452/mjs.vol44no2.5
Malaysian Journal of Science 44(2): 52-62 (June 2025)

Our simulation of parameter sets A, B, C, E, F, and G demonstrated the persistence of a COVID-19 variation. We examined the manner in which a pandemic could occur based on initial conditions, even with a small infected population, in addition to analyzing infection and mortality rates. We believe that the codimension two bifurcation diagram could provide valuable insight into forecasting the impact of any future COVID-19 variants.

6. Acknowledgement

I would like to acknowledge the Indonesian Mathematical Society (IndoMS) for the research visit grant and give my warmest thanks to Dr. Wirawan Chinviriyasit (King Mongkut's University of Technology Thonburi, Thailand), who made this work possible. I am indebted to Dr. Johan Matheus Tuwankotta for his continuous support and feedback throughout the research process. Furthermore, I also acknowledge the financial support from Lembaga Penelitian dan Pengabdian Masyarakat (LPPM), Parahyangan Catholic University.

7. References

Agusto, F. B. (2013). Optimal isolation control strategies and cost-effectiveness analysis of a two-strain avian influenza model. Biosystems, 113(3), 155-164.

Duan, L., Huang, L., & Huang, C. (2021). Spatial dynamics of a diffusive SIRI model with distinct dispersal rates and heterogeneous environment. Communications on Pure and Applied Analysis, 20(10), 3539-3560.

European Centre for Disease Prevention and Control. Available online: https://www.ecdc.europa.eu/en/infectious-disease-topics/z-disease-list/covid-19/ facts/transmission-covid-19 (accessed on Februari 26, 2024).

Martins, J., & Pinto, A. (2017). Bistability of evolutionary stable vaccination strategies in the reinfection SIRI model. Bulletin of mathematical biology, 79, 853-883.

McMahon, A., & Robb, N. C. (2020). Reinfection with SARS-CoV-2: Discrete SIR (susceptible, infected, recovered) modeling using empirical infection data. JMIR public health and surveillance, 6(4), e21168.

Ndaïrou, F., Area, I., Nieto, J. J., & Torres, D. F. (2020). Mathematical modeling of COVID-19 transmission dynamics with a case study of Wuhan. Chaos, Solitons & Fractals, 135, 109846.

Nurjanah, A., & Prawoto, B. P. (2022). Dinamika Model Siri Covid-19 Dengan Adanya Pengaruh Kerumunan. MATHunesa: Jurnal Ilmiah Matematika, 10(2), 280-288.

Office for National Statistics (ONS) - Coronavirus (COVID-19) Infection Survey in UK. Available online: https://www.ons.gov.uk/peoplepopulationandcommunity/healthandsocialcare/conditionsanddiseases/datasets/coronaviruscovid19infectionsurveydata (accessed on October 19, 2022).

Our World in Data. SARS-CoV-2 sequences by variant. Available online: https://ourworldindata.org/explorers (accessed on May 2, 2023).

Pinto, L. M., Nanda, V., Sunavala, A., & Rodriques, C. (2021). Reinfection in COVID-19: A scoping review. medical journal armed forces india, 77, S257-S263.

Salman, A. M., Ahmed, I., Mohd, M. H., Jamiluddin, M. S., & Dheyab, M. A. (2021). Scenario analysis of COVID-19 transmission dynamics in Malaysia with the possibility of reinfection and limited medical resources scenarios. *Computers in biology and medicine*, *133*, 104372.

Saxena, S. K. (Ed.). (2020). Coronavirus disease 2019 (COVID-19): epidemiology, pathogenesis, diagnosis, and therapeutics. Springer nature.

Sharma, S., Badshah, V. H., & Gupta, V. K. (2017). Analysis of a SIRI Epidemic Model with Modified Nonlinear Incidence Rateand Latent Period. Asian Journal of Mathematics and Statistics, 10, 1-12.

Strogatz, S. H. (2018). Nonlinear dynamics and chaos with student solutions manual: With applications to physics, biology, chemistry, and engineering. CRC press.

Ud Din, R., Shah, K., Ahmad, I., & Abdeljawad, T. (2020). Study of transmission dynamics of novel COVID-19 by using mathematical model. Advances in Difference Equations, 2020, 1-13.

Van den Driessche, P. (2017). Reproduction numbers of infectious disease models. Infectious disease modelling, 2(3), 288-303.

Wangari, I. M., Sewe, S., Kimathi, G., Wainaina, M., Kitetu, V., & Kaluki, W. (2021). Mathematical modelling of COVID-19 transmission in Kenya: a model with reinfection transmission mechanism. *Computational and Mathematical Methods in Medicine*, *2021*, 1-18.

Wituła, R., & Słota, D. (2010). Cardano's formula, square roots, Chebyshev polynomials and radicals. Journal of Mathematical Analysis and Applications, 363(2), 639-647.

Yale Medicine. Will BA.2.86 ('Pirola'), the New Coronavirus Variant, Increase COVID-19 Cases?. Available online: https://www.yalemedicine.org/news/new-covid-variant-ba286-pirola (accessed on September 1, 2023).

DOI:https//doi.org/10.22452/mjs.vol44no2.5
Malaysian Journal of Science 44(2): 52-62 (June 2025)

Yang, Y., Zhou, J., & Hsu, C. H. (2019). Threshold dynamics of a diffusive SIRI model with nonlinear incidence rate. Journal of Mathematical Analysis and Applications, 478(2), 874-896.

Yong, B., Owen, L., & Hoseana, J. (2022). Mathematical Analysis of an Epidemic Model for COVID-19. Letters in Biomathematics, 9(1), 3–22.

Yong, B., Hoseana, J., & Owen, L. (2022). A design of governmental policies for the eradication of COVID-19 in Jakarta using an SIR-type mathematical model. Commun. Math. Biol. Neurosci., 2022 (2022), Article ID 26

World Health Organization (WHO). COVID-19 weekly epidemiological update. Available online: https://www.who.int/publications/m/item/weekly-epidemiological-update-on-covid-19 1-september-2023 (accessed on September 1, 2023).

DOI:https//doi.org/10.22452/mjs.vol44no2.5
Malaysian Journal of Science 44(2): 52-62 (June 2025)

MALAYSIAN JOURNAL OF SCIENCE
MJS
ISSN 1394-3065

Regular Issue

Malaysian Journal of Science 44 (2): 63-68 (June 2025) https://mjs.um.edu.my

Probing the Rotation Curve of NGC 4501 Galaxy using Two Different Models

Israa Abdulqasim Mohammed Ali[1a*], Hareth Saad Mahdi[2b], Zamri Zainal Abidin[3c] and Danial Ahmad Ariffin Lee[4c]

Abstract: Rotation curves of spiral galaxies have become an important tool for investigating their physical properties and is usually used as evidence for dark matter presence in their haloes. This research aims to probe the rotation curve of the spiral galaxy NGC 4501. The HI data of this galaxy have been collected from Very Large Array (VLA) and nonlinear fitting techniques have been used in this research for different components: stars, gas and halo. Particularly, kinematic analysis of NGC 4501's rotation curve has been carried out in this research using two different profile models: pseudo-isothermal profile and the Moore profile. The results of this study clearly showed that pseudo-isothermal model is better at reproducing the rotation curve of NGC 4501 than Moore model. The reduced chi-square, $\chi^2_{\rm red}$ of pseudo-isothermal is found to be close to one whereas Moore model does not agree with observational data. This is due to the fact that the pseudo-isothermal model is characterized primarily by the linearity of its behavior within the inner region together with the flat profile at large radii. As a result, the dark matter distribution in NGC 4501 is one that may be represented by a core halo model.

Keywords: *Dark matter, evolution, galaxies: individual (NGC 4501).*

1. Introduction

Initial rotation curve studies of spiral galaxies showed that some of the matter in these objects were "missing" (See for example: Bosma, 1981; Sofue & Rubin, 2001; Ali et al., 2018). Since then, this "missing" substance has become an aspect of cosmology. A complex framework has been developed to explain and detail the characteristics of the Universe incorporating a constant (Λ) and Cold Dark Matter (CDM) that does not interact. The ΛCDM model offers an understanding of the Universe as evidenced by findings, like the WMAP results (Spergel et al., 2007) and the Planck results (Planck Collaboration et al. 2015). However, challenges persist on scales within galaxies as highlighted in studies, by Klypin et al. (1999). Moore et al. (1999).

Studying how galaxies rotate has proven to be quite valuable, in understanding their kinematics and mass distribution of galaxies (Oort, 1927; Babcock, 1939; de Swart, 2017). Previous studies note that the flat rotation curve profile on the outside of a galaxy. This contrasts with Kepler's Law, which predicts a decline in rotational velocity further away from the center. Others have stated that the rotational velocity should increase in the outskirts of a galaxy (Freeman, 1970). The observed flat rotational velocity implies a significant disparity between theoretical expectations and actual observations, specifically arising from inconsistencies in the distribution of light (luminous matter) compared to the matter distribution inferred from the rotation curve (Zwicky, 1933; Kahn, 1959; Ali et al., 2021). Specifically, this disagreement may be seen in the way that rotational velocity behaves. It is hypothesized that the structure of galaxies must have a component called the dark matter halo. This is thought to have a mass density that might supply galaxies with a rotation curve that is flat. Dark matter is also necessary on larger scales in order to have consistency with dynamics and the creation of structures based on observations (Bertone, 2005).

On the other hand, modified gravity theories were also suggested as an attempt to describe the behavior of the galactic rotation curves instead of dark matter theory. Gaining a knowledge of the characteristics and fundamentals of dark matter represents one of the most difficult and important topics in modern cosmological studies (Mannheim, 2006; Moffat, 2013).

NGC 4501 (or M88) is a spiral galaxy in Coma Berenices, which is between 50 and 60 million light-years away. It was one of the first galaxies of its kind to be discovered within the Virgo Cluster (Binggeli, 1985). According to Mollenhoff et al., (2001), the spiraling arms of the galaxy exhibit an exceptionally regular pattern that can be tracked into the center of the galaxy. A type 2 Seyfert galaxy displays narrow line emissions caused by ionised gas located at its core. A concentrated mass of gas measuring 230 parsecs in diameter can be identified at the core of this galaxy. The condensation is mainly supported by the flow coming from the spiral arms as mentioned by Onodera et al. in 2002. Numerous previous studies have delved into the properties of NGC 4501 and similar galaxies with diverse characteristics to comprehend the structure of galaxies. This research provides a study of the rotation curve of NGC 4501 and fitting two different models to the observational data of HI.

Authors information:

[a]Department of Remote Sensing, College of Remote Sensing and Geophysics, Al-Karkh University of Science, Baghdad, 10003, IRAQ. Email: israa.aq88@gmail.com/israa.aq88@kus.edu.iq[1]

[b]Astronomy and Space Department, College of Science, University of Baghdad, Baghdad, IRAQ. Email: hareth@uobaghdad.edu.iq[2]

[c]Department of Physics, Faculty of Science, Universiti Malaya, 50603 Kuala Lumpur, MALAYSIA. Email: zzaa@um.edu.my[3]; danny_9112@yahoo.com[4]

*Corresponding Author: zzaa@um.edu.my

Received: July, 2023
Accepted: June, 2024
Published: June, 2025

DOI:https//doi.org/10.22452/mjs.vol44no2.6
Malaysian Journal of Science 44(2): 63-68 (June 2025)

2. Data

Data for NGC4501 is available publicly and obtained via the Very Large Array (VLA) radio telescope. Observations were carried out on January 20th, 1991, and required 552060s of integration time. The spectra were collected using 63 channels at LL and RR polarizations with a bandwidth of 3.027 MHz, and a primary focus on the HI 21-cm line. The 27-antenna C configuration was used for the L-band observations.

The Common Astronomy Software Application (CASA) was used for the image processing and data reduction tasks. The task 'uvconsub' gives the HI map cube from the continuum subtracted instabilities. Multi scale clean with Briggs weighting produces the cleaned images. Beam size is 16.83"× 16.41" with PA = 140º, corresponding to the angular linear scales of 1.38 ×1.35 kpc at distance of 17 Mpc (see Figure 1).

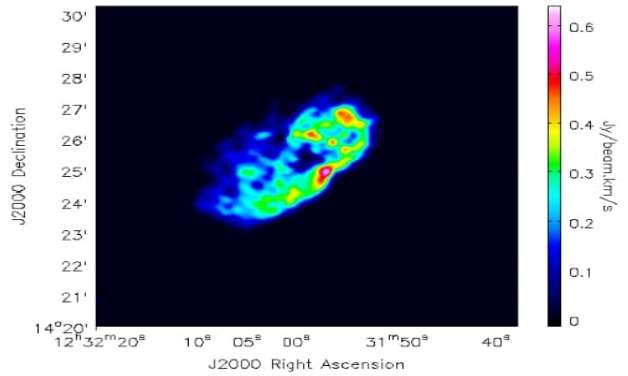

Figure 1. Integrated-intensity image of NGC 4501 at 21cm.

3. Methodology and Results

Rotation Curve of NGC 4501

Using the 3DBarolo software (Teodoro & Fraternali, 2015), we obtained rotation curves from the HI data cube of NGC 4501. The software produces tilted-ring models and compares them in 3D, allowing for comprehensive control of observational effects, particularly beam smearing, which can alter the derivation of rotational velocities within galaxies.

Three geometrical parameters define the model: the galaxy center coordinates (x0, y0), position angle (PA), and inclination (i). The kinematic parameters include the redshift (z), rotation velocity (Vrot), and velocity dispersion (σ). The systemic velocity, Vsys, was assumed to be 2280 km/s, and all rings were centered on the center of NGC 4501 as in Chung et al. (2009) (see Table 1). After considering these assumptions, the only fitting parameters that remain are i, PA, Vrot, and σ. To obtain initial estimates for the kinematic parameters (i and PA), 3DBarolo fitted the HI cube map and used the results as starting points. Two steps were used to determine the rotation and dispersion: an initial fit with all four parameters left free, followed by fixing the geometric parameters and performing a new fit with only Vrot and σ.

The 3DBarolo software is a tool used for analysing galaxy rotation curves using VLA cube data. It surpasses methods, like Woods et al. (1990) Guhathakurta et al. (1988) Sofue et al. (2003). Nehlig et al. (2016) by incorporating 3D fitting to address challenges such as beam smearing of solely depending on velocity field maps. Its reliability, capability to detect sources and ability to predict conditions greatly enhance the efficiency of automated analysis especially when dealing with datasets. This software is an asset for scientists those studying galaxies, with different data resolutions.

Figures 2 and 3 reveal the velocity and variations, between the model and actual data using a position velocity (PV) chart along both the major and minor axes. The rotating velocity of the galaxy is shown to increase linearly from its innermost core to its farthest regions, remains almost constant at the outside. The rotation curve can be described as a combination of influences, from stars, gas and halo components (Ali et al. 2018).

$$V_{\text{total}}^2 = V_{\text{disc}}^2 + V_{\text{gas}}^2 + V_{\text{halo}}^2 \quad (1)$$

Using Mathematica software, the rotation curve's contribution from each component is calculated. We might determine the star, gas, and halo values that are the most correct by adding up the disk, gas, and halo components in all possible configurations before choosing the one that best fits the observed data (Tan et al., 2022).

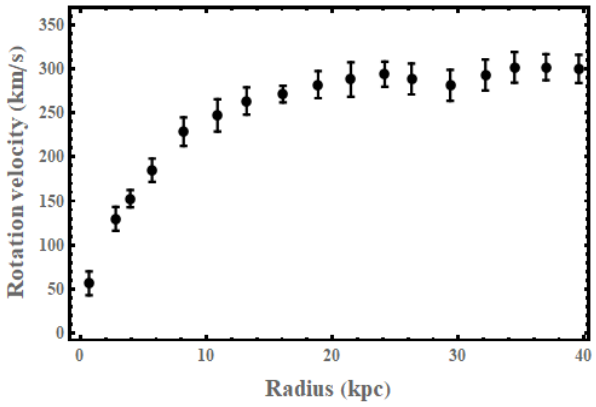

Figure 2. Velocities at different radii of NGC 4501 obtained from data cube with 3DBarolo, indicating the rotation curve profile.

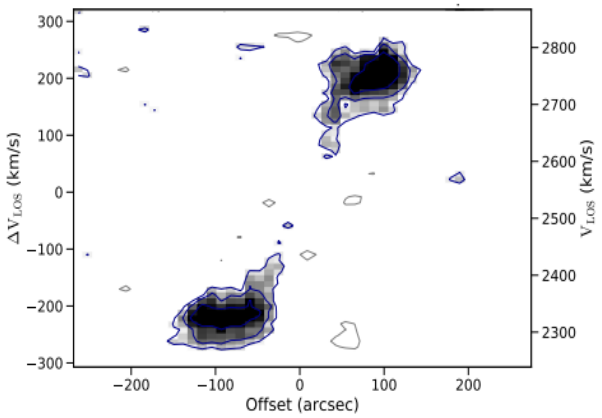

Figure 3. PV diagrams of galaxy NGC 4501 along major axes. The data are shown in grey, while the model is shown in blue.

DOI:https//doi.org/10.22452/mjs.vol44no2.6
Malaysian Journal of Science 44(2): 63-68 (June 2025)

Table 1. Properties of galaxy NGC 4501.

Parameter	Value
R.A.	12h31m59s.0
Dec.	$+14°25'10.0''$
Adopted distance	17 Mpc
PA	140°
i	59°
Systemic velocity	2280 km s^{-1}
z	0.007641

Dark Halo Profile

Researchers are expanding their study of dark matter by employing a broader theoretical framework in order to provide better tools for studying it directly. Our analysis of the NGC 4501 rotation curve considers both core and cusp dark halo profiles, allowing us to find the dark matter mass and distribution. The cored profile used is Pseudo-isothermal. While we used the Moore profile for the cuspy profile.

The density of a pseudoisothermal profile indeed approaches a constant density, typically denoted as ρ_0 at the center and transitions to a power-law behavior at larger radii. (de Blok et al., 2001). Simultaneously, the mass distribution adheres to a power law with a dependence on radius (R) of R^{-2} at large radii, ultimately approaching zero at infinity. Here are the dark matter density and velocity equations (Jimenez et al., 2003; Ali et al., 2021) for the pseudoisothermal profile:

$$\rho_{Iso}(R) = \frac{\rho_0}{1+(R/R_c)^2} \quad (2)$$

$$V_{\mathrm{ISO}}(R) = \sqrt{4\pi G\rho_0 R_c^2\left(1-\frac{R}{R_c}\mathrm{atan}\left(\frac{R}{R_c}\right)\right)} \quad (3)$$

Where G represents the gravitational constant, ρ_0 and R_C are the central density and the core radius of the halo. The definitions of these parameters are exactly the same for another model. Dark halo density and velocity are given by Moore model (Moore et al., 1999):

$$\rho_{Moore}(R) = \frac{\rho_0}{\left(\frac{R}{R_c}\right)^{1.5}\left(1+\left(\frac{R}{R_c}\right)^{1.5}\right)} \quad (4)$$

$$V_{Moore}^2(r) = \frac{8.38G\rho_0 R_c^3}{R}\left(\ln\left(1+\left(\frac{R}{R_c}\right)^{1.5}\right)\right) \quad (5)$$

Baryonic Velocities

Star Velocity

The majority of the luminosity is taken up by stars, while the remainder, which is less than 10%, is made up of interstellar gas. As a result, the distribution of the luminosity of the star disc nearly represents the distribution of the luminous mass (Sofue 2013). The velocity of the star disc (exponential disc) is given by the equation below

$$V_{disc}^2 = \frac{GM_d R^2}{2R_d}(I_o K_o - I_1 K_1) \quad (6)$$

Where I_n and K_n are the first and second kinds of modified Bessel functions, respectively, measured at 1.6x, where x = $\frac{R}{R_d}$. R_d is the disc scale length, which is measured in kpc and M_d represents the mass of the galactic disc, which is the total mass of the flattened, rotating disk component within a galaxy, and it is treated as a free parameter in our analysis. The assumed disc scale length for NGC 4501 is 45.53 arcsec (Möllenhoff 2001), which corresponds to 5.75 kpc.

Gas Velocity

The gas velocity of NGC 4501 can be calculated by taking into account the equation shown below (Ali et al., 2018),

$$V_{gas}(r) = \sqrt{\frac{GM_{HI}(R)}{R}}, \quad (7)$$

where M_{HI} is the mass of the HI gas as determined by the following equation:

$$M_{HI}(R) = 2\pi\int_0^R r\,\Sigma\,(R)dR \quad (8)$$

where Σ represents the surface density of the HI gas, calculated using 3D-Barolo as shown in Figure 4. The HI mass value of galaxy NGC 4501 galaxy can then be determined. Therefore, the rotational velocity of the HI gas might be estimated as revealed in Figure 5.

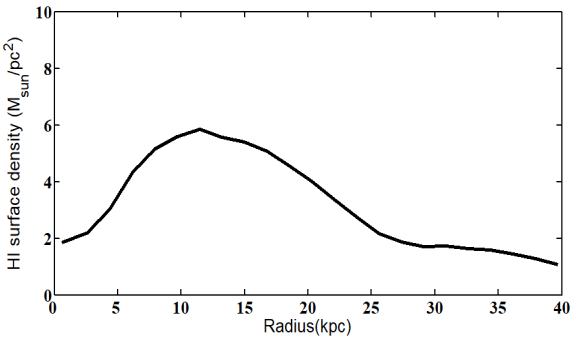

Figure 4. HI gas surface density of NGC 4501.

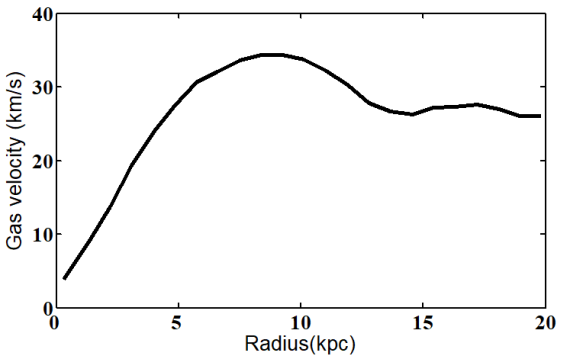

Figure 5. HI velocity of NGC 4501.

DOI:https//doi.org/10.22452/mjs.vol44no2.6
Malaysian Journal of Science 44(2): 63-68 (June 2025)

4. Discussion

In this study, the nonlinear least square approach was utilized to match observations with equation (1) by taking into consideration either the ISO model (see Eq. 3) or the Moore model (see Eq. 5). In order to evaluate a model, it is common practice to compare the actual data to the expected data from the model and find the correlation between the two. Consequently, we performed the chi-square function to evaluate rotation curve fitting. The parameter, χ^2, that needs to be minimized is (Bevington et al., 1969):

$$\chi^2 = \sum_{i=1}^{N} \left(\frac{(y_i - y(x_i,a,b,c))^2}{\sigma_i^2} \right) \quad (9)$$

Where y_i and σ_i refer to number i of data points and their associated uncertainty for the NGC 4501 galaxy, respectively. $y(x_i, a, b, c)$ represents the model function values computed at the radius, x_i and (a, b, c) are the fit parameters. Then, we applied the reduced chi-square, χ^2_{red} to perform the goodness-of-fit test. A good model would give a χ^2_{red} value close to one.

The rotation curve obtained in Figure 6 and the χ^2_{red} test in Table 2 show that the rotation curve of pseudo-isothermal model has a linear increase in the inner region, but it flattens out as the radius gets larger. Over this, the pseudo-isothermal model is able to obtain the best fitting with χ^2_{red} equal to 0.89, which is the value that is closest to one and NGC 4501 has a core missing matter distribution. However, at radii less than 10kpc, the Moore profile generates a dark matter velocity that exceeds the total rotational velocity. Above 10 kpc to larger radii, the Moore profile constantly gives a lower dark matter velocity than the total rotational velocity. Based on our results, the Moore profile is inappropriate for NGC 4501.

The expected curve falls inside the confidence bands also provides support for the best-fit V_{ISO} model (χ^2_{red} value ~ 1). Figures 7 and 8 show the confidence bands that were calculated using the two different models. It shows graphically how well the match of the data and the best-fit curve. Confidence bands for the rotation velocity as a function at various points from the galactic centre are shown in purple here as solid purple lines, with the corresponding purple shaded area representing the 68% confidence level. The error bars on the rotation curves seen can also be viewed as confidence bands, with 95% confidence that the curves are contained within the blue bands. The green shaded area, representing a 99% confidence bands, can be interpreted in the same way. Otherwise, one data point with an error bar in Figure 8 is seen to be outside these confidence limits.

Furthermore, we estimated the mass of pseudo-isothermal dark matter (M_{Iso}) to be approximately $7.4\times10^{11}\ M_{\odot}$. This value exceeds the total luminous mass ($1.41\times10^{11}\ M_{\odot}$) of the entire galaxy, which includes the disk and the gas. These findings emphasize the significant contribution of dark matter to the overall mass distribution in NGC 4501 (see Figure 9).

This research makes a contribution to the study of how dark matter's distribution within galaxies. Our study shows a remarkable consistency between the mass models and observed rotation curves providing evidence for the presence of dark matter in galaxy systems (Frusciante et al., 2012; Hashim et al., 2015). This study stands out when compared to analyses of previous rotation curves. It is especially noteworthy given the controversy in the scientific literature concerning the distribution of cuspy profile (Ali et al., 2018). Since it is consistent with the cored profile trend, our research contributes significant new information to the ongoing debate on the nature of the dark matter distribution in galaxies, underscoring the requirement for a deeper and more thorough comprehension of galactic dynamics.

Table 2. Free parameters with χ^2_{red} for the two dark halo profiles.

Halo models	M_D ($M_{\odot}$)	ρ_0 ($M_{\odot}$ kpc^{-3})	R_c (kpc)	χ^2_{red}
Pseudo-isothermal	$(1.25\pm0.12)\times10^{11}$	$(1.16\pm0.38)\times10^{7}$	15.57	0.89
Moore	$(8\pm6.93)\times10^{10}$	$(1.77\pm6.24)\times10^{6}$	29.34	4.59

5. Conclusion

Studying the rotation curves is a way to investigate the existence and characteristics of dark matter in galaxies. Using a gradient-based nonlinear least-squares fitting method, we find that the best-fitting model function, ISO model, is a fits well with the measured rotation curve of the NGC4501galaxy, as compared to another model, Moore model. According to this result, a cored dark matter halo should be expected for the NGC4501 galaxy if ISO model is used to explain the dark matter distribution. Therefore, we can describe the structure of the NGC4501 galaxy's missing matter, which tends more toward a cored missing matter distribution with a halo mass of $7.4\times10^{11}\ M_{\odot}$.

DOI:https//doi.org/10.22452/mjs.vol44no2.6
Malaysian Journal of Science 44(2): 63-68 (June 2025)

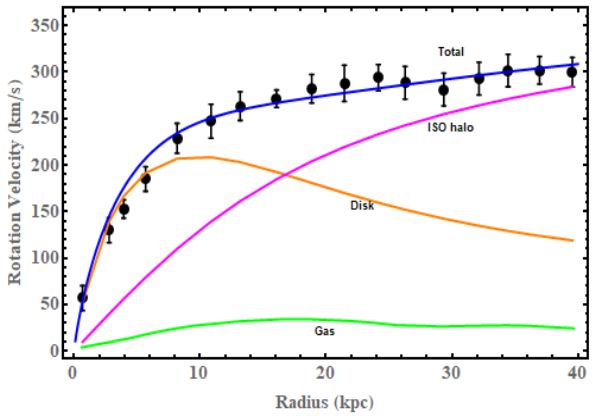

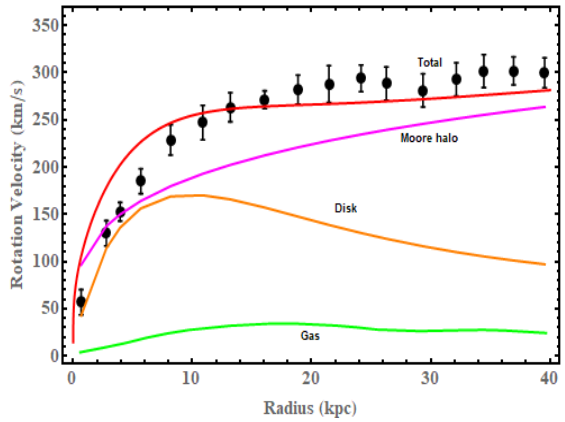

Figure 6. The nonlinear rotational velocity of NGC 4501 by employing two halo models. The contributions of dark matter halo, star, and gas velocities are represented, respectively, in purple, orange, and green.

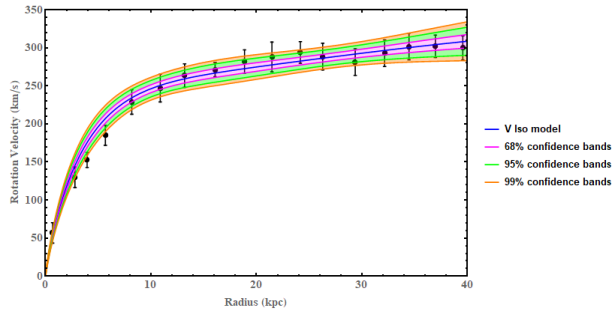

Figure 7. Confidence level band with Pseudoisothermal model.

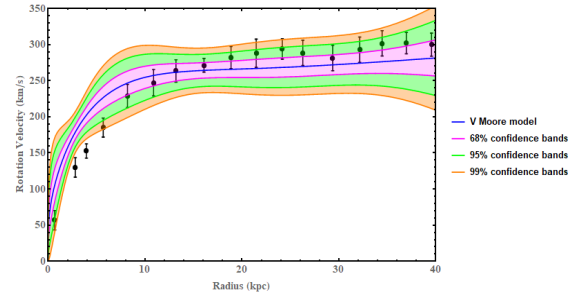

Figure 8. Confidence level band with Moore model.

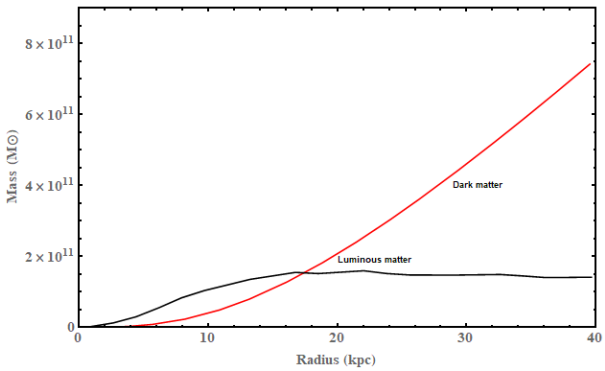

Figure 9. Variation of dark matter and luminous matter in the galaxy NGC 4501 as a function of radius.

6. References

Ade, P. A., Aghanim, N., Arnaud, M., Ashdown, M., Aumont, J., Baccigalupi, C., ... & Matarrese, S. (2016). Planck 2015 results-xiii. cosmological parameters. *Astronomy & Astrophysics*, 594, A13.

Ali, I. A. M. (2021). Testing Two Halo Models by Galactic Rotation Curve. In Journal of Physics: Conference Series (Vol. 1818, No. 1, p. 012197). IOP Publishing.

Ali, I. A. M., Hashim, N., & Abidin, Z. Z. (2018). The dark matter distribution of NGC 5921. *Indian Journal of Physics* 92(4): 409-415.

Babcock, H. W. (1939). The rotation of the Andromeda Nebula. Lick observatory bulletin, 19, 41-51.

Bertone, G., Hooper, D., & Silk, J. (2005). Particle dark matter: Evidence, candidates and constraints. *Physics reports* 405(5-6): 279-390.

Bevington, P. R., & Robinson, D. K. (1969). *Data reduction and error analysis for the physical sciences.* New York, 19692, 235.

Binggeli, B., Sandage, A., & Tammann, G. A. (1985). Studies of the Virgo Cluster. II-A catalog of 2096 galaxies in the Virgo Cluster area. *The Astronomical Journal* 90: 1681-1759.

Bosma, A. (1981). 21-cm line studies of spiral galaxies. II. The distribution and kinematics of neutral hydrogen in spiral galaxies of various morphological types. *The Astronomical Journal 86*: 1825-1846.

Chung, A., Van Gorkom, J. H., Kenney, J. D., Crowl, H., & Vollmer, B. (2009). VLA imaging of virgo spirals in atomic gas (VIVA). I. The atlas and the H i properties. *The Astronomical Journal 138*(6): 1741.

de Blok, E., McGaugh, S., & Rubin, V. (2001). High-resolution rotation curves of LSB galaxies: Mass Models. arXiv preprint astro-ph/0107366.

DOI:https//doi.org/10.22452/mjs.vol44no2.6
Malaysian Journal of Science 44(2): 63-68 (June 2025)

de Swart, J., Bertone, G., & van Dongen, J. How dark matter came to matter. Nature Astron. 1, 0059 (2017). arXiv preprint arXiv:1703.00013.

Freeman, K. C. (1970). On the disks of spiral and S0 galaxies. *The Astrophysical Journal* 160: 811.

Frusciante, N., Salucci, P., Vernieri, D., Cannon, J.M. & Elson, E.C. (2012). The distribution of mass in the Orion dwarf galaxy. *Monthly Notices of the Royal Astronomical Society* 426(1): 751-757.

Guhathakurta, P., Van Gorkom, J. H., Kotanyi, C. G., & Balkowski, C. (1988). A VLA HI survey of the Virgo cluster spirals. II-Rotation curves. Astronomical Journal (ISSN 0004-6256), vol. 96, Sept. 1988, p. 851-866., 96, 851-866.

Hashim, N., Abidin, Z. Z., Ibrahim, U. F. S. U., Hassan, M. S. R., Hamidi, Z. S., Umar, R., & Ibrahim, Z. A. (2015). The nonlinear least square fitting for rotation curve of Orion dwarf spiral. *Sains Malaysiana*, 44(3), 457-462.

Jimenez, R., Verde, L., & Oh, S. P. (2003). Dark halo properties from rotation curves. *Monthly Notices of the Royal Astronomical Society* 339(1): 243-259.

Kahn, F. D., & Woltjer, L. (1959). Intergalactic Matter and the Galaxy. *The Astrophysical Journal* 130: 705.

Klypin, A., Kravtsov, A. V., Valenzuela, O., & Prada, F. (1999). Where are the missing galactic satellites?. The Astrophysical Journal, 522(1), 82.

Mannheim, P. D. (2006). Alternatives to dark matter and dark energy. P*rogress in Particle and Nuclear Physics* 56(2): 340-445.

Moffat, J. W., & Rahvar, S. (2013). The MOG weak field approximation and observational test of galaxy rotation curves. *Monthly Notices of the Royal Astronomical Society* 436(2): 1439-1451.

Möllenhoff, C., & Heidt, J. (2001). Surface photometry of spiral galaxies in NIR: structural parameters of disks and bulges. *Astronomy & Astrophysics* 368(1): 16-37.

Moore, B., Quinn, T., Governato, F., Stadel, J., & Lake, G. (1999). Cold collapse and the core catastrophe. *Monthly Notices of the Royal Astronomical Society* 310(4): 1147-1152.

Nehlig, F., Vollmer, B., & Braine, J. (2016). Effects of environmental gas compression on the multiphase ISM and star formation-The Virgo spiral galaxies NGC 4501 and NGC 4567/68. Astronomy & Astrophysics, 587, A108.

Onodera, S., Sofue, Y., Koda, J., Nakanishi, H., & Kohno, K. (2002). CO (J= 1-0) Observations of the Non-Barred Seyfert 2 Galaxy NGC 4501. In 8th Asian-Pacific Regional Meeting, Volume II (pp. 199-200).

Oort, J. H. (1927). Observational evidence confirming Lindblad's hypothesis of a rotation of the galactic system. *Bulletin of the Astronomical Institutes of the Netherlands* 3: 275.

Sofue, Y., & Rubin, V. (2001). Rotation curves of spiral galaxies. *Annual Review of Astronomy and Astrophysics* 39(1): 137-174.

Sofue, Y., Koda, J., Nakanishi, H., & Onodera, S. (2003). The virgo high-resolution CO survey: II. Rotation curves and dynamical mass distributions. Publications of the Astronomical Society of Japan, 55(1), 59-74.

Sofue, Y. (2013). The mass distribution and rotation curve in the galaxy. arXiv preprint arXiv:1307.8215.

Spergel, D. N., Bean, R., Doré, O., Nolta, M. R., Bennett, C. L., Dunkley, J., ... & Wright, E. L. (2007). Three-year Wilkinson Microwave Anisotropy Probe (WMAP) observations: implications for cosmology. *The Astrophysical Journal Supplement Series* 170(2): 377.

Tan, W. S., Abidin, Z. Z., & Hashim, N. (2022). A comprehensive analysis using 9 dark matter halo models on the spiral galaxy NGC 4321. *Indian Journal of Physics* 96(3): 671-687.

Teodoro, E. D., & Fraternali, F. (2015). 3D BAROLO: a new 3D algorithm to derive rotation curves of galaxies. *Monthly Notices of the Royal Astronomical Society* 451(3): 3021-3033.

Woods, D., Madore, B. F., & Fahlman, G. G. (1990). Luminosity-velocity diagrams for Virgo Cluster spirals. I-Inner rotation curves. The Astrophysical Journal, 353, 90-102.

Zwicky, F. (1933). Die rotverschiebung von extragalaktischen nebeln. Helvetica Physica Acta, Vol. 6, p. 110-127, 6, 110-127.

DOI:https//doi.org/10.22452/mjs.vol44no2.6
Malaysian Journal of Science 44(2): 63-68 (June 2025)

MALAYSIAN JOURNAL OF SCIENCE
MJS
ISSN 1394-3065

Regular Issue

Malaysian Journal of Science 44 (2): 69-77 (June 2025) https://mjs.um.edu.my

Carbon-Based Materials/Latex Composite from *Euphorbia Tirucalli* Plant for Potential Bone Fracture Treatment

Supardi[1a], Pranita Wardani[2a], and Wipsar Sunu Brams Dwandaru[3a]*

Abstract: This study aims to investigate the preparation and characterization of carbon-based materials (CMs)/latex composites from the *Euphorbia tirucalli* plant for potential bone fracture treatment. The primary objectives are to: i) determine the antibacterial property of the CMs/latex composites against *Staphylococcus aureus* bacteria; and ii) determine the tensile strength of the CMs/latex composites via chicken bones as the model. The CMs were prepared using a simple heating method, using an oven at a temperature of 250 oC. The CMs/latex composites were prepared by mixing 3 ml of the latex and CMs solutions with concentrations of 10%, 20%, and 40% in 10 ml of distilled water. The CMs were characterized using UV-Vis, PL, and FTIR spectroscopies. The antibacterial property and tensile strength of the CMs/latex composites were tested using the diffusion method and an ultimate testing machine, respectively. The results obtained demonstrate that the CMs had absorption and emission peaks at wavelengths of 287 nm and 499 nm, respectively, resulting in cyan luminescence. The FTIR test of the CMs indicated the existence of the C=C, O-H, and N=C=S functional groups. The CMs/latex composites produced the highest diameter of inhibition zone and tensile strength of 3.24 mm and 0.02 kN, respectively. These findings show the potential application of CMs/latex composites for bone fracture treatment with antibacterial properties.

Keywords: *CMs, CMs/latex composites, bone fracture treatment, Euphorbia tirucalli plant.*

1. Introduction

Euphorbia tirucalli (*E. tirucalli*) has been known as an herbal plant, especially in Asian countries (da Silva et al., 2022). Various parts of the *Euphorbia* plant, such as its latex, stems, and twigs, have certain benefits, especially in traditional and/or herbal medicine. In various Asian countries, this plant is claimed to have many benefits for treating various diseases, e.g., cancer (Mali & Panchal, 2017). *Euphorbia* latex can treat fractures and accelerate wound healing, while the twigs can reduce bone and nerve pains (da Silva et al., 2022; Maver et al., 2015). The latex comes out from the surrounding branches that have been cut. Although latex is claimed to be able to treat fractures, research on this is relatively rare. The branches of the *Euphorbia* plant contain flavonoids and tannins, which produce anti-bacterial activity and potentially prevent wound infections (Pallavali et al., 2019). The latex and stem extracts from *E. tirucalli* were tested as antimicrobials against *Staphylococcus aureus* (*S. aureus*), *Bacillus subtilis* (*B. subtilis*), and *Pseudomonas aeruginosa* (*P. aeruginosa*) bacteria (Mali & Panchal, 2017). Moreover, converting the unused parts of the plant into carbon-based materials (CMs) may increase the applicability of the *Euphorbia* plant.

CMs hold a critical role in the development of functional materials. CMs include graphite, graphene and its derivatives, fullerene, carbon nanotubes (CNTs), biochar, and carbon nanodots (Cdots) (Sabzehmeidani et al., 2021; Liu et al., 2020). For example, Cdots are 0-dimensional (0D) nanomaterials with sizes of 1 nm to 10 nm. They comprise carbon atoms as the core and functional groups such as carbonyl, carboxyl, hydroxyl, or amine as the surface state (Xia et al., 2019). They are favorable to be mass produced because they have novel properties, e.g., good solubility, strong luminescence, biocompatibility, and non-toxicity (Kaur & Verma, 2022; Ghosh et al., 2022). CMs, especially Cdots, can be prepared from various organic carbon precursors, viz.: nam-nam fruit (Dwandaru et al., 2020), Arabic gum (Thakur et al., 2014), guar gum (Rahmani & Ghaemy, 2019), latex of *E. mili* (Bano et al., 2019), and also wastes such as watermelon peel (Liu et al., 2016) and chicken bone (Dwandaru & Sari, 2020). Various preparation methods can produce CMs: Hummer's method (Sabzehmeidani et al., 2021), hydrothermal (Khajuria et al., 2018; Bano et al., 2019; Dwandaru et al., 2019), microwave (Baipai et al., 2019; Pires et al., 2015; de Medeiros et al., 2019), pyrolysis (Weber & Quicker, 2018), and carbonization at low temperatures (Liu et al., 2016).

CMs have been widely utilized for various applications, including biosensors, photocatalysts, drug delivery systems, antibacterial agents, heat and power production, and soil amendment (Zhai et al., 2012; Wang & Hu, 2017; Weber & Quicker, 2018). For some examples, Cdots have been used for antibacterials with conjunctions to other antimicrobial reagents, such as H_2O_2, Na_2CO_3, and AcOH (acetic acid) (Dong et al., 2017). Cdots can help antimicrobial reagents to inhibit bacterial activities. In addition, N-doped Cdots/hydroxyapatite nanocomposites have also been developed for bone repair. Adding Cdots significantly improves bone regeneration and repair (Khajuria et al., 2018; Shao et al., 2017). Furthermore, C-dots can be conjugated with latex

Authors information:
[a]Physics Education Department, Faculty of Mathematics and Natural Sciences, Universitas Negeri Yogyakarta, Jl. Colombo No. 1, Karangmalang, Yogyakarta, 55281, INDONESIA. E-mail: supardi@uny.ac.id[1]; ranita.anita2016@student.uny.ac.id[2]; wipsarian@uny.ac.id[3]
*Corresponding Author: wipsarian@uny.ac.id

Received: September, 2023
Accepted: June 20, 2024
Published: June, 2025

DOI:https//doi.org/10.22452/mjs.vol44no2.7
Malaysian Journal of Science 44(2): 69-77 (June 2025)

materials, such as XSBR, which can be used as nano-filters (Sreenath et al., 2020).

The handling of bone fractures is typically carried out using plates, pins, wires, and couplers. The problem is that these objects are metals, foreign objects in the body. The use of plates and couplers requires drilling the bone. In this study, we offer another alternative in treating bone fractures using CMs from *E. tirucalli* as an additive for the fracture treatment. The chicken bone is used as a model for the bone fracture. The *E. tirucalli* latex is mixed with the CMs to form a CMs/latex composite. The characteristics of the resulting CMs are examined using ultraviolet-visible (UV-Vis) spectrophotometry, photoluminescence (PL) spectroscopy, and Fourier transform infrared (FTIR) spectroscopy. The tensile strength of the CMs/latex composites applied to the chicken bone is examined using the universal testing machine (UTM). The antibacterial properties of the CMs and CMs/latex composites based on the diameter inhibition zone (DIZ) against *S. aureus* bacteria are also determined.

This study explores the potential of a composite material, i.e., CMs/latex, for bone fracture treatment. There are limited studies in the related literature on applying *E. tirucalli* for bone fracture treatment. Furthermore, the combination of CMs and *E. tirucalli* latex has not been extensively investigated. By assessing the antibacterial properties and mechanical strength of this composite material, this study contributes to the development of bone fracture treatment. This study highlights its approach, interdisciplinary relevance, and potential contribution to advancing CMs and healthcare. It offers a novel and interdisciplinary investigation at the crossroads of CMs and medicine. It addresses the utilization of *E. tirucalli*-derived CMs and *E. tirucalli* latex in treating bone fractures, which has seen limited exploration thus far. By combining the inherent antibacterial properties of *E. tirucalli* with the advanced properties of CMs, we aim to develop a composite material with enhanced mechanical strength and antibacterial properties, providing a potential alternative to conventional approaches in bone fracture treatment.

The antibacterial ability of the CMs/latex composites provides a safe treatment of bone fractures and prevents infection when applied to the bones. Moreover, the improved tensile strength of the CMs/latex composites provides a better and safer support and/or buffer in the healing process of the bone fracture. Hence, the specific objectives of this study are i) to determine the antibacterial property of the CMs/latex composites against *S. aureus* bacteria; and ii) to determine the tensile strength of the CMs/latex composites via chicken bones as the model bones. The CMs produced in this study, their incorporation into latex, antibacterial assessments, and mechanical testing on a chicken bone model, offer a comprehensive examination of the composite's potential efficacy. In this case, the chicken bones are used as a real-life model for bones. Of course, the chicken bones used in this study do not respond to the treatment, as no living cells exist. However, in this study we do not directly investigate the respond of the bones to the treatment and leave this for future studies. In addition to its immediate applications in medicine, the findings of this study could hold broader implications for the advancement of CMs and their tailored use in medical contexts.

2. Method

The latex was extracted from the *E. tirucalli* plant. This was conducted by cutting the branches of the *E. tirucalli* plants. The latex came out drop by drop from the ends of the cut branches. The latex was collected into a container and tightly sealed to prevent drying. This process can be observed in Figure 1.

Figure 1. Latex collection of the *E. tirucalli* plant, i.e., a) cutting the branches; b) collecting the latex in a cup, c) pouring the latex into a sample container, and d) tightly sealing the latex in the sample container.

The CMs were prepared by washing 50 grams of *E. tirucalli* branch wastes, then cutting them into small pieces. Next, the branches were dried in the sun for 6 hours. The branches were heated in a Mitseda Electric Oven at a temperature of 250 ^{o}C for 2 hours and then mashed into powder. The powder was filtered to ensure that the powder size was homogeneous. The oven is heated to 250 °C for 20 minutes. The powder was then dissolved in distilled water at a ratio of 1:1, stirred, and left alone for 24 hours. The solution was then filtered twice using a 110 μm filter paper. Hence, the CMs solution was produced.

The CMs were characterized using a UV-Vis spectrophotometer, a PL spectrometer, and an FTIR spectrometer. The UV-Vis (Shimadzu 2450 Series) spectrophotometer was used to determine the wavelengths at the absorption peaks of the CMs.

DOI:https//doi.org/10.22452/mjs.vol44no2.7
Malaysian Journal of Science 44(2): 69-77 (June 2025)

The PL spectrometer was self-assembled using an Ocean Optics USB 4000 Fiber Optic spectrometer and a laser (405 nm) source to determine the emission wavelength produced by the CMs. Finally, an FTIR (Thermo Nicolet Avatar 360 IR) spectrometer was employed to identify the functional groups produced by the CMs.

The CMs/latex composite was prepared by mixing 10 ml of distilled water, 3 ml of latex solution, and CMs solution with concentrations of 10%, 20%, and 40%. Then, the mixture was heated and stirred to obtain CMs/latex solution with a sticky texture and white color. Hence, three samples of CMs/latex composites were produced, i.e., CMs/latex A, B, and C for 10%, 20%, and 40% CMs concentrations, respectively (Figure 2).

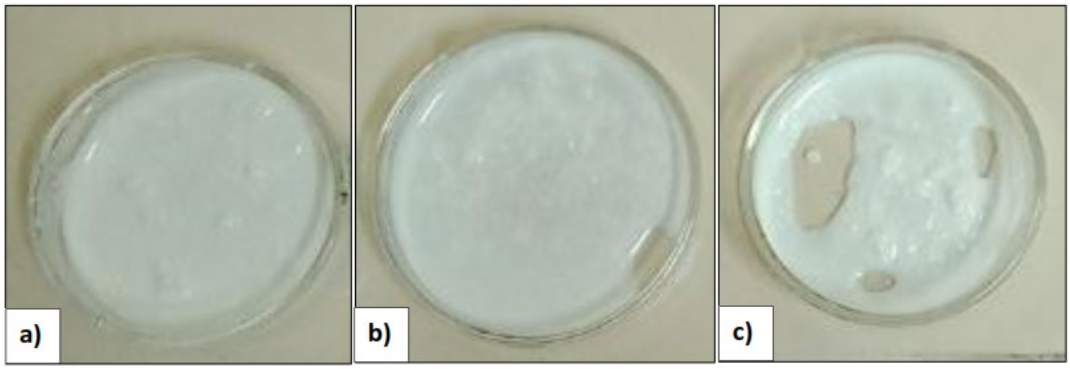

Figure 2. Samples of CMs/latex composites of (a) A, (b) B, and (c) C.

Figure 3. Chicken bones covered by (a) *E. tirucalli* latex and (b) CMs/latex composites.

The antibacterial activity of CMs and CMs/latex composites (A, B, and C) was tested against *S. aureus* bacteria using the diffusion method. The bacteria were purchased from the Medical Faculty of Universitas Gadjah Mada, Indonesia. All equipment for the antibacterial test was provided by the Microbiology laboratory, Universitas Negeri Yogyakarta, Indonesia. The DIZ was determined to identify the anti-bacterial activity of the samples. The bacterial culture was grown on nutrient agar (NA) and nutrient Broth (NB) media. The bacteria were then cultured in a medium on a petri dish. Paper disks were immersed in the sample solutions for 15 minutes, and then placed on solidified NA media and in a sterile room at 37 ^{o}C. Three petri dishes were given various samples of the paper disks, i.e., CMs (A, B, and C), *E. tirucalli* latex (2 ml, 3 ml, and 4 ml), and CMs/latex composites (A, B, and C). This test was carried out for 24 hours, with the DIZ measured every 3 hours using a caliper.

Finally, the latex and CMs/latex composites were applied to chicken bones as a simple model of treating bone fractures. This was conducted by drying and breaking the chicken bones around their middle parts. The chicken bones were then re-attached and covered (wrapped) by the latex and CMs/latex. This can be observed in Figure 3. The test on the chicken bones was conducted to determine the tensile strength of the latex and CMs/latex composites. The tensile strength test was conducted at the Faculty of Engineering, Universitas Negeri Yogyakarta using the UTM. In principle, UTM pulled the tested material until it broke. This produced the peak tensile force required to split the chicken bones wrapped by the latex and CMs/latex composites. Moreover, the tissue layers of the chicken bone without coating, chicken bone coated by CMs, and CMs/latex were also observed using a light microscope (Optilab Microscope).

DOI:https//doi.org/10.22452/mjs.vol44no2.7
Malaysian Journal of Science 44(2): 69-77 (June 2025)

3. Results and Discussion

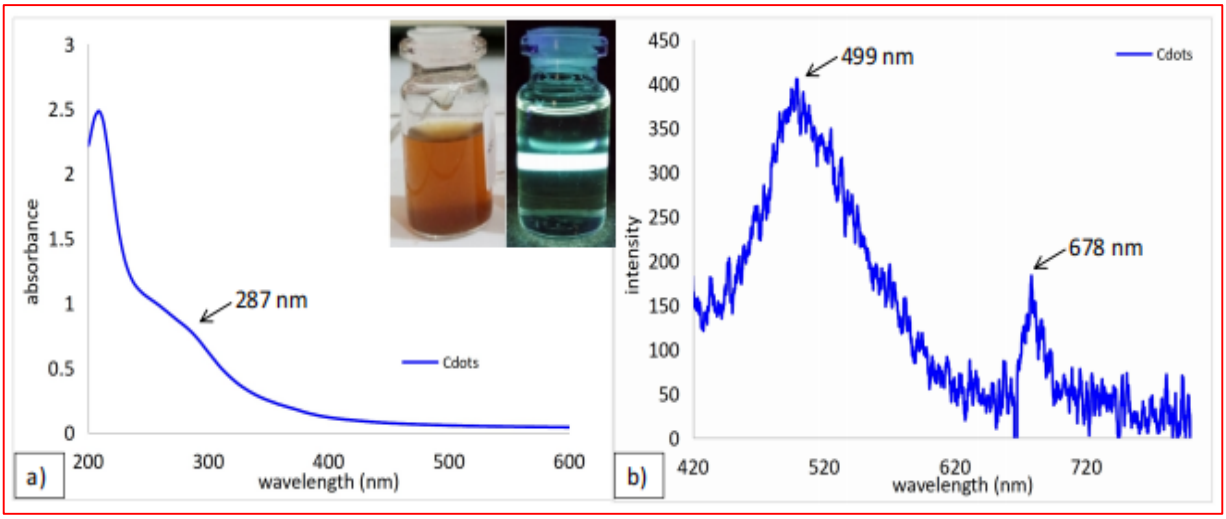

Figure 4. The (a) absorption and (b) emission spectra of the CMs.

The results of the UV-Vis and PL characterizations of the CMs are presented in Figures 4(a) and 4(b), respectively. Figure 4(a) shows an absorption peak at a wavelength of 287 nm, which is attributed to the π → π* transition of C=C (Rahmani & Ghaemy, 2019; Mewada et al., 2015). Figure 4(b) shows two intensity peaks. The first dominant peak is at a wavelength of 499 nm, which belongs to the cyan wavelength range, i.e., 495 nm to 570 nm. This suggests that the CMs sample has a cyan luminescence in accordance with the luminescence shown in the inset of Figure 4 (right picture), which is obtained by exposing the CMs solution with a UV/violet laser (a wavelength of 405 nm). In addition to the first dominant intensity peak, a second peak is produced at a wavelength of 678 nm. This latter wavelength belongs to the red emission spectrum, i.e., 620 nm to 750 nm. This second peak indicates the presence of *chlorophyll* in the CMs sample (Dwandaru et al., 2020; Li et al., 2017). It is possible that the *chlorophyll* from the branches of *E. tirucalli* still remains, although the branches have been heated. However, the intensity is small compared to the first intensity peak. The CMs solution has a brownish appearance under sunlight (inset Figure 4, left picture).

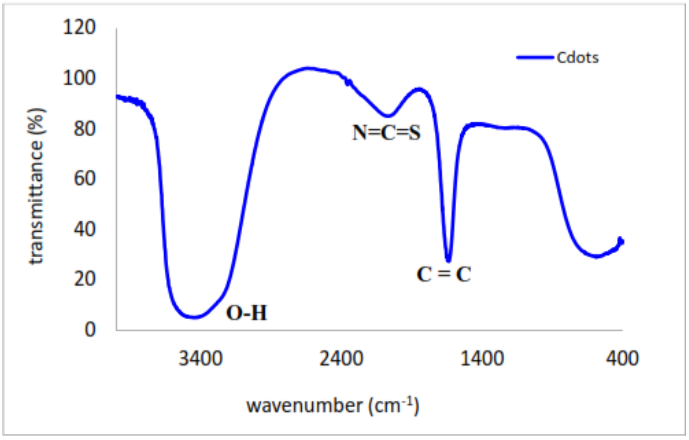

Figure 5. IR spectrum of the CMs.

DOI:https//doi.org/10.22452/mjs.vol44no2.7
Malaysian Journal of Science 44(2): 69-77 (June 2025)

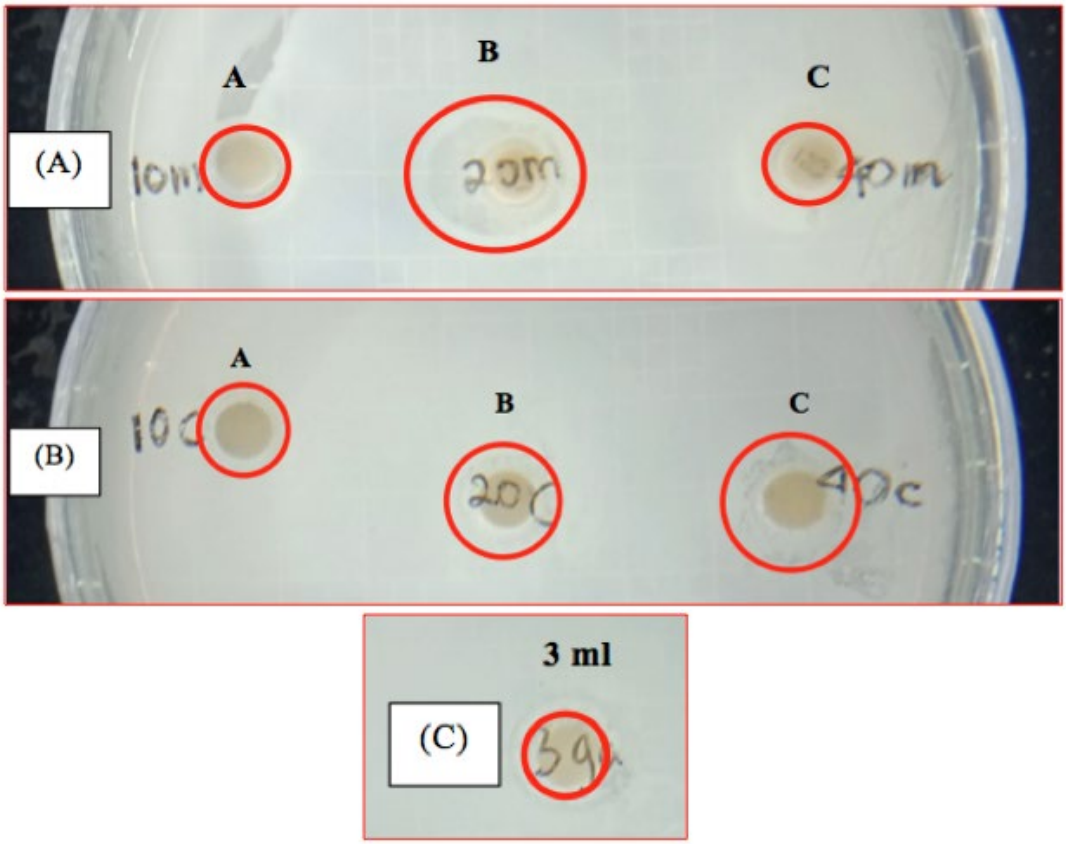

Figure 6. DIZs after 24 hours of the CMs (A), CMs/latex composites (B), and *E. tirucalli* latex (C).

The IR spectrum of the CMs is depicted in Figure 5. The FTIR spectrum shows bands of C=C, O-H, and N=C=S functional groups at 1633 cm^{-1}, 3446 cm^{-1}, and 2067 cm^{-1}, respectively. The functional group of C=C is in accordance with the UV-Vis result shown in Figure 4(a). Furthermore, the functional group of OH has a water solubility property that makes the CMs easy to conjugate with other materials, e.g., the latex.

The CMs solution was then combined with *E. tirucalli* latex to produce the CMs/latex composites. The latter has a sticky texture like glue and white color following the latex (see Figure 2). Furthermore, higher concentrations of the CMs resulted in a thicker composite. In order to study the antibacterial property of the composites, the antibacterial tests were conducted. The antibacterial activities of the CMs and CMs/latex composites are observed against *S. aureus* by measuring the DIZ of the aforementioned samples. The DIZs after 24 hours are shown in Figure 6. The DIZs of the samples can be observed inside the red circles in the figure. The average DIZ of each sample is shown in Table 1.

Table 1. The average DIZs of the samples.

No.	CMs		Latex		CMs/latex composites	
	Sample	Average ± 0.05 (mm)	Volume (ml)	Average ± 0.05 (mm)	Sample	Average ± 0.05 (mm)
1.	A	1.44			A	1.37
2.	B	2.59	3	1.24	B	2.08
3.	C	1.90			C	3.24

It can be observed in Table 1 that the highest DIZ of 3.24 ± 0.05 mm is obtained for sample C of the CMs/latex composites consisting of 40% CMs solution. In the case of the CM/latex composites, the higher the concentration of the CMs, the higher the antibacterial activity, which is indicated by the higher DIZ results. This is expected as the composite of the two materials, i.e., CMs/latex composites, produces better antibacterial properties compared to the individual components, i.e., CMs and latex. In addition, the latex naturally has antibacterial properties (Mali & Panchal, 2017). This is evidenced by the average DIZ obtained by the latex (3 ml) of 1.24 ± 0.05 mm.

On the other hand, the CMs samples also have antibacterial properties, with the highest DIZ of 2.59 ± 0.05 mm for sample B. All A, B, and C samples of the CMs and CMs/latex composites have higher DIZs compared to the DIZ of the pure latex. This indicates that the antibacterial property of CMs and CMs/latex composites performs better than that of pure latex. However, pure CMs of samples A and B have DIZs higher than the CMs/latex composites

DOI:https//doi.org/10.22452/mjs.vol44no2.7
Malaysian Journal of Science 44(2): 69-77 (June 2025)

of A and B, respectively. Only sample C of the CMs/latex composites has a higher DIZ compared to the pure CMs of sample C. This partially indicates that preparing composite materials of CMs/latex produces better antibacterial properties as expected. Therefore, the composite of CMs with the latex can significantly improve the antibacterial ability against *S. aureus* and can be further used as an antibacterial agent. The antibacterial properties of CMs can be extracted from the precursor of CMs, namely the branches of *the E. tirucalli plant,* which have natural antibacterial components. Furthermore, CMs are smaller in size compared to the latex. Hence, the former are more effective in inhibiting the growth of *S. aureus* bacteria (Muktha et al., 2020).

S. aureus is a gram-positive bacterium that can cause various harms to human health, particularly in this case concerning, e.g., bones and joint infections (Bouiller & David, 2023) and fracture-related infection (FRI) in orthopedic surgery (Li et al., 2023). Hence, this justifies the preparation of CMs/latex composites with antibacterial properties against *S. aureus*. For a comparison, the highest DIZ of 3.24 ± 0.05 mm of the CMs/latex composites is lower than the DIZ of CM core-shell/SiO_2 (SiO_2@C) and AgNP/Cdots nanocomposites of 6.7 mm to 11.2 mm and 9.80 mm, respectively (Khemthong et al., 2023; Wang et al., 2022). The difference in the values of the DIZ is most likely caused by the various concentrations used for each composite. Hence, modifying the concentration of the composite's components may be conducted to increase the DIZ of the CMs/latex composites.

Moreover, we argue that the antibacterial activity of the CMs/latex composites is a synergetic mechanism between the individual components of the composites, i.e., CMs and latex. The latex is essentially a complex emulsion consisting of proteins, starches, alkaloids, sugars, and gums with sources of carbon, oxygen, nitrogen, and sulfur (Bano et al., 2018). Some of these compounds are responsible for the antibacterial activity of the latex in the form of antimicrobial compounds (AMCs) and/or antimicrobial peptides (AMPs), e.g., proteins and alkaloids. These AMCs and AMPs can penetrate the bacterial cell membranes, especially the AMPs being hydrophobic (Gracz-Bernaciak et al., 2021). On the other hand, many antimicrobial mechanisms can be attributed to the CMs, e.g., physical or mechanical destruction, oxidative stress via reactive oxygen species (ROS), and photodynamic effects (Xin et al., 2018). Hence, the synergy between CMs and latex improves the physical or mechanical penetration strength towards the bacterial cell membranes. The combination of AMCs, AMPs, and CMs produces mechanical damage to the outer membranes of *S. aureus* cell walls. The damage that is exerted upon the bacterial cell membranes depends on the contact interaction between the CMs/latex composites and *S. aureus,* depending on the dimensionalities of the composites.

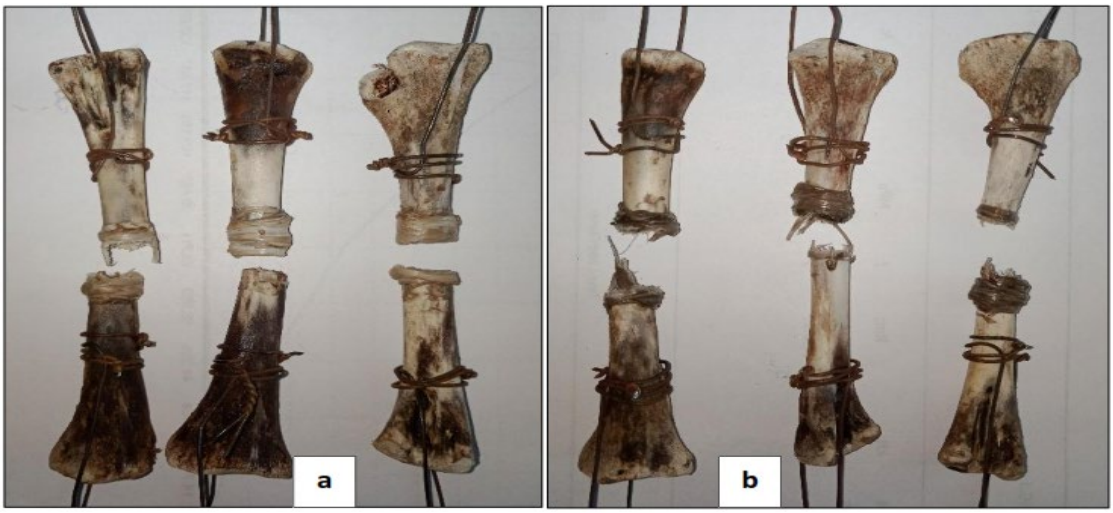

Figure 7. Tensile strength test of the latex (a) and CMs/latex composites (b) wrapped on chicken bones.

A fractured chicken bone model was used to investigate the tensile strength of the latex and CMs/latex composites. The latex and CMs/latex composites are intended as an alternative to commonly used metal objects in the process of healing and/or repositioning the bone fracture. Samples of chicken bones wrapped in the latex and CMs/latex composites are shown in Figure 3. Physically, the latex covering the bone fracture has a white color, while CMs/latex composites have a darker grey color. This color difference is due to the addition of CMs in the CMs/latex composites. The model is tested for tensile strength using the UTM. The results of the UTM tests can be seen in Figure 7. The peak tensile force of the tested chicken bones wrapped with the latex and CMs/latex composites are shown in Table 2.

DOI:https//doi.org/10.22452/mjs.vol44no2.7
Malaysian Journal of Science 44(2): 69-77 (June 2025)

Table 2. The peak tensile force of the latex and CMs/latex composites.

No.	Sample	Peak tensile force of latex ± 0.0005 (kN)	Peak tensile force of CMs/latex ± 0.0005 (kN)
1.	1	0.0110	0.0240
2.	2	0.0150	0.0250
3.	3	0.0160	0.0110
Average		0.0140	0.0200

The UTM test shows the force required to break the material. The greater the force required, the stronger the material. A strong wrapping is required to keep the fractured bones in good shape during the healing period. It may be observed in Table 2 that the highest average tensile force is obtained for the chicken bones wrapped with CMs/latex composites, with an average of 0.02 kN, while the chicken bones wrapped with latex have an average tensile strength value of 0.014 kN. This indicates that the CMs/latex composites have the ability to withstand higher tensile stress than the sample of the latex. Hence, the addition of CMs increases the strength of the latex as an alternative fracture treatment.

Finally, Figure 8 shows the images of the chicken bone layers without coating [Figure 8(a)], coated with latex [Figure 8(b)], and coated with CMs/latex composites [Figure 8(c)]. The chicken bone layer without coating clearly shows elongated fibrous surface like threads. Hence, the texture of the surface layer appears to be uneven. On the other hand, the image of the chicken bone coated by latex shows a smooth surface, while the chicken bone coated by CMs/latex composites has a smooth and dense surface. This means that the latex and CMs/latex composites are able to cover the bone fibers. Moreover, the CMs/latex composites are able to densely cover the chicken bone layer compared to the latex. The CMs added to the latex fill in the gaps in the chicken bone layers better than the pure latex. This makes CMs/latex composites look denser and can cover the chicken bone better than the latex alone. These results also reinforce the tensile strength test results, where the chicken bone wrapped with CMs/latex composites has a greater tensile strength compared to the pure latex. Since the latex is a sticky emulsion, the addition of CMs particles makes the composites denser, hence improving the strength of the CMs/latex composites.

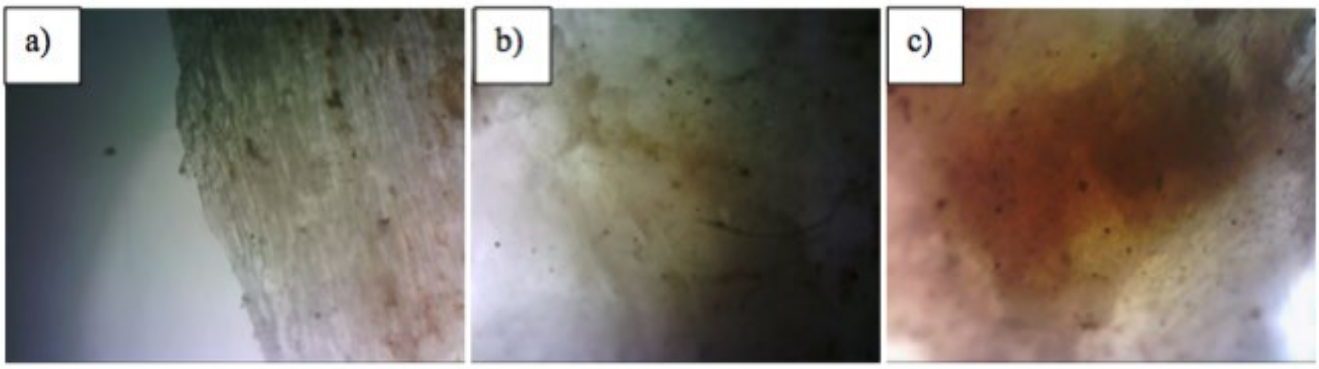

Figure 8. Images of the chicken bone layer without coating (a), coated with latex (b), and coated with CMs/latex composites (c) with a magnification of 5.3X.

4. Conclusion

The CMs were successfully prepared through heating at a low temperature from the branches of the *E. tirucalli* plant. The CMs/latex composites have the highest DIZ against *S. aureus* bacteria compared to the latex and CMs, which shows that the antibacterial ability is improved if the latex and CMs are combined. The fractured chicken bone wrapped with CMs/latex composites has the highest tensile strength because CMs/latex have a smooth and dense surface, so that they can bind the chicken bone better than the latex alone. Hence, the CMs/latex composites can be developed as an alternative for bone fracture treatment. Further characterization of the CMs and CMs/latex composites can be conducted for future study, such as using a high-resolution transmission electron microscope (HR-TEM). Further studies can also be conducted on the application of the CMs/latex composites to various parts of the bones.

5. Acknowledgement

The authors would like to thank the Faculty of Mathematics and Natural Science, Universitas Negeri Yogyakarta, for supporting this study.

DOI:https//doi.org/10.22452/mjs.vol44no2.7
Malaysian Journal of Science 44(2): 69-77 (June 2025)

5. References

Bajpai S K., D'Souza A., Suhail B. (2019). Carbon dots from Guar Gum: Synthesis, characterization and preliminary in vivo application in plant cells *Mater. Sci. Eng. B.* 241.

Bano D., Kumar V., Singh V K., Chandra S., Singh D K., Yadav P K., Talat M., Hasan S H. (2019). A facile and simple strategy for the synthesis of label free carbon quantum dots from the latex of *Euphorbia mili* and its peroxidase-mimic activity for the naked eye detection of glutathione in a human blood serum *ACS Sustainable Chem. Eng.* 7: 1923.

Bouiller K., David M Z. (2023). Staphylococcus aureus genomic analysis and outcomes in patients with bone and joint infections *Int. J. Mol. Sci.* 24(4): 3234.

da Silva R F., Carneiro C N., do C. de Sousa C B., Gomez F J V., Espino M., Boiteux J., Fernandez M A., Silva M F., Dias F S. (2022). Sustainable extraction bioactive compounds procedures in medicinal plants based on the principles of green analytical chemistry: A review *Microchem. J.* 175: 107184.

de Medeiros T V., Manioudakis J., Noun F., Macairan J –R., Victoria F., Naccache R. (2019). Microwave-assisted synthesis of carbon dots and their applications *J. Mater. Chem. C.* 7: 7175-7195.

Dong X., Awak M A., Tomlinson N., Tang Y., Sun Y –P., Yang L. (2017). Antibacterial effects of carbon dots in combination with other antimicrobial reagents *PloS One* 12: e0185324.

Dwandaru W S B., Bilqis S M., Wisnuwijaya R I., Isnaeni (2019). Optical properties comparison of carbon nanodots synthesized from commercial granulated sugar using hydrothermal method and microwave *Mater. Res. Express.* 6: 105041.

Dwandaru W S B., Fadli A L., Sari E K., Isnaeni (2020). Cdots and Cdots/S synthesis from nam-nam fruit (*Cynometra cauliflora l.*) via frying method using cooking oil *Dig. J. Nanomater. Biostructures.* 15: 555.

Dwandaru W S B., Sari E K. (2020). Chicken bone wastes as precursor for C-dots in olive oil *J. Phys. Sci.* 31: 113.

Ghosh T., Das T K., Das P., Banerji P., Das N Ch. (2022). Current scenario and recent advancement of doped carbon dots: a short review scientocracy update (2013–2022) *Carbon Lett.* (2022).

Gracz-Bernaciak J., Mazur O., Nawrot R. (2021). Functional studies of plant Latex as a rich source of bioactive compounds: focus on proteins and alkaloids Int. *J. Mol. Sci.* 22(22): 1242.

Kaur P., Verma G. (2022). Converting fruit waste into carbon dots for bioimaging applications *Mater. Today Sustain.* 18: 100137.

Khajuria D K., Kumar V B., Gigi D., Gedanken A., Karasik D. (2018). Accelerated bone regeneration by nitrogen-doped carbon dots functionalized with hydroxyapatite nanoparticles *ACS Appl. Mater. Interfaces.* 10: 19373.

Khemthong P., Phanthasri J., Youngjan S., Wanmolee W., Samun Y., Sosa N., Rungnim C., Kraithong W., Sangkhun W., Panthong J., Butburee T, Thanee K., Nakajima H., Supruangnet R., Towiwat P., Chanvorachote P., Sukrong S. (2023). Effect of the ethanol-to-water ratio on the properties of silica-carbon core-shell materials for prolonged antibacterial activity of thymol *Applied Surface Science* 635: 157716.

Li J., Leung S S Y., Chung Y L., Chow S K H., Alt V., Rupp M., Brochhause C., Chui C S., Ip M., Cheung W-H., Wong R M Y. (2023). Hydrogel delivery of DNase I and liposomal vancomycin to eradicate fracture-related ethicillin-resistant staphylococcus aureus infection and support osteoporotic fracture healing Acta Biomaterialia 164: 223.

Li L., Zhang R., Lu C., Sun J., Wang L., Qu B., Li T., Liu Y., Li S. (2017). In situ synthesis of NIR-Light emission carbon dots derived from spinach for bio-imaging application *J. Mater. Chem. B.* 5: 7328.

Liu J., Li R., Yang B. (2020). Carbon dots: a new type of carbon-based nanomaterial with wide applications *ACS Cent. Sci.* 12: 2179.

Liu X., Pang J., Xu F., Zhang X. (2016). Simple approach to synthesize amino-functionalized carbon dots by carbonization of chitosan *Sci. Rep.* 6: 31100.

Mali P Y., Panchal S S. (2017). Euphorbia tirucalli L.: Review on morphology, medicinal uses, phytochemistry and pharmacological activities *Asian Pac. J. Trop. Med.* 7: 603.

Maver T., Maver U., Kleinschek K S., Smrke D M., Kreft S. (2015). A review of herbal medicines in wound healing *Int. J. Dermatol.* 54: 740-751.

Mewada A., Vishwakarma R., Patil B., Phadke C., Kalita G., Sharon M., Sharon M. (2015). Non-blinking dendritic crystals from C-dot solution *Carbon Lett.* 16: 211.

Muktha H., Sharath R., Kottam N., Smrithi S P., Samrat K., Ankitha P. (2020). Green synthesis of carbon dots and evaluation of its pharmacological activities *BioNanoSci.* 10: 731.

Pallavali R R., Avula S., Degati V L., Penubala M., Damu A G., Durbaka V R P. (2019). Data of antibacterial activity of plant leaves crude extract on bacterial isolates of wound infections *Data in Brief* 24: 103896.

Pires N R., Santos C M W., Sousa R R., de Paula R C M., Cunha P L R., Feitosa J P A. (2015). Novel and fast microwave-assisted

DOI:https//doi.org/10.22452/mjs.vol44no2.7
Malaysian Journal of Science 44(2): 69-77 (June 2025)

synthesis of carbon quantum dots from raw cashew gum *J. Braz. Chem. Soc.* 26: 1274.

Rahmani Z., Ghaemy M. (2019). One-step hydrothermal-assisted synthesis of highly fluorescent N-doped carbon dots from gum tragacanth: luminescent stability and sensitive probe for Au^{3+} ions *Opt. Mater.* 97.

Sabzehmeidani M M., Mahnaee S., Ghaedi M., Heidari H., Roy V A L. (2021). Carbon based materials: a review of adsorbents for inorganic and organic compounds *Mater. Adv.* 2: 598.

Shao D., Lu M., Xu D., Zheng X., Pan Y., Song Y., Xu J., Li M., Zhang M., Li J., Chi G., Chen L., Yang B. (2017). Carbon dots for tracking and promoting osteogenic differentiation of mesenchymal stem cells *Biomater. Sci.* 5: 1820.

Sreenath P R., Mandal S., Panigrahi H., Das P., Kumar K D. (2020). Carbon dots: fluorescence active, covalently conjugated and strong reinforcing nanofiller for polymer latex *Nano-Struct. Nano-Objects.* 23: 100477.

Thakur M., Pandey S., Mewada A., Patil V., Khade M., Goshi E., Sharon M. (2014). Antibiotic conjugated fluorescent carbon dots as a theranostic agent for controlled drug release, bioimaging, and enhanced antimicrobial activity *J. Drug Deliv*. 2014.

Wang P., Song Y., Mei Q., Dong W-F., Li L. (2022). Silver nanoparticles@carbon dots for synergistic antibacterial activity *Applied Surface Science* 600: 154125.

Wang Y H., Hu A. (2017). Carbon quantum dots: synthesis, properties and applications *J. Mater. Chem. C.* 2: 6921.

Weber K., Quicker P. (2018). Properties of biochar *Fuel* 217: 240.

Xia C., Zhu S., Feng T., Yang M., Yang B. (2019). Evolution and synthesis of carbon dots: from carbon dots to carbonized polymer dots *Adv. Sci.* 6: 1901316.

Xin Q., Shah H., Nawaz A., Xie W., Akram M Z., Batool A., Tian L., Jan S U., Boddula R., Guo B., Liu Q., Gong J R. (2018). Antibacterial carbon-based nanomaterials *Adv. Mater.* 2018: 1-15.

Zhai X., Zhang P., Liu C., Bai T., Li W., Dai L., Liu W. (2012). Highly luminescent carbon nanodots by microwave-assisted pyrolysis *Chem. Commun.* 48: 7955.

DOI:https//doi.org/10.22452/mjs.vol44no2.7
Malaysian Journal of Science 44(2): 69-77 (June 2025)

MALAYSIAN JOURNAL OF SCIENCE
MJS
ISSN 1394-3065

Regular Issue

Malaysian Journal of Science 44 (2): 78-85 (June 2025) https://mjs.um.edu.my

Effect of Cu and Si Wafer Substrates in Increasing Raman Signal of Surface-Enhanced Raman Scattering-Based Au Nanoparticles

Affi Nur Hidayah[1ab], Djoko Triyono[2a]*, Yuliati Herbani[3b] and Rosari Saleh[4a]

Abstract: Surface-enhanced Raman spectroscopy (SERS) has attracted considerable research interest over the last four decades because of its rapid vibrational spectroscopic detection, high sensitivity, and nondestructive technique for enhancing the generally weak signal from Raman scattering. Here, SERS substrates were fabricated by drop-casting Au nanoparticles (NPs) onto two substrates (Cu and Si wafers). The AuNPs (diameter = 7.3 nm) were synthesized from an Au metal ion solution with a concentration of 4.22×10^{-4} M via photochemical reduction using a femtosecond laser. The SERS substrates were tested for their ability to enhance the Raman signal of paraquat pesticides at 10 ppm. Six vibration peaks of the paraquat pesticides at 671, 838, 1187, 1294, 1530, and 1643 cm^{-1} were successfully detected and enhanced. The results showed that the SERS substrate on the Si wafer increased the Raman signal more than the Cu wafer.

Keywords: *SERS substrates, Au nanoparticles, silicon wafer, copper wafer.*

1. Introduction

The unique chemical, physical, optical, catalytic, and electronic capabilities of metallic nanoparticles (NPs) have attracted significant research attention because these properties are influenced by plasmonic oscillations. The plasmonic oscillations of metal NPs strongly rely on various variables, such as the material, size, shape, nanostructure composition, and the dielectric constant of the surrounding medium (Minho, Jung-Hoon & Jwa-Min, 2019). Plasmon resonance exhibits sensitivity toward alterations in the refractive index of the surrounding medium, which can arise from the adsorption or binding of molecules onto material surfaces. This property renders plasmon resonance valuable for the development of environmental sensing applications, including colorimetry (Xu, Jin & Li, 2021), surface-enhanced Raman scattering (SERS) (Israelsen, Hanson, and Vargis, 2015), and biosensing applications (Unser, Bruzas, He & Sagle, 2015) (Huan et al, 2021).

SERS has been developed as a straightforward and nondestructive testing method for the detection of dangerous chemical substances and food contaminants, e.g., antibiotics, melamine, and pesticides (Craig, Franca, & Irudayaraj, 2013). In addition, SERS has demonstrated its efficacy in detecting various biological entities, such as micro-RNA, DNA, viruses, bacteria, and cancer cells (Pilot et al., 2019). Noble metallic elements, including Au, Ag, and Cu, are commonly utilized in the form of metal NPs for SERS-substrate modification (Roguska et al., 2011). In a study by Wang, K G et al. (2019), AgNPs exhibited sharp and narrow plasmon peaks, resulting in a high intensity. This characteristic enabled the AgNPs to more effectively amplify the Raman signal compared with AuNPs. Nevertheless, Ag is highly susceptible to oxidation and exhibits potentially harmful characteristics that can adversely affect the analyte under investigation (Ferdous & Nemmar, 2020). AuNPs have attracted significant attention in the medical field because of their remarkable biocompatibility (Janina et al., 2010). This interest has been further fueled by the high plasmonic stability of Au attributed to its elevated chemical and physical stability (Ilyas et al., 2021) (Hidayah et al., 2022).

The use of SERS substrates has been demonstrated to enhance the typically low signal strength obtained from Raman spectroscopy. This enhancement occurs when biomolecules, which are the targets or analytes for environmental pollution, interact with the plasmonic nanostructures on the substrate surface (Pérez-Jiménez et al., 2020). The plasmonic oscillation of metal NPs can manifest in two separate effects. Initially, the phenomenon of extinction or scattering results in a displacement of the spectral peak toward long wavelengths. It has been observed that plasmonic nanostructures can increase nonelastic optical phenomena on molecules or quantum entities through local field enhancement (Lia, Cushinga & Wua, 2015). Surface plasmons (SPs), specifically localized SPs at the metal surface, interact with incident photons and Raman-scattered vibrations emitted by analyte molecules. These interactions result in a substantial enhancement of Raman-scattered photons,

Authors information:
[a]School Department of Physics, Universitas Indonesia, Kampus UI Depok, INDONESIA. E-mail: djoko.triyono@sci.ui.ac.id[2]; rosari.saleh@ui.ac.id[4]
[b]Research Center for Photonics, National Research and Innovation Agency, Kawasan PUSPIPTEK Building 442, Tangerang Selatan 15314, INDONESIA. E-mail: affi001@brin.go.id[1]; yuli018@brin.go.id[3]
*Corresponding Author: djoko.triyono@sci.ui.ac.id

Received: June, 2023
Accepted: June, 2024
Published: June, 2025

DOI:https//doi.org/10.22452/mjs.vol44no2.8
Malaysian Journal of Science 44(2): 78-85 (June 2025)

commonly known as electromagnetic enhancement (EM). Chemical enhancement (CM) can yield additional performance enhancements when the molecule establishes a chemical bond with the metal surface, leading to the transfer of charge, involving the metal and molecule. The aforementioned processes are considered the basis for SERS (Kahraman et al., 2017).

AuNPs are a popular choice for SERS substrates. However, the shape of the NPs (Au nanospheres, nanorods, nanotriangles, nanowires, nanoplates, and nanocubes), substrate type (Si, glass, quartz, and paper), and analyte used impacts the process of increasing the Raman signal on an AuNP SERS substrate (Lopez-Lorente, 2021). Numerous AuNPs that are used as SERS substrates are still produced using chemical reduction techniques that involve reducing agents, such as stainless steel (Lopez-Lorente, 2014), trisodium citrate (Brust, 1994), $NaBH_4$, or ascorbic acid (Saim, 2021). The chemical reduction approach is complicated and can result in chemical residues on the AuNPs, which could be harmful if utilized in medical applications. Thus, using a femtosecond laser to create AuNPs via the chemical photoreduction process could be beneficial because it is simpler, faster, and does not require chemicals.

AuNP SERS substrates have been used to detect a range of analytes, including pesticides, such as phosmet (Luo, 2016), carbaryl (Alsammarraie, 2017), thiram (Zhang, 2014), cypermethrin (Li, 2019), esfenvalerate (Wang, K., 2019), pestisida thiabendazole (Alsammarraie, 2018) and paraquat pesticides. Currently, chemical reduction to fabricate AuNPs is the only approach used for AuNP-based SERS substrates in the detection of pesticides. There are several methods for performing the SERS-substrate measurement process for detecting paraquat pesticides. They include combining the pesticide with AuNPs and dropping them onto a glass substrate (Lin, 2021), aluminum engraved using a laser and coating with AuNPs (Kamkrua, 2023), or dropping AuNPs onto glass and drying in a vacuum oven for 6 h (Chen, 2022). No reports have been made regarding the production of SERS substrates on Cu and Si wafers for the detection of paraquat pesticides. Although the use of paraquat insecticide has begun to be outlawed in Europe and America, farmers in Indonesia continue to use it. Paraquat pesticides are commonly used by farmers to kill pests on coffee and oil palm trees (Pusat Standarisasi-Kementerian Lingkungan Hidup dan Kehutanan, 2020). Thus, the advancement of the field of spectroscopy in Indonesia is critically dependent on the development of a SERS substrate based on AuNPs.

The fabrication techniques employed for the production of SERS substrates include spin coating (Gushiken et al., 2020), electron beam lithography (Chen et al., 2019), and physical vapor deposition (Khalil et al., 2019). Nevertheless, it might be argued that the aforementioned methods are highly complex, difficult, and costly. The quality of SERS substrates can impact SERS signals. The present study fabricated SERS substrates by the application of a drop-casting technique, which was confirmed to be rapid and cost-effective. AuNPs were used as the primary material, and they were coated onto Cu and Si wafers. The initial step in the production of the AuNPs involves the use of a femtosecond laser for photochemical reduction, commonly referred to as the green synthesis method. This approach prevents the use of strong chemical reduction agents. The AuNPs were produced by diluting Au salts in a water solution, placing them in a glass cuvette, and irradiating them using the femtosecond laser. When a femtosecond laser interacts with a solution of Au ions, it generates a strong reducing agent that can convert Au ions into AuNPs. This study was aimed at evaluating the impact of various substrate types on the enhancement of the Raman signal of paraquat pesticides.

2. Materials and Methods

Materials

An AuNP solution was synthesized by reducing a solution of Au ions using the femtosecond laser. The Au ion solution was prepared by diluting potassium gold (III) chloride metal salt ($KAuCl_4$; 98% purity, Sigma Aldrich) with distilled water to a concentration of 4.22×10^{-4} M. Furthermore, a capping agent, polyvinylpyrrolidone (PVP; 99.9% purity, Sigma Aldrich), was utilized. The PVP had a molecular weight of 40,000 incorporated into the solution at a concentration of 0.01 wt%.

Paraquat pesticides (Sigma Aldrich) were selected as analytes for the quality testing of the present SERS substrates. The paraquat pesticide (1 g) was diluted multiple times to achieve a concentration of 10 ppm.

Methods

The AuNP SERS substrates were fabricated on two distinct substrates: Si and Cu wafers. The AuNPs were first produced via a photoreduction process with a femtosecond laser and subsequently placed on the wafers to create SERS substrates using the drop-casting method. The use of a femtosecond laser created NPs without chemicals or strong reduction agents, offering a rapid and more eco-friendly alternative to chemical techniques.

To synthesize colloidal AuNPs, a solution containing Au ions was introduced into a quartz cuvette (10 × 10 × 45 mm), resulting in a total volume of 3 mL. The solution was subsequently exposed to a femtosecond laser, with a fundamental wavelength of 800 nm, power output of 2 mJ, and repetition rate of 1 kHz. The experiment was conducted for 15-min irradiation times. The laser beam was directed at a right angle to the side wall of the glass cuvette using an aspheric lens (numerical aperture = 0.5; focal length = 8 mm). The schematic representation of the experimental setup has been previously illustrated (Hidayah et al., 2022). After the irradiation process, the ultraviolet–visible (UV–VIS) absorption of the synthesized AuNPs was analyzed using a modular UV–VIS spectrophotometer (Maya2000 Pro) and a broadband light source (DH-Mini, Ocean Optics). The colloidal AuNPs were deposited on grids with a carbon coating (Ted Pella, Inc.) and allowed to dry for at least 24 h. Afterward, their morphology was investigated via transmission electron microscopy (TEM) (FEI Tecnai G2 20 S-Twin) at an acceleration voltage of 200 kV.

The SERS substrates were fabricated by drop casting the

DOI:https//doi.org/10.22452/mjs.vol44no2.8
Malaysian Journal of Science 44(2): 78-85 (June 2025)

colloidal AuNPs (1 mL) onto the Si wafers and Cu substrates (0.5 × 0.5 cm) placed on a hot plate at 40°C. The hot plate was set to 40°C to minimize coffee ring formation and alterations in the characteristics of the AuNPs. Prior to a quality assessment of the SERS substrate, normal Raman spectra of the standard paraquat pesticide were evaluated. The paraquat pesticide (2 µL, 10 ppm) was dropped onto the SERS Cu and Si substrates, which were dried at room temperature. SERS experiments were conducted using a Raman spectrometer with a 785-nm excitation source and gratings of 1800 grooves per millimeter (HR 550, Horiba). Figure 1 illustrates the production of the SERS substrate and the measurement using Raman spectroscopy.

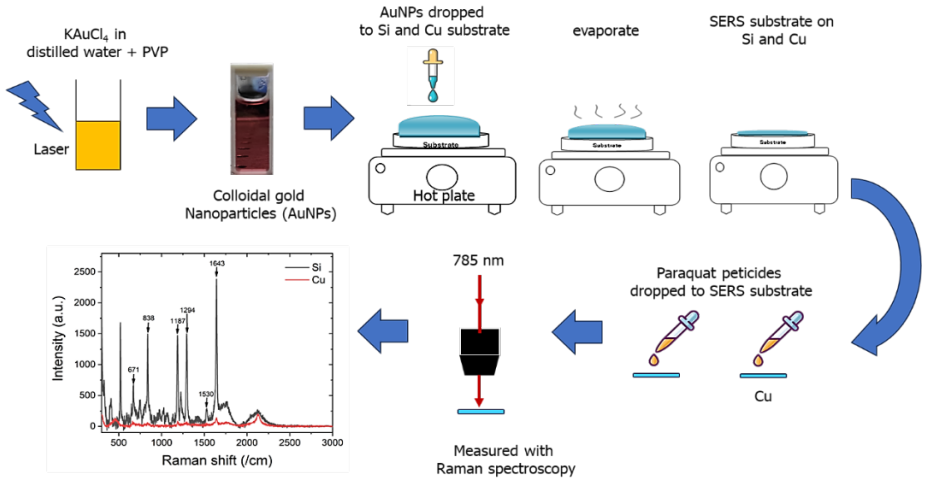

Figure 1. Production of SERS substrates and Raman measurements.

3. Results and Discussion

First, the AuNPs were generated from a solution of Au ions, which were placed in cuvettes and exposed to a femtosecond laser for 15 min. This was performed prior to the production of SERS substrates on Si and Cu wafers. The femtosecond laser was used to irradiate the Au ion solution, which is a mixture of water (H_2O) and $K^+[AuCl4]^-$. The interaction between the H_2O and the tightly focused laser created plasmas containing reactive radicals, such as hydrated electrons (e^-_{aq}-), hydrogen peroxide (H_2O_2), and hydroxyl radicals (OH). The hydrogen radicals and hydrated electrons acted as strong reducing agents and reduced $K^+[AuCl_4]^-$ to AuNPs (Meader et al, 2017).

The absorbance of the AuNP solution was measured, and the findings are illustrated in Figure 2, depicting the localized surface plasmon resonance (LSPR) value at 522 nm. Furthermore, the NPs were characterized by TEM, and the results are shown in Figure 3, illustrating the spherical morphology of the NPs with a diameter of 7.3 nm.

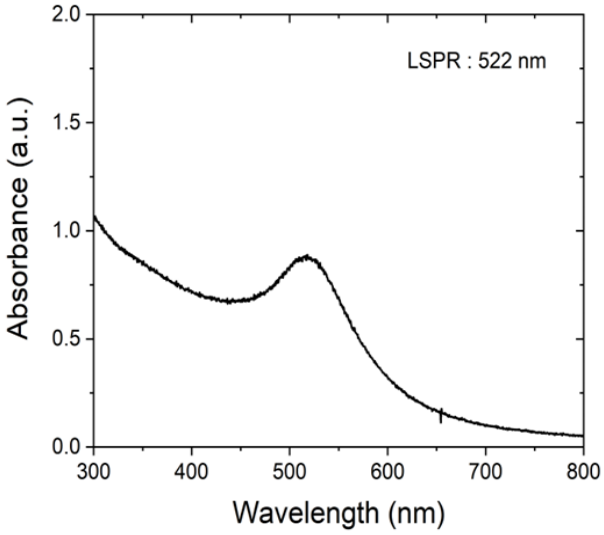

Figure 2. Localized surface plasmon resonance of AuNPs.

DOI:https//doi.org/10.22452/mjs.vol44no2.8
Malaysian Journal of Science 44(2): 78-85 (June 2025)

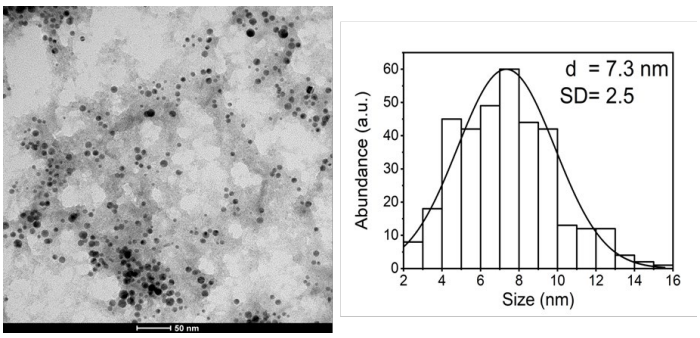

Figure 3. TEM images of morphology and particle size of AuNPs.

The colloidal AuNPs were subsequently coated onto the Si and Cu wafers, respectively, using a hot plate. The Si SERS substrate was characterized via field-emission scanning electron microscopy (FE-SEM; Figure 4).

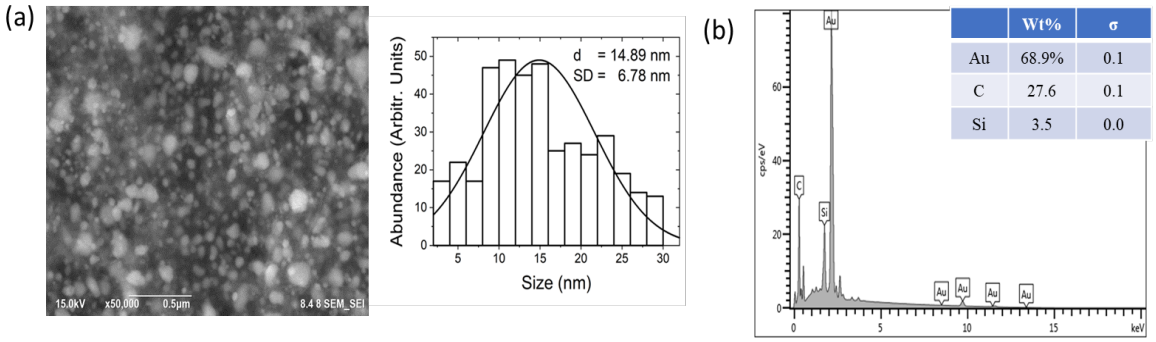

Figure 4. (a) FE-SEM images of the morphology and particle size. (b) Energy-dispersive X-ray spectroscopy.

The experimental findings indicated that AuNPs, when applied as a coating on a Si wafer substrate, were larger than the NPs in the solution suspension. This implies that the transfer mechanism of the colloidal AuNPs onto the substrate, in conjunction with the impact of the temperature of the hot plate, resulted in the heightened aggregation and enlargement of the NPs. The weight percentage of the NPs successfully coated on the Si wafer substrate was 68.9%. When colloidal AuNPs are deposited on a substrate and evaporate, the capillary flow from the center to the edge within the droplets causes the NPs to aggregate at the edge of the droplet, leading to their cohesion (Kumar, 2020). The van der Waals interaction between the NPs and heating on the hot plate accelerated the evaporation process, leading to a faster aggregation of the NPs. Once the NPs were adhered to the substrate, the heating process continued in the thin film. The heat produced by the hot plate follows principles, such as the annealing process on thin films. This process involves heating to enhance the crystallinity of the film and enlarges the size of NPs in the thin film (Kabir, 2019). This technique results in a coffee ring effect, causing the particles to be more concentrated at the edges than in the middle (Eral, 2013).

Standard paraquat pesticide powder ($C_{12}H_{14}Cl_2N_2$; Sigma Aldrich) was subjected to Raman spectroscopy prior to evaluating the quality of the SERS substrate. Six signal peaks corresponding to the paraquat pesticide were observed in the Raman spectrum (Figure 5) at the following wave numbers: 654.87, 841.87, 1199.29, 1300.54, 1552.08, and 1655.5 cm^{-1}.

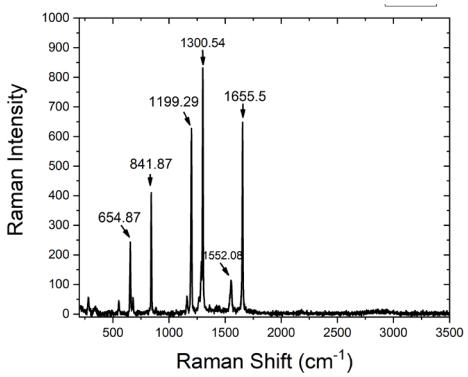

Figure 5. Raman shift of standard paraquat pesticide powder.

DOI:https//doi.org/10.22452/mjs.vol44no2.8
Malaysian Journal of Science 44(2): 78-85 (June 2025)

The quality testing of the SERS substrates was conducted on Si and Cu wafers. A droplet (2 µL) of paraquat pesticide solution was applied to each substrate, which was subsequently dried at room temperature. To assess the efficacy of the AuNPs in enhancing the Raman signal of paraquat pesticides, two sets of measurements were conducted. The first set involved an empty Si wafer substrate devoid of NPs and pesticides. The second set involved an empty Si substrate without NPs, onto which the paraquat pesticide (2 µL) was applied; the substrate was subsequently dried at room temperature. Figure 6 shows a comparative analysis of Raman signal outcomes from three samples: empty Si wafer substrates, Si wafers without NPs treated with paraquat pesticides, and SERS substrates treated with pesticides.

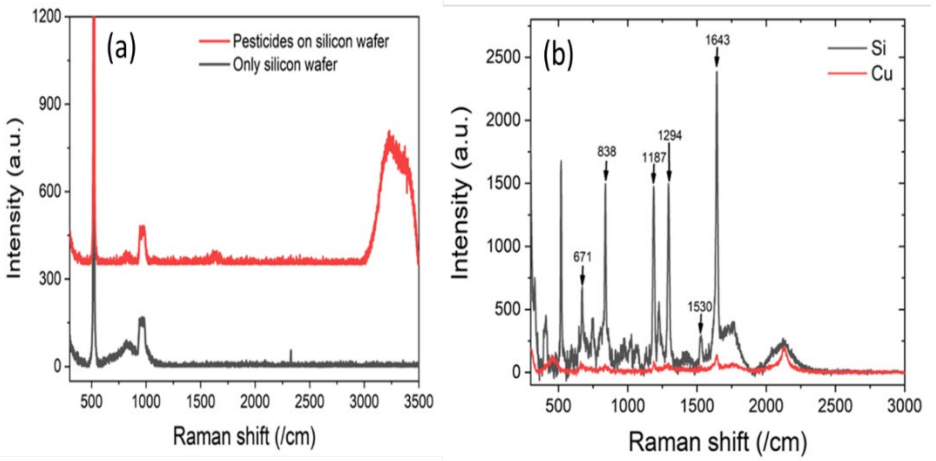

Figure 6. Raman shifts of (a) only Si wafer, pesticides on Si wafer, and (b) pesticides on SERS substrate on Si and Cu wafers.

The Raman spectroscopy of a blank Si wafer revealed distinct peaks at 500 and 1000 cm^{-1} (Figure 6a). No Raman peaks resulting from paraquat pesticides were observed for the uncoated Si wafer substrate and the Si wafer substrate that was not treated with NPs and pesticides. Here, the use of SERS substrates on Si and Cu wafers enhanced the detection of six distinct paraquat pesticide peaks. These peaks were observed at 671, 838, 1187, 1294, 1530, and 1643 cm^{-1}, which represent the C–Cl stretching vibration, C–N stretching vibration, C=C symmetrical stretching vibration, C–C deformation vibration, C–C deformation vibration, and C=N stretching vibration (Chen, 2022). This showed that the presence of NPs with plasmonic characteristics on the SERS substrate enabled the modulation and interaction of electromagnetic waves, Raman scattering, with the molecular vibrations of paraquat pesticides. Six paraquat pesticide peaks of the Raman shift observed for the SERS substrate exhibited slight deviations compared with the Raman spectra obtained for powdered paraquat pesticide. These deviations were attributable to the impact of plasmonic interactions occurring on the NPs. This influenced the enhancement of the incident laser source and the vibrational behavior of the paraquat pesticide molecules, contrary to the molecular vibrations of powdered paraquat pesticides, which were only affected by the laser source passing through the molecule (Liao, 2007).

The observed enhancement in the Raman signal of the paraquat insecticide on the SERS Si substrate was greater than that on the Cu substrate. The SERS enhancement factor (EF) combines two multiplicative contributions from CM and EM. Thus, the augmentation of the Raman signal was influenced by both EM and CM. This experiment evaluated the efficacy of the SERS substrate using the paraquat pesticide as the analyte. Two distinct substrate types were used to assess the quality of the SERS substrate. In this experiment, the EM process influenced the enhancement of the Raman signal of the paraquat pesticides more than the CM because the amplification of the Raman signal was solely influenced by the plasmonic properties of the NPs. The plasmonic characteristics exhibited by AuNPs coated on a Si wafer substrate are governed by the surface plasmon polariton (SPP) phenomenon. This effect is governed by the dielectric properties of the substrate in which the NPs are implanted (Le Ru, 2009).

SPP signals can be amplified using different methods depending on the material used. The dielectric value of the material had an effect on the SPP by strengthening the Raman signals. Once NPs are placed on the SERS substrate, LSPR and polaritons begin to form. Polaritons are caused by electron oscillations moving through the substrate material. The material can strengthen the electric field around the NPs owing to polaritons. Plasmon effects that increase electromagnetic waves are caused by SPP and the interaction between NPs and the dielectric constant of the

DOI:https//doi.org/10.22452/mjs.vol44no2.8
Malaysian Journal of Science 44(2): 78-85 (June 2025)

substrate. To determine the field on the SERS material, lasers with electric fields of EInc to the polariton mode were used. The Raman signal enhancement was affected by the factor, MLoc = |ELoc/EInc|, for increasing the local field strength (LFIEF). The electric field of the SERS ELoc substrate is changed by the polariton electric field, which works with the dielectric electric field (E_1) and metal electric field (E_2). The factor for increasing the LFIEF was determined using the following equation:

$$M = \frac{|E_1(0)|^2}{|E_{Inc}(0)|^2} = \frac{2|\epsilon|}{\epsilon_M \epsilon''} I_m \left(\epsilon \sqrt{\frac{1}{\epsilon + \epsilon_M}}\right) \eta \sqrt{\epsilon_{Inc} cos_{\theta_{Inc}}}, \quad (1)$$

where E_{Inc} is the electric field of the laser, ϵ_{Inc} is the dielectric where the wave arrives, θ_{Inc} is the angle of incidence, Im is the imaginary part, ϵ is the substrate dielectric, ϵ'' is the imaginary substrate dielectric, and ϵ_M is the medium dielectric (Le Ru, 2009). The dielectric constant of the SERS substrate impacts signal growth and the EF value.

The Raman signal amplification on the Si wafer substrate exceeded that on the Cu substrate, mostly attributable to the disparity in dielectric constants. The dielectric constant of the Si wafer substrate (11.7) exceeded that of the Cu substrate (1.68). The Si wafer substrate, with its higher dielectric constant, had a higher influence on the plasmonic characteristics of the SERS substrate. The stronger plasmonic coupled and increased the Raman vibration of the pesticide molecules, as represented by the higher Raman peak compared with that of the SERS Cu substrate. The EF for the SERS Si substrate was 2.38×10^4, higher than that for the Cu substrate (1.39×10^2). The EF is determined using (ISERS/IRaman) × (NRaman/NSERS), where ISERS represents the SERS intensity, IRaman is the standard Raman intensity, NRaman is the analyte concentration in standard Raman measurements, and NSERS is the analyte concentration in SERS measurements (Ru, 2013).

4. Conclusion

This study effectively fabricated SERS substrate-based AuNPs on Si and Cu wafer substrates. The SERS substrates were fabricated via the drop-casting method, and AuNPs (diameter = 7.3 nm), synthesized from Au metal salts dissolved in water and irradiated with a femtosecond laser, were deposited onto both substrates. The quality assessment of the SERS substrate relied on its ability to enhance the Raman signal of the paraquat pesticides. The experimental findings showed that the AuNPs could enhance the Raman signal, leading to the successful detection of six Raman peaks associated with the paraquat insecticide. The SERS substrate on a Si wafer significantly amplified the Raman signal for the paraquat insecticide compared with the Cu substrate. This was due to the higher dielectric constant of the Si wafer than that of the Cu wafer. The higher dielectric constant influenced the behavior of the localized SPPs, facilitating the coupling of the Raman scattering vibrations of the paraquat pesticide molecules. Further investigation is required to investigate the impact of other substrates, in addition to Si and Cu wafers, on the amplification of Raman signals for analytes under examination.

5. Acknowledgement

This paper was supported by Rumah Program ORNM Badan Riset dan Inovasi Nasional and Universitas Indonesia under Grant PUTI NKB-4502/UN2.RST/HKP.05.00/2020.

6. References

Alsammarraie, F K., Lin, M S. (2017). Using standing gold nanorod arrays as surface-enhanced Raman spectroscopy (SERS) substrates for detection of carbaryl residues in fruit juice and milk. J. Agric. Food Chem. 65 : 666−674.

Alsammarraie, F K., Lin, M S., Mustapha, A., Lin, H T., Chen, X., Chen, Y H., Wang, H., Huang, M Z. (2018). Rapid determination of thiabendazole in juice by SERS coupled with novel gold nanosubstrates. Food Chem. 259 : 219−225.

Anema J R., Li J F., Yang Z L., Ren B. and Tian Z. Q. (2011). Shell-isolated nanoparticle-enhanced Raman spectroscopy: expanding the versatility of surface-enhanced Raman scattering, Annual Review of Analytical Chemistry 4:129-150.

Brust, M., Walker, M., Bethell, D., Schiffrin, D.J., Whyman, R. (1994). Synthesis of thiolderivatised gold nanoparticles in a two-phase Liquid-Liquid system, J. Chem. Soc., Chem. Commun 7 : 801e802.

Chen Y T., Pan L., Horneber A., Berg M., Miao P., Xu P., Adam P M., Meixner A J., and Zhang D. (2019). Charge transfer and electromagnetic enhancement processes revealed in the SERS and TERS of a CoPc thin film, Nanophotonics 8(9), 1533-1546.

Chen, W., Li, C., Yu, Z., Song, Y., Zhang, X., Ni, D., Zhang, D., Liang, P. (2022). Optimum synthesis of cactus-inspired SERS substrate with high roughness for paraquat detection, Spectrochimica Acta Part A: Molecular and Biomolecular Spectroscopy 268 : 120703.

Craig A P., Franca A S., and Irudayaraj J. (2013). Surface-Enhanced Raman Spectroscopy Applied to Food Safety, Annu. Rev. Food Sci. Technol. 4:369–80.

Eral, H., Oh, J. (2013). Contact angle hysteresis: a review of fundamentals and applications, Colloid Polym. Sci. 291 : 247–260.

Ferdous Z. and Nemmar A. (2020). Health Impact of Silver Nanoparticles: A Review of the Biodistribution and Toxicity Following Various Routes of Exposure, Int. J. Mol. Sci. 21(7):2375.

Gushiken N K., Paganoto G T., Temperini M L A., Teixera F S. and Salvadori M C. (2020). Substrate for Surface-Enhanced Raman Spectroscopy Formed by Gold Nanoparticles Buried in Poly (methyl methacrylate), ACS Omega 5(18):10366-10373.

DOI:https//doi.org/10.22452/mjs.vol44no2.8
Malaysian Journal of Science 44(2): 78-85 (June 2025)

Hidayah, A.N., Herbani, Y., Steven, E., Subhan, A., Triyono, D., Isnaeni, Suliyanti, M. M., and Shiddiq, M. (2022). Tuning the electrical properties of colloidal nanoalloys by varying their composition, Colloids and Surfaces A: Physicochemical and Engineering Aspects 641:128496.

Hidayah, A N., Triyono, D., Herbani, Y., and Saleh, R. (2022). Liquid Surface-Enhanced Raman Spectroscopy (SERS) Sensor-Based Au-Ag Colloidal Nanoparticles for Easy and Rapid Detection of Deltemthrin Pesticide in Brewed Tea, Crystals 12:24.

Huan Q., Liu Y., Chang S., Chen H., and Chen J. (2016). Surface Plasmonic Sensors: Sensing Mechanism and Recent Applications, Sensors 21(16):5262.

Ilyas H., Zeeshan T., Sattar N. A., Ramay S. M., Mahmood A., Abbas H. G., Saleem M. (2021). First principle and experimental investigations of monodispersed Au plasmonic nanoparticles on TiO_2, Chemical Physics Letters 783:139080.

Israelsen N D., Hanson C. and Vargis E. (2015). Nanoparticles Properties and Synthesis Effects on Surface-Enhanced Raman Scattering Enhancement Factor: An Introduction, The Scientific World Journal 2015: 124582.

Kabir, M H., Ali, M. M., Kaiyum, M A., and Rahman, M S. (2019). Effect of annealing temperature on structural morphological and optical properties of spray pyrolized Al-doped ZnO thin films, J. Phys. Commun. 3 : 105007.

Kahraman M., Mullen E R., Korkmaz A. and Wachsmann-Hogiu S. (2017). Fundamentals and Applications of SERS-based bioanalytical sensing, Nanophotonics 6(5).

Kamkrua, N., Ngernsutivorakul, T., Limwichean, S., Eiamchai, P., Chananonnawathorn, C., Pattanasetthakul, V., Ricco, R., Choowongkomon, K., Horprathum, M., Nuntawong, N., Bora, T., and Botta, R. (2023). Au Nanoparticle-Based Surface-Enhanced Raman Spectroscopy Aptasensors for Paraquat Herbicide Detection, ACS Appl. Nano Mater. 6 : 1072−1082.

Khalil I., Chou C M., Tsai K L., Hsu S., Yehye W A., and Hsiao V K S. (2019). Gold Nanofilm-Coated Porous Silicon as Surface-Enhanced Raman Scattering Substrate, Appl. Sci. 9: 4806.

Kneipp J., Kneipp H., Wittig B., and Kneipp K. (2010). Novel optical nanosensors for probing and imaging live cells, Nanomedicine 6(2):214–226.

Kumar, A K S., Zhang, Y., Li, D., Compton. R G. (2020). A mini-review: How reliable is the drop casting technique?. Electrochemistry Communications 121 : 106867.

Le Ru, E. and Etchegoin P. (2009). Principles of Surface Enhanced Raman Spectroscopy. Pp. 134-135, UK, Oxford: Elsivier.

Le Ru, E C., and Etchegoin, P G. (2013). Quantifying SERS enhancements, MRS (Materials Research Society) Bulletin 38 : 631 – 640.

Lia M., Cushinga S K., and Wua N. (2015). Plasmon-enhanced optical sensors: a review, Analyst 140 (2):386–406.

Liao, Q., Li, M Y., Hao, R., Ai, X C., Zhang, J P., Wang, Y. (2007). Surface-enhanced Raman scattering and DFT computational studies of cyanuric chloride derivative, Vibrational Spectroscopy 4 : 351-356.

Li, X Z., Yang, T Y., Song, Y T., Zhu, J H., Wang, D L., Li, W. (2019). Surface-enhanced Raman spectroscopy (SERS)-based immunochromatographic assay (ICA) for the simultaneous detection of two pyrethroid pesticides. Sens. Actuators, B 283 : 230−238.

Lin, M H., Sun, L., Kong, F., Lin, M. (2021). Rapid detection of paraquat residues in green tea using surface-enhanced Raman spectroscopy (SERS) coupled with gold nanostars, Food Control 130 : 108280.

Lopez-Lorente, A. I., Simonet, B.M., Valc_arcel, NM., Eppler, S., Schindl, R., Kranz, C., Mizaikoff, B. (2014). Characterization of stainless steel assisted bare gold nanoparticles and their analytical potential, Talanta 118 : 321e327.

Lopez-Lorente, A. I. (2021). Recent developments on gold nanostructures for surface enhanced Raman spectroscopy: Particle shape, substrates and analytical applications. A review, Analytica Chimica Acta 1168 : 338474.

Luo, H R., Huang, Y Q., Lai, K Q., Rasco, B A., Fan, Y X. (2016). Surface-enhanced Raman spectroscopy coupled with gold nanoparticles for rapid detection of phosmet and thiabendazole residues in apples. Food Control 68 : 229−235.

Meader V K., John M G., Rodrigues C J., Tibbetts K M. (2017). Roles of Free Electrons and H2O2 in the Optical Breakdown-Induced Photochemical Reduction of Aqueous [$AuCl_4$], J. Phys. Chem. A 121:6742–6754.

Minho K., Jung-Hoon L., Jwa-Min N. (2019). Plasmonic Photothermal Nanoparticles for Biomedical Applications, *Adv. Sci*. 6:1900471.

Pusat Standarisasi Instrumen Kualitas Lingkungan Hidup, Kementerian Lingkungan Hidup dan Kehutanan Republik Indonesia. (2020). *Konversi Rotterdam: Pro dan Kontra Paraquat Dichloride*. Maret 2024. (https://psiklh.bsilhk.menlhk.go.id/v2/?p=11619).

Pérez-Jiménez A I., Lyu D., Lu Z., Liu G., and Ren B. (2020). Surface-enhanced Raman spectroscopy: benefits, trade-offs and future developments, Chem. Sci. 11:4563-4577.

DOI:https//doi.org/10.22452/mjs.vol44no2.8
Malaysian Journal of Science 44(2): 78-85 (June 2025)

Pilot R., Signorini R., Durante C., Orian L. (2019). Manjari Bhamidipati and Laura Fabris, A Review on Surface-Enhanced Raman Scattering, Biosensors 9:57.

Pissuwan D., Camilla G., Mongkolsuk S., Cortie M. B. (2019). Single and multiple detections of foodborne pathogens by gold nanoparticle assays, WIREs Nanomed. Nanobiotechnol. 12:1584.

Roguska A., Kudelski A., Pisarek M., Opara M., and Janik-Czachor M. (2011). Surface-enhanced Raman scattering (SERS) activity of Ag, Au and Cu nanoclusters on TiO_2-nanotubes/Ti substrate, Appl. Surf. Sci. 257(19):8182–8189.

Saim, A K., Kumah, F N., Oppong, M N. (2021). Extracellular and intracellular synthesis of gold and silver nanoparticles by living plants: a review, Nanotechnol. Environ. Eng. 6 : 1.

Unser S., Bruzas I., He J. and Sagle L. (2015). Localized Surface Plasmon Resonance Biosensing: Current Chalengges and Aprroaches, Sensors 15(7):15684-15716.

Wang K., Sun D W., Pu H. and Wei Q. (2019). Shell thickness-dependent Au@Ag nanoparticles aggregates for high-performance SERS applications, Talanta 195:506-515.

Wang, K G., Sun, D W., Pu, H B., Wei, Q Y. (2019). Surface enhanced Raman scattering of core-shell Au@Ag nanoparticles aggregates for rapid detection of difenoconazole in grapes. Talanta 191 : 449−456.

Xu N., Jin S., and Li W. (2021). Metal nanoparticles-based nanoplatforms for colorimetric sensing: A review, Reviews in Analytical Chemistry 40: 1–11.

Yonzon C R., Haynes C L., Zhang X., Walsh J T., Van Duyne R P. (2004). A glucose biosensor based on surface-enhanced Raman scattering: improved partition layer, temporal stability, reversibility, and resistance to serum protein interference, *Anal. Chem.* 76(1):78-85.

Zhang D., Pu H., Huang L., and Sun D. (2021). Advances in flexible surface-enhanced Raman scattering (SERS) substrates for nondestructive food detection: Fundamentals and recent applications, *Trends in Food Science & Technology* 109:690-701.

Zhang, Y Z., Wang, Z Y., Wu, L., Pei, Y W., Chen, P., Cui, Y P. (2014). Rapid simultaneous detection of multi-pesticide residues on apple using SERS technique. Analyst 139 : 5148−5154.

Zhao Y., Gan S., Zhang G., Dai X. (2019). High sensitivity refractive index sensor based on surface plasmon resonance with topological insulator, Results in Physics 14:102477.

DOI:https//doi.org/10.22452/mjs.vol44no2.8
Malaysian Journal of Science 44(2): 78-85 (June 2025)

MALAYSIAN JOURNAL OF SCIENCE
MJS
ISSN 1394-3065

Regular Issue

Malaysian Journal of Science 44 (2): 86-103 (June 2025) https://mjs.um.edu.my

Exploring Fertilizer-Microbiome Interactions Through Next-Generation Sequencing (NGS): Insights for Sustainable Agriculture

Mohd Khairil Radzali[1a], Amalia Mohd Hashim[2ab], Miratul Hada Mohd Ali[3a], Wan Zuhainis Saad[4a]*, Zakiah Anis Nawawi[5a]

Abstract: With the global demand for food production escalating, concerns about the long-term sustainability and environmental impact of traditional farming practices, particularly the application of chemical fertilizers, have gained prominence. Recognizing the importance of addressing these issues, this review explores the evolving dynamic between fertilizers and microbial communities, emphasizing the need for a more profound understanding of these interactions. The transformative impact of next-generation sequencing (NGS) technologies in unraveling microbial intricacies within agricultural ecosystems is highlighted as a crucial tool for advancing this understanding. Investigation extends to discerning the nuanced effects of both chemical and non-chemical fertilizers on soil microbiomes, considering variations in soil type and crop specificity. Linking these findings to the Sustainable Development Goals (SDGs), the review highlights the critical connection between fertilizer use, microbial diversity, and the achievement of sustainability objectives. Despite the potential of NGS, the review acknowledges current limitations, sparking discussions on potential technological advancements and methodological improvements. Emphasizing the necessity for interdisciplinary collaboration, it advocates for comprehensive insights that bridge gaps between microbiology, agriculture, and sustainability. In conclusion, the article synthesizes historical perspectives, cutting-edge technologies, and sustainable development objectives to provide a holistic understanding of the intricate interplay between fertilizers, microbial diversity, and the imperative path toward a more sustainable agricultural future.

Keywords: *Fertilizers, microbial diversity, sustainable agricultural practices, next-generation sequencing (NGS) technologies, sustainable development goals (SDGs)*

1. Introduction

Background

Agriculture is the backbone of human civilization, providing sustenance, economic stability, and a foundation for societal development. Its global significance is indisputable, as it not only supports the basic human need for food but also fuels economies (Shen et al., 2023), shapes landscapes (Martello et al., 2023), and influences cultural identities (Zheng et al., 2023). The unprecedented growth of the world's population and the escalating demand for food resources have intensified the pressure on agricultural systems, necessitating innovative approaches to ensure sustainable food production.

At the core of modern agricultural practices lies the pivotal role of fertilizers. Fertilizers have become vital tools for farmers seeking to enhance crop yields and meet the escalating demands of a growing population (Mustafa et al., 2023). These chemical and non-chemical formulations offer valuable nutrients to plants, augmenting soil fertility and addressing nutrient deficiencies. While fertilizers have played a critical role in boosting agricultural productivity, their widespread use has raised concerns about environmental impact, including soil acidification, greenhouse gas emissions, depletion of the ozone layer, and loss of biodiversity (Bai et al., 2020; Mustafa et al., 2023). As we delve into the intricate relationship among fertilizers and microbial communities, it becomes apparent that a nuanced understanding of these dynamics is essential for sustainably shaping the future of agriculture. This review investigates the transformative potential of Next Generation Sequencing (NGS) in unraveling the complex interplay between fertilizers and microorganisms, offering insights that can pave the way for achieving Sustainable Development Goals (SDGs) in agriculture.

Rationale for the Review

The escalating global demand for food production drives the imperative to reassess and optimize agricultural practices. With the world's population steadily climbing, the need for increased food yields places unprecedented pressure on the agricultural sector. This heightened demand necessitates a critical evaluation of existing farming methods to ensure both quantity and the quality and sustainability of our food supply. Simultaneously, the reliance on conventional fertilizers has sparked environmental and sustainability challenges that cannot be ignored. Runoff from these chemical inputs contributes to water pollution, adversely

Authors information:
[a]Department of Microbiology, Faculty of Biotechnology and Biomolecular Sciences, Universiti Putra Malaysia, 43400, Serdang, Selangor, MALAYSIA. E-mail: gs50774@student.upm.edu.my[1]; amalia@upm.edu.my[2]; miratulali@gmail.com[3]; mohdtermizi@upm.edu.my[4]; zuhainis@upm.edu.my[5]; zakiahanisnawawi@gmail.com[6]
[b]Halal Produt Research Institute, Universiti Putra Malaysia, 43400, Serdang, Selangor, MALAYSIA. E-mail: amalia@upm.edu.my[2]
*Corresponding Author: zuhainis@upm.edu.my

Received: January, 2024
Accepted: July, 2024
Published: June, 2025

DOI: https//doi.org/10.22452/mjs.vol44no2.9
Malaysian Journal of Science 44(2): 86-103 (June 2025)

impacting aquatic ecosystems, while the accumulation of excess nutrients in the soil can lead to degradation and long-term loss of fertility (AbdelRahman et al., 2022; Li et al., 2022a). Addressing these challenges requires a major shift towards more environmentally conscious and sustainable agricultural practices.

Amidst these challenges, the introduction of NGS emerges as a transformative tool to deepen our understanding of microbial dynamics in agriculture. NGS technologies, including both shotgun and amplicon sequencing, enable researchers to investigate the genetic landscapes of microbial communities, offering unparalleled insights into their composition, diversity, and functional potential (Liu et al., 2021a; de Vries et al., 2023; Maretto et al., 2023; Tang et al., 2023). It holds the promise of unraveling the complex relationships between fertilizers and microorganisms and guiding the development of sustainable agricultural practices for the future (Chouhan et al., 2023). This review aims to investigate the synergy between fertilizer use, microbial dynamics, and NGS technologies, highlighting on the path toward achieving Sustainable Development Goals in agriculture.

2. Fertilizers and Microbial Diversity: a Historical Perspective

Historically, the relationship between fertilizers and microorganisms has been focused primarily on nutrient provision to plants. Traditional agricultural practices often treated soil as a mere substrate for plant growth (Thompson, 1992; Lafaille, 2017), with little consideration for the intricate web of microbial life beneath the surface. While effective in boosting crop yields, this limited perspective failed to account for the broader ecological consequences of altering microbial ecosystems. It aimed to replenish essential nutrients without heavily understanding the dynamic interplay between these chemical inputs and the diverse microbial communities inhabiting the soil and plant root systems (Russel & Williams, 1977; Inubushi & Acquaye, 2004). However, the traditional mindset that viewed soil merely as a medium for plant growth is gradually transforming into a holistic approach that considers the soil as a living ecosystem (Ponge, 2015).

As agriculture evolved and intensified, the limitations of these traditional views became increasingly apparent that the indiscriminate use of chemical fertilizers led to soil degradation, negative impacts on microbial biodiversity, and environmental pollution (Feng et al., 2022; Mukhles et al., 2022; Wang et al., 2022; Nguyen et al., 2023). The emergence of these challenges underscored the need for a deeper understanding of the intricate relationships between fertilizers and microorganisms. The dynamic nature of microbial communities, their symbiotic relationships with plants, and their roles in nutrient cycling and soil health became focal points for researchers seeking sustainable agricultural solutions (Abid et al., 2021; Iqbal et al., 2023; Wei et al., 2023a; Zhang et al., 2023a). Acknowledging the complexity of these interactions is vital for mitigating the unintended consequences of fertilization and steering agricultural practices toward greater ecological resilience.

The historical shift towards environmentally-friendly agricultural practices, as highlighted in the Sustainable Development Goals (SDGs) and underscored by scholars like Dubey et al. (2021) and Shahmohamadloo et al. (2021), reflects a growing awareness of the complex interplay between human activities and the environment. This departure from historical practices, often focused solely on maximizing yields with little regard for long-term ecological consequences, is now characterized by a commitment to biodiversity conservation, climate resilience, and reducing ecological footprint. Aligning agricultural strategies with sustainable development objectives underscores a historical trajectory towards a more responsible and conscientious approach, recognizing the importance of integrating sustainable practices to ensure the long-term well-being of ecosystems and harmony between food production and ecological health preservation.

3. Next Generation Sequencing: Revolutionizing Agricultural Microbiology

The aim of sustainable agriculture relies on microbial diversity. These microscopic organisms, including bacteria, fungi, and archaea, contribute to soil fertility, nutrient cycling, and plant health (May et al., 2023; Xiang et al., 2023). A rich and diverse microbial community can enhance plant tolerance to soil salinity (Feng et al., 2023; Wang et al., 2023), suppress pathogenic organisms (Ehau-Taumaunu & Hockett, 2023; Yang et al., 2023a), and improve nutrient availability for plants (Arunrat et al., 2023; Li et al., 2023a). As the agricultural community recognizes the multifaceted benefits of microbial diversity, there is a growing shift towards holistic and regenerative practices that aim to maximize crop yields and foster long-term soil health.

NGS technologies have emerged as powerful tools, propelling agricultural microbiology into a new era of precision and depth. Two primary methodologies, shotgun and amplicon sequencing, form the cornerstone of NGS applications in studying microbial communities. Shotgun Sequencing involves the random sequencing of DNA fragments, providing a comprehensive snapshot of the entire genetic content present in a sample (Doni et al., 2023). Amplicon sequencing, on the other hand, targets specific gene regions such as 16S ribosomal RNA (16S) and Internal Transcribed Spacer (ITS), allowing for a more focused analysis of microbial diversity (Liu et al., 2021a). These approaches help researchers to investigate the genetic complexities of microbial communities with unprecedented resolution, shedding light on the composition, functional potential, and dynamics of these microscopic ecosystems (Liu et al., 2021a; de Vries et al., 2023; Maretto et al., 2023; Tang et al., 2023).

By unlocking the genetic codes of diverse microorganisms through NGS technologies, researchers can elucidate their roles in nutrient cycling, plant-microbe interactions, and overall soil health (Windisch et al., 2021; Kim et al., 2022; Xiang et al., 2023). NGS aids in the identification and quantification of microbial species, offering insights into their functional capabilities and interactions. By exploring the microbial ecosystems, NGS enables

DOI: https//doi.org/10.22452/mjs.vol44no2.9
Malaysian Journal of Science 44(2): 86-103 (June 2025)

the comprehensive analysis of microbial diversity at a scale and precision unattainable by traditional methods such as PCR-Denaturing Gradient Gel Electrophoresis (PCR-DGGE), Terminal Restriction Fragment Length Polymorphism (T-RFLP), and Fluorescent in Situ Hybridization (FISH) (Wolsing & Priemé, 2004; Caracciolo et al., 2005; Wenhui et al., 2007; Bokulich & Mills, 2012). This transformative capability extends beyond taxonomy, allowing a deeper understanding of the functional attributes governing microbial contributions to agricultural ecosystems.

The application of NGS in agricultural microbiology goes beyond mere taxonomic identification and explores the functional dynamics of microbial communities. Metagenomics, a primary application of NGS, enables the direct study of genomic material extracted from environmental samples, providing valuable insights into the functional potential of microbial communities (Tas et al., 2021). Metatranscriptomics further extends this capability by analyzing the actively expressed genes, allowing researchers to analyze real-time functional activities within microbial ecosystems (Mukherjee & Reddy, 2020). This understanding of genetic composition and functional activities empowers scientists to identify microbial contributions to nutrient cycling, disease suppression, and plant resilience (Chuckran et al., 2021; Mendes et al., 2023; Pande et al., 2023). The integration of metagenomic and metatranscriptomic data opens avenues for targeted interventions, allowing for the development of precision agricultural practices that leverage the specific functions of microbial communities to improve crop health and yield.

The shift from traditional to NGS-based approaches represents a paradigmatic leap in our capacity to assess microbial diversity. NGS offers several advantages over outdated conventional methods, including higher throughput, reduced cost per base pair, and the ability to detect rare and novel microbial taxa (Zhao et al., 2020; Adhikari et al., 2021; Greay et al., 2021). The technology's capacity to provide quantitative data on microbial abundances, community structures, and functional potentials in a single experiment is unparalleled (Hiiesalu et al., 2012; Azarbad et al., 2022). NGS minimizes biases inherent in cultivation-dependent methods, allowing for the identification of previously unculturable microorganisms (Chaudhary et al., 2019; Qaisrani et al., 2019; Sessou et al., 2023; Deinert et al., 2023). It is a transformative tool that broadens our understanding of microbial ecosystems and guides the development of targeted strategies for enhancing agricultural productivity and resilience toward sustainable practices.

4. Fertilizer Impact on Microbial Communities: Insights from NGS Studies

Chemical Fertilizers and Their Effects on Microbiomes

The widespread application of chemical fertilizers in modern agriculture has significantly changed the dynamics of soil microbial communities, prompting a closer examination of their impacts through the NGS. Chemical fertilizers, rich in nitrogen (N), phosphorus (P), and potassium (K), are known to influence soil pH, nutrient availability, and overall soil structure (Li et al., 2020a; Liu et al., 2020). However, the consequences of these alterations on microbial diversity and function have become increasingly apparent with the application of NGS technologies.

Apart from demonstrating an increase in the abundance of the denitrification-related gene nirK (Carrascosa et al., 2023), chemical fertilization exhibited an increased abundance of genes associated with methane oxidation, soil nitrogen degradation, nitrification, and anammox, emphasizing a distinct influence on nutrient cycling as shown by the 16S amplicon studies (Hu et al., 2022a). The NPK fertilization also positively influenced acidophilic groups, such as nitrifiers and denitrifiers, based on 16S and ITS amplicon sequencing, and concurrently increased the alpha diversity of arbuscular mycorrhizal (AM) fungi in the root endosphere (Semenov et al., 2020; Ma et al., 2021). According to Hu et al. (2022b), nitrogen (N) fertilization induced the saprotroph fungal functional group, which may suggest its potential role in decomposing and absorbing organic matter from dead or decaying organisms using the ITS sequencing approach.

Recent studies using shotgun metagenomic sequencing are further discussed and have revealed novel insights into how the taxonomic makeup of soil microorganisms changes when exposed to chemical fertilizers. High inorganic nitrogen fertilizer led to higher relative abundance in Bacillaceae and Carnobacteriaceae families, while certain bacterial families like Pseudonocardiaceae, Clostridiaceae, Cytophagaceae, Micromonosporaceae, and others were relatively less abundant (Enebe & Babalola, 2021). Apart from increasing soil nutrient availability, excessive K2SO4 application in tobacco-planting soil increased copiotrophic groups such as Burkholderiaceae and Rhodospirillaceae families, as well as Ellin6067 genus, while negatively impacting oligotrophic taxa (Lu et al., 2022). Li et al. (2020b) found that applying NPK fertilizer reduced Proteobacteria and Bradyrhizobium at the genus level and increased Acidobacteria at the phylum level. In a separate study, Li et al. (2022b) reported that NPK fertilizer resulted in decreased Proteobacteria abundance, increased Actinobacteria abundance, the lowest Acidobacteria abundance, and the highest Chloroflexi abundance. Fadiji et al. (2020) found that using inorganic fertilizer (NK) led to the dominance of Dothideomycetes at the class level and endophytic Leptosphaeria at the genus level. Leptosphaeria sp. has been reported to promote plant growth by increasing root volume and plant tolerance to salinity and drought (Poveda, 2022; Zhao et al., 2024). These findings highlight the impact of nutrient changes on microorganisms, influencing specific groups that, in turn, can promote plant growth, emphasizing the potential for targeted approaches to enhance overall plant health and productivity.

These studies uncover previously overlooked microorganisms, revealing details of nutrient cycling, organic matter decomposition, and plant-microbe interactions. By integrating data from diverse ecosystems and crops, these investigations offer a complete understanding of the intricate connections between chemical fertilizers and microbial communities. This awareness aids in refining fertilizer applications, lessening environmental impact, and fostering robust and productive farming practices. The research also takes economic factors into

DOI: https//doi.org/10.22452/mjs.vol44no2.9
Malaysian Journal of Science 44(2): 86-103 (June 2025)

account, directing efforts toward cost-effective and sustainable approaches. Moreover, it addresses social considerations by advocating for microbiome-conscious agriculture, contributing to a more promising future.

Non-Chemical Fertilizers and Their Influence on Microbial Diversity

In contrast to chemical fertilizers, non-chemical alternatives, such as organic or bio-based fertilizers, have gained prominence in agricultural systems aiming for sustainability and reduced environmental impact. The impact of these non-chemical fertilizers on microbial diversity has become a focal point of the investigation, leveraging the capabilities of NGS to delve into the subtleties of microbial responses.

NGS studies have facilitated a signified comparative analysis of the impacts of non-chemical and chemical fertilizers on microbial diversity. By adopting a comparative approach, researchers have unraveled the intricate interactions between diverse fertilizer types and the soil microbiome, with multiple studies highlighting the beneficial effects of both organic matter and fertilizers on agriculture. Zhu et al. (2023a) found that composting enhances microbial diversity, promoting the activity of beneficial genera like Corynebacterium and Lactobacillus, while influencing nutrient cycling and emissions. Composting also showcases Marinimicrobium and Thermobifida's crucial roles in ammonia assimilation, highlighting the diverse microbial contributions (Zhu et al., 2023b). Moreover, bark compost boosts beneficial fungi, including Penicillium and Inocybe, with potential benefits for nutrient uptake and plant health (Malewski et al., 2023) whereas the combination of compost and citrus rootstocks significantly influences rhizobiome bacterial abundance and diversity, correlating with essential nutrient concentrations for plant health and productivity (Castellano-Hinojosa et al., 2023). Sophora alopecuroides L., or Kudouzi in China, traditionally used for medicinal purposes, is also employed as an organic fertilizer, enhancing sugar content and promoting beneficial microorganisms, as indicated by Hua et al. (2023).

Manure serves as an alternative to compost for organic fertilizer. Khatri et al. (2023) claim that green manure applications lead to higher microbial abundance, reduced disease development, and increased abundance of beneficial phyla, thereby contributing to sustainable agriculture. Erythrobacter sp. YH-07-inoculated organic manure enhances microbial diversity, suppresses Fusarium wilt, and alters community composition. This demonstrates its potential for disease control, as Tang et al. (2023) highlighted. Another finding reveals that Hanwoo manure positively impacts soil organic matter, crude ash, and phosphorus, providing a valuable alternative to chemical fertilizers (Lee et al., 2023). Lastly, implementing reduced tillage with green manure for a decade enhances soil organic carbon and total nitrogen, maintaining almond yields and promoting sustainability, albeit with changes in the bacterial community structure (Özbolat et al., 2023). These findings showcase their significant potential in fostering sustainable agriculture, enhancing soil health, and mitigating disease risks, emphasizing a promising shift towards eco-friendly farming practices.

One notable trend from the comparative studies is the potential for non-chemical fertilizers to foster greater microbial diversity than their chemical counterparts. Organic amendments, for instance, introduce a spectrum of organic matter that serves as a substrate for a diverse array of microorganisms (Saunders et al., 2012; Verma et al., 2020). This diversity, in turn, contributes to enhanced nutrient cycling, disease suppression, and overall soil health as discussed previously. The comparative insights gained from NGS studies not only inform on the immediate impacts of fertilizer choices but also provide a foundation for developing strategies that optimize microbial diversity in ways that align with sustainable development goals in agriculture (Meuniern & Bayır, 2021; Ashraf et al., 2022).

The Role of Soil Type and Crop Specificity in Shaping Microbial Communities

The relationships between fertilizers and microbial communities are not only influenced by the type of fertilizer. However, they are equally shaped by the unique characteristics of soil types and the specific crops being cultivated. NGS studies have been instrumental in elucidating the complex interplay between soil types, crop specificity, and the dynamic microbial ecosystems they harbor.

Understanding the impact of soil type on microbial communities is crucial, as various soils possess distinct physical and chemical properties that influence microbial life. NGS technologies have unveiled how microbial compositions respond differently to fertilizers in clayey, loamy, and sandy soils. High clay content in the soil offered enhanced physicochemical protection for microbial biomass pools and mitigated water stress, impacting the efficacy of N fertilization on soil microbial communities (Kallenbach & Grandy, 2011; Fierer et al., 2012; Yu et al., 2019). The 16S rRNA sequencing results indicated shifts in bacterial composition post-fertilization, which led to a decrease in the relative abundance of Chloroflexi, Acidobacteria, and Nitrospirae at the phylum level while increasing Proteobacteria and Actinobacteria (Liu et al., 2021b). The relative abundance of Gemmatimonadota and Firmicutes significantly increased with NPK treatments, accompanied by a decrease in Bacteroidetes (Chen et al., 2023).

On the contrary, sandy loam soils demonstrate a well-rounded capacity for water retention, stable structure formation, adequate aeration, and maintenance of a moderate soil temperature (Lakesh et al., 2022). Fertilizer applications resulted in a major shift in microbial composition, with a lower relative abundance of Bacteroidetes and elevated levels of Proteobacteria and Verrucomicrobia compared to the control (Zhang et al., 2022a). Meanwhile, fertilized sandy loam soils exhibit significant increases in Ambispora, Funneliformis, and Glomus, accompanied by a marked decline in Paraglomus at the genus level of the arbuscular mycorrhizal fungal community (Liu et al., 2022). These findings collectively highlight the multifaceted impact of

DOI: https//doi.org/10.22452/mjs.vol44no2.9
Malaysian Journal of Science 44(2): 86-103 (June 2025)

fertilization on microbial attributes, influencing bacterial and fungal communities in different soil types.

In addition, the crop specificity of microbial communities adds another layer of complexity to the fertilization equation in the NGS studies. A study by Zhang et al. (2023b) reveals that rotating rice and oilseed rape crops significantly enhances soil microbes, particularly those associated with nitrogen, phosphorus, and overall soil quality. A similar study on crop rotation of peppers and eggplants created helpful microbes that protected bananas from diseases, aiding in sustainable banana farming (Hong et al., 2023). Compared to annually rotated crops, corn and soybean crops influenced bacterial communities differently, with grass cover crops having minimal impact, emphasizing the greater role of soil pH and organic matter for bacteria (Chamberlain et al., 2020).

Biochar had different effects on wheat and mash bean soils, increasing specific genes in both, with wheat showing an additional gene increase; the crop type played a major role in how biochar and fertilizer influenced microbes in mash bean soils (Azeem et al., 2020). A study by Woo et al. (2022) found that pea farming clearly reduced microbe diversity compared to wheat, pea-wheat rotations, and fallow fields, impacting diverse fungi, and influencing nitrogen, water, as well as both beneficial and harmful fungi in the Canadian prairies. Consequently, the choice of fertilizer can exert variable effects on microbial communities based on the specific crop it is intended for (Dincă et al., 2022; Gupta et al., 2022; Williams et al., 2023). Integrating crop-specific insights from NGS studies into fertilizer management can enhance nutrient uptake, disease resistance, and overall crop performance. These studies offer a roadmap for customizing agricultural practices based on the intricate relationships among fertilizers, soil types, and crop specificity. This holistic approach acknowledges unique microbial dynamics in diverse agroecosystems, which are crucial for creating sustainable and resilient agricultural systems in the face of global challenges.

5. Sustainable Development Goals (SDGS) and Agricultural Microbial Diversity

Linking Fertilizer Use, Microbial Diversity, and SDGs

The intersection of fertilizer use, microbial diversity, and the ambitious targets set by the SDGs forms a critical nexus in pursuing a more sustainable and equitable global agriculture (Figure 1). Fertilizers, both chemical and non-chemical, play a pivotal role in meeting the SDG mandate to eradicate hunger (SDG 2) by bolstering crop yields (Heidkamp et al., 2021; Saqib et al., 2020; Ishfaq et al., 2023). However, the implications of fertilizer use extend beyond mere productivity, resonating with several other SDGs that collectively underscore the need for holistic and environmentally responsible agricultural practices (United Nations, 2023).

Microbial diversity emerges as a linchpin in achieving these broader sustainability goals. NGS studies have illuminated the intricate relationships between fertilizers and microbial communities, revealing their profound impact on soil health, nutrient cycling, and ecosystem resilience (Ma et al., 2023; May et al., 2023; Xiang et al., 2023). Recognizing the symbiotic alliances between plants and microorganisms facilitated by appropriate fertilization (Li et al., 2023b) aligns with SDG 15 (Life on Land), promoting the conservation, restoration, and sustainable use of terrestrial ecosystems (Kumawat et al., 2023). Moreover, fostering microbial diversity through judicious fertilizer management contributes to SDG 13 (Climate Action) by enhancing soil carbon sequestration and mitigating greenhouse gas emissions (Jiang et al., 2021; Zhou et al., 2022). The potential to reduce agriculture's environmental footprint while simultaneously increasing its productivity positions microbial-conscious fertilization as a key player in the global effort to combat climate change.

Furthermore, the relationship between fertilizer use, microbial diversity, and the SDGs extends into water resource management, aligning with SDG 6 (Clean Water and Sanitation). Proper fertilization practices that promote microbial diversity contribute to enhanced water retention in soils (Wang et al., 2021; Xu et al., 2023a), reducing the risk of nutrient runoff and contamination of water bodies (Menzies Pluer et al., 2020). By mitigating water pollution and ensuring sustainable water use in agriculture, this integrated approach addresses a critical aspect of the SDGs related to clean and accessible water. Implementing microbial-conscious fertilization supports agricultural productivity and safeguards vital water resources, marking a significant stride towards achieving the broader agenda of sustainable development.

Linking fertilizer application, microbial diversity, and SDGs demonstrates the need for an integrative approach to agricultural practices. Harnessing the insights gleaned from NGS studies, this linkage provides a pathway for sustainable intensification, ensuring that the gains in crop production are harmonized with environmental conservation, social equity, and the overarching objectives of the Sustainable Development Agenda.

DOI: https//doi.org/10.22452/mjs.vol44no2.9
Malaysian Journal of Science 44(2): 86-103 (June 2025)

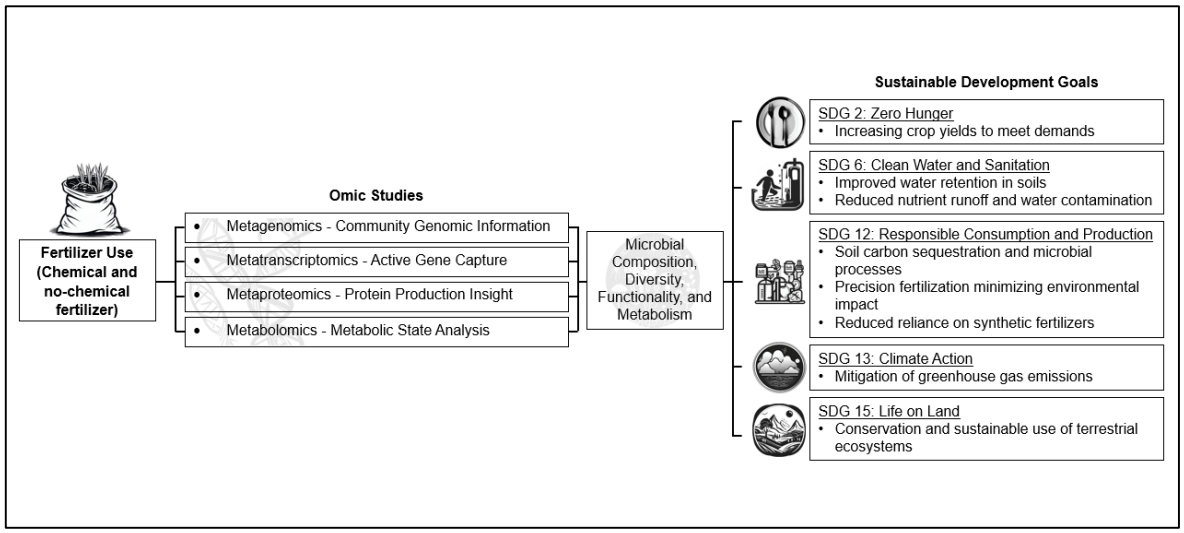

Figure 1. An illustration showing how fertilizer applications and multi-omics studies contribute to the achievement of Sustainable Development Goals

NGS as a Tool for Aligning Agricultural Practices with Sustainability Goals

NGS is a transformative tool that dissects the complex relationships between fertilizers, microbial diversity, and agricultural ecosystems and aligns agricultural practices with the broader canvas of sustainability goals. In the context of the SDGs, NGS acts as a linchpin by providing a comprehensive understanding of microbial communities' responses to different fertilizers and their implications for sustainable agriculture.

NGS offers a holistic view of the soil microbiome, enabling researchers and practitioners to identify microbial signatures associated with sustainable practices. By delineating the impacts of various fertilizers on microbial diversity, NGS facilitates the development of precision fertilization strategies that optimize crop yields efficiently while minimizing environmental harm (Kurzemann et al., 2020; Iqbal et al., 2022; Wyszkowska et al., 2022). This aligns with SDG 12 (Responsible Consumption and Production) by reducing the need for excessive resource consumption, minimizing environmental degradation, and supporting the goal of ensuring sustainable consumption and production patterns for a healthier planet.

Furthermore, NGS-driven insights contribute to achieving SDG 2 (Zero Hunger) by fostering resilient agricultural systems. Better understanding the microbial dynamics in response to fertilizers enables the design of strategies that enhance nutrient availability, improve soil health, and, consequently, increase food security (Kurzemann et al., 2020; Nwachukwu & Babalola, 2022; Arunrat et al., 2023). NGS's capacity to uncover microbial contributions to carbon sequestration (Zhou et al., 2022) aligns with SDG 13 (Climate Action), offering methods to reduce climate change through sustainable agriculture.

Moreover, NGS contributes significantly to the pursuit of SDG 15 (Life on Land) by shedding light on the impact of fertilizers on microbial diversity and its cascading effects on terrestrial ecosystems. The ability of NGS to uncover the intricate relationships between microbial communities and the surrounding environment enables a nuanced understanding of the role of these microorganisms in promoting biodiversity and ecosystem resilience (Wang & Xiong, 2022; Meng et al., 2023; Xu et al., 2023b). This aligns with the broader objective of conserving land ecosystems, restoration, and sustainable use (Küfeoğlu, 2022). Through soil analysis, NGS helps farmers boost agricultural productivity and support ecosystem health. Integrating NGS data into land management strategies preserves biodiversity, prevents soil degradation, and promotes species coexistence. NGS is a powerful tool aligning agriculture with sustainability goals by understanding fertilizer-microbe interactions, enabling precision agriculture for enhanced productivity, environmental protection, and fulfillment of SDGs.

Addressing Global Challenges Through a Microbial Perspective

Embracing a microbial perspective in agriculture is pivotal for addressing the multifaceted global challenges outlined in the SDGs. Using NGS to explore soil microorganisms presents an unprecedented opportunity to address global challenges by gaining insights into their effects on soil health and ecosystem resilience. Agriculture gains a tool for fostering sustainable practices that simultaneously enhance productivity and mitigate environmental impact from the lens of microbial diversity. The microbial perspective contributes directly to SDG 15 (Life on Land) by emphasizing terrestrial ecosystems' conservation and sustainable use (Kumawat et al., 2023; Li et al., 2023b). Besides that, climate change-induced abiotic stresses exacerbate agricultural challenges, particularly when compounded by chemical fertilizer application, which degrades soil health (Wijitkosum, 2018; Azahari & Sukarman, 2023). Nonetheless, leveraging beneficial microorganisms presents a sustainable solution, aligning with SDG 15 by fostering soil resilience and enhancing plant stress tolerance, thus promoting sustainable agricultural practices in the face of climate change.

DOI: https//doi.org/10.22452/mjs.vol44no2.9
Malaysian Journal of Science 44(2): 86-103 (June 2025)

Understanding and optimizing microbial communities through precision fertilization strategies aligns with SDG 12 (Responsible Consumption and Production), optimizing the application of fertilizers to enhance plant growth while minimizing environmental impact. Precision fertilization leverages microbial processes, such as nitrogen fixation, to make nutrients available to plants, thereby reducing the reliance on synthetic fertilizers (Shi et al., 2021; Lin et al., 2021). This aligns with responsible consumption and production, lowering the environmental footprint of chemical input production and use.

Moreover, a microbial perspective offers innovative solutions to combat climate change (SDG 13). Microorganisms contribute to combating climate change by enhancing soil fertility and structure through the breakdown of organic matter and storing carbon in the soil as a natural sink (Kozjek et al., 2023). Additionally, certain microbes, such as methanotrophic bacteria, play a crucial role in converting methane, a potent greenhouse gas, into less harmful byproducts, aiding in the reduction of overall greenhouse gas emissions (He et al., 2023). The understanding and harnessing microbial processes offer innovative solutions for managing greenhouse gas dynamics, contributing to global efforts to mitigate climate change (Hussain et al., 2022). Harnessing NGS technologies to decipher the microbial contributions to climate mitigation provides a pathway for agriculture to address global climate challenges proactively. By acknowledging the central role of microorganisms in the intricate balance of agroecosystems, the global community can forge a path toward achieving the broader aspirations of the Sustainable Development Agenda.

6. Challenges and Future Directions

Current Limitations in NGS-Based Studies

While NGS has revolutionized our understanding of microbial dynamics in response to fertilizers, several challenges persist in NGS-based studies. One notable limitation is the sheer volume and complexity of generated data (Larson et al., 2023). The extensive datasets produced by NGS technologies present storage, processing, and analysis challenges, demanding sophisticated computational infrastructure and expertise (Larson et al., 2023). This computational bottleneck poses challenges for researchers, particularly those with limited access to high-performance computing resources.

Additionally, the inherent biases and errors introduced during the sequencing process can impact the accuracy and reliability of results. Amplification biases, sequencing errors, and variations in bioinformatics pipelines may contribute to artifacts in the data, necessitating stringent quality control measures (Beckers et al., 2017; Notario et al., 2023). Addressing these technical challenges is vital to ensure the fidelity of NGS-generated information and to foster confidence in the conclusions drawn from such studies. The interpretability of NGS data remains a challenge. As our knowledge of microbial functions and interactions expands, so does the complexity of interpreting the functional implications of microbial diversity changes revealed by NGS (Toole et al., 2021). Integrating multi-omics data and advancing bioinformatics tools are essential for unraveling the functional significance of microbial shifts, thereby bridging the gap between taxonomic identification and ecological understanding.

In addition to technical challenges, issues related to standardization and comparability across studies pose hurdles in NGS-based agricultural microbiome research. The lack of standardized protocols for sample collection, DNA extraction, and data analysis can lead to variations in results, reducing the comparability of findings across other related studies (Serrano-Silva & Calderon-Ezquerro, 2018; Malczynski et al., 2021). Establishing a set of best practices and guidelines for NGS-based studies in agricultural microbiome research would enhance the consistency and reliability of results (Forry et al., 2023; Hiergeist et al., 2023). Collaborative efforts within the scientific community to develop and adopt standardized methodologies will build a more robust foundation for interpreting and synthesizing insights from diverse studies (Biswas et al., 2023). By addressing technical and standardization challenges, NGS can more effectively contribute to advancing our understanding of microbial responses to fertilizers and supporting the development of sustainable agricultural practices.

As NGS continues to be at the forefront of agricultural microbiome research, addressing these limitations will be pivotal for maximizing the technology's potential and ensuring that insights gained contribute meaningfully to developing sustainable agricultural practices. The ongoing refinement of methodologies, improvement in computational tools, and collaborative efforts across scientific disciplines will shape the future directions of NGS-based studies in unraveling the intricate relationships between fertilizers and microbial communities.

Potential Technological Advancements and Methodological Improvements

The future of NGS studies in agricultural microbiome research holds promise with anticipated technological advancements and methodological innovations. One area ripe for improvement is the enhancement of sequencing technologies themselves. Ongoing efforts to increase read lengths, reduce error rates, and elevate sequencing throughput will alleviate existing challenges in data generation (Callahan et al., 2021; Zhou et al., 2021), making NGS studies more accessible and cost-effective for a broader range of research endeavors. Long-read sequencing platforms like Oxford Nanopore and PacBio offer longer read lengths than traditional short-read platforms (Cook et al., 2024). Error correction tools such as Nanocorr and Canu help improve the accuracy of long-read data (Hu et al., 2020; Marić et al., 2024). For hybrid assembly pipelines, tools such as Unicycler and St. Petersburg Genome Assembler (SPAdes) combine long-read and short-read data for more accurate assemblies (Latorre-Pérez et al., 2020; Xu et al., 2022).

Moreover, the integration of multi-omics approaches is poised to refine our understanding of microbial responses to fertilizers. Coupling metagenomics with meta-transcriptomics, meta-proteomics, and metabolomics can provide a comprehensive view of microbial functions, shedding light on the dynamic interplay between microbial communities and their environment

DOI: https//doi.org/10.22452/mjs.vol44no2.9
Malaysian Journal of Science 44(2): 86-103 (June 2025)

(Yamazaki et al., 2021; Qiu et al., 2023; Yang et al., 2023b). Moreover, integrating metagenomic and metatranscriptomic analyses using NGS has allowed researchers to move beyond taxonomic identification and understand the functional consequences of chemical fertilizer applications at the molecular level. Metagenomic studies reveal the complete genetic makeup of microbial communities, exposing the genes and pathways involved in important ecological processes. In contrast, metatranscriptomics captures actively expressed genes, offering insights into the functional dynamics of microbial communities (Qian et al., 2020). These advanced analyses have revealed shifts in gene expression associated with nutrient uptake, stress response, and the synthesis of secondary metabolites (Chevrette et al., 2022; Law et al., 2022; Tartaglia et al., 2023). Identifying specific functional genes involved in these processes enhances our ability to predict and manage the ecological outcomes of chemical fertilizer use.

The integration between metagenomics and metabolomics also provides a comprehensive understanding of microbial functionality by revealing both the taxonomic composition of microbial communities and insights into the actual biochemical processes and metabolites. Zhao et al. (2023) demonstrates that long-term fertilization enhances soil quality by promoting the growth of beneficial bacteria and fungi and releasing essential compounds to support plant growth and maintain overall productivity. Additionally, Tian et al. (2023) found that mulching reduces NO3−-N content and influences specific genes (nxrA and nasA), accelerating microbial metabolism and stimulating the production of various metabolites linked to key biological processes. The P-fertilizer application resulted in a decrease in the diversity of bacterial and fungal genes in the soil. The fertilizer also affected the soil metabolite spectrum, notably influencing seven primary metabolic pathways related to amino acids, plant hormones, and secondary metabolites (Cheng et al., 2022). Integrating metagenomic and metabolomic approaches is crucial for developing sustainable fertilization strategies that optimize nutrient use, minimize environmental impact, and foster a resilient soil microbiome, translating microbial diversity data into actionable insights for sustainable agriculture.

Advancements in bioinformatics tools will play a pivotal role in overcoming current data analysis and interpretation limitations. Machine learning algorithms, for instance, have the potential to discern complex patterns within large and intricate datasets, facilitating more accurate taxonomic assignments and functional predictions (Lee et al., 2022; Zhang et al., 2022b; Cheng et al., 2023). Additionally, user-friendly pipelines that streamline data processing and enhance accessibility will democratize the use of NGS technologies, enabling researchers with diverse backgrounds to leverage these powerful tools.

As technology continues to evolve, the integration of advanced studies, like NGS commonly used in medicine, along with other emerging technologies such as high-resolution imaging and remote sensing (Wang et al., 2020; Zhang et al., 2020; Wei et al., 2023b), holds promise for gaining a more holistic understanding of agroecosystems. These multidisciplinary approaches will enable researchers to explore microbial dynamics at various scales, from the microscopic to the field-level, fostering a more nuanced comprehension of the intricate relationships between fertilizers, microbial communities, and sustainable agricultural practices.

The Importance of Interdisciplinary Collaboration for Comprehensive Insights

Addressing the complex challenges and unlocking the full potential of NGS in agricultural microbiome research requires a concerted effort in interdisciplinary collaboration (Chiusano, 2015). Integrating expertise from diverse fields such as microbiology, agronomy, bioinformatics, and data science is imperative for advancing our understanding of the relationships between fertilizers and microbial communities.

Microbial responses to fertilizers unfold within the broader context of agroecosystems, encompassing soil health, plant-microbe interactions, and environmental sustainability. An interdisciplinary approach ensures that researchers can navigate this complexity, drawing on various disciplines' insights to interpret NGS-generated data comprehensively. Microbiologists contribute their knowledge of microbial ecology, agronomists provide insights into crop-specific needs, and bioinformaticians bring essential tools for processing and analyzing large-scale genomic datasets.

Furthermore, collaboration between academia, industry, and policy-making entities is essential to bridge the gap between research findings and real-world applications (John et al., 2023). Industry professionals can offer practical insights into the scalability and feasibility of implementing NGS-informed strategies in diverse agricultural settings. Policymakers play a crucial role in translating research into actionable guidelines that promote sustainable and microbiome-conscious agricultural practices on a broader scale.

The challenges NGS studies face in agricultural microbiome research are multifaceted, and their resolution demands a collective effort. By fostering a culture of interdisciplinary collaboration, researchers can harness the strengths of different fields, enriching the depth and applicability of insights gained from NGS technologies. As we look to the future, synergy between diverse disciplines will be pivotal for overcoming challenges and realizing the full potential of NGS in shaping the sustainable future of agriculture.

4. Conclusion

In the journey through the nexus of fertilizers, microbial communities, and sustainable agriculture, this review has unveiled findings elucidated by NGS. NGS studies have provided unprecedented insights into the dynamic relationships between chemical and non-chemical fertilizers, soil types, crop specificity, and microbial diversity. Through comprehensive analyses, researchers have deciphered fertilizer applications' taxonomic and functional implications, offering a deeper understanding of agroecosystem dynamics. These insights underscore the pivotal role of microbial diversity in shaping resilient and sustainable

DOI: https//doi.org/10.22452/mjs.vol44no2.9
Malaysian Journal of Science 44(2): 86-103 (June 2025)

agricultural systems.

The potential impact of NGS on reshaping agricultural practices cannot be overstated. The depth and precision of information provided by NGS technologies empower farmers, researchers, and policymakers to make informed decisions that balance productivity with environmental and social considerations. NGS lays the foundation for a paradigm shift in agriculture from precision fertilization strategies tailored to specific soil types and crops to the development of microbiome-conscious agricultural policies. The technology's capacity to uncover microbial functions, predict ecosystem responses, and guide sustainable practices positions NGS as a transformative force with far-reaching implications for the future of global agriculture.

As we stand at the cusp of agricultural innovation, a resounding call to action echoes from the insights gained through NGS studies. It is incumbent upon the global community, including farmers, researchers, policymakers, and industry stakeholders, to embrace sustainable and microbiome-conscious agricultural practices. Leveraging the knowledge derived from NGS, we can design and implement strategies that enhance crop yields and prioritize soil health, biodiversity conservation, and climate resilience. This call to action implores us to bridge the gap between scientific knowledge and practical application, fostering a holistic approach that aligns with the principles of the SDGs. Through collaborative efforts, informed decision-making, and a commitment to stewardship of our agroecosystems, we could shape a productive but also sustainable, resilient, and harmonious agricultural future with the microbial world beneath our feet.

5. References

AbdelRahman, M. A., Metwaly, M. M., Afifi, A. A., D'Antonio, P., & Scopa, A. (2022). Assessment of soil fertility status under soil degradation rate using geomatics in West Nile Delta. *Land*, *11*(8), 1256. https://doi.org/10.3390/land11081256

Abid, M., Wu, J., Seyedsalehi, M., Hu, Y. Y., & Tian, G. (2021). Novel insights of impacts of solid content on high solid anaerobic digestion of cow manure: Kinetics and microbial community dynamics. *Bioresource Technology*, *333*, 125205. https://doi.org/10.1016/j.biortech.2021.125205

Adhikari, M., Kim, S. W., Kim, H. S., Kim, K. Y., Park, H. B., Kim, K. J., & Lee, Y. S. (2021). Bacterial Community and Diversity from the Watermelon Cultivated Soils through Next Generation Sequencing Approach. *The Plant Pathology Journal*, *37*(6), 521. https://doi.org/10.5423%2FPPJ.OA.07.2021.0106

Arunrat, N., Sereenonchai, S., Sansupa, C., Kongsurakan, P., & Hatano, R. (2023). Effect of Rice Straw and Stubble Burning on Soil Physicochemical Properties and Bacterial Communities in Central Thailand. *Biology*, *12*(4), 501. https://doi.org/10.3390/biology12040501

Ashraf, M. F., Hou, D., Hussain, Q., Imran, M., Pei, J., Ali, M., Shehzad, A., Anwar, M., Noman, A., Waseem, M., & Lin, X. (2022). Entailing the next-generation sequencing and metabolome for sustainable agriculture by improving plant tolerance. *International Journal of Molecular Sciences*, *23*(2), 651. https://doi.org/10.3390/ijms23020651

Azahari, D. H. (2023, September). Impact of chemical fertilizer on soil fertility of oil palm plantations in relation to productivity and environment. In *IOP Conference Series: Earth and Environmental Science* (Vol. 1243, No. 1, p. 012020). IOP Publishing. https://doi.org/10.1088/1755-1315/1243/1/012020

Azarbad, H., Tremblay, J., Bainard, L. D., & Yergeau, E. (2022). Relative and quantitative rhizosphere microbiome profiling results in distinct abundance patterns. *Frontiers in Microbiology*, *12*, 798023. https://doi.org/10.3389/fmicb.2021.798023

Azeem, M., Sun, D., Crowley, D., Hayat, R., Hussain, Q., Ali, A., Tahir, M. I., Jeyasundar, P. G. S. A., Rinklebe, J., & Zhang, Z. (2020). Crop types have stronger effects on soil microbial communities and functionalities than biochar or fertilizer during two cycles of legume-cereal rotations of dry land. *Science of The Total Environment, 715*, 136958. https://doi.org/10.1016/j.scitotenv.2020.136958

Bai, Y. C., Chang, Y. Y., Hussain, M., Lu, B., Zhang, J. P., Song, X. B., Lei, X. S., & Pei, D. (2020). Soil chemical and microbiological properties are changed by long-term chemical fertilizers that limit ecosystem functioning. *Microorganisms*, *8*(5), 694. https://doi.org/10.3390/microorganisms8050694

Beckers, M., Mohorianu, I., Stocks, M., Applegate, C., Dalmay, T., & Moulton, V. (2017). Comprehensive processing of high-throughput small RNA sequencing data including quality checking, normalization, and differential expression analysis using the UEA sRNA Workbench. *RNA*, *23*(6), 823-835. https://doi.org/10.1261/rna.059360.116

Biswas, A., Kumari, A., Gaikwad, D. S., & Pandey, D. K. (2023). Revolutionizing Biological Science: The Synergy of Genomics in Health, Bioinformatics, Agriculture, and Artificial Intelligence. OMICS: *A Journal of Integrative Biology, 27*(12), 550-569. https://doi.org/10.1089/omi.2023.0197

Bokulich, N. A., & Mills, D. A. (2012). Next-generation approaches to the microbial ecology of food fermentations. *BMB Reports*, *45*(7), 377-389. http://dx.doi.org/10.5483/BMBRep.2012.45.7.148

Callahan, B. J., Grinevich, D., Thakur, S., Balamotis, M. A., & Yehezkel, T. B. (2021). Ultra-accurate microbial amplicon sequencing with synthetic long reads. *Microbiome*, *9*(1), 1-13. https://doi.org/10.1186/s40168-021-01072-3

DOI: https//doi.org/10.22452/mjs.vol44no2.9
Malaysian Journal of Science 44(2): 86-103 (June 2025)

Caracciolo, A. B., Grenni, P., Ciccoli, R., Di Landa, G., & Cremisini, C. (2005). Simazine biodegradation in soil: analysis of bacterial community structure by in situ hybridization. *Pest Management Science: formerly Pesticide Science, 61*(9), 863-869. https://doi.org/10.1002/ps.1096

Carrascosa, A., Pascual, J. A., López-García, Á., Romo-Vaquero, M., De Santiago, A., Ros, M., Petropoulos, S. A., & Alguacil, M. D. M. (2023). Effects of inorganic and compost tea fertilizers application on the taxonomic and functional microbial diversity of the purslane rhizosphere. *Frontiers in Plant Science, 14*, 1159823. https://doi.org/10.3389/fpls.2023.1159823

Castellano-Hinojosa, A., Albrecht, U., & Strauss, S. L. (2023). Interactions between rootstocks and compost influence the active rhizosphere bacterial communities in citrus. *Microbiome, 11*(1), 1-16. https://doi.org/10.1186/s40168-023-01524-y

Chamberlain, L. A., Bolton, M. L., Cox, M. S., Suen, G., Conley, S. P., & Ane, J. M. (2020). Crop rotation, but not cover crops, influenced soil bacterial community composition in a corn-soybean system in southern Wisconsin. *Applied Soil Ecology, 154*, 103603. https://doi.org/10.1016/j.apsoil.2020.103603

Chaudhary, D. K., Khulan, A., & Kim, J. (2019). Development of a novel cultivation technique for uncultured soil bacteria. *Scientific Reports*, *9*(1), 6666. https://doi.org/10.1038/s41598-019-43182-x

Chen, M., Zhang, S., Liu, L., & Ding, X. (2023). Influence of organic fertilization on clay mineral transformation and soil phosphorous retention: Evidence from an 8-year fertilization experiment. *Soil and Tillage Research*, *230*, 105702. https://doi.org/10.1016/j.still.2023.105702

Cheng, H., Yuan, M., Tang, L., Shen, Y., Yu, Q., & Li, S. (2022). Integrated microbiology and metabolomics analysis reveal responses of soil microorganisms and metabolic functions to phosphorus fertilizer on semiarid farm. *Science of the Total Environment, 817*, 152878. https://doi.org/10.1016/j.scitotenv.2021.152878

Cheng, Z., Zheng, Q., Shi, J., He, Y., Yang, X., Huang, X., Wu, L., & Xu, J. (2023). Metagenomic and machine learning-aided identification of biomarkers driving distinctive Cd accumulation features in the root-associated microbiome of two rice cultivars. *ISME Communications*, *3*(1), 14. https://doi.org/10.1038/s43705-023-00213-z

Chevrette, M. G., Thomas, C. S., Hurley, A., Rosario-Meléndez, N., Sankaran, K., Tu, Y., Hall, A., Magesh, S., & Handelsman, J. (2022). Microbiome composition modulates secondary metabolism in a multispecies bacterial community. *Proceedings of the National Academy of Sciences, 119*(42), e2212930119. https://doi.org/10.1073/pnas.2212930119

Chiusano, M. L. (2015). On the multifaceted aspects of bioinformatics in the next generation era: the run that must keep the quality. *Next Generation: Sequencing & Applications*, *2*, e106. http://dx.doi.org/10.4172/jngsa.1000e106

Chouhan, A., Kushwaha, E. M., & Mahalakshmi, P. (2023). 7 AGRICULTURE BIOINFORMATICS IN THE AGE OF NEXT-GENERATION SEQUENCING. *Applications of Environmental Biotechnology for Global Sustainability*, 51.

Chuckran, P. F., Fofanov, V., Hungate, B. A., Morrissey, E. M., Schwartz, E., Walkup, J., & Dijkstra, P. (2021). Rapid response of nitrogen cycling gene transcription to labile carbon amendments in a soil microbial community. *MSystems, 6*(3), e00161-21. https://doi.org/10.1128/msystems.00161-21

Cook, R., Brown, N., Rihtman, B., Michniewski, S., Redgwell, T., Clokie, M., Stekel, D. J., Chen, Y., Scanlan, D. J., Hobman, J. L., Nelson, A., Jones, M. A., Smith, D., & Millard, A. (2024). The long and short of it: benchmarking viromics using Illumina, Nanopore and PacBio sequencing technologies. *Microbial Genomics, 10*(2), 001198. https://doi.org/10.1099/mgen.0.001198

de Vries, J., Saleem, F., Li, E., Chan, A. W. Y., Naphtali, J., Naphtali, P., Paschos, A., & Schellhorn, H. E. (2023). Comparative Analysis of Metagenomic (Amplicon and Shotgun) DNA Sequencing to Characterize Microbial Communities in Household On-Site Wastewater Treatment Systems. *Water*, *15*(2), 271. https://doi.org/10.3390/w15020271

Deinert, L., Ikoyi, I., Egeter, B., Forrestal, P., & Schmalenberger, A. (2023). Short-Term Impact of Recycling-Derived Fertilizers on Their P Supply for Perennial Ryegrass (*Lolium perenne*). *Plants, 12*(15), 2762. https://doi.org/10.3390/plants12152762

Dincă, L. C., Grenni, P., Onet, C., & Onet, A. (2022). Fertilization and soil microbial community: a review. *Applied Sciences*, *12*(3), 1198. https://doi.org/10.3390/app12031198

Doni, L., Martinez-Urtaza, J., & Vezzulli, L. (2023). Searching pathogenic bacteria in the rare biosphere of the ocean. *Current Opinion in Biotechnology*, *80*, 102894. https://doi.org/10.1016/j.copbio.2023.102894

Dubey, P. K., Singh, A., Chaurasia, R., Pandey, K. K., Bundela, A. K., Dubey, R. K., & Abhilash, P. C. (2021). Planet friendly agriculture: Farming for people and the planet. *Current Research in Environmental Sustainability, 3*, 100041. https://doi.org/10.1016/j.crsust.2021.100041

Ehau-Taumaunu, H., & Hockett, K. L. (2023). Passaging phyllosphere microbial communities develop suppression towards bacterial speck disease in tomato. *Phytobiomes*

DOI: https//doi.org/10.22452/mjs.vol44no2.9
Malaysian Journal of Science 44(2): 86-103 (June 2025)

Journal, 7(2), 233-243. https://doi.org/10.1094/PBIOMES-05-22-0030-FI

Enebe, M. C., & Babalola, O. O. (2021). The influence of soil fertilization on the distribution and diversity of phosphorus cycling genes and microbes community of maize rhizosphere using shotgun metagenomics. *Genes, 12*(7), 1022. https://doi.org/10.3390/genes12071022

Fadiji, A. E., Ayangbenro, A. S., & Babalola, O. O. (2020). Organic farming enhances the diversity and community structure of endophytic archaea and fungi in maize plant: A shotgun approach. *Journal of Soil Science and Plant Nutrition, 20*, 2587-2599. https://doi.org/10.1007/s42729-020-00324-9

Feng, Q., Cao, S., Liao, S., Wassie, M., Sun, X., Chen, L., & Xie, Y. (2023). *Fusarium equiseti*-inoculation altered rhizosphere soil microbial community, potentially driving perennial ryegrass growth and salt tolerance. *Science of The Total Environment*, *871*, 162153. https://doi.org/10.1016/j.scitotenv.2023.162153

Feng, Y., Delgado-Baquerizo, M., Zhu, Y., Han, X., Han, X., Xin, X., Li, W., Guo, Z., Dang, T., Li, C., Zhu, B., Cai, Z., Li, D., & Zhang, J. (2022). Responses of soil bacterial diversity to fertilization are driven by local environmental context across China. *Engineering*, *12*, 164-170. https://doi.org/10.1016/j.eng.2021.09.012

Fierer, N., Lauber, C. L., Ramirez, K. S., Zaneveld, J., Bradford, M. A., & Knight, R. (2012). Comparative metagenomic, phylogenetic and physiological analyses of soil microbial communities across nitrogen gradients. *The ISME Journal*, *6*(5), 1007-1017. https://doi.org/10.1038/ismej.2011.159

Forry, S. P., Servetas, S. L., Kralj, J. G., Soh, K., Hadjithomas, M., Cano, R., Carlin, M., de Amorim, M. G., Auch, B., Bakker, M. G., Bartelli, T. F., Bustamante, J. P., Cassol, I., Chalita, M., Dias-Neto, E., Del Duca, A., Gohl, D. M., Kazantseva, J., Haruna, M. T., Menzel, P., Moda, B. S., Neuberger-Castillo, L., Nunes, D. N., Patel, I. R., Peralta, R. D., Saliou, A., Schwarzer, R., Sevilla, S., Takenaka, I. K. T. M., Wang, J. R., Knight, R., Gevers, D., & Jackson, S. A. (2023). Variability and Bias in Microbiome Metagenomic Sequencing: an Interlaboratory Study Comparing Experimental Protocols. *bioRxiv*, 2023-04. https://doi.org/10.1101/2023.04.28.538741

Greay, T. L., Evasco, K. L., Evans, M. L., Oskam, C. L., Magni, P. A., Ryan, U. M., & Irwin, P. J. (2021). Illuminating the bacterial microbiome of Australian ticks with 16S and Rickettsia-specific next-generation sequencing. *Current Research in Parasitology & Vector-Borne Diseases, 1,* 100037. https://doi.org/10.1016/j.crpvbd.2021.100037

Gupta, A., Singh, U. B., Sahu, P. K., Paul, S., Kumar, A., Malviya, D., Singh, S., Kuppusamy, P., Singh, P., Paul, D., Rai, J. P., Singh, H. V., Manna, M. C., Crusberg, T. C., Kumar, A., & Saxena, A. K. (2022). Linking soil microbial diversity to modern agriculture practices: A review. *International Journal of Environmental Research and Public Health*, *19*(5), 3141. https://doi.org/10.3390/ijerph19053141

He, Z., Shen, J., Zhu, Y., Feng, J., & Pan, X. (2023). Enhanced anaerobic oxidation of methane with the coexistence of iron oxides and sulfate fertilizer in paddy soil. *Chemosphere*, *329*, 138623. https://doi.org/10.1016/j.chemosphere.2023.138623

Heidkamp, R. A., Piwoz, E., Gillespie, S., Keats, E. C., D'Alimonte, M. R., Menon, P., Das, J. K., Flory, A., Clift, J. W., Ruel, M. T., Vosti, S., Akuoku, J. K., Bhutta, Z. A. (2021). Mobilising evidence, data, and resources to achieve global maternal and child undernutrition targets and the Sustainable Development Goals: an agenda for action. *The Lancet*, *397*(10282), 1400-1418. https://doi.org/10.1016/S0140-6736(21)00568-7

Hiergeist, A., Ruelle, J., Emler, S., & Gessner, A. (2023). Reliability of species detection in 16S microbiome analysis: Comparison of five widely used pipelines and recommendations for a more standardized approach. *PLoS One, 18*(2), e0280870. https://doi.org/10.1371/journal.pone.0280870

Hiiesalu, I., Öpik, M., Metsis, M., Lilje, L., Davison, J., Vasar, M., Moora, M., Zobel, M., Wilson, S. D., & Pärtel, M. (2012). Plant species richness belowground: higher richness and new patterns revealed by next-generation sequencing. *Molecular Ecology, 21*(8), 2004-2016. https://doi.org/10.1111/j.1365-294X.2011.05390.x

Hong, S., Yuan, X., Yang, J., Yang, Y., Jv, H., Li, R., Jia, Z., & Ruan, Y. (2023). Selection of rhizosphere communities of diverse rotation crops reveals unique core microbiome associated with reduced banana *Fusarium* wilt disease. *New Phytologist*, *5*(238), 2194-2209. https://doi.org/10.1111/nph.18816

Hu, X., Gu, H., Liu, J., Wei, D., Zhu, P., Zhou, B., Chen, X., Jin, J., Liu, X., & Wang, G. (2022a). Metagenomics reveals divergent functional profiles of soil carbon and nitrogen cycling under long-term addition of chemical and organic fertilizers in the black soil region. *Geoderma, 418*, 115846. https://doi.org/10.1016/j.geoderma.2022.115846

Hu, X., Gu, H., Liu, J., Zhou, B., Wei, D., Chen, X., & Wang, G. (2022b). High variation of fungal communities and associated potential plant pathogens induced by long-term addition of N fertilizers rather than P, K fertilizers: A case study in a Mollisol field. *Soil Ecology Letters, 4*(4), 348-361. https://doi.org/10.1007/s42832-021-0120-4

DOI: https//doi.org/10.22452/mjs.vol44no2.9
Malaysian Journal of Science 44(2): 86-103 (June 2025)

Hu, Y., Fang, L., Nicholson, C., & Wang, K. (2020). Implications of error-prone long-read whole-genome shotgun sequencing on characterizing reference microbiomes. *IScience, 23*(6). https://doi.org/10.1016/j.isci.2020.101223

Hua, L. Q., Yang, S. Q., Xia, Z. F., & Zeng, H. (2023). Application of *Sophora alopecuroides* organic fertilizer changes the rhizosphere microbial community structure of melon plants and increases the fruit sugar content. *Journal of the Science of Food and Agriculture, 103*(1), 164-175. https://doi.org/10.1002/jsfa.12126

Hussain, M. M., Farooqi, Z. U. R., Rasheed, F., & Din, W. M. U. (2022). Role of microorganisms as climate engineers: Mitigation and adaptations to climate change. In *Climate Change and Microbes* (pp. 1-24). Apple Academic Press.

Inubushi, K., & Acquaye, S. (2004). Role of microbial biomass in biogeochemical processes in paddy soil environments. *Soil Science and Plant Nutrition*, *50*(6), 793-805. https://doi.org/10.1080/00380768.2004.10408539

Iqbal, A., He, L., Ali, I., Yuan, P., Khan, A., Hua, Z., Wei, S., & Jiang, L. (2022). Partial substation of organic fertilizer with chemical fertilizer improves soil biochemical attributes, rice yields, and restores bacterial community diversity in a paddy field. *Frontiers in Plant Science*, *13*, 895230. https://doi.org/10.3389/fpls.2022.895230

Iqbal, A., Tang, X., Ali, I., Yuan, P., Khan, R., Khan, Z., Adnan, M., Wei, S., & Jiang, L. (2023). Integrating low levels of organic fertilizer improves soil fertility and rice yields in paddy fields by influencing microbial communities without increasing CH_4 emissions. *Applied Soil Ecology*, *189*, 104951. https://doi.org/10.1016/j.apsoil.2023.104951

Ishfaq, M., Wang, Y., Xu, J., Hassan, M. U., Yuan, H., Liu, L., He, B., Ejaz, I., White, P. J., Cakmak, I., Chen, W.-S., Wu, J., van der Werf, W., Li, C., Zhang, F., & Li, X. (2023). Improvement of nutritional quality of food crops with fertilizer: a global meta-analysis. *Agronomy for Sustainable Development*, *43*(6), 74. https://doi.org/10.1007/s13593-023-00923-7

Jiang, Z., Yang, S., Pang, Q., Xu, Y., Chen, X., Sun, X., Qi, S., & Yu, W. (2021). Biochar improved soil health and mitigated greenhouse gas emission from controlled irrigation paddy field: Insights into microbial diversity. *Journal of Cleaner Production*, *318*, 128595. https://doi.org/10.1016/j.jclepro.2021.128595

John, T., Cordova, K. E., Jackson, C. T., Hernández-Mondragón, A. C., Davids, B. L., Raheja, L., Milić, J. V., & Borges, J. (2023). Engaging Early-Career Scientists in Global Policy-Making. *Angewandte Chemie International Edition*, *62*(34), e202217841. https://doi.org/10.1002/anie.202217841

Kallenbach, C., & Grandy, A. S. (2011). Controls over soil microbial biomass responses to carbon amendments in agricultural systems: A meta-analysis. *Agriculture, Ecosystems & Environment*, *144*(1), 241-252. https://doi.org/10.1016/j.agee.2011.08.020

Khatri, S., Dubey, S., Shivay, Y. S., Jelsbak, L., & Sharma, S. (2023). Organic farming induces changes in bacterial community and disease suppressiveness against fungal phytopathogens. *Applied Soil Ecology, 181*, 104658. https://doi.org/10.1016/j.apsoil.2022.104658

Kim, H., Park, Y. H., Yang, J. E., Kim, H. S., Kim, S. C., Oh, E. J., Moon, J., Cho, W., Shin, W., & Yu, C. (2022). Analysis of major bacteria and diversity of surface soil to discover biomarkers related to soil health. *Toxics*, *10*(3), 117. https://doi.org/10.3390/toxics10030117

Kozjek, K., Manoharan, L., Urich, T., Ahrén, D., & Hedlund, K. (2023). Microbial gene activity in straw residue amendments reveals carbon sequestration mechanisms in agricultural soils. *Soil Biology and Biochemistry, 179,* 108994. https://doi.org/10.1016/j.soilbio.2023.108994

Küfeoğlu, S. (2022). SDG-15: Life on Land. In *Emerging Technologies: Value Creation for Sustainable Development* (pp. 469-486). Cham: Springer International Publishing. https://doi.org/10.1007/978-3-031-07127-0_17

Kumawat, A., Yadav, D., Srivastava, P., Babu, S., Kumar, D., Singh, D., Vishwakarma, D. K., Sharma, V. K., & Madhu, M. (2023). Restoration of agroecosystems with conservation agriculture for food security to achieve sustainable development goals. *Land Degradation & Development, 11,* 34, 3079-3097. https://doi.org/10.1002/ldr.4677

Kurzemann, F. R., Plieger, U., Probst, M., Spiegel, H., Sandén, T., Ros, M., & Insam, H. (2020). Long-term fertilization affects soil microbiota, improves yield and benefits soil. *Agronomy*, *10*(11), 1664. https://doi.org/10.3390/agronomy10111664

Lafaille, N. (2017, January). The development of fertilizer from the early years to today©. In *Proceedings of the 2017 Annual Meeting of the International Plant Propagators' Society 1212* (pp. 213-216). https://doi.org/10.21273/HORTTECH.15.1.0024

Larson, N. B., Oberg, A. L., Adjei, A. A., & Wang, L. (2023). A clinician's guide to bioinformatics for next-generation sequencing. *Journal of Thoracic Oncology*, *18*(2), 143-157. https://doi.org/10.1016/j.jtho.2022.11.006

Latorre-Pérez, A., Villalba-Bermell, P., Pascual, J., & Vilanova, C. (2020). Assembly methods for nanopore-based metagenomic

DOI: https//doi.org/10.22452/mjs.vol44no2.9
Malaysian Journal of Science 44(2): 86-103 (June 2025)

sequencing: a comparative study. *Scientific Reports, 10*(1), 13588. https://doi.org/10.1038/s41598-020-70491-3

Law, S. R., Serrano, A. R., Daguerre, Y., Sundh, J., Schneider, A. N., Stangl, Z. R., Castro, D., Grabherr, M., Näsholm, T., Street, N. R., & Hurry, V. (2022). Metatranscriptomics captures dynamic shifts in mycorrhizal coordination in boreal forests. Proceedings of the National Academy of Sciences, 119(26), e2118852119. https://doi.org/10.1073/pnas.2118852119

Lee, J., Jo, N. Y., Shim, S. Y., Linh, L. T. Y., Kim, S. R., Lee, M. G., & Hwang, S. G. (2023). Effects of Hanwoo (Korean cattle) manure as organic fertilizer on plant growth, feed quality, and soil bacterial community. *Frontiers in Plant Science, 14*, 1135947. https://doi.org/10.3389/fpls.2023.1135947

Lee, J.-Y., Mitchell, H. D., Burnet, M. C., Wu, R., Jenson, S. C., Merkley, E. D., Nakayasu, E. S., Nicora, C. D., Jansson, J. K., Burnum-Johnson, K. E., & Payne, S. H. (2022). Uncovering hidden members and functions of the soil microbiome using de *novo* metaproteomics. *Journal of Proteome Research*, *21*(8), 2023-2035. https://doi.org/10.1021/acs.jproteome.2c00334

Li, N., Sheng, K., Zheng, Q., Hu, D., Zhang, L., Wang, J., & Zhang, W. (2023a). Inoculation with phosphate-solubilizing bacteria alters microbial community and activates soil phosphorus supply to promote maize growth. *Land Degradation & Development*, *34*(3), 777-788. https://doi.org/10.1002/ldr.4494

Li, T., Li, R., Cao, Y., Tao, C., Deng, X., Ou, Y., Liu, H., Shen, Z., & Shen, Q. (2022b). Soil antibiotic abatement associates with the manipulation of soil microbiome via long-term fertilizer application. *Journal of Hazardous Materials, 439*, 129704. https://doi.org/10.1016/j.jhazmat.2022.129704

Li, T., Zhang, Y., He, B., Wu, X., & Du, Y. (2022a). Nitrate loss by runoff in response to rainfall amount category and different combinations of fertilization and cultivation in sloping croplands. *Agricultural Water Management*, *273*, 107916. https://doi.org/10.1016/j.agwat.2022.107916

Li, W. X., Wang, C., Zheng, M. M., Cai, Z. J., Wang, B. R., & Shen, R. F. (2020a). Fertilization strategies affect soil properties and abundance of N-cycling functional genes in an acidic agricultural soil. *Applied Soil Ecology*, *156*, 103704. https://doi.org/10.1016/j.apsoil.2020.103704

Li, Y., Wang, C., Wang, T., Liu, Y., Jia, S., Gao, Y., & Liu, S. (2020b). Effects of different fertilizer treatments on rhizosphere soil microbiome composition and functions. *Land, 9*(9), 329. https://doi.org/10.3390/land9090329

Li, Y., Wang, C., Wu, J., Zhang, Y., Li, Q., Liu, S., & Gao, Y. (2023b). The Effects of Localized Plant–Soil–Microbe Interactions on Soil Nitrogen Cycle in Maize Rhizosphere Soil under Long-Term Fertilizers. *Agronomy*, *13*(8), 2114. https://doi.org/10.3390/agronomy13082114

Lin, Y., Ye, G., Luo, J., Di, H. J., Lindsey, S., Fan, J., Liu, D., & Ding, W. (2021). Long-term organic fertilization regulates the abundance of major nitrogen-cycling-related genes in aggregates from an acidic Ultisol. *Applied Soil Ecology*, *165*, 104014. https://doi.org/10.1016/j.apsoil.2021.104014

Liu, K. L., Han, T. F., Huang, J., Asad, S., Li, D. M., Yu, X. C., Huang, Q. H., Ye, H. C., Hu, H. W., Hu, Z. H., & Zhang, H. M. (2020). Links between potassium of soil aggregates and pH levels in acidic soils under long-term fertilization regimes. *Soil and Tillage Research*, *197*, 104480. https://doi.org/10.1016/j.still.2019.104480

Liu, Y. X., Qin, Y., Chen, T., Lu, M., Qian, X., Guo, X., & Bai, Y. (2021a). A practical guide to amplicon and metagenomic analysis of microbiome data. *Protein & Cell*, *12*(5), 315-330. https://doi.org/10.1007/s13238-020-00724-8

Liu, Y., Lv, Z., Hou, H., Lan, X., Ji, J., & Liu, X. (2021b). Long-term effects of combination of organic and inorganic fertilizer on soil properties and microorganisms in a Quaternary Red Clay. *Plos One*, *16*(12), e0261387. https://doi.org/10.1371/journal.pone.0261387

Liu, Z., Chen, R., Wang, J., Liu, J., Li, M., Lin, X., & Hu, J. (2022). Long-term moderate carbon input benefited arbuscular mycorrhizal fungal community diversity and vitality in a sandy loam soil. *Ecological Indicators*, *136*, 108679. https://doi.org/10.1016/j.ecolind.2022.108679

Lu, Y., Cong, P., Kuang, S., Tang, L., Li, Y., Dong, J., & Song, W. (2022). Long-term excessive application of K2SO4 fertilizer alters bacterial community and functional pathway of tobacco-planting soil. *Frontiers in Plant Science, 13*, 1005303. https://doi.org/10.3389/fpls.2022.1005303

Ma, X., Zhou, Z., Chen, J., Xu, H., Ma, S., Dippold, M. A., & Kuzyakov, Y. (2023). Long-term nitrogen and phosphorus fertilization reveals that phosphorus limitation shapes the microbial community composition and functions in tropical montane forest soil. *Science of the Total Environment*, *854*, 158709. https://doi.org/10.1016/j.scitotenv.2022.158709

Ma, Y., Zhang, H., Wang, D., Guo, X., Yang, T., Xiang, X., Walder, F., & Chu, H. (2021). Differential responses of arbuscular mycorrhizal fungal communities to long-term fertilization in the wheat rhizosphere and root endosphere. *Applied and Environmental Microbiology, 87*(17), e00349-21. https://doi.org/10.1128/AEM.00349-21

Malczynski, M., Zhu, A., Zembower, T., & Qi, C. (2021). Diagnostic performance of Ion 16S metagenomics kit and Ion reporter

DOI: https//doi.org/10.22452/mjs.vol44no2.9
Malaysian Journal of Science 44(2): 86-103 (June 2025)

metagenomics workflow for bacterial pathogen detection in culture-negative clinical specimens from sterile sources. *Diagnostic Microbiology and Infectious Disease, 101*(2), 115451. https://doi.org/10.1016/j.diagmicrobio.2021.115451

Malewski, T., Borowik, P., Olejarski, I., Rutkiewicz, A., Okorski, A., & Oszako, T. (2023). Addition of Organic Matter to Pine Plantations on Agricultural Land Positively Alters the Mycobiome of Agricultural Soils. *Applied Sciences, 13*(9), 5800. https://doi.org/10.3390/app13095800

Maretto, L., Deb, S., Ravi, S., Della Lucia, M. C., Borella, M., Campagna, G., Squartini, A., Concheri, G., Nardi, S., & Stevanato, P. (2023). 16S metabarcoding, total soil DNA content, and functional bacterial genes quantification to characterize soils under long-term organic and conventional farming systems. *Chemical and Biological Technologies in Agriculture*, *10*(1), 78. https://doi.org/10.1186/s40538-023-00450-3

Marić, J., Križanović, K., Riondet, S., Nagarajan, N., & Šikić, M. (2024). Comparative analysis of metagenomic classifiers for long-read sequencing datasets. *BMC Bioinformatics, 25*(1), 15. https://doi.org/10.1186/s12859-024-05634-8

Martello, F., dos Santos, J. S., Silva-Neto, C. M., Cássia-Silva, C., Siqueira, K. N., de Ataíde, M. V. R., Ribeiro, M. C., & Collevatti, R. G. (2023). Landscape structure shapes the diversity of plant reproductive traits in agricultural landscapes in the Brazilian Cerrado. *Agriculture, Ecosystems & Environment*, *341*, 108216. https://doi.org/10.1016/j.agee.2022.108216

May, A., Coelho, L. F., Pedrinho, A., Batista, B. D., Mendes, L. W., Mendes, R., Morandi, M. A. B., Barth, G., Viana, R. S., & Vilela, E. S. D. (2023). The use of indigenous bacterial community as inoculant for plant growth promotion in soybean cultivation. *Archives of Agronomy and Soil Science*, *69*(1), 135-150. https://doi.org/10.1080/03650340.2021.1964017

Mendes, L. W., Raaijmakers, J. M., De Hollander, M., Sepo, E., Gómez Expósito, R., Chiorato, A. F., Mendes, R., Tsai, S. M., & Carrión, V. J. (2023). Impact of the fungal pathogen *Fusarium oxysporum* on the taxonomic and functional diversity of the common bean root microbiome. *Environmental Microbiome, 18*(1), 68. https://doi.org/10.1186/s40793-023-00524-7

Meng, H., Wang, S., Zhang, J., Wang, X., Qiu, C., & Hong, J. (2023). Effects of coal-derived compound fertilizers on soil bacterial community structure in coal mining subsidence areas. *Frontiers in Microbiology, 14*, 1187572. https://doi.org/10.3389/fmicb.2023.1187572

Menzies Pluer, E. G., Schneider, R. L., Morreale, S. J., Liebig, M. A., Li, J., Li, C. X., & Walter, M. T. (2020). Returning degraded soils to productivity: an examination of the potential of coarse woody amendments for improved water retention and nutrient holding capacity. *Water, Air, & Soil Pollution, 231*, 1-14. https://doi.org/10.1007/s11270-019-4380-x

Meunier, R., & Bayır, S. (2021). Metagenomics approaches in microbial ecology and research for sustainable agriculture. *TATuP-Zeitschrift Für Technikfolgenabschätzung in Theorie Und Praxis*, *30*(2), 24-29. https://doi.org/10.14512/tatup.30.2.24

Mukherjee, A., & Reddy, M. S. (2020). Metatranscriptomics: an approach for retrieving novel eukaryotic genes from polluted and related environments. *3 Biotech, 10*(2), 71. https://doi.org/10.1007/s13205-020-2057-1

Mukhles, M. B., Rahman, M. M., Rana, M. R., Huda, N., Ferdous, J., Rahman, F., Rafi, M. H., & Biswas, S. K. (2022). Effect of pesticides on nitrification activity and its interaction with chemical fertilizer and manure in long-term paddy soils. *Chemosphere, 304,* 135379. https://doi.org/10.1016/j.chemosphere.2022.135379

Mustafa, G., Hayat, N., & Alotaibi, B. A. (2023). How and why to prevent over fertilization to get sustainable crop production. In *Sustainable Plant Nutrition* (pp. 339-354). Academic Press. https://doi.org/10.1016/B978-0-443-18675-2.00019-5

Nguyen, S. H., Nguyen, D. N., Nguyen Thu, N., Pham, H. H., Phan, H. A., & Dao, C. D. (2023). Current Soil Degradation Assessment in the Thua Thien Hue Province, Vietnam, by Multi-Criteria Analysis and GIS Technology. *Sustainability, 15*(19), 14276. https://doi.org/10.3390/su151914276

Notario, E., Visci, G., Fosso, B., Gissi, C., Tanaskovic, N., Rescigno, M., Marzano, M., & Pesole, G. (2023). Amplicon-Based Microbiome Profiling: From Second-to Third-Generation Sequencing for Higher Taxonomic Resolution. *Genes*, *14*(8), 1567. https://doi.org/10.3390/genes14081567

Nwachukwu, B. C., & Babalola, O. O. (2022). Metagenomics: A tool for exploring key microbiome with the potentials for improving sustainable agriculture. *Frontiers in Sustainable Food Systems, 6,* 886987. https://doi.org/10.3389/fsufs.2022.886987

Özbolat, O., Sánchez-Navarro, V., Zornoza, R., Egea-Cortines, M., Cuartero, J., Ros, M., Pascual, J. A., Boix-Fayos, C., Almagro, M., de Vente, J., Díaz-Pereira, E., & Martínez-Mena, M. (2023). Long-term adoption of reduced tillage and green manure improves soil physicochemical properties and increases the abundance of beneficial bacteria in a Mediterranean rainfed almond orchard. *Geoderma, 429*, 116218. https://doi.org/10.1016/j.geoderma.2022.116218

Pande, P. M., Azarbad, H., Tremblay, J., St-Arnaud, M., & Yergeau, E. (2023). Metatranscriptomic response of the wheat holobiont

DOI: https//doi.org/10.22452/mjs.vol44no2.9
Malaysian Journal of Science 44(2): 86-103 (June 2025)

to decreasing soil water content. *ISME Communications, 3*(1), 30. https://doi.org/10.1038/s43705-023-00235-7

Ponge, J. F. (2015). The soil as an ecosystem. *Biology and Fertility of Soils*, *51*, 645-648. https://doi.org/10.1007/s00374-015-1016-1

Poveda, J. (2022). Effect of volatile and non-volatile metabolites from *Leptosphaeria maculans* on tomato calli under abiotic stresses. *Plant Stress, 3*, 100054. https://doi.org/10.1016/j.stress.2021.100054

Qaisrani, M. M., Zaheer, A., Mirza, M. S., Naqqash, T., Qaisrani, T. B., Hanif, M. K., Rasool, G., Malik, K. A., Ullah, S., Jamal, M. S., Mirza, Z., Karim, S., & Rasool, M. (2019). A comparative study of bacterial diversity based on culturable and culture-independent techniques in the rhizosphere of maize (*Zea mays* L.). *Saudi Journal of Biological Sciences*, *26*(7), 1344-1351. https://doi.org/10.1016/j.sjbs.2019.03.010

Qian, X. B., Chen, T., Xu, Y. P., Chen, L., Sun, F. X., Lu, M. P., & Liu, Y. X. (2020). A guide to human microbiome research: study design, sample collection, and bioinformatics analysis. *Chinese Medical Journal, 133*(15), 1844-1855.

Qiu, Q., Xiang, D., Li, Q., Wang, H., Wan, Y., Wu, Q., Ye, X., Jiang, L., Fan, Y., Liu, B., Liu, Y., Li, H., & Liu, C. (2023). Interkingdom multi-omics analysis reveals the effects of nitrogen application on growth and rhizosphere microbial community of Tartary buckwheat. *Frontiers in Microbiology*, *14*. https://doi.org/10.3389%2Ffmicb.2023.1240029

Russel, D. A., & Williams, G. G. (1977). History of chemical fertilizer development. *Soil Science Society of America Journal*, *41*(2), 260-265. https://doi.org/10.2136/sssaj1977.03615995004100020020x

Saqib, M., Yasin, R., & Akhtar, J. (2020). Inorganic Fertilizers: Necessity to Achieve Global Zero Hunger Target. *Zero Hunger*, 414-424. https://doi.org/10.1007/978-3-319-95675-6_29

Saunders, O. E., Fortuna, A. M., Harrison, J. H., Cogger, C. G., Whitefield, E., & Green, T. (2012). Gaseous nitrogen and bacterial responses to raw and digested dairy manure applications in incubated soil. *Environmental Science & Technology*, *46*(21), 11684-11692. https://doi.org/10.1021/es301754s

Semenov, M. V., Krasnov, G. S., Semenov, V. M., & van Bruggen, A. H. (2020). Long-term fertilization rather than plant species shapes rhizosphere and bulk soil prokaryotic communities in agroecosystems. *Applied Soil Ecology, 154*, 103641. https://doi.org/10.1016/j.apsoil.2020.103641

Serrano-Silva, N., & Calderon-Ezquerro, M. C. (2018). Metagenomic survey of bacterial diversity in the atmosphere of Mexico City using different sampling methods. *Environmental Pollution, 235*, 20-29. https://doi.org/10.1016/j.envpol.2017.12.035

Sessou, P., Keisam, S., Gagara, M., Komagbe, G., Farougou, S., Mahillon, J., & Jeyaram, K. (2023). Comparative analyses of the bacterial communities present in the spontaneously fermented milk products of Northeast India and West Africa. *Frontiers in Microbiology, 14.* https://doi.org/10.3389%2Ffmicb.2023.1166518

Shahmohamadloo, R. S., Febria, C. M., Fraser, E. D., & Sibley, P. K. (2022). The sustainable agriculture imperative: A perspective on the need for an agrosystem approach to meet the United Nations Sustainable Development Goals by 2030. *Integrated Environmental Assessment and Management, 18*(5), 1199-1205. https://doi.org/10.1002/ieam.4558

Sharma, L. K., Zaeen, A., & Bali, S. (2022). Growing potatoes. In L. K. Sharma, A. Zaeen, & S. Bali (Eds.), *Insect Pests of Potato (Second Edition): Global Perspectives on Biology and Management* (pp. 7-14). Insect Pests of Potato. https://doi.org/10.1016/B978-0-12-821237-0.00025-1

Shen, F., Yang, L., Zhang, L., Guo, M., Huang, H., & Zhou, C. (2023). Quantifying the direct effects of long-term dynamic land use intensity on vegetation change and its interacted effects with economic development and climate change in Jiangsu, China. *Journal of Environmental Management*, *325*, 116562. https://doi.org/10.1016/j.jenvman.2022.116562

Shi, W., Zhao, H. Y., Chen, Y., Wang, J. S., Han, B., Li, C. P., Lu, J. Y., & Zhang, L. M. (2021). Organic manure rather than phosphorus fertilization primarily determined asymbiotic nitrogen fixation rate and the stability of diazotrophic community in an upland red soil. *Agriculture, Ecosystems & Environment*, *319*, 107535. https://doi.org/10.1016/j.agee.2021.107535

Tang, S., Ma, Q., Marsden, K. A., Chadwick, D. R., Luo, Y., Kuzyakov, Y., Wu, L., & Jones, D. L. (2023). Microbial community succession in soil is mainly driven by carbon and nitrogen contents rather than phosphorus and sulphur contents. *Soil Biology and Biochemistry*, *180*, 109019. https://doi.org/10.1016/j.soilbio.2023.109019

Tang, T., Sun, X., Liu, Q., Dong, Y., & Zha, M. (2023). Treatment with organic manure inoculated with a biocontrol agent induces soil bacterial communities to inhibit tomato *Fusarium* wilt disease. *Frontiers in Microbiology, 13*, 1006878. https://doi.org/10.3389/fmicb.2022.1006878

Tartaglia, M., Ranauda, M. A., Falzarano, A., Maisto, M., Postiglione, A., Prigioniero, A., Scarano, P., Zuzolo, D., Sciarrillo, R., & Guarino, C. (2023). Metatranscriptomics of pastures under drought stress show a rhizospheric meta-organism reshape.

DOI: https//doi.org/10.22452/mjs.vol44no2.9
Malaysian Journal of Science 44(2): 86-103 (June 2025)

Rhizosphere, 26, 100687. https://doi.org/10.1016/j.rhisph.2023.100687

Taş, N., de Jong, A. E., Li, Y., Trubl, G., Xue, Y., & Dove, N. C. (2021). Metagenomic tools in microbial ecology research. *Current Opinion in Biotechnology, 67*, 184-191. https://doi.org/10.1016/j.copbio.2021.01.019

Thompson Jr, W. R. (1992). Importance of water solubility in phosphate fertilizers. In *Proceedings of the Annual Meeting Fertilizer Industry Round Table (USA)*.

Tian, L., Zhang, F., Zhang, L., Gao, X., & Feng, B. (2023). Use of metagenomics and metabolomics to quantify changes in rhizosphere soil microbial function in response to mulching regimes. *Land Degradation & Development, 34*(10), 3033-3048. https://doi.org/10.1002/ldr.4666

Toole, D. R., Zhao, J., Martens-Habbena, W., & Strauss, S. L. (2021). Bacterial functional prediction tools detect but underestimate metabolic diversity compared to shotgun metagenomics in southwest Florida soils. *Applied Soil Ecology*, *168*, 104129. https://doi.org/10.1016/j.apsoil.2021.104129

United Nations. (2023). Sustainable Development Goals Report 2023. United Nations. Retrieved January 7, 2024, from https://sdgs.un.org/goals

Verma, B. C., Pramanik, P., & Bhaduri, D. (2020). Organic fertilizers for sustainable soil and environmental management. *Nutrient Dynamics for Sustainable Crop Production*, 289-313. https://doi.org/10.1007/978-981-13-8660-2_10

Wang, B., Wang, X., Wang, Z., Zhu, K., & Wu, W. (2023). Comparative metagenomic analysis reveals rhizosphere microbial community composition and functions help protect grapevines against salt stress. *Frontiers in Microbiology*, *14*, 1102547. https://doi.org/10.3389/fmicb.2023.1102547

Wang, L., & Xiong, X. (2022). Long-Term Organic Manure Application Alters Urease Activity and Ureolytic Microflora Structure in Agricultural Soils. *Agronomy, 12*(12), 3018. https://doi.org/10.3390/agronomy12123018

Wang, S., Ai, J., Cui, P., Zhu, Y., Wu, H., & Zhang, W. (2020). Diagnostic value and clinical application of next-generation sequencing for infections in immunosuppressed patients with corticosteroid therapy. *Annals of Translational Medicine*, *8*(5), 227. https://doi.org/10.21037%2Fatm.2020.01.30

Wang, W., Yang, S., Zhang, A., & Yang, Z. (2021). Synthesis of a slow-release fertilizer composite derived from waste straw that improves water retention and agricultural yield. *Science of the Total Environment, 768*, 144978. https://doi.org/10.1016/j.scitotenv.2021.144978

Wang, Z. J., Yue, F. J., Wang, Y. C., Qin, C. Q., Ding, H., Xue, L. L., & Li, S. L. (2022). The effect of heavy rainfall events on nitrogen patterns in agricultural surface and underground streams and the implications for karst water quality protection. *Agricultural Water Management*, *266*, 107600. https://doi.org/10.1016/j.agwat.2022.107600

Wei, W., Cao, J., Wu, X. C., Cheng, L. P., Shen, X. N., Sha, W., & Sun, Q. (2023b). Diagnostic performance of metagenomic next-generation sequencing in non-tuberculous mycobacterial pulmonary disease when applied to clinical practice. *Infection*, *51*(2), 397-405. https://doi.org/10.1007/s15010-022-01890-z

Wei, Z., Sixi, Z., Xiuqing, Y., Guodong, X., Baichun, W., & Baojing, G. (2023a). Arbuscular mycorrhizal fungi alter rhizosphere bacterial community characteristics to improve Cr tolerance of Acorus calamus. *Ecotoxicology and Environmental Safety*, *253*, 114652. https://doi.org/10.1016/j.ecoenv.2023.114652

Wenhui, Z., Zucong, C., Lichu, Y., & He, Z. (2007). Effects of the long-term application of inorganic fertilizers on microbial community diversity in rice-planting red soil as studied by using PCR-DGGE. *Acta Ecologica Sinica*, *27*(10), 4011-4018. https://doi.org/10.1016/S1872-2032(07)60084-5

Wijitkosum, S. (2018). Fuzzy AHP for drought risk assessment in Lam Ta Kong watershed, the north-eastern region of Thailand. *Soil and Water Research, 13*(4), 218-225. https://doi.org/10.17221/158/2017-swr

Williams, A., Birt, H. W., Raghavendra, A., & Dennis, P. G. (2023). Cropping system diversification influences soil microbial diversity in subtropical dryland farming systems. *Microbial Ecology*, *85*(4), 1473-1484. https://doi.org/10.1007/s00248-022-02074-w

Windisch, S., Sommermann, L., Babin, D., Chowdhury, S. P., Grosch, R., Moradtalab, N., Walker, F., Höglinger, B., El-Hasan, A., Armbruster, W., Nesme, J., Sørensen, S. J., Schellenberg, I., Geistlinger, J., Smalla, K., Rothballer, M., Ludewig, U., & Neumann, G. (2021). Impact of long-term organic and mineral fertilization on rhizosphere metabolites, root–microbial interactions and plant health of lettuce. *Frontiers in Microbiology*, *11*, 597745. https://doi.org/10.3389/fmicb.2020.597745

Wolsing, M., & Priemé, A. (2004). Observation of high seasonal variation in community structure of denitrifying bacteria in arable soil receiving artificial fertilizer and cattle manure by determining T-RFLP of *nir* gene fragments. *FEMS Microbiology Ecology*, *48*(2), 261-271. https://doi.org/10.1016/j.femsec.2004.02.002

Woo, S. L., De Filippis, F., Zotti, M., Vandenberg, A., Hucl, P., & Bonanomi, G. (2022). Pea-wheat rotation affects soil microbiota

DOI: https//doi.org/10.22452/mjs.vol44no2.9
Malaysian Journal of Science 44(2): 86-103 (June 2025)

diversity, community structure, and soilborne pathogens. *Microorganisms, 10*(2), 370. https://doi.org/10.3390/microorganisms10020370

Wyszkowska, J., Borowik, A., & Kucharski, J. (2022). The role of grass compost and *Zea Mays* in alleviating toxic effects of tetracycline on the soil bacteria community. *International Journal of Environmental Research and Public Health, 19*(12), 7357. https://doi.org/10.3390/ijerph19127357

Xiang, L., Harindintwali, J. D., Wang, F., Bian, Y., Zhao, Z., Wang, Z., Wang, Y., Mei, Z., Jiang, X., Schaffer, A., & Xing, B. (2023). Manure-and straw-derived biochars reduce the ecological risk of PBDE and promote nitrogen cycling by shaping microbiomes in PBDE-contaminated soil. *Chemosphere*, *312*, 137262. https://doi.org/10.1016/j.chemosphere.2022.137262

Xu, G., Zhang, L., Liu, X., Guan, F., Xu, Y., Yue, H., Huang, J.-Q., Chen, J., Wu, N., & Tian, J. (2022). Combined assembly of long and short sequencing reads improve the efficiency of exploring the soil metagenome. *BMC Genomics, 23*(1), 37. https://doi.org/10.1186/s12864-021-08260-3

Xu, J., Si, L., Zhang, X., Cao, K., & Wang, J. (2023b). Various green manure-fertilizer combinations affect the soil microbial community and function in immature red soil. *Frontiers in Microbiology*, 14. https://doi.org/10.3389%2Ffmicb.2023.1255056

Xu, P., Gao, Y., Cui, Z., Wu, B., Yan, B., Wang, Y., Wen, M., Wang, H., Ma, X., & Wen, Z. (2023a). Application of Organic Fertilizers Optimizes Water Consumption Characteristics and Improves Seed Yield of Oilseed Flax in Semi-Arid Areas of the Loess Plateau. *Agronomy, 13*(7), 1755. https://doi.org/10.3390/agronomy13071755

Yamazaki, S., Mardani-korrani, H., Kaida, R., Ochiai, K., Kobayashi, M., Nagano, A. J., Fujii, Y., Sugiyama, A., & Aoki, Y. (2021). Field multi-omics analysis reveals a close association between bacterial communities and mineral properties in the soybean rhizosphere. *Scientific Reports*, *11*(1), 8878. https://doi.org/10.1038/s41598-021-87384-8

Yang, J., He, J., Jia, L., & Gu, H. (2023b). Integrating metagenomics and metabolomics to study the response of microbiota in black soil degradation. *Science of The Total Environment*, *899*, 165486. https://doi.org/10.1016/j.scitotenv.2023.165486

Yang, K., Wang, X., Hou, R., Lu, C., Fan, Z., Li, J., Wang, S., Xu, Y., Shen, Q., Friman, V. P., & Wei, Z. (2023a). Rhizosphere phage communities drive soil suppressiveness to bacterial wilt disease. *Microbiome*, *11*(1), 1-18. https://doi.org/10.1186/s40168-023-01463-8

Yu, H., Ling, N., Wang, T., Zhu, C., Wang, Y., Wang, S., & Gao, Q. (2019). Responses of soil biological traits and bacterial communities to nitrogen fertilization mediate maize yields across three soil types. *Soil and Tillage Research*, *185*, 61-69. https://doi.org/10.1016/j.still.2018.08.017

Zhang, C., Zhao, X., Liang, A., Li, Y., Song, Q., Li, X., Li, D., & Hou, N. (2023a). Insight into the soil aggregate-mediated restoration mechanism of degraded black soil via biochar addition: Emphasizing the driving role of core microbial communities and nutrient cycling. *Environmental Research, 228,* 115895. https://doi.org/10.1016/j.envres.2023.115895

Zhang, H., Luo, G., Wang, Y., Fei, J., Xiangmin, R., Peng, J., Tian, C., & Zhang, Y. (2023b). Crop rotation-driven change in physicochemical properties regulates microbial diversity, dominant components, and community complexity in paddy soils. *Agriculture, Ecosystems & Environment, 343*, 108278. https://doi.org/10.1016/j.agee.2022.108278

Zhang, H., Wang, X., Li, Y., & Ding, W. (2022a). Effect of long-term fertilization on bacterial community in a sandy loam soil and its relation to organic carbon accumulation. In *E3S Web of Conferences* (Vol. 338, p. 01007). EDP Sciences. https://doi.org/10.1051/e3sconf/202233801007

Zhang, X., Feng, J., Su, X., Lei, Y., Wu, W., & Cheng, X. (2020). Next generation sequencing reveals a synchronous trilateral lung adenocarcinoma case with distinct driver alterations of EGFR 19 deletion or EGFR 20 Insertion or EZR-ROS1 fusion. *OncoTargets and Therapy*, 12667-12671. https://doi.org/10.2147/OTT.S283617

Zhang, Z., Zhang, Q., Cui, H., Li, Y., Xu, N., Lu, T., Chen, J., Penuelas, J., Hu, B., & Qian, H. (2022b). Composition identification and functional verification of bacterial community in disease-suppressive soils by machine learning. *Environmental Microbiology*, *24*(8), 3405-3419. https://doi.org/10.1111/1462-2920.15902

Zhao, G., Wu, K., An, T., Wen, L., Zi, S., Fan, Z., Zhou, F., Ouyang, C., Yang, Y., Wu, B., & Fullen, M. A. (2023). Integrated analysis of changes in soil microbiota and metabolites following long-term fertilization in a subtropical maize-wheat agroecosystem. *Pedosphere, 33*(3), 521-533. https://doi.org/10.1016/j.pedsph.2022.06.055

Zhao, S., Zhang, C., Mu, J., Zhang, H., Yao, W., Ding, X., Ding, J., & Chang, Y. (2020). All-in-one sequencing: An improved library preparation method for cost-effective and high-throughput next-generation sequencing. *Plant Methods*, *16*(1), 1-14. https://doi.org/10.1186/s13007-020-00615-3

Zhao, Y., Rodić, N., Liaskos, M., Assimopoulou, A. N., Lalaymia, I., & Declerck, S. (2024). Effects of fungal endophytes and

DOI: https//doi.org/10.22452/mjs.vol44no2.9
Malaysian Journal of Science 44(2): 86-103 (June 2025)

arbuscular mycorrhizal fungi on growth of *Echium vulgare* and alkannin/shikonin and their derivatives production in roots. *Fungal Biology, 128*(1), 1607-1615. https://doi.org/10.1016/j.funbio.2023.12.004

Zheng, Q., Zhang, S., Liang, J., Chen, Y., & Ye, W. (2023). The Impact of Cultural Memory and Cultural Identity in the Brand Value of Agricultural Heritage: A Moderated Mediation Model. *Behavioral Sciences*, *13*(2), 79. https://doi.org/10.3390/bs13020079

Zhou, W., Kang, L., Duan, H., Qiao, S., Tao, L., Chen, Z., & Huang, Y. (2021). A virtual sequencer reveals the dephasing patterns in error-correction code DNA sequencing. *National Science Review*, *8*(5), nwaa227. https://doi.org/10.1093/nsr/nwaa227

Zhou, Y., Zhang, J., Xu, L., Nadeem, M. Y., Li, W., Jiang, Y., Ding, Y., Liu, Z., & Li, G. (2022). Long-term fertilizer postponing promotes soil organic carbon sequestration in paddy soils by accelerating lignin degradation and increasing microbial necromass. *Soil Biology and Biochemistry*, *175*, 108839. https://doi.org/10.1016/j.soilbio.2022.108839

Zhu, L., Huang, C., Li, W., Wu, W., Tang, Z., Tian, Y., & Xi, B. (2023a). Ammonia assimilation is key for the preservation of nitrogen during industrial-scale composting of chicken manure. *Waste Management, 170*, 50-61. https://doi.org/10.1016/j.wasman.2023.07.028

Zhu, L., Li, W., Huang, C., Tian, Y., & Xi, B. (2023b). Functional redundancy is the key mechanism used by microorganisms for nitrogen and sulfur metabolism during manure composting. *Science of The Total Environment,* 169389. https://doi.org/10.1016/j.scitotenv.2023.169389

DOI: https//doi.org/10.22452/mjs.vol44no2.9
Malaysian Journal of Science 44(2): 86-103 (June 2025)

MALAYSIAN JOURNAL OF SCIENCE
MJS
ISSN 1394-3065

Regular Issue

Malaysian Journal of Science 44 (2): 104-114 (June 2025) https://mjs.um.edu.my

Study on Machinability Issues of Hard to Machining Inconel 718 - A Review

Kishor K Powar[1ag], Anupama N Kallol[2b], Shivakumar S[3c], Manjunath G Avalappa[4d*], Balachandra P[5e] and Nikhil Rangaswamy[6f]

Abstract: In the aerospace and automobile industries, there has been a recent growing demand for tough and heat-resistant materials. Processing these materials is difficult, primarily due to their mechanical properties, which include strong wear resistance, abrasion resistance, and low heat conductivity. This results in short tool lifetimes and high cutting temperatures and forces. Variations in machinability may be brought on by changes in material microstructures brought on by changes in chemical composition, forging methods, casting, and heat treatment. Because of their remarkable greater efficiency and effectiveness, Inconel 718 nickel superalloys are employed in numerous automotive, marine, and aviation applications. In contrast, Inconel 718's poor thermal conductivity and quick strain hardening made fabrication difficult and compromised the surface's machining ability. This study examines Inconel 718 machining problems, and the issue of dry machining and machining with nanofluids, which demonstrates advancements in research on improving surface quality and material removal rate by reviewing the properties of alumina (Al_2O_3)-based nanofluids.

Keywords: *Inconel 718, microstructure, machinability, tool wear, nanofluids.*

1. Introduction

Having an alloy proportion of more than 4%, high-alloy cast irons fall under this category of materials. Low-alloy cast iron, which has a Brinell hardness range of 350–550, is defined as cast iron with less than 4% alloy (HB). High alloy cast iron (450-850 HB) has significantly higher wear, heat, and corrosion resistance compared to unalloyed or Cast iron with low or moderate levels of alloy [1-5]. Nickel, vanadium, molybdenum, chromium, and copper are cast iron alloys most commonly used. Based on the amount of alloy in these materials, they are labelled Ni-Hard, Cr-Hard, etc. With a Rockwell C (HRC) hardness range of 58–65 and wear resistance, Ni-Hard is a high-alloy white cast iron.

Authors information:
[a]Research Scholar, Department of Mechanical Engineering, KLS Gogte Institute of Technology, Visvesvaraya Technological University, Belagavi, 590008, INDIA. E-mail: kishor.powar5570@gmail.com[1]
[b]Department of Mechanical Engineering, K. L. S. Gogte Institute of Technology, Belagavi, 590008, INDIA. E-mail: ankallol@git.edu[2]
[c]School of Management, G M University, Davanagere, 577006, INDIA. E-mail: gitshiva@gmail.com[3]
[d]Department of Mechanical Engineering, K. L. S. Gogte Institute of Technology, Belagavi, 590008, INDIA. E-mail: manjunathga@git.edu[4]
[e]Department of Mathematics, S J B Institute of Technology, Bengaluru, 560060, INDIA. E-mail: balachandrapsjbit@gmail.com[5]
[f]Department of Mechatronics Engineering, School of Mechanical Engineering, REVA University, Bengaluru, 560064, INDIA. E-mail: nikhil.rangaswamy@reva.edu.in[6]
[g]Department of Mechanical Engineering, DKTE Society's Textile and Engineering Institute, Ichalkaranji – 416115, INDIA. E-mail: kishor.powar5570@gmail.com[1]
*Corresponding Author: manjunathga@git.edu

The result of these two factors is the material's resistance to corrosion. It is a nickel-based alloy commonly employed in aerospace applications with heat resistance and exceptional strength. With the alloy's extraordinary hardness and work-hardening properties, Inconel 718 machining is becoming increasingly difficult. Some researchers investigated the machinability of Inconel 718 by studying the effects of cutting conditions.

Cutting Condition

The cutting situations for white cast iron and its results, such as average surface roughness (Ra) and cutting force (Fc), were predicted and optimised using Taguchi's L18 orthogonal array (Ni-Hard). Output factor (Fc and Ra) to select the exact cutting parameters use “smaller-is-better" to evaluate the (Input) signal-to- (output) noise (S/N) ratio for the machining [18,26].

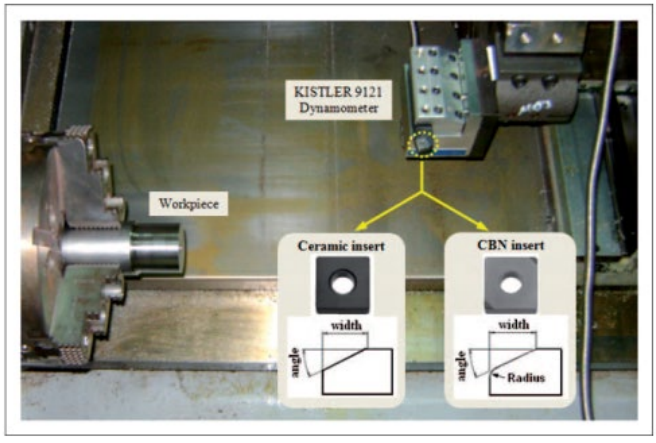

Figure 1. Experimental setup for turning operation of Inconel 718 bar [25]

DOI:https//doi.org/10.22452/mjs.vol44no2.10
Malaysian Journal of Science 44(2): 104-114 (June 2025)

Figure 1 shows the experimental setup for turning the Inconel bar. Multiple researchers introduce various cutting conditions in Fig. 1. The cutting conditions include the Hardness of the workpiece, which is cast and has a hardness of 50 HRC, and after cooling, it has a hardness of 62 HRC. It is also in a vacuum furnace, with a pressure of 3 bar, and the job is tempered for a homogeneous microstructure. This indicates that for experimentation, we must prepare for cutting conditions.

The pineapple is believed to originate from Brazil. Once discovered, the pineapple was imported to Europe. Christopher Columbus and his men are thought to have tasted the pineapple initially. The word pineapple started to be used in English in 1938 which refers to the organs of conifer trees (Jungle Dragon, 2024). The European pioneers named the fruit as a 'pineapple' according to what is known as a pinecone. The term pinecone was first recorded in 1694, that is to supplant the importance of the pineapple (Hoque *et al*., 2019). According to Sun, (2015), the pineapple or *Ananas comosus L. Merr*. is widely accepted to have come from South America, Argentina, and Paraguay. The pineapple is known by the people of South America just before Christopher Columbus arrived in 1493. The European pilgrims use the word pineapple to present the natural product as to have come from pinecones. Meanwhile, the word Ananas is the initial name of the natural product that comes from the word for pine 'nanas' and 'comosus' referring to the tuft of the stem of the natural product (Jungle Dragon, 2024).

Pineapple is a significant nourishment crop which is planted widely in the tropical and sub-tropical regions of the world. It is a significantly produced natural product for business in Malaysia and is, for the most part, utilized as organic ingredients for pastry or to produce canned pineapple as cuts or rings, squeezes, and sticks. There are five assortments of pineapples in Malaysia; these include the Morris, Sarawak, Gandol, Josapine and N36 (Lasekan & Hussein, 2018). Pineapple processing such as canning and juice produces wastes including pineapple peels. Discharge of pineapple peels during this process will produce waste and lead to serious environmental pollution. In artificial practices, pineapple waste is either used as animal feed or disposed to the soil as waste. Natural enzyme contained in pineapple is called bromelain. Bromelain is an enzyme which is believed to have numerous benefits and is veritably promising to the development of food and medicinal diligence. Bromelain can be found in several parts of the pineapple. The specific part from which it is extracted lends its name to the enzyme; thus, we have fruit bromelain and stem bromelain (Bala *et al*., 2012). Bromelain activity has been reported to be within a pH range of 3 to 8 and a temperature range of 30–70 ºC (Kumar *et al*., 2011;Liang *et al*., 2012;Ramli *et al*., 2018). The natural bromelain enzyme has been used as a meat tenderizer, anti-browning agent and in the processing of formulas for babies (Tochi et al., 2008). As a protease, it hydrolyses proteins in these formulas, therefore making amino acids more readily available to babies. Bromelain is utilized in some applications including cosmetic and pharmaceutical and in textile industry as reported by (Aehle, 2007;B.K. Bhattacharrya, 2008;Ataide *et al*., 2018;Sancesario *et al*., 2018).

Some successful methods have been used for bromelain extraction and purification. Purification of enzymes is important to determine the three-dimensional structure of an enzyme and its impact on the functionality of the enzyme (A. Illanes, 2008). The successful methods in bromelain purification include aqueous two phase systems (Ketnawa *et al*., 2010;Ferreira *et al*., 2011), ammonium sulphate precipitation (G & Viswanathan, 2013;Gautam *et al*., 2010), ethanol precipitation (Martins *et al*., 2014), ion exchange chromatography (G & Viswanathan, 2013;Gautam *et al*., 2010; Bresolin *et al*., 2013), membrane separation (Seguí & Fito Maupoey, 2018) and adsorption using functionalized Santa Barbara Acid-15 (Arumugam & Ponnusami, 2013).

The pineapple variety Josapine was chosen because it is abundantly planted in Malaysia which covers about 41.5% or 6725 hectares. This shows that the waste produced by the pineapple industry is large at about 150 000 kg. Other than that, the pineapple variety Josapine was easily obtained and the price was affordable and cheap. Also, the pineapple variety Josapine was suitable for the canning industry (MPIB, 2022). The main reason to select the maturity index 5 and 7 is to determine whether there is a significant difference of bromelain activity among them. As a justification, the maturity index 3 and 4 is not chosen because their difference is too narrow while maturity index 5 is in the middle and maturity index 7 is overripe. Maturity index 1 is too young while maturity index 2 is usually selected for harvesting. Thus, the aim of this study was to determine the bromelain activity, protein content and specific enzyme activity of bromelain extracted from pineapple variety Josapine peel with maturity indices 2, 5 and 7.

2. Materials and Methods

Tool Life

Tool The challenges encountered when machining nickel-based alloys include shorter tool lifespans, low metal removal rates, high cutting pressures, increased power consumption, swarf disposal issues, and reduced metal removal efficiency. It emphasises the importance of CVD and PVD tool coatings in addressing these challenges. The study also examines the quality and consistency achieved through high-speed complex machining of hardened D2 tool steel using PCBN inserts. The research investigates the crystal and electrical structure analysis, micromechanical properties assessment, and resistance to short-term oxidation. Furthermore, it investigates the performance of coated tools in machining hardened H13 tool steel, nickel-based superalloys, and Ti alloys such as TiAl6V4 during ball nose end milling. The study includes tool life measurements with uncoated carbide inserts under varying coolant pressures and environments.

Received: December, 2023
Accepted: May, 2024
Published: June, 2025

DOI:https//doi.org/10.22452/mjs.vol44no2.10
Malaysian Journal of Science 44(2): 104-114 (June 2025)

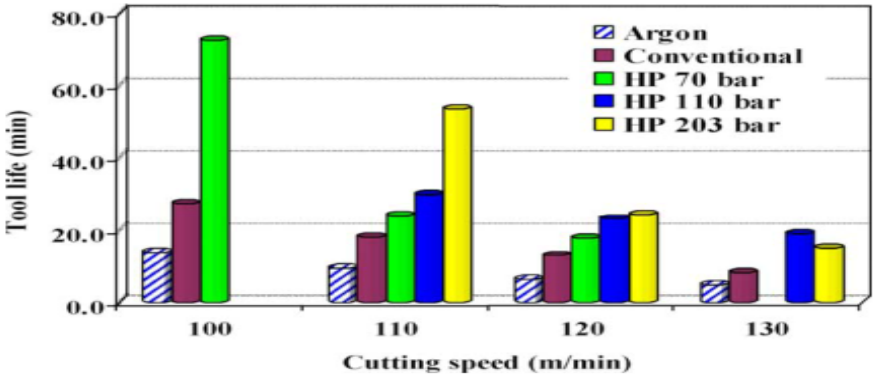

Figure 2a. Tool life Graph for uncoated carbide inserts [31]

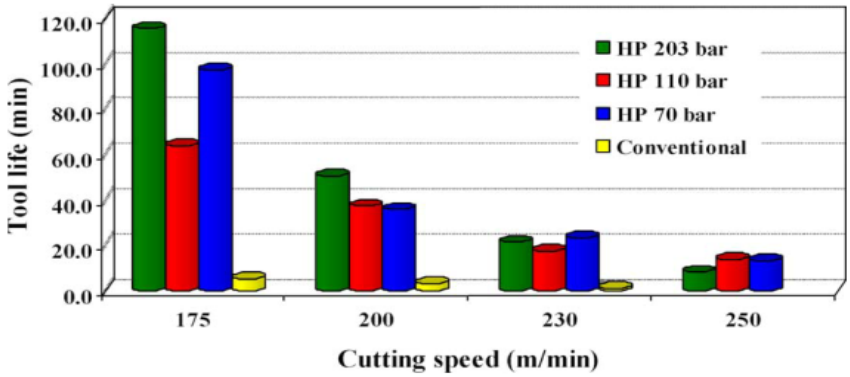

Figure 2b. Tool life Graph for uncoated Polycrystalline tool [31]

Figure 2b Tool life measurements were made when cutting titanium alloy with Polycrystalline diamond inserts and conventional coolant.

Tool wear

The research investigates various types of damage and wear in cutting operations. Different loading scenarios were used to simulate wear reliably in PCBN inserts. Understanding wear mechanisms significantly impacting component quality is essential to improve tool materials, primarily by reducing flank wear rates. It explores high-speed complex machining (HSHM) with hardened D2 tool steel, using PCBN inserts. It also investigates the use of CBN-TiN-coated inserts for turning tough materials. Additionally, it examines the effects of process parameters such as depth of cut, tool feed rate, cutting speed, and cutting pressures on surface finish, tool wear, and machining cost. The study identifies wear processes, including tribochemical reactions, fracture, abrasion, material transfer, and plastic flow, influenced by thermal and mechanical demands on the tool. Additionally, the research assesses the cutting environment's impact on the machinability of Inconel 718, using performance indicators like workpiece surface roughness, insert flank wear, and cutting pressures when utilizing a CNC lathe.

Turning is performed using coated carbide inserts with a standard of K05-K25 and a grade of WNMA 060408. The tool's average burn rate is relatively low at slower cutting speeds since the cutting zone has a low temperature. Faster tool wear-out at high cutting speeds leads to more severe patterns of tool failure, like severe notching. Better tool performance of a coating results from the tool being unable to operate within a particular temperature range. The performance of Inconel 718 with carbide tips was found to be inferior while cutting at a high pace. Due to the integrity of the surface being compromised by high cutting speeds, uncoated carbide tips are recommended over coated tips. Coated tips cannot improve high-speed performance. The tool-life wear diminishes below 250 m/min, and the maximum tool-life is found.

Diffusion loss occurs due to heat when cutting Inconel 718 using carbide tools. Figure 3a illustrates the wear of the tool as observed under the microscope. The measured levels for level 7 consist of a depth of cut of 0.25 mm, a feed rate of 100 mm/min, a spindle speed of 10,000 rpm, and tools with and without coating. Figures 3a and 3b show the tool effect of material loss for both tools (uncoated and coated).

DOI:https//doi.org/10.22452/mjs.vol44no2.10
Malaysian Journal of Science 44(2): 104-114 (June 2025)

Figure 3a. Coated tool b) Uncoated tool [16]

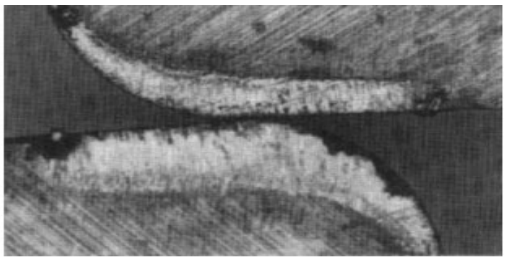

Figure 3b. Worn Tool [16]

The workpiece typically only receives 10% of the heat produced during machining, with the remaining 90% going to the chip and cutting tool. Figure 3a illustrates the coated tool's minimal wear. The induction heat source's radiant and friction heat harm the uncoated tool. The used tool is shown in Figure 3b after being machined. Figure 3c shows that the tool chip contact duration was reduced on the worn inserts' rake faces when cutting with a high-pressure coolant supply. [31]. This impact is displayed in Figure 4.

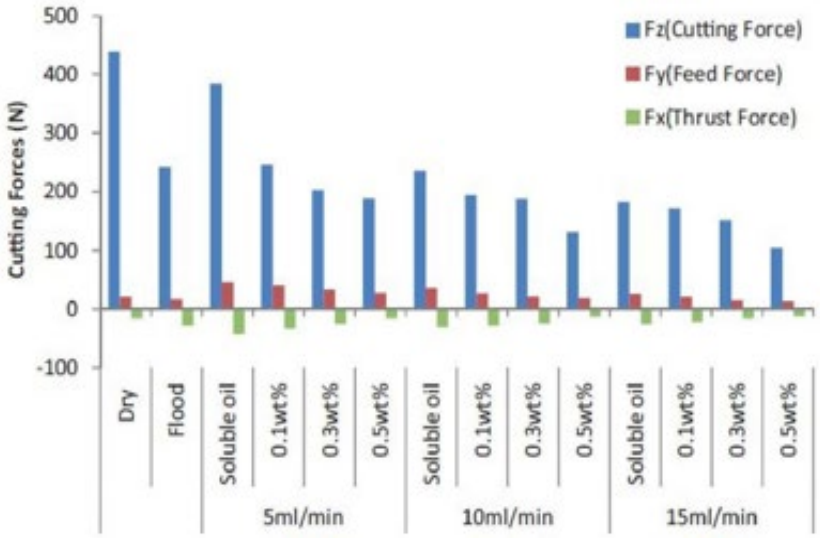

Figure 4. Variation in cutting forces with a cemented carbide tool under changing cutting parameters [3]

This might be the case because when air pressure rises, oil vaporises faster, forming tiny droplets of aerosol that get smaller as air pressure increases. This little aerosol is easy to insert into the tool, providing a low-cost heat-removal interface that reduces tool wear [33]. Tool life in the machining process utilising a CuO-based Nano fluid was investigated by Vazquez et al. By using CuO Nano fluid, the tool's service life was increased by 604%. CuO nanoparticles exhibit an anti-wear property. This results in a lower frictional coefficient caused by rolling action and CuO deposition on worn surfaces [33,34].

Effect of Contact Angle on Tool Wear

Using Al2O3 as a nano fluid, Mathew et al. adjusted the cutting parameters and nanoparticle concentration during the turning of EN8. Speed, feed, depth of cut, and nanoparticle concentration were the process variables used to evaluate surface roughness. Surface roughness was most significantly influenced by feed and nanoparticle concentration, according to analysis of variance (ANOVA) [37]. Several experiments evaluated the performance of the surface roughness of the H3BO3 microfluid and the MoS2 nanofluid in the MQL system while spinning the AISI 1040. They claim that while nano and

DOI:https//doi.org/10.22452/mjs.vol44no2.10
Malaysian Journal of Science 44(2): 104-114 (June 2025)

microfluidic systems function nearly similarly at low speeds, nanofluidic systems outperform microfluidic systems at high speeds due to their superior lubricating and cooling abilities. Compared to H3BO3, MoS2 has a 30% lower surface roughness. This is due to reduced friction and associated effects caused by stable and consistent nanofluid lubrication.

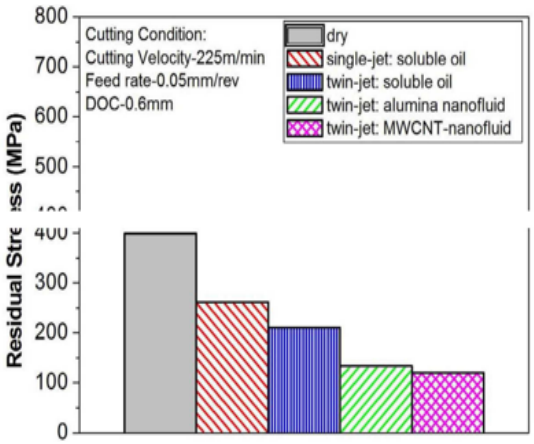

Figure 5. Residual stress on the machine surface under different cutting environments [7]

The researcher examined SiC nanoparticles for EN-24 material with 0.5, 1, and 1.5 weight percent and discovered that 1.5 weight percent SiC nanofluid showed the least surface roughness. This might be due to the cooling effect caused by the 0.5 weight percent SiC nanofluid, which has the maximum thermal conductivity and lowest coefficient of friction. As a result, decreased tool wear and surface roughness were produced [40]. Surface roughness diminishes gradually with increasing air pressure, but it lowers quickly up to 6 bar, according to research by Huang et al. on the MQL system. The creation of tiny droplets of oil aerosol, whose size decreases with rising air pressure, may cause a decrease in surface roughness because the flow rate increases as the air pressure rises. This small aerosol enters the tool with ease thanks to a low-cost interface that removes heat and, as a result, reduces surface roughness [41]. Table 1 provides a thorough analysis of surface roughness.

Table 1. Summary of surface roughness analysis.

Size	Nanoparticle	Process	Proportion	Base fluid	Remark	References
-	Al_2O_3	Turning	0.1,0.5& 1wt. %	Water	By Anova, nanoparticle concentration is the most influential factor, followed by F, S & Doc	36
90 &100	MoS2 & H3 BO3	Turning	0.25 wt %	Coconut Oil	Nanofluid provides 30% less Ra than Microfluid	37
80nm	Graphite	Running	0.3 wt %	Conventional water-soluble oil	For mist application with nanofluid Ra decreased by 42 %, 30 &, and 28% dry cut	35
30-40nm	Graphene	Turning	0,0.2,0.6,1 wt %	90 % water + 5 % servo cut the oil	Ra reduces at a higher % of grapheme in 95 % water, nano fluid with a high 5% servo cutting vel. & lower cutting 50% FR & DOC	36

DOI:https//doi.org/10.22452/mjs.vol44no2.10
Malaysian Journal of Science 44(2): 104-114 (June 2025)

2-50 nm	MWCNT	Turning	0.6 vol %	Cutting oil	12 % improvement was observed in surface roughness	27
< 80 nm	Nano graphite	Turning	0,0.1,0.3, and 0.5 wt% %.	Water	Surface roughness was reduced with increasing nanoparticle concentration.	26
40 nm and 20 nm	CuO and Al_2O_3	Turning	0,0.25,0.5,1 %	Water-based oil	minimum surface roughness	24

Microstructure

Since the initial hardness of parts created using alloy 718 SLM print technology is larger than that made using wrought techniques, post-treatment is necessary to produce the desired conditions and characteristics. As a pre-aging treatment, these post-treatments must assess the effects on microstructure, hardening properties, and microsegregation at 1100 °C or 1250 °C. Printed samples are more complex than solutions composed of heat-treated samples because of the quantity of cooling and heating passes made during manufacturing. At the subgrain boundary, the components and leaves are thoroughly dissolved at 1200 °C for heat treatment. A coarsening effect on the grain was discovered following recrystallization during the solution treatment [27–36]. Figure 4 shows the Inconel 718 microstructure after 21 minutes of machining.

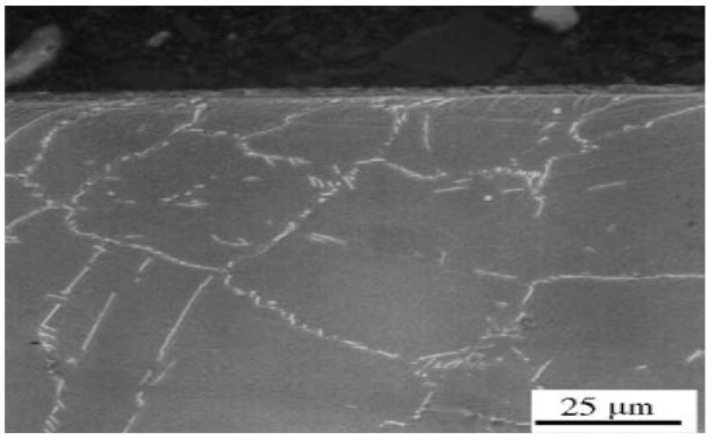

Figure 4. Inconel 718 microstructure following 21 minutes of machining with self-propelled rotary tools [31]

Grain Size

Compared to conventional material, the alloy Inconel 718 made using SLM techniques demonstrated excellent gamma size and diffusion dislocation. Both alloys' microstructures were fine-tuned, and their microhardness was raised due to the superalloy's higher torsion pressure. [21]

Hardness

Poor machinability and shorter tool life as a result of precipitated phases "Inconel 718's high hardness is also a result of and. Carbides form at temperatures between 600 and 670°C, and samples are reinforced at temperatures between 600 and 648°C ", the highest hardness rating of which has been validated and demonstrated to be 360 HV. [27,28]

Microstructure Study and Mechanical Testing

The workpiece's microstructure affected the cutting process's stability and the tool wear rate during machining the hard-to-machine titanium alloys (9Ti-6Al-4V and Ti-555). The results show that cutting tools wear differently while cutting the Ti-555 alloy than when cutting with a Ti-6Al-4V insert.

Microstructure and machining parameter research uses scanning electron microscopy (SEM), high-resolution photography as characterization techniques, transmission electron microscopy (TEM), and optical microscopy (OM).

CBN tool at the cutting conditions: v = 200 m/min, f = 0.08 mm/rev, and d = 0.2 mm result.

DOI:https//doi.org/10.22452/mjs.vol44no2.10
Malaysian Journal of Science 44(2): 104-114 (June 2025)

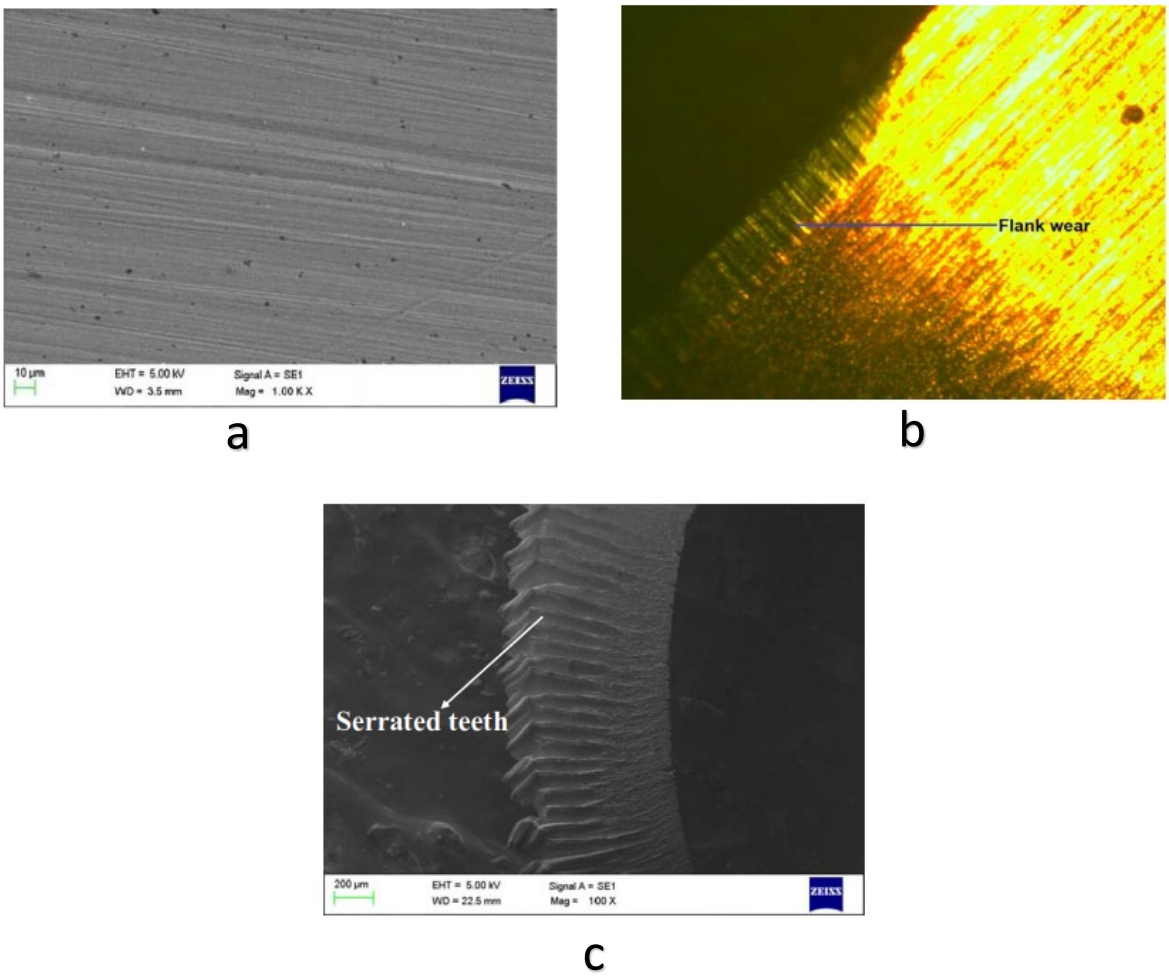

Figure 5. a) View of a machined surface using SEM [32] b) optical Image of flank wear in a CBN tool [32] c) SEM observation of chip morphology [32]

Figure 5 (A) shows a flat surface with a regular, smooth pattern and relatively few undulations, long scratch marks, and fine feed marks caused by shearing the machined work surface under the cutting edge, indicating a better surface finish. An acceptable level of surface roughness for the surface finish (Ra < 1.0 µm) was produced due to the exclusion of chatter formation, no chip entanglement, and less plastic deformation of the machined surface during machining. The scanning electron microscope (SEM) image of the challenging turned component, Figure 5 (b), shows the optical micrograph of the tool wear profile of the cBN tool at the flank face. The primary wear mechanism observed in hard turning is abrasion.

Machinability Issues

In terms of Inconel 718, significant developments and findings in its machining are discussed. Some alternatives to using coolants and various coating techniques have been researched to facilitate the switch to dry machining.

Machining Issues with Inconel 718

This study gives the significance of various cutting fluids when working with hard materials, which describes the characteristics of hard-to-machine materials and how to review and recognize them. Key environmental and health concerns related to using various coolants in the material cutting business are also examined. Finally, the review and discussion of the progress made in lowering fluid usage, reduction, or elimination. [24] By way of residual stresses, surface roughness, work hardening layers, and white layer, surface integrity (SI) issues have been characterized. Lowering constraints, the factors that most directly affect the SI of a hard-machined component are those related to the workpiece's material properties, the cutting tool's characteristics, the machine tool stiffness, and the cutting fluid qualities.[17]

DOI:https//doi.org/10.22452/mjs.vol44no2.10
Malaysian Journal of Science 44(2): 104-114 (June 2025)

Phase and Structural Microstructure Study

Table 2. Techniques used to find various output parameters of complex machining.

Technique	Remarks	References
X-ray diffraction	Detailed microstructures and spots are scanned using a resolution between 11nm and 13nm during tool wear analysis.	15, 20
Scanning Electron Microscopy	The surface of the sample in 3D, the grain size, the tool wear morphology, and the material's texture	18

Effect of Nanofluid

Thermal conductivity increased by 19.74 % and 36.21% for Al2O3 and CuO nanofluid, respectively. For machining operation, a better heat transfer fluid was obtained at an optimum value of 0.3 volume % for Al2O3 and 0.15 volume % for CuO [22].

Table 3. The percentage of Al_2O_3 and CuO.

Reference	Base Fluid	Nanoparticle	Flow Rate	Wt Ratio
[11]	vegetable oil	Al_2O_3	100ml/h	0%, 4%, 6%vol
[12]	soluble cutting oil	Al_2O_3	-	0%, 0.1% wt.
[13]	Oil10 (SAE 10W)	CuO and AL_2O_3	-	0.2% to 1% and 0.5% to 2%
[14]	Soluble Cutting oil	Al2O3	40 ml/h	0.2%,0.4%,0.6% wt%1wt%
[15]	vegetable oil	Al2O3	2.5 mi/min	0.25,0.75and 1.25 vol%
[37]	distilled water	CuO and Al_2O_3	-	0.25%, 0.5%, 0.75% and 1.0% (wt. percentage)
[36]	Vegetable Oil	Al_2O_3	40 ml/hr	0% 2% 4% nano additives 0.2 g
[34]	E2000	Al_2O_3 and MWCNT	40 ml/hr	0, 2 and 4%
[32]	water	Al_2O_3 and CuO	-	0.05, 0.15,0.3, 0.5 and 1 vol. %.

From table 3, the percentage of Al2O3 and CuO used in the base fluid is analyzed and is shown in Figure 6.

DOI:https//doi.org/10.22452/mjs.vol44no2.10
Malaysian Journal of Science 44(2): 104-114 (June 2025)

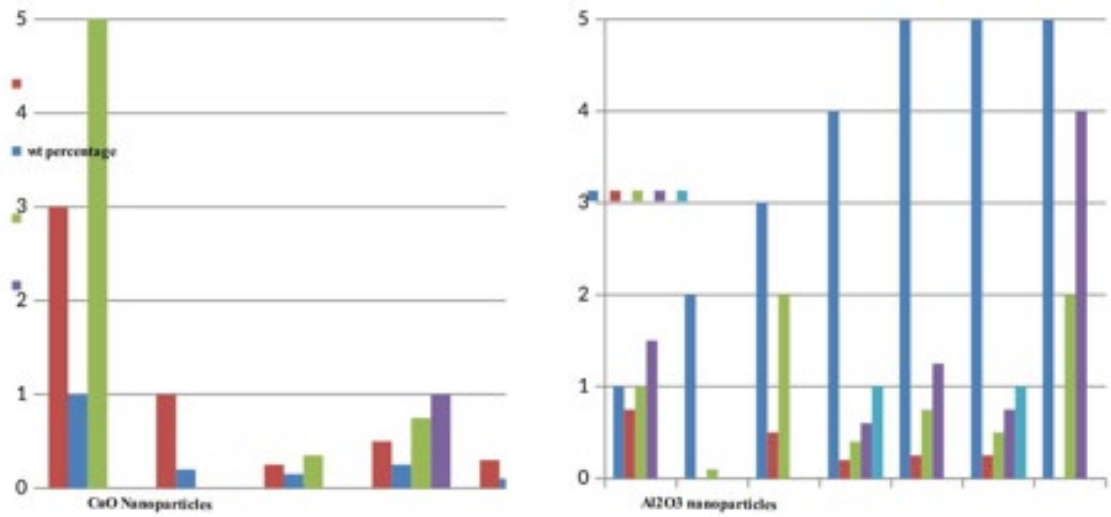

Figure 6. Weight of CuO and Al2O3 nanoparticles used by different researchers.

2. Conclusion

According to the above literature review, studies by various researchers identified several issues in terms of Machining Inconel 718

i. Since conductivity is low, thermal changes and microstructure changes make this material difficult to machine. Tool wear morphology, Grain size, material texture, and a 3D representation of the sample's surface were all examined using scanning electron microscopy.
ii. Tool wear analysis, spot scan, and microstructure area scan were performed using X-ray diffraction.
iii. Information about surface integrity and the formation of white layers is also included in the study.
iv. Investigating how to cut Inconel 718 material quickly results in BUC chips
v. Concluding that the use of coolant and dry machining has different effects on surface finish and MRR.
vi. Recognizing how tool wear and surface finish are affected by nanofluid.
vii. Recognizing how the nanofluid affects the surface roughness machining output parameter.

3. References

Amrita, M.; Srikant, R. R.; Sitaramaraju, A. V. (2014). Performance Evaluation of Nanographite-Based Cutting Fluid in Machining Process. Mater. Manuf. Process., 29 (5), 600–605. https://doi.org/10.1080/10426914.2014.893060.

Amrita, M.; Srikant, R. R.; Sitaramaraju, A. V.; Prasad, M. M. S.; Krishna, P. V. (2013). Experimental Investigations on Influence of Mist Cooling Using Nanofluids on Machining Parameters in Turning AISI 1040 Steel. Proc. Inst. Mech. Eng. Part J J. Eng. Tribol., 227 (12), 1334–1346. https://doi.org/10.1177/1350650113491934.

Anthony Xavior M, Duchosal A, Jeyapandiarajan P. (2018). Experimental Investigation on Work Hardening and Residual Stress during Machining of Inconel718. Mater Today Proc;5(5):13301-13308. doi:10.1016/j.matpr.2018.02.322

Chaudhari, S. S.; Chakule, R. R.; Talmale, P. S. (2019). Experimental Study of Heat Transfer Characteristics of Al2O3 and CuO Nanofluids for Machining Application. Mater. Today Proc., 18, 788–797. https://doi.org/10.1016/j.matpr.2019.06.499.

Chaudhari, S. S.; Chakule, R. R.; Talmale, P. S. (2019). Experimental Study of Heat Transfer Characteristics of Al2O3 and CuO Nanofluids for Machining Application. Mater. Today Proc., 18, 788–797. https://doi.org/10.1016/j.matpr.2019.06.499.

Davies MA, Burns TJ, Evans CJ. (2021). On the dynamics of chip formation in machining hard metals. CIRP Ann - Manuf Technol. 46(1):25-30. doi:10.1016/s0007-8506(07)60768-9

Endrino JL, Fox-Rabinovich GS, Gey C. (2006). Hard AlTiN, AlCrN PVD coatings for machining of austenitic stainless steel. Surf Coatings Technol. 200(24):6840-6845. doi:10.1016/j.surfcoat.2005.10.030

Fox-Rabinovich GS, Kovalev AI, Aguirre MH. (2009). Design and performance of AlTiN and TiAlCrN PVD coatings for machining of hard to cut materials. Surf Coatings Technol.;204(4):489-496. doi:10.1016/j.surfcoat.2009.08.021

Gupta K, Paulo Davim J. (2020). High-speed machining. High-Speed Mach.; 41:1-311. doi:10.1016/C2017-0-02542-9

Gupta, M. K.; Jamil, M.; Wang, X.; Song, Q.; Liu, Z.; Mia, M.; Hegab, H.; Khan, A. M.; (2019). Collado, A. G.; Pruncu, C. I.; et al. Performance Evaluation of Vegetable Oil-Based Nano-Cutting

DOI:https//doi.org/10.22452/mjs.vol44no2.10
Malaysian Journal of Science 44(2): 104-114 (June 2025)

Fluids in Environmentally Friendly Machining of Inconel-800 Alloy. Materials (Basel)., 12 (7). https://doi.org/10.3390/ma12172792.

Huang, W. T.; Chen, J. T. (2020). Application of Intelligent Modeling Methods to Enhance the Effectiveness of Nanofluid / Micro Lubrication in Microdeep Drilling Holes Machining. J. Adv. Mech. Des. Syst. Manuf., 14 (7), 1–26. https://doi.org/10.1299/jamdsm.2020jamdsm0099.

Iuliana BC. (2015). Factors-influencing-surface-integrity-in-hard-machining-of-steels-A-review.doc. Int J Sci Eng Res.;6(5):38-43.

Khalil, A. N. M.; Ali, M. A. M.; Azmi, A. I. (2015). Effect of Al2O3 Nanolubricant with SDBS on Tool Wear During Turning Process of AISI 1050 with Minimal Quantity Lubricant. Procedia Manuf. 2(February),130–134. https://doi.org/10.1016/j.promfg.2015.07.023.

Kim EJ, Lee CM. (2019). A study on the optimal machining parameters of the induction assisted milling with Inconel 718. Materials (Basel). 12(2). doi:10.3390/ma12020233

Kramar D, Kopač J. (2009). High-pressure cooling in the machining of hard-to-machine materials. Stroj Vestnik/Journal Mech Eng.55(11):685-694.

Krishna, P. V.; Parimala, N. (2019). Effectiveness of Coconut Oil Based Nanofluids in Machining of Steel.2 (1), 49–57.

Mani, N. K.; Mathew, C.; Kallanickal, P. M. (2015). Optimization of Cutting Parameters & Nanoparticle Concentration in CNC Turning of EN8 Steel Using Al2O3 Nanofluids as Coolant. Int. J. Eng. Trends Technol. 29 (6), 290–294. https://doi.org/10.14445/22315381/ijett-v29p254.

Öndin, O.; Kıvak, T.; Sarıkaya, M.; Yıldırım, Ç. V. (2020). Investigation of the Influence of MWCNTs Mixed Nanofluid on the Machinability Characteristics of PH 13-8 Mo Stainless Steel. Tribol. Int.148.https://doi.org/10.1016/j.triboint.2020.106323.

Parida AK, Maity KP. (2016). An Experimental Investigation to Optimize Multi-Response Characteristics of Ni-Hard Material Using Hot Machining. Adv Eng Forum.16:16-23. doi:10.4028/www.scientific.net/aef.16.16.

Pasam, V. K.; Srikant Revuru, R.; Gugulothu, S. (2018). Comparing the Performance & Viability of Nano and Microfluids in Minimum Quantity Lubrication for Machining AISI1040 Steel. Mater. Today Proc. 5 (2), 8016–8024. https://doi.org/10.1016/j.matpr.2017.11.486.

Paturi UMR, B. VD, Reddy NS. Progress of machinability on the machining of Inconel 718:A comprehensive review on the perception of cleaner machining. Clean Eng Technol. 2021;5:100323. doi:10.1016/j.clet.2021.100323

Rahman M, Seah WKH, Teo TT. (1997). The machinability of Inconel 718. J Mater Process Technol. 63(1-3):199-204. doi:10.1016/S0924-0136(96)02624-6

Rizvi SA, Ali W, Ahmad M, Delhi N. (2016). SOME STUDY OF MACHINABILITY BY TURNING PROCESS-A. II(6):1-20.

Roy, S.; Ghosh, A. (2014). High-Speed Turning of AISI 4140 Steel by Multi-Layered TiN Top-Coated Insert with Minimum Quantity Lubrication Technology and Assessment of near Tool-Tip Temperature Using Infrared Thermography. Proc. Inst. Mech. Eng. Part B J. Eng. Manuf., 228 (9), 1058–1067. https://doi.org/10.1177/0954405413514570.

Sahin Y, Sur G. (2004). The effect of Al2O3, TiN and Ti (C, N) based CVD coatings on tool wear in machining metal matrix composites. Surf Coatings Technol. 179(2-3):349-355. doi:10.1016/S0257-8972(03)00802-8

Sharma, A. K.; Singh, R. K.; Dixit, A. R.; Tiwari, A. K.; Singh, M. (2019). An Investigation on Tool Flank Wear Using Alumina/MoS2 Hybrid Nanofluid in Turning Operation; Springer International Publishing, 1. 156-189, https://doi.org/10.1007/978-3-319-99353-9_23.

Sharma, K. A.; Tiwari, A. K.; Dixit, A. R. (2015). Mechanism of Nanoparticles Functioning and Effects in Machining Processes: A Review. Mater. Today Proc., 2 (4–5), 3539–3544. https://doi.org/10.1016/j.matpr.2015.07.331.

Shokrani A, Dhokia V, Newman ST. (2012). Environmentally conscious machining of difficult-to-machine materials with regard to cutting fluids. Int J Mach Tools Manuf. 57:83-101. doi:10.1016/j.ijmachtools.2012.02.002

Singh PN, Raghukandan K, Rathinasabapathi M, Pai BC. (2004). Electric discharge machining of Al-10%SiCP as-cast metal matrix composites. J Mater Process Technol. 155-156(1-3):1653-1657. doi:10.1016/j.jmatprotec.2004.04.321

Singh, R. K.; Sharma, A. K.; Bishwajeet; Mandal, V.; Gaurav, K.; Nag, A.; Kumar, A.; Dixit, A. R.; Mandal, A.; Kumar Das, A. (2018). Influence of Graphene-Based Nanofluid with Minimum Quantity Lubrication on Surface Roughness and Cutting Temperature in Turning Operation. Mater. Today Proc.,5 (11), 24578–24586. https://doi.org/10.1016/j.matpr.2018.10.255.

Sreejith PS, Ngoi BKA. (2000). Dry machining: Machining of the future. J Mater Process Technol. 101(1):287-291. doi:10.1016/S0924-0136(00)00445-3

Su Y, He N, Li L, (2007). Refrigerated cooling air cutting of difficult-to-cut materials. Int J Mach Tools Manuf;47(6):927-933. doi:10.1016/j.ijmachtools.2006.07.005

DOI:https//doi.org/10.22452/mjs.vol44no2.10
Malaysian Journal of Science 44(2): 104-114 (June 2025)

Thakur, A.; Manna, A.; Samir, S. (2020) Multi-Response Optimization of Turning Parameters during Machining of EN-24 Steel with SiC Nanofluids Based Minimum Quantity Lubrication. Silicon, 12 (1), 71–85. https://doi.org/10.1007/s12633-019-00102-y.

Vasu, V.; Reddy, G. P. K. (2012) Effect of Minimum Quantity Lubrication with Al 2O 3 nanoparticles on Surface Roughness, Tool Wear and Temperature Dissipation in achining Inconel 600 Alloy. Proc. Inst. Mech. Eng. Part N J. Nanoeng. Nanosyst., 225 (1), 3–15. https://doi.org/10.1177/1740349911427520.

Venkatesan K, Ramanujam R. (2018) Statistical approach for optimization of influencing parameters in laser assisted machining (LAM) of Inconel alloy. Meas J Int Meas Confed. 89:97-108. doi:10.1016/j.measurement.2016.04.021

Wang ZY, Rajurkar KP. (2000) Cryogenic machining of hard-to-cut materials. Published online:168-175.

Yücel E, Günay M. (2013) Modelling and optimization of the cutting conditions in hard turning of high-alloy white cast iron (Ni-Hard). Proc Inst Mech Eng Part C J Mech Eng Sci. 227(10):2280-2290. doi:10.1177/0954406212471755.

DOI:https//doi.org/10.22452/mjs.vol44no2.10
Malaysian Journal of Science 44(2): 104-114 (June 2025)